# C. Elegans & anorectic herbal extracts: defining molecular-genetic responses & life-cycle consequences

Imanikia, Soudabeh

*Awarding institution:*
King's College London

# *C. elegans* & Anorectic Herbal Extracts:

## *Defining Molecular-Genetic Responses & Life-Cycle Consequences*

---

Thesis Presented To The Faculty Of Life Sciences & Medicine, King's College London

In Partial Fulfilment Of The Requirements For The Degree Of

Doctor Of Philosophy

***Soudabeh Imanikia***

***PhD in Genetic & Environmental Toxicology***
***2014***

**Dedication**

*To my mother, Dr. M. Imani, whose love and sacrifice are limitless, the one and only person who has been the rock of my life… Nothing can express my gratitude towards her.*

*Thank you!*

## *Acknowledgements*

Hereby I would like to express my gratitude towards everyone who has been by my side throughout these four years of research. Special thanks to the invaluable guidance and constant support of my supervisors Prof. Stephen Stürzenbaum and Prof. Peter Hylands whose knowledge and patience have helped me from the first day in the Laboratory of Molecular Genetics, King's College London.

This study was supported by King's International Graduate Scholarships (KINGS) and King's Alumni Bursary (KAB), in addition to the generous funds from the Centre of Natural Medicine Research. All worm strains and *E. coli* OP50 were kindly provided by the Caenorhabditis Genetics Center (CGC) (University of Minnesota, Minneapolis, MN, USA). Furthermore I wish to acknowledge Dr. Matthew Arno, manager of the KCL Genomics Centre and Dr. Estibaliz Aldecoa-otalora Astarloa, for printing the arrays and the use of genomic facilities.

I cannot express my gratefulness enough towards my beloved family, specifically to my grandfather whose words of wisdom lit my life from a toddler to date. To my precious mother without whom I could not make it through all these years and to my stepfather who believed in me more than I believed in me. In addition, many thanks to friends who never stop cheering for me even when I was down and could not carry on, for the ones who scientifically and emotionally supported me particularly, Dr. Martina Hockner, Dr. Nisha Hirani and Dr. Sabine Schnell.

## List Of Abbreviations

| Abbreviation | Actual name |
|---|---|
| **FLIM** | Fluorescent Life-time Imaging Technique |
| **PBS** | Phosphate Buffered Saline |
| **NGM** | Nematode Growth Medium |
| **LB** | Luria-Bertani Broth |
| **BMI** | Body Mass Index |
| **WHO** | World Health Organization |
| **TAG** | Triacylglycerol |
| **MRWB** | Modified Ruvkun Witches Brew |
| **RNAi** | RNA interference |
| **AMP** | Adenosine Monophosphate |
| **TOR** | Target OF Rapamycin |
| **SREBP** | Sterol Regulatory Element Binding Protein |
| **LDL** | Low Density Lipoprotein |
| **HDL** | High Density Lipoprotein |
| **NPY** | NeuroPeptide Y |
| **CARS** | Coherent Anti-Stokes Raman Scattering |
| **EM** | Electron Microscopy |
| **ATP** | Adenosine Triphosphate |
| **Nhr** | Nuclear Hormone Receptor |
| **PPAR** | Peroxisome proliferator-activated receptor |
| **TCA** | **tricarboxylic acid cycle** |
| **NADH** | Nicotinamide adenine dinucleotide |
| **FADH2** | Flavin adenine dinucleotide |
| **C/EBP** | CCAAT/enhancer binding protein transcription factor |
| **FABP** | Fatty Acid Binding Protein |
| **ACBP** | Acyl-CoA Binding Protein |
| **CPT transporter** | Carnitine Palmitoyltransferase transporter |
| **ABC transporter** | ATP-binding cassette transporter |
| **IIS** | Insulin/IGF-like Signaling pathway |
| **CR** | Calorie Restriction |
| **DR** | Dietary Restriction |
| **IGF-1** | Insulin-like Growth Factor |
| **GO** | Gene Onthology |
| **TAE** | Tris-Acetate-EDTA |
| **M-MLV** | Moloney Murine Leukemia Virus |
| **dNTP** | Deoxynucleotide |
| **RT-qPCR** | Real Time quantitative Polymerase Chain Reaction |
| **Bp, kb** | Basepair, kilo-basepair |
| **cDNA** | Complementary DNA |
| **AMV** | Avian Myeloblastosis Virus |
| **EDTA** | Ethylenediaminetetraacetic acid |
| **PFA** | Paraformaldehyde |
| **DMSO** | Dimethyl sulfoxide |

| | |
|---|---|
| **Rpm** | Rounds per minute |
| **CGC** | Caenorhabditis Genetics Center |
| **LRO** | Lysosome related organelles |
| **FRET** | Förster resonance energy transfer |
| **PMT** | Photo Multiplier Tube |
| **OD** | Optical Density |
| **SEM** | Standard Error of the Mean |
| **UV** | Ultra Violate |
| **UPL** | Universal Probe Library |
| **LNA** | Locked Nucleic Acids |
| **FABP** | Fatty Acid Binding Protein |
| **NMR** | Nuclear magnetic resonance |
| **HPLC** | High-performance liquid chromatography |
| **HR-MS** | High resolution Mass Spectrometry |
| **CNS** | Central Nervous System |
| **LC-MS** | Liquid Chromatography Mass Spectrometry |
| **ASI** | Amino acid Starvation-Induced p |
| **NMC** | Nicotinamide Mononucleotide uptake permease PnuC |
| **HUFA** | Highly Unsaturated Fatty Acid |
| **MUFA** | Mono Unsaturated Fatty Acid |
| **UTR** | Untranslated Region |
| **dsRNA** | Double stranded DNA |
| **FOXO** | Forkhead Box O |
| **ROS** | Reactive Oxygen Species |
| **NADPH** | Nicotinamide adenine dinucleotide phosphate |
| **FDA** | Food and Drug Administration |
| **TGF- β** | Transforming Growth Factor β |

## *Abstract*

An imbalance between energy uptake and energy expenditure can lead to obesity and increase the risk of coronary heart disease, high blood pressure, stroke, type II diabetes and some cancers. Given that key elements of energy pathway are evolutionary conserved, invertebrate research is an attractive alternative that overcomes the many legislative, financial and experimental hurdles typical of research with higher metazoan animals. The nematode *Caenorhabditis elegans* is a premier invertebrate model and has been utilized to study a wide range of topics of biomedical research including obesity, aging, toxicology, pharmaceutical and drug delivery approaches. Previous studies have suggested that raw extracts from a South African succulent (*Hoodia gordonii*) and P57 (the main active compound of the extracts) may exert an appetite suppressant effect. To investigate this notion in more detail, this present study aimed to pinpoint phenotypic, genetic and genomic-level responses of *C. elegans* treated with *H. gordonii* extract. Supplementing the bacterial food source with *H. gordonii* extract resulted in a significant reduction in growth parameters and the pharyngeal pumping rate as well as the fecundity. Likewise, it diminished the overall level of Nile Red positive compartments, which is indicative of a change in lipid metabolism. Comprehensive transcriptomics revealed that several genes involved in aging, lipid transport and reproduction were modulated following the exposure to the crude extract and pure P57. Based on these results, selected deletion mutants were studied in more detail, including *fat-5* (a member of the Δ9 desaturases) and *cyp-35A2* (a member of the cytochrome P450 family). The creation of a *fat-5(tm420);cyp-35A2(gk317)* mutant uncovered that the deletion of both genes resulted in a strain which is marked by a reduced fat content and an extended lifespan. Taken together, the results suggest the presence of a putative correlation between longevity and dietary restriction and given that both genes have human homologs, this finding may offer a new lead to investigate in higher organisms.

# CONTENTS

**List Of Figures:**

# Chapter One

## *General Introduction*

# 1 General introduction

## 1.1 Obesity, a global epidemic

Energy levels are tightly controlled by nutrient-sensing systems, metabolic enzymes and the nervous system. An imbalance of energy homeostasis (energy uptake vs. expenditure) can lead to obesity. Although a proportion of any population is seemingly resistant to excessive weight gain, levels of obesity have mushroomed (WHO, 2013).

On a global scale, obesity levels have doubled since 1980 and some 65% of the population now lives in countries where overweight rather than underweight is one of the main factors that influence the death rate. Annually, approximately 2.8 million individuals die as a result of obesity, which is now ranked as one of the top five life-threatening diseases. Overall, 44% of diabetic cases, 32% of ischemic heart problems and 7- 41% of certain types of cancer have been linked to overweight or obesity (WHO, 2013). Clearly, due to the complexity of the fat-metabolism pathway, it is impossible to provide a comprehensive list that encompasses all associated diseases but chronic heart diseases, diabetes type II, hypertension and stroke, respiratory complications and even sleep disorders are all related to metabolic disorders (Kopelman, 2000).

The body fat level can be evaluated by means of the Body Mass Index (BMI), a simplistic measure that calculates a ratio based on the weight in kilograms divided by the square of the height in meters. The WHO has used the BMI index to classify obesity (Table 1.1). Although the BMI correlates well with densitometry measurements of fat mass, its major disadvantage is that it cannot distinguish between fat mass and lean mass, which will differ markedly between an overweight person and an athlete. Alternative approaches include waist

circumference that is taken at the midpoint between the lower border of ribs and the upper border of the pelvis, this method assesses upper body fat content but cannot evaluate the intra-abdominal fat composition. Skinfold thickness is measured with calipers to allow a more precise assessment from different areas of the body, a method that lacks the ability to measure abdominal and intramuscular fat. In order to distinguish between the fat level and the muscle content, the Bio-impedance method can be utilized which quantifies the electrolyte solution resistance when a weak current is applied across the extremities and provides an estimation of lean mass rather than the fat mass using an empirically derived equation (Kopelman, 2000, WHO, 2013).

| **BMI index number** | Definition |
|---|---|
| **≤ 18.5** | Underweight |
| **18.5 - 24.9** | Normal |
| **25.0 - 29.9** | Grade 1 overweight |
| **30.0 - 39.9** | Grade 2 overweight (obese) |
| **≥ 40.0** | Grade 3 overweight (obese) |

**Table 1.1 The Body Mass Index (BMI).** The index is calculated from the weight in kilograms divided by the square of the height in meters, provides a rapid method of categorizing weight status. From (Kopelman, 2000, Imanikia and Stürzenbaum, 2013, WHO, 2013).

It is not only the modern lifestyle and its associated "toxic" effects that contribute to obesity, but a genetic mutation can cause anything from a mild hypomorphism to complete loss of function of essential enzymes linked to metabolic activities (Schlegel and Stainier, 2007).

Overweight and obesity have increased dramatically and since both terms are non-communicable diseases, they are preventable. Changing the eating habit of individuals by providing healthier, less calorie-dense food and encouraging citizens to be more physically active can be the starting point (WHO, 2013). In addition, life-threatening effects (such as cardiovascular diseases) may remain silent, as capillaries are less likely to be blocked by fat particles in a short period of time. Obesity is not a one-dimensional illness and due to the complexity of lipid pathways, all genetic and environmental factors involved in fat metabolism need to be taken into consideration. For all these reasons pharmacognosy and pharmacology of weight loss have become enormously attractive to the pharmaceutical industries. The number of approved synthetically manufactured drugs, which target obesity is surprisingly low however remedies of natural and herbal origin have become an incredibly popular alternative to the prescribed anti-obesity drugs. Often ignored are the potential side effects or the long-term exposure consequences of consuming herbal remedies to tackle overweight and obesity. The precise chemical structure(s) of a plant extract is/are often unknown, additives are not disclosed and the mechanisms of action are not fully understood. In order to address these shortfalls, there is a presenting need to study the pharmaceutical aspects of non-chemically manufactured anti-obesity pills. One approach is to utilize model organism ranging from invertebrates to mammals to explore the toxicogenetics underlying these drugs.

## 1.2 Model organisms

The side effects of previously marketed anti-obesity drugs have highlighted the need to improve our understanding of energy metabolism, including the drivers

of appetite, energy distribution and metabolic processes. Genetic model organisms offer powerful research tools to study metabolism and energy synthesis/breakdown pathways. Whilst the advantages of a vertebrate model organism approach are apparent, ethical issues cannot be ignored. In 1959 Russell and Burch proposed the principals of the "three Rs", namely the vision to Replace, Reduce and Refine the use of animals in biomedical research. In this context, replacement refers to the use of non-animal methods to substitute, where applicable, the use of animals; reduction can be justified by the deployment of enhanced methods to lower the number of animals in research; and refinement, where alternative methodologies will lead to less pain being applied to the animals during research (Wilson-Sanders, 2011). Invertebrate model organisms are promising surrogates for vertebrate research. To date, two invertebrate models have been utilized extensively mainly due to their molecular and genetic tractability, namely the fruit fly *Drosophila melanogaster* and the nematode *Caenorhabditis elegans*. A recent report has emphasized the importance of invertebrate models in the discovery of ground- breaking achievements of direct relevance to biomedicine (Wilson-Sanders, 2011). Besides the fly and the worm, further invertebrates are now used in basic and applied biomedical research such as the sea star *Astrerias forbesii* (Wessel et al., 2010), the sea squirt *Ciona intestinalis* (Holland and Gibson-Brown, 2003, Passamaneck and Di Gregorio, 2005), the reef coral *fungia scutaria* (Jokiel and Bigger, 1994), the water flea *Daphnia magna* (Gorr et al., 2006, Romero et al., 2007), the grasshopper *Dissosteira Carolina* (Bonner and O'Connor, 2000) and the star ascidian *Botryllus schlosseri* (Lightner et al., 2008).

## 1.3 Introducing the nematode *C. elegans*

### 1.3.1 General aspects

Over the last four decades invertebrates have emerged as model organisms within several areas of biological and biomedical research. In 1998 *C. elegans* was the first multi-cellular organism to be fully sequenced, which was a major advance aiding forward and reverse genetic approaches (Hope, 1999).

*C. elegans* is an omnipresent, free-living, soil dwelling, bacteriovorus round worm (Hope, 1999). A fully-grown adult hermaphrodite is about 1mm in length and produces 250-300 eggs. At 20°C and food *ad libitum* the L1 larva grows into a fully developed gravid adult within 3 days (or 5 days if maintained at 15°C). The life span varies between 14-21 days (Figure 1.1). Under extreme conditions (such as food deprivation, stress, crowding etc.) the L1 larva undergoes a protection phase and enters "Dauer" (Figure 1.1). This alternative pathway allows the worm to survive up to five months and resume development by entering the L4 stage once external conditions improve (Wood, 1988b, Wood, 1988a).

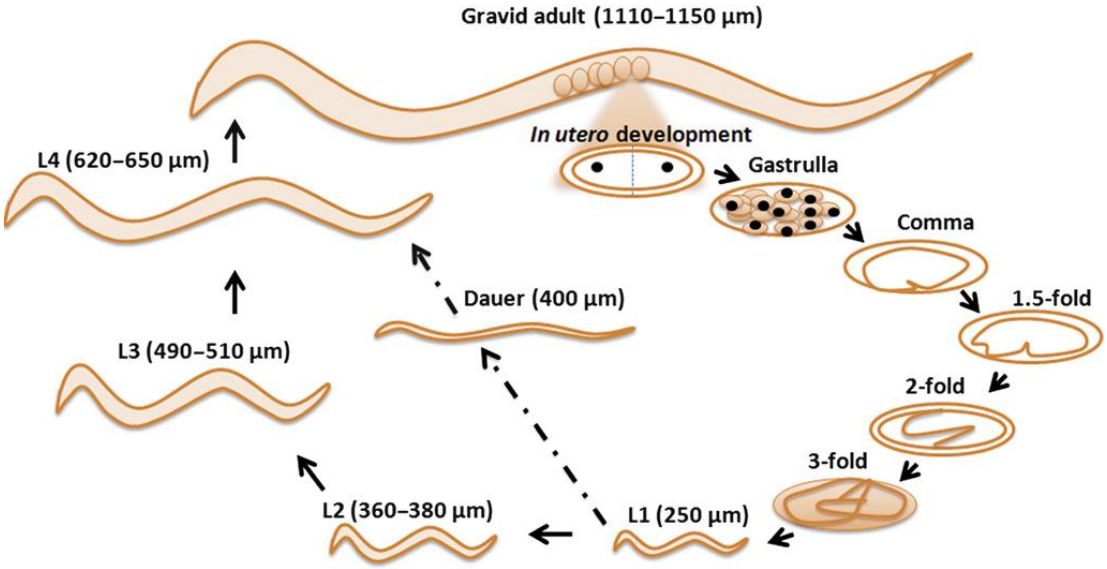


**Figure 1.1 A simplified presentation of the *C. elegans* life cycle.** The egg is laid at gastrulla stage. When exposed to undesirable conditions (stress, crowding or lack of food) the first larval stage (L1) enters "dauer," a stage that allows the worm to survive up to five months. Once conditions improve, the dauer animal develops into an L4 worm and oogenesis commences. Under optimal growth conditions, the entire life cycle (egg to egg) is completed within three days (Altun and Hall, 2009, Imanikia and Stürzenbaum, 2013).

Males are rare (less than 0.2 % of a wild-type population raised at 20°C) and karyotipic analysis confirmed that the male nematode is XO, resultant from the non-disjunction of the X chromosome at meiosis (Jorgensen and Mango, 2002). The male nematode has distinct phenotypic features and can be recognized by the fan-like structure of its tail (Figure 1.2) (Wood, 1988b).

The hermaphrodite *C. elegans* is made up of 959 somatic cells, of which 302 are neurons and 95 are muscle cells. Its body consists of a range of tissues and organs that are comparable to higher organisms including muscle cells, nerves, epidermis and a large gastrointestinal tract, which occupies almost the entire body (Wood, 1988a, Hope, 1999).

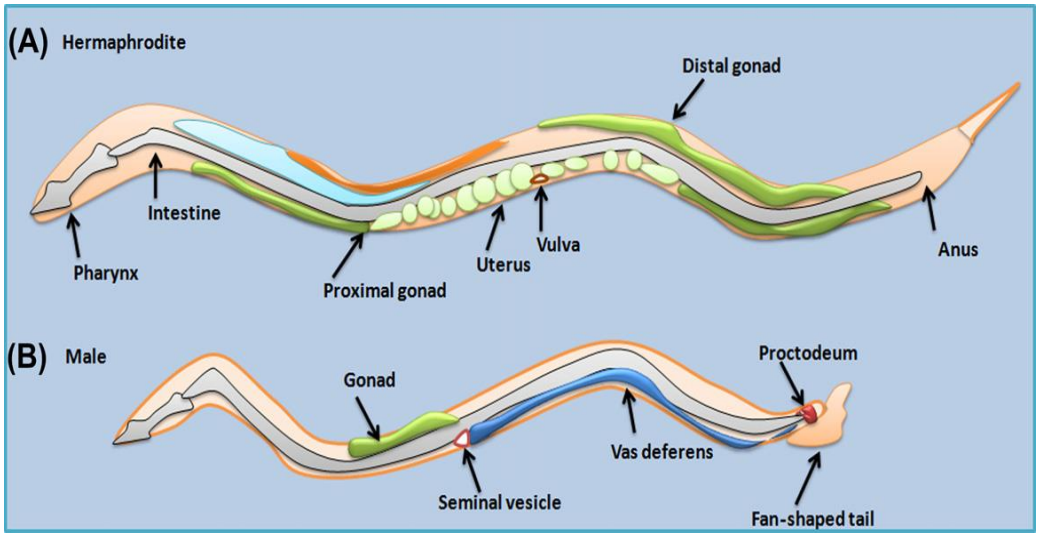


**Figure 1.2 Schematic overview of the hermaphrodite and male *C. elegans*.** (A) Schematic drawing of a gravid hermaphrodite nematode. The hermaphrodite has two gonads (proximal and distal) and is self-fertilizing in the absence of males. The adult is about 1 mm in length and consists of 959 cells. (B) The male nematode is smaller in size and more active (compared to its hermaphroditic counterpart). The posterior end of the male worm comprises a distinct fan-shaped tail, which is required for the mating process with hermaphrodites. The male *C. elegans* consists of 1031 cells (Altun and Hall, 2009, Imanikia and Stürzenbaum, 2013).

A further remarkable feature is its transparency that allows the study of different endpoints within the intact body of the live animal. For example, pharyngeal pumping rate, changes in cellular morphology and physiological alterations can be followed and studied without invasive methods. Moreover, fluorescent tags can be observed in the body of live animals (Wood, 1988a).

### 1.3.2 Behavior

*C. elegans* displays several behavioral characteristics which are mirrored in higher organisms, the most significant being locomotion and chemotaxis. *C. elegans* also responds to stimuli including taste, smell, temperature, touch and osmotic change. In addition to these primary behaviors nematodes display social modes of communication, learning and memory skills. Complex behavioral

factors can be tested to study the effects of drugs on the nervous system, including alcohol, nicotine or serotonin-related drugs such as the antidepressant Fluoxetine (Rankin, 2002).

Initially, *C. elegans* was chosen as an experimental model organism to target developmental and neural processes, and was instrumental in uncovering the mechanisms of programmed cell death (Kaufmann and Hengartner, 2001). *C. elegans* is now a prime choice to study diverse areas related to mammalian biology, such as cell-cell signaling, aging and gender determination. These are possible due to the presence of evolutionary conserved pathways between worm and man (Carroll and Fitzgerald, 2003).

### 1.3.3 Genome

The genome of *C. elegans* is made up of 100,291,840 bp (Hillier et al., 2005). There are several examples in which nematodes have been utilized as disease-models, including age-related neurodegenerative diseases such as Alzheimer's, Parkinson's and Huntington's that are mainly due to protein aggregations. By using the nematodes it is possible to adapt experimental tools to aid our understanding of the fundamentals underlying neurodegenerative diseases. However one of the shortcomings of the worm model is that some factors are specific to mammals and therefore cannot be studied in a simple invertebrate model (Link et al., 2003). As most neurodegenerative illnesses are inheritable through genetic mutations, it is of great importance to find the core mutations that give rise to such illnesses. For instance, Parkinson's disease is at least in part, the result of mutations in the human PARKIN protein, which has a *C.*

*elegans* homolog, named PDR-1. Moreover, Alzheimer's disease which has been linked to mutations in PRESENILIN-1 (PS1) and PRESENILIN-2 (PS2) also has sequence similarity with the *C. elegans* SEL-12 (Li and Greenwald, 1996). Not only for neurodegenerative diseases but also in metabolic disorders, nematodes share several homologies with humans. For example obesity can be studied using the model organism *C. elegans,* by exploring genes and pathways involved in adipogenesis. Two of the mammalian genes involved in fat accumulation are SREBP and C/EBP (Rosen et al., 2000, McKay et al., 2003). The *C. elegans* homolog, *sbp-1,* is expressed in endodermal fat-storing cells and a mutation in *sbp-1* results in pale and slim worms marked by larval arrest (McKay et al., 2003).

### 1.3.4 Fat accumulation in *C. elegans*

Lipids extracted and fractionated from whole animals by means of column/thin-layer chromatography or gas-chromatography/mass spectrometry (GC/MS) have confirmed that *C. elegans* store lipids, similar to higher organisms, as Triglycerides (Ashrafi, 2007). Phospholipids, the other major fat bodies in the worm, consist of several components such as Ethanolamine glycerophospholipids 55%, Choline glycerophospholipids 32%, Sphingomyelin 8% and in minor parts Cardiolipins, Inositol glycerophospholipids and Lyso-choline glycerophospholipids. The exact composition varies depending on the diet, growth stage and the temperature in which the nematode lives. In addition to saturated, unsaturated and polyunsaturated fatty acids, *C. elegans* retains a wide spectrum of elongases and desaturases that are also found in plants and

other animals, thereby ensuring a supply of essential linoleic and linolenic acids. Conversely, mutations within the elongase or desaturase gene families disrupt the fat metabolism and other physiological, metabolic and behavioral mechanisms. Being a cholesterol auxotroph, *C. elegans* obtains cholesterol via its food. Given that cholesterol is only required in small quantities, it is believed that cholesterol is utilized only for specific sterol-derived hormonal activities rather than being a membrane or structural requirement (Ashrafi, 2007).

Due to their hydrophobic properties, fatty acids play important roles in membrane permeability, fluidity and signal transfers within different cells. Tri-AcylGlycerides (TAGs) are stored in lipid droplets or yolk and thereby act as energy reservoirs. TAGs are utilized during embryogenesis, food shortage and in the dauer stage in which nematodes seize to feed (Watts, 2009). Due to the transparency of the nematodes, lipid droplets can be visualized using vital dye and fixative staining methods. Whilst the vital dye Nile Red allows a rapid and convenient detection of fat bodies, Sudan Black and Oil Red O require a more laborious preparation. Similarly, fat content can readily be assessed by means of standard biochemical assays. Nematodes store fat either in their intestinal cells or under their skin-like epidermis (Ashrafi, 2007).

The mechanism by which nematodes consume and digest food is that the bacterial food source enters the pharynx and is mechanically crushed by the grinder then enters the intestine. The *C. elegans* intestine consists of column-shaped epithelial and polar cells, and surface microvilli play an important role in nutrient absorption. The intestinal cells are involved in the secretion of lipases and peptidases, for example, the *C. elegans* genome contains genes which encode for eight α/β hydrolase lipases, seven of which are predicted to produce signal

peptides targeted for secretion into the gut, unlike the lipases of the mammalian pancreas and digestive system which are also secreted from the α/β hydrolase lipase family (Mullaney and Ashrafi, 2009).

Because the nematode lacks adipocytes, the cells of the intestine are the main sites for lipid storage. Electron Microscopy and genome-wide RNAi studies have advanced our knowledge regarding the lipid depots in nematodes, however very little is known about the precise membrane characteristics or molecular composition of target proteins. Although some mammalian fat related genes and proteins are not found in the nematodes, others have been studied in great detail and have provided sufficient data to support the notion that the major fat regulatory pathways are conserved (Mullaney and Ashrafi, 2009).

### 1.3.5 The conserved fat-regulatory genes and pathways in *C. elegans*

The balance between energy intake and energy expenditure is vital, hence several energy regulatory pathways are conserved among eukaryotic organisms ranging from invertebrates to mammals, including humans. Lipids are important as they are a major component of cellular membranes and because they are energy storage sites. Mammals have both peripheral and central regulatory sites for fat metabolism although nematodes lack this complexity they have key genes that play essential roles. There is still an uncertainty about how lipids are stored in *C. elegans* and to what degree they exhibit a fat storage system that is analogous to mammals. Having said that, it is known that *C. elegans* store fat droplets in intestinal and skin-like hypodermal cells (Ashrafi, 2007, Hellerer et al., 2007) and lipid storage and breakdown involve several conserved pathways including,

the AMP-activated protein and target of rapamycin (TOR) kinases, the sterol response element binding protein (SREBP) and CCAAT/enhancer binding protein (C/EBP) transcription factors (Hara et al., 2002, McKay et al., 2003, Apfeld et al., 2004, Jia et al., 2004, Yang et al., 2006).

In addition, lipids and proteins are transported from intestinal cells into oocytes via a shuttling system using a low-density lipoprotein (LDL) family receptor and receptor-mediated endocytosis (Grant and Hirsh, 1999). Fatty acid transporters and lipid-binding proteins are also found in worms (Plenefisch et al., 2000).

Yeast, worms and flies lack dedicated fat storage organs and tissues (liver and adipocytes) however SREBP homologs are responsible for the majority of lipid and cholesterol related processes in these organisms. When membrane fluidity is changed, the expression of specific transcription factors is altered. This feature is evolutionarily conserved with additional organism-specific modifications, for example in fission yeast it helps in monitoring oxygen level. Whilst in flies it controls their phospholipid levels and in higher organisms such as mammals SREBP functions in the control of cholesterol synthesis (Brown and Goldstein, 1997, Dobrosotskaya et al., 2002, Hughes et al., 2005). The role of the *C. elegans* SREBP in membrane lipid metabolism is not yet fully explored, although there is evidence that this gene may play a vital role in fat regulatory pathways (Jones and Ashrafi, 2009).

Certain neuronal and endocrine regulators of lipid metabolism in *C. elegans* resemble those of the mammalian insulin fat metabolism and aging pathways. Additionally, serotonin signaling in the nervous system and the feeding behavior control fat synthesis/breakdown. Of course fat metabolism comprises of a complex network including different pathways, redundant mechanisms and

positive/negative feedback loops. In most mammalian studies, pathways are only studied in isolation (via single gene knock-in/out) however homeostatic responses are far more complex. In mice for example, the neuropeptide Y (NPY) is expressed in the hypothalamus in a leptin-dependent manner. When NPY is administrated, hyperphagia and obesity occur, but mice, which are NPY deficient, show no symptoms of either abnormal feeding or elevated fat levels. Interestingly, once NPY-deficient mice are crossed with leptin-deficient *ob/ob*, then leptin and NPY show cross activity (Jones and Ashrafi, 2009). For mammalian studies, it is usually not applicable to perform multiple knock downs/outs because they are frequently lethal. However, in *C. elegans* studies, gene manipulations are much easier and genome-wide studies via RNAi or microarray analyses are less labor-intensive.

Feeding behavior does not only rely on gastrointestinal signals but are also regulated by olfactory signals, visual and several other sensory key factors. Moreover, environmental factors also affect the feeding rate. For instance, dauer formation is mainly in response to environmental changes such as food shortage, temperature fluctuations or over-population. Many lipid-regulatory genes that are involved in *C. elegans* dauer formation have human homologs including the insulin signaling pathway and an AMP-activated protein kinase (Hu, 2007, Narbonne and Roy, 2009). Recent studies have revealed that several developmental modulations depend on the nutrient sensing signals by which, upon food deprivation, larvae arrest as a result of insulin regulatory pathways (Baugh and Sternberg, 2006, Fukuyama et al., 2006).

Interestingly, in *C. elegans* food availability is correlated with the feeding rate (pharyngeal pumping) in addition to the egg-laying and locomotion patterns.

Nematodes also share similarities with humans in metabolic responses such as serotonin pathway (Tecott et al., 1995, Sawin et al., 2000). Correspondingly, nematodes receive fat regulatory signals from peripheral lipid sites (Srinivasan et al., 2008), and worms have a remarkable behavioral ability to interact with each other and stimulate feeding activities via a homolog of the NPY receptor (de Bono and Bargmann, 1998). In addition to food availability, food quality and previous experience of the food can affect the feeding behavior of nematodes (Shtonda and Avery, 2006). Satiety signaling pathways can also be studied in nematodes because these mechanisms are evolutionary conserved (You et al., 2008).

There are several mutations involved in longevity that have been initially discovered in nematodes. There is enough evidence that Insulin/IGF signaling pathway is directly involved in aging, by which a reduction in IIS needs the Forkhead FoxO transcription factor *daf-16*. Furthermore, lifespan is also extended via suppression of TOR/SM6 kinase pathway activity at different stages such as TOR kinase and S6 kinase that is a homolog of the pro-aging yeast SCH9. Moreover, a target of TOR signaling, autophagy is essential in order to increase the survival rate. There are many other key factors of TOR signaling pathway, which are involved in longevity, which may act independently or via several parallel pathways (such as an alteration HIF-1 activity) (Fontana et al., 2010).

Dietary restriction can be implied to *C. elegans* by different methods. Including, mutations in key regulators of pharyngeal pumping or changes in bacterial food source such as, the removal of bacteria, dilution of live or dead bacteria in solid or liquid media and/or dilution of peptone and axenic cultures(Mair and Dillin, 2008). There are other factors affecting lifespan in nematodes rather than dietary

restriction, diffusible substances may be released from bacterial food source that result in a reduction in the survival of worms (Smith et al., 2008). It has been confirmed via rodent studies that a combination of dietary restriction and heat shock factor-1 protects the animal from proteotoxicity leading to age-related diseases (Steinkraus et al., 2008).

It is also important to know that dietary restriction can be implied via different approaches that may work independently or in parallel to each other. The mechanisms by which DAF-16 extends *C. elegans* lifespan is different from the pathways responsible for the long-lived *eat* mutants. This also emphasizes the complexity of parallel pathways (Greer and Brunet, 2009). Nutrient sensing pathways play an important role in response to dietary restriction. TOR pathway influences autophagy and HIF-1 that are both well known to be involved in dietary restriction. In addition, IIS is involved in DAF-16-mediated dietary restriction responses as well as the AMP-activated protein kinase (AMPK) (Greer and Brunet, 2009). Moreover, there are other transcription factors including *pha-4* (with co-factor SMK-1) and SKN-1 that are partially responsible in some of the dietary restriction methods. *Pha-4* is the orthologous of mammalian Foxa family of forkhead transcription factors, with an essential role in metabolic homeostasis (Carrano et al., 2009). Nematodes have an orthologous of mammalian Nfe211 and Nfe212 transcription factors namely SKN-1, involved in induction of the phase II detoxification pathway. Having said that, an increase in SKN-1 activity ultimately makes worms longer-lived (Tullet et al., 2008, Fontana et al., 2010).

A wide range of desaturases are found in nematodes that are also found in plants and animals such as Δ12, ω3 and Δ5, Δ6, Δ9 desaturases, respectively (Castro et

al., 2012). Briefly, Δ5 desaturase is responsible for catalyzing the synthesis of highly unsaturated fatty acids (HUFAs), Δ6 desaturase is a membrane-bound enzyme that is involved in the catalysis step during the formation of poly-unsaturated fatty acids (PUFAs), and Δ12 is mainly found in plants and (similar to other desaturases) plays a role in desaturation of long chain fatty acids as well as ω3 (Nakamura and Nara, 2004, Castro et al., 2012). In the nematodes, each member of the FAT protein family is responsible for one of these desaturases, including FAT-1 that has a ω3-resembling function, FAT-2 is responsible for the Δ12 activity, FAT-3 and FAT-4 are analogs of Δ6 and Δ5 desaturases, respectively. Moreover, FAT-5, 6 and 7 are involved in Δ9 desaturase activity (Zhou et al., 2011, Watts and Browse, 2002, Watts, 2013).

In detail, Δ9 desaturase enzymes are mainly responsible for limiting the formation rate of monounsaturated fatty acids (MUFAs), which are the preferred substrate for the production of various lipids such as phospholipids, triglycerides and cholesteryl esters. In addition, Δ9 desaturases play an essential role in membrane fluidity by changing the ratio of branched fatty acids. Due to the fundamental roles of desaturases, they are likely to be a therapeutic target for several metabolic disorders including obesity, diabetes and some coronary heart diseases (Castro et al., 2012).

In humans, stearoyl-CoA desaturase-1 (SCD) is the homolog of the nematode Δ9 desaturase, which codes for an important enzyme in fatty acid metabolism for the production of polyunsaturated fatty acids and specifically, oleic acid. The SCD gene has putative homologs in other mammalian organisms such as, *Pan troglodytes* (Chimpanzee), *Macaca mulatta* (Rhesus Monkey) and *Mus musculus* (House Mouse). Lower organisms also share gene homology with the human

SCD, for instance *Drosophila melanogaster* (Fruit fly), *Anopheles gambiae* (Mosquitos) and the nematode *C. elegans* (NCBI, 2014). Stearoyl-CoA desaturase (SCD-1) is responsible for the catalysis of a double bond at the Δ9 position of palmitoyl-CoA (16:0) (Shanklin et al., 1994, Watts and Browse, 2000).

Previous studies have reported that in *Scd1* deficient mice the hepatic levels of triglycerides are reduced and in parallel the insulin sensitivity increases. Moreover, when the *Scd* deficient mouse model is fed a low fat and high-carbohydrate lipogenic diet, high-density lipoprotein (HDL) is essentially absent and the mutants develop cholestasis, however recover once the animals are fed mono- and poly-unsaturated fat (Attie et al., 2007).

Moreover, cytochrome P450s are essential for oxidizing exogenous compounds and metabolizing endogenous molecules. The oxidation process is essential for processing toxic or foreign compounds (especially from a toxicological aspect). Mammalian studies have revealed that cytochrome P450s play a vital role when relatively long-chain fatty acids, including linoleic and arachidonic acids, are converted into bioactive forms (Aarnio et al., 2011).

The *C. elegans* genome encodes 77 members of the cytochrome P450 superfamily. There is experimental evidence that a number of the cytochrome family members are involved in maintaining a healthy fat composition in worms (Ashrafi *et al*., 2003; Menzel *et al.*, 2007). In *C. elegans* genome, *cyp*- genes are on chromosome V and are located next to each other as well as harbouring *cyp-34* family as a neighbor. Interestingly, CYPs that are clustered together are appeared to be more involved in xenobiotic activities in contrasted to the more

isolated *cyp*-members (Thomas, 2007, Aarnio et al., 2011). Human CYP-1 and CYP-2 are the closest members to *cyp-35*s, which are involved in metabolizing both exogenous and endogenous compounds such as omega-3 and 6 fatty acids (Schwarz et al., 2004, Fer et al., 2008, Arnold et al., 2010, Aarnio et al., 2011). Furthermore, Aarnio's study reconfirmed that inactivation of cyp-35 members leads to a lower intestinal fat accumulation therefore suggesting that CYPs are necessary for lipid storage but not sufficient (Aarnio et al., 2011). In addition to this, signal transduction enzymes, transporters, receptors and energy metabolism enzymes were pinpointed through that study with an emphasis on a major fat storage regulator namely NHR-49. This regulator is associated with 13 energy metabolism genes (Van Gilst et al., 2005a, Van Gilst et al., 2005b). The Aarnio et al., study then suggested the involvement of several energy metabolism genes including *fat-5, fat-6* and *fat-7* to overlap with other regulators including *cyp-35* members. Finally, it was concluded that CYPs and NHRs may share common energy regulatory pathways associated with lipid storage (Aarnio et al., 2011).

Mutations in *cyp-35A2, cyp-35A3, cyp-35A4* and *cyp-35A5* result in a deficient fatty acid metabolism. The CYP-35A protein family is widely expressed within the gut cells, which are also the main sites of fat storage (Aarnio *et al*., 2011). Similar studies have also reported the involvement of additional members of the CYP protein family in lipid pathways, such as CYP-29A3 and CYP-33E2 which are metabolizers of eicosapentaenic acid, and CYP-31A2 and CYP-31A3 that are both essential for metabolizing lipids throughout developmental stages (Kulas et al., 2008, Ashrafi et al., 2003, Benenati et al., 2009, Aarnio et al., 2011). These

findings emphasize the complexity of metabolic pathways even in a relatively simple organism such as the nematode *C. elegans.*

## 1.4 *C. elegans*: a model organism for obesity research

Approximately 60% of *C. elegans* genome displays sequence similarity to the human genome, this feature renders the nematode an ideal candidate for the study of conserved pathways and metabolic activities. *C. elegans* occupies an interesting niche between *in vitro* and cell culture studies (which, though cost efficient and fast, lack the whole animal aspect) and rodent experiments (which are time consuming and expensive, but clearly of value due to their evolutionary closeness to humans).

Characteristics such as the short lifespan, large progeny number (which are essentially cloned if random mutations are not discounted) and the rapid life cycle are some of the benefits of utilizing nematodes in biomedical research. However, one should not forget that *C. elegans* is maintained under highly tailored laboratory conditions, for instance they are grown on Nematode Growth Media (NGM) supplemented with a Uracil auxotroph strain of *E. coli*, namely OP50. This bacterial strain has a reduced growth rate therefore, provides a thin layer of food lawn that does not overgrow the worms. Since the nematode's diet can influence its fat accumulation and composition, it is paramount to control and keep a constant food source, as any changes may introduce experimental variations. It is also important to ensure that nematodes do not enter the dauer form, which induces structural changes that directly elevate fat storage (Zheng and Greenway, 2012). Despite the physiological, genetic and functional

conservations between worms and mammals, one should not forget that the architecture of nematodes is simple.

*C. elegans* has been used to explore the link between dietary restriction and life extension. For example, the pharyngeal nicotinic acetylcholine receptor mutant, *eat-2*, is characterized by a reduced feeding rate (i.e., fewer pharyngeal pumps per minute) and also lives longer. However pumping rate and fat accumulation do not necessarily correlate; indeed many mutations and conditions promote an increase in pharyngeal pumping and a loss in total body fat and vice versa (Zheng and Greenway, 2012).

A developing (wild-type) nematode typically accumulates fat in lipid droplets within the intestinal cells and the fat storage capacity is increased by elevating the quantity and size of the droplets. CARS (Coherent Anti-stokes Raman Scattering) microscopy has revealed that the larger droplets mainly accumulate in the gut granules whereas smaller fat droplets in the epidermal cell. Notably, during development and exposure to environmental stress the size, number and distribution of the droplets can change (Mullaney and Ashrafi, 2009).

Measuring lipids in nematodes is an essential step by which one could be able to analyze alteration in lipid profile of *C. elegans* benefiting from the transparency of the nematodes. It is worth employing diverse approaches to quantify lipid droplets in worms and not to draw conclusion only by applying one certain technique. Not only the overall lipid content but also the distribution of fat must be taken into account when choosing a lipid visualization and/or quantification method. Two mutants with the same fat levels may have significantly dissimilar lipid distribution within different tissues and cells resulting in the need for

conducting different approaches to target lipid droplets within these strains (Lemieux and Ashrafi, 2014).

There are several different methods of visualizing lipids in nematodes, a recent review by Lemieux and Ashrafi has summarized different techniques as well as the pros and cons of each method. There are fixed- and vital-dye staining procedures that can be utilized based on the purpose of the study. Fixed staining includes Sudan Black and Oil Red O through which, the cuticle needs to be permeabilized in order to absorb the dye. This method is error prone due to the use of organic solvents, which may potentially lead to dissolving certain types of fatty acids and false negative results. Vital dye labeling consist of Nile Red, LipidTox and BODIPY, despite being an easier approach, vital staining fails to stain all types of lipids as well as giving false positive results due to auto-fluorescence. Furthermore, there are analytical approaches such as TLC[1] and GC/MS[2], by which the former allows quantifying triacylglycerols, phospholipids and free fatty acids and the latter unravels the abundance of single fatty acid chains (Lemieux and Ashrafi, 2014).

Recently, label-free microscopy approaches have been employed to visualize and eventually quantify lipid droplets in *C. elegans*. Two methods of CARS[3] and SRS[4], based on Raman-simulated vibrational emission, are suggested and have been in use however despite the fact that label-free methods are highly complex they are highly labor intensive and require expensive equipment and the turnover time is considerably slow (Lemieux and Ashrafi, 2014).

[1] Thin Layer Chromatography
[2] Gas Chromatography- Mass Spectrometry
[3] Coherent Anti-Stokes Raman Scattering
[4] Stimulated Raman Scattering

Therefore, because of the diverse environment that lipid droplets are stored within the body of the animals, makes it a challenge to utilize a universal method targeting all types of fatty acids and fat.

## 1.5 Fat pathways in mammals and nematodes

Fat accumulation and fat transport are coordinated by intricate networks involving transcriptional, translational and in some cases post-translational regulations. The *C. elegans sbp-1*, a homolog of the mammalian SREBP, plays a major role in fat accumulation in nematodes. The knockout or silencing (by RNAi) of *sbp-1* results in a dramatic decrease in body fat, a finding which was confirmed by Electron Microscopy (EM), biochemical assays and staining methodologies (Mullaney and Ashrafi, 2009). As in mammals, other SREBP transcriptional end points are dependent on *sbp-1*, including acetyl-CoA carboxylase, ATP-citrate lyase, fatty acid synthase, glycerol 3-phosphate acyltransfrase and malic enzyme. Likewise, the *C. elegans* nuclear hormone receptor *nhr-49* is an ortholog of the mammalian peroxisome proliferator-activated receptors (PPARs). Suppression of *nhr-49* (in worms) or PPAR (in mice) results in elevated levels of fat. Both genes are involved in the transcriptional regulation of fatty acid β-oxidation, lipid binding and fatty acid desaturation (Mullaney and Ashrafi, 2009).

The fundamental mechanisms underlying the sugar, fat and energy metabolism are conserved between *C. elegans* and higher organisms, therefore justifying the study of energy homeostasis pathways in a simple model organism (Figure 1.3). The TCA cycle also known as the Krebs cycle, has one main goal of harvesting electrons from carbon sources. The cycle is not responsible for energy generation, it removes electrons from Acyl CoA and then transfers the electrons onto NADH and $FADH_2$. Thereafter electrons that are released from re-oxidation of NADH and $FADH_2$ are transported across a wide range of membrane proteins (electron-transport chain), upon which a proton gradient is created along the membrane.

These protons pass through ATP synthase in order to generate ATP from ADP and other inorganic phosphate. It is essential to have oxygen in citric acid cycle to act as the electron acceptor in the last part of the electron-transport chain to produce $NAD^+$ and FAD (Berg et al., 2002). Moreover, cytochrome b5 reductase (CBR) is an electron donor for cytochrome b5, which is an abundant electron carrier involved in a wide range of metabolic pathways such as steroid biosynthesis, desaturation and elongation of fatty acids and P450-dependent reactions. There are two forms of CBRs found in cells, one is bound to the membrane of endoplasmic reticulum and the other is soluble and located in erythrocytes (information adapted from Interpro IPR001834, www.ebi.ac.uk).

Transcriptional and translational regulatory processes modulate the transfer of energy between cells. Sensory and metabolic pathways are connected via neuroendocrine signaling and neuromodulatory pathways control the entire network.

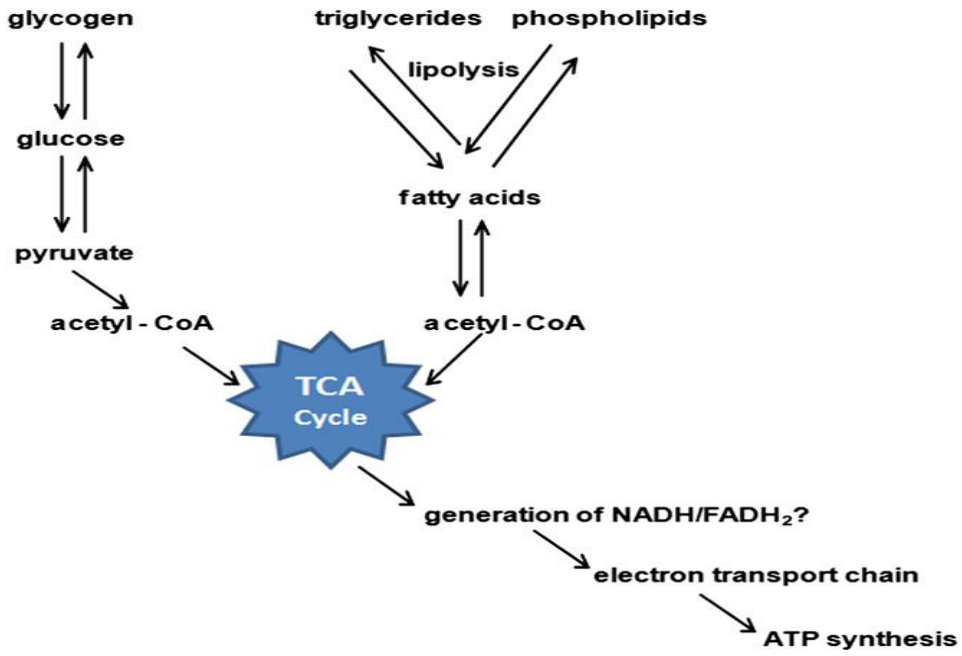


**Figure 1.3 An overview of major fat/sugar biosynthesis and breakdown mechanisms.** Acetyl-CoA fuels the sugar and lipid pathways. In lipid biosynthesis, conversion of fatty acetyl-CoAs to phospholipids involves tightly regulated sequential steps. ATP, adenosine triphosphate; FADH2, reduced form of flavine adenine dinucleotide; NADH, reduced form of nicotinamide adenine dinucleotide; TCA, tricarboxylic acid cycle (Ashrafi, 2007, Imanikia and Stürzenbaum, 2013).

ATP, the energy supplier in cells, is produced when carbohydrates, amino acids and fats are broken down. For example, glycolytic enzymes break down carbohydrate macromolecules into pyruvate and then acetyl-CoA. Acetyl-CoA is then used to generate NADH and $FADH_2$ via the tricarboxylic acid cycle (TCA). NADH and $FADH_2$ are oxidized by phosphorilation to synthesize ATP (Figure 3.1). Stored triacylglycerides are transferred by lipolytic enzymes such as the hormone sensitive lipase, thereafter fatty acid components are turned into their respective acyl-CoA derivate by acyl-CoA synthases or ligases. β-oxidation enzymes in mitochondria or proxisomes are responsible for converting acyl-CoAs to acetyl-CoA (Ashrafi, 2007, Imanikia and Stürzenbaum, 2013).

Many conserved *C. elegans* pathways are involved in carbohydrate and lipid synthesis and break down, however it is the insulin-signaling pathway that has been studied in fine detail mainly due to its central role in the animal's life. The down-regulation of the insulin pathway results in an extension of the adult lifespan and mutants harboring the loss of function of *daf-2* (the insulin receptor) accumulate fat in a different manner. The metabolism of dauer larva and *daf-2* mutants is altered however the change in lipid distribution and the overall fat content is not the same as calorie restricted nematodes (Ashrafi, 2007, Braeckman et al., 2002, Burnell et al., 2005, Gems, 1999, Halaschek-Wiener et al., 2005, Larsen et al., 2006).

A *C. elegans* RNAi experiment incorporating essentially a genome-wide analysis pinpointed a comprehensive list of genes involved in fat metabolism when lipids were visualized by vital dye Nile Red staining. Upon silencing, 305 genes resulted in reduced body fat, 112 genes in an increased fat storage and 261 genes reduced body fat combined with larval arrest, sterility and embryonic lethality. These 261 genes were shown to be predominantly involved in essential pathways such as fat biosynthesis and metabolism (acetyl-CoA carboxylase, fatty acid synthase and the fatty acid desaturase *fat-7* (Ashrafi, 2007).

Overall, three conserved pathways are deemed to be important in the homeostatic control of energy levels, fat storage and breakdown (Long et al., 2002, McKay et al., 2003, Apfeld et al., 2004), namely the TOR, SREBP and C/EBP pathways (Table 1.2).

| Pathway | Abbreviation |
|---|---|
| **AMP-activated protein and target of rapamycin kinase** | TOR |
| **Sterol response element-binding protein** | SREBP |
| **CCAAT/enhancer binding protein transcription factor** | C/EBP |

**Table 1.2 Conserved *C. elegans* Pathways Involved in Lipid Storage and Metabolism** (Long et al., 2002, McKay et al., 2003, Apfeld et al., 2004, Imanikia and Stürzenbaum, 2013).

Irrespective of size, organisms have to transport lipids and fat droplets between cells and tissues. For example fatty acids are transported from intestinal cells into oocytes by means of a low-density lipoprotein (LDL) family receptor and receptor-mediated endocytosis. The core structures of this transport machinery are well conserved between the worm and vertebrates (Grant and Hirsh, 1999, Jones and Ashrafi, 2009, Imanikia and Stürzenbaum, 2013).

## 1.6 Lipid uptake and transport

Clearly, the mechanisms of fat transport are more complex in vertebrates than in worms, yet similarities can be found at the cellular level. Several *C. elegans* proteins share sequence homology to fatty acid translocases (FAT/CD36), fatty acid transport proteins (FATP), fatty acid binding proteins (FABPs), acylCoA binding proteins (ACBPs), carnitine-palmytoyl transferases (CPTs) and ATP-binding cassette (ABC) transporter proteins. The respective mammalian orthologs transport fatty acids between lipid bilayers and are responsible for the

intracellular shuttling of fatty acyl CoAs and a change in the expression can result in obesity or insulin resistance. Similarly, the knockdown (by RNAi) or the loss of function of particular members of the FABP, ACBP, CPT or ABC transporter family alters the fat level in the intestine of the worm (Ashrafi et al., 2003).

The mode of nutrient delivery from intestinal cells to the developing embryo via lipid uptake and transport systems is well characterized in *C. elegans*. A complex containing fats and cholesterol are stored in yolk proteins, the vitellogenins (these are functionally and structurally related to LDL-type proteins), which are then secreted into the pseudocoelom and sequentially absorbed, through receptor-mediated endocytosis, by the developing embryo (Fares and Grant, 2002).

## 1.7 Feeding behavior in nematodes

The *C. elegans* pharynx continuously pumps, even in the absence of food. However, the pumping rate is modulated by the availability of food (Avery and Horvitz, 1990). Nematodes sense food and their locomotion patterns change according to food availability and quality (Hills et al., 2004, Sawin et al., 2000). The pharyngeal pumping rate is controlled by serotonin. Indeed, exposing *C. elegans* to serotonin can influence the pumping pattern or imipramine (the serotonin uptake inhibitor) and mutations in the serotonergic receptors disable or reduce the stimulatory effects that lead to pumping (Hobson et al., 2006). Although the overlap between neuronally controlled feeding, behavioral food searching patterns and the central fat regulatory system is apparent, the precise

interconnections are at large unknown (Ashrafi, 2007, Imanikia and Stürzenbaum, 2013).

## 1.8 The link between lipid metabolism and diseases

The *C. elegans* insulin/insulin-like growth factor signaling (IIS) is interwoven with longevity, reproduction and the immune response. Interestingly, almost all intermediates of this pathway seem to have vertebrate orthologs. An imbalance of the IIS pathway (as induced by gene mutations) can lead to changes in growth and body size of the animals, but also the quantity and composition of lipids in fat reservoirs. This evidence aligns well with the observation that calorie restriction in mice and bariatric surgery in humans promotes health and longevity (Schlegel and Stainier, 2007). Furthermore, it is well known that obesity is the base for several metabolic diseases such as diabetes type II, which is due to an over-active adipose tissue, and as a response the level of fatty acids increases significantly in the liver. In order to maintain the lipid homeostasis, hepatic insulin resistance increases whereas hepatic insulin clearance decreases. The challenge is keeping blood sugar at normal levels, which is achieved by elevated pancreatic insulin secretion. Eventually, islet cells become over-worked and fail to function properly leading to hyperglycemia and in turn type II diabetes mellitus (Lawrence and Kopelman, 2004, Lewis et al., 2002).

Dyslipidemia can also arise from obesity, insulin resistance and hyper-insulinemia. As a result, hepatic triglyceride production increases because there are more free fatty acids available, and LDL particles become denser while HDL level decreases. Dyslipidemia is marked by an increase in plasma concentrations

of triglycerides, LDL cholesterol and in contrast decreased HDL cholesterol (Lemieux and Ashrafi, 2014).

Hypertension is another unwell-being associated with overweight and obesity. Despite the fact that the mechanism by which obesity leads to hypertension is not clear. It could be due to triggering sympathic nervous system, physical pressure being applied to kidneys, an influence on cytokine and an elevated reabsorption of sodium. There are other disorders that stem from overweight and obesity including sleep deprivation, fatty liver, cardiovascular and thrombolic malfunctions and cancer (Lawrence and Kopelman, 2004, Lemieux and Ashrafi, 2014).

## 1.9 The "fat and aging" connection

Lipids play a crucial role in the biology and physiology of metazoan animals (Hou and Taubert, 2012, Fahy et al., 2009, Subramaniam et al., 2011). Lipids such as diacylglycerol, fatty acids, phosphatidylinositols, sterols, ceramides and sphingolipids can directly contribute to signaling cascades (e.g. cell membrane receptor signaling or Nuclear Hormone Receptor (NHR signaling) or indirectly via the palmitoylation and prenylation of proteins. Interestingly, NHRs are not only affected by lipids but they can also modulate fat bodies in response to their downstream regulatory processes. Metazoan NHRs are evolutionarily conserved and play a crucial role in the physiology and development of the animal's life. The *C. elegans* genome accommodates 284 NHRs, which exceeds by far the number observed in the human genome. Surprisingly, most NHRs seem to originate from the same ancestral root and are related to HNF4, the Hepatocyte

Nuclear Receptor that is instrumental for pancreatic and liver development in mammals (Robinson-Rechavi et al., 2005, Maestro et al., 2007, Gonzalez, 2008). In flies, HNF4 is a fat transporter and is also involved in the β-oxidation of fatty acids (Palanker et al., 2009). It is conceivable that *C. elegans* fats bind to and/or regulate specific nematode NHRs, which are involved in a healthy lifespan.

The link between calorie/dietary restriction and the delay in cell decay was firstly observed in *Saccharomyces cerevisiae*, where CR was shown to extend the yeast's lifespan by activating a deacetylase. Furthermore, it has been shown that the deactivation of the insulin-like growth factor 1 (IGF-1) pathway extends the lifespan of nematodes, flies and mice (Cohen et al., 2004).

## 1.10 Drug entry route into *C. elegans*

It has been reported that drugs enter the nematode's body via three distinct paths: through the skin-like epidermis, via exposed sensory neuronal endings and by ingestion. Ingestion is a slow process consisting of several steps. The animal senses its food source (including the drug) via chemosensory neurons. Since the drug is typically applied via the food source (i.e., it is mixed with the *E. coli* OP50), therefore is taken up by the animal if it is not chemo-repulsive. Given that the neuromuscular contractions of the pharynx relies on satiety and food availability hence the pharyngeal muscle contractions enables the drug to enter the nematode's gut and is absorbed by intestinal cells. Similar to the human stomach, the nematodes' apical surface of intestinal cells is covered in microvilli, which ultimately increase the absorption area. Through the body cavity the drug is finally distributed to the target (Kaletta and Hengartner, 2006).

## 1.11 Aims

The use of natural herbal medication to combat overweight and obesity has gained momentum mainly due to the shortcomings of certified chemical anti-obesity drugs. However, no study has, to date, investigated the physiological and genomic effects of long-term treatment.

Appetite suppressants of natural origin have occupied a large share of the pharmaceutical industry. For example *Hoodia gordonii* a South African succulent with thirst-quenching and anorectic effects is one of the market leading anti-obesity supplements, yet very little post-application research has been conducted.

The initial aim of this project was to assess the phenotypic effects of *H. gordonii* extract exposure in the model organism *C. elegans*. Furthermore, by conducting a genome-wide microarray assay, it was anticipated to generate a list of influenced genes that are modulated upon exposure to different doses of *H. gordonii* extract, and classify them into groups based on the Gene Onthology (GO) terms. The main active compound isolated from *H. gordonii* extract is P57 (MacLean and Luo, 2004). Therefore, several experimental procedures were performed to assess the downstream effects of pure P57 treatment and to compare these results to the exposure to *H. gordonii* plant extract.

Since longevity and maintaining a healthy lipid profile have been considered to be highly important to mankind (Jones and Ashrafi, 2009), several research groups have been trying to find ways in order to revert aging and/or to tackle abnormal fat accumulation in the body. The ultimate goal of this study was to explore putative pathways linking fat metabolism and aging in response to herbal medication. With the established homology between nematodes and mammals, it

was deemed to be of interest to find such leads in a lower metazoan animal like nematodes and further apply it to higher organisms.

# Chapter Two

## *Materials & Methods*

# 2 Materials & Methods

## 2.1 Reagents and chemicals

Below is a list of materials that were used throughout the project (Table 2.1).

| Reagent | Supplier |
|---|---|
| **Sodium chloride, extra pure** | ACROS ORGANICS, Leicestershire, UK |
| **Sodium phosphate, dibasic, 99%** | ACROS ORGANICS, Leicestershire, UK |
| **Potassium phosphate, monobasic, 99%** | ACROS ORGANICS, Leicestershire, UK |
| **Calcium chloride dehydrate** | Fisher Scientific, Leicestershire, UK |
| **Magnesium sulfate** | SIGMA-ALDRICH, Dorset, UK |
| **LB Broth** | Sigma Life Science, Dorset, UK |
| **LB Agar** | Sigma Life Science, Dorset, UK |
| **Bacto™ Agar** | Becton, Dickinson & Company, Nottingham, UK |
| **Bacto™ Peptone** | Becton, Dickinson & Company, Nottingham, UK |
| **Potassium chloride** | Fisher Scientific, UK Limited, Leicestershire, UK |
| **Triton® X-100** | Fisher Scientific, New Jersey, USA |
| **Paraformaldehyde** | Fluka Chemika, Germany |
| **Tris, Ultra pure** | MP Biomedicals, UK |
| **Proteinase K** | Machenery-Nagel, GmbH & Co., Germany |
| **Phosphate Buffered Saline (Dulbecco A), pH=7.3 ± 0.2 at 25°C** | OXOID Limited, Hampshire, England |
| **2-Mercaptoethanol** | National Diagnostics, UK |
| **Glycerol for Molecular Biology** | Fisher Scientific Limited, Leicestershire, UK |
| **10X TAE (Tris-Acetate-EDTA)** | Fisher Bioreagents, Leicestershire, UK |

| | |
|---|---|
| **Ethidium Bromide solution** | Fisher Scientific, Leicestershire, UK |
| **Agarose electrophoresis grade** | MP Biomedicals Inc., France |
| ***Hoodia gordonii* capsules-500 mg** | RedRose Manufacturing company, UK |
| **Sudan Black B** | ACROS ORGANICS, Leicestershire, UK |
| **Oil Red O** | SIGMA-ALDRICH, Germany |
| **Water, sterile, Nuclease free** | Amresco-Inc., VWR Internationals, Lutterworth, UK |
| **Ethanol absolute** | VWR, BDH PROLABO, UK |
| **Methanol** | Fisher Scientific, Leicestershire, UK |
| **Acetone** | Fisher Scientific, Leicestershire, UK |
| **Chloroform** | Fisher Scientific, Leicestershire, UK |
| **Propan-2-ol** | Fisher Scientific, Leicestershire, UK |
| **Hydrochloric acid SG 1.18, 37%** | Fisher Scientific, Leicestershire, UK |
| **P57** | ChromaDex, Inc., LGC Standards, Middlesex, UK |
| **Custom designed primers** | Sigma Life Science, Dorset, UK |
| **Nystatin suspension** | Sigma Life Science, Dorset, UK |
| **Ampicillin sodium salt** | Sigma Life Science, Dorset, UK |
| **Cholesterol** | Sigma Life Science, Dorset, UK |
| **Gelatin from porcine skin, Type A** | Sigma Life Science, Dorset, UK |
| **Nile Red B3013** | SIGMA-ALDRICH, Dorset, UK |
| **PIPES sesquisodium salt, 97%** | ACROS ORGANICS, Leicestershire, UK |
| **Sodium hypochlorite solution** | SIGMA-ALDRICH, Dorset, UK |
| **Spermidine, 99%** | ACROS ORGANICS, Leicestershire, UK |
| **Spermine, 97%** | ACROS ORGANICS, Leicestershire, UK |
| **TRI Reagent** | Sigma Life Science, Dorset, UK |
| **IPTG, Dioxane-Free0** | Promega, Southampton, UK |
| **M-MLV Reverse Transcriptase** | Promega, Southampton, UK |
| **Deoxynucleotide Triphosphates (dNTPs)** | Promega, Southampton, UK |
| **GoTaq® Flexi DNA Polymerase** | Promega, Southampton, UK |

| | |
|---|---|
| ***E. coli* OP50** | Fire Lab, Cambridge, USA |
| **RNAi library** | Ahringer Library |
| **Real time PCR probes (Universal Probe Library)** | Roche Diagnostics Limited, West Sussex, UK |
| **100bp DNA ladder** | Promega, Southampton, UK |
| **1kb DNA ladder** | Promega, Southampton, UK |
| **Glass beads, acid-washed (425-600µm)** | Sigma Life Science, Dorset, UK |
| **Real time qPCR MasterMix** | Roche Diagnostics Limited, West Sussex, UK |
| **M-MLV Reverse Transcriptase** | Promega, Southampton, UK |
| **TWEEN-20** | CALBIOCHEM, Hertfordshire, UK |
| **$NPO_4$** | Sigma, Southampton, UK |

**Table 2.1 Reagents and chemicals with the supplier company names.**

## 2.2 Nematode strains

Mutant strains of *C. elegans* were supplied by the *Caenorhabditis* Genetics Center (CGC), University of Minnesota, and the Tokyo Women's Medical College (Table 2.2).

| Strain | Genotype | Allele | Location | Origin |
|---|---|---|---|---|
| N2 Bristol | wild-type | N/A | N/A | CGC |
| BX107 | *fat-5* | *tm420* | V | CGC |
| CE541 | *sbp-1* | *ep79* | III | CGC |
| DA531 | *eat-1* | *ad427* | IV | CGC |
| DA465 | *eat-2* | *ad465* | II | CGC |
| VC710 | cyp-35A2 | *gk317* | V | CGC |
| GR1307 | *daf-16* | *mgDf50* | I | CGC |
| FX01780 | *acl-12* | *tm1780* | X | TWMC |
| FAT-5;CYP-35A2 | *fat-5;cyp-35A2* | *tm420;gk317* | V | SRS Lab |

**Table 2.2 An overview of mutant strains used in this study.** Genotype, allele, origin and the chromosomal location of each strain are listed (where CGC is *Caenorhabditis* Genetics Center, TWMC is Tokyo Women's Medical College and SRS is Stephen Richard Stürzenbaum).

## 2.3 Methods

### 2.3.1 Maintenance

#### *2.3.1.1 NGM Agar preparations and* E. coli *OP50 bacterial food source*

*C. elegans* is kept under laboratory conditions on Nematode Growth Medium (NGM) agar plates seeded with an *E. coli* strain OP50. Different sizes of Petri dishes were used throughout the project based on the purpose of the assay, including 90 mm (Fisher Scientific, UK), 55 mm, 35 mm and 12-well plates (Greiner bio-one, Germany). Plate preparation and bacterial inoculation were all performed under aseptic conditions using a Laboratory Laminar Flow hood (FASTER, Italy). NGM agar plates were prepared in reference to the Brenner's method as follows: 17 grams of Bacto agar, 3 grams of Sodium chloride and 2.3 grams of Bacto peptone were measured and mixed together in 975 mL of $dH_2O$. The mixture was autoclaved in a Rapid Bench Autoclave (Prestige Medical, England). Once the mixture was cooled down to 60°C, 25 mL $KH_2PO_4$ (1M), 1 mL of $MgSO_4$ (1M), $CaCl_2$ (1M) and Cholesterol (5mg/mL in ethanol) were added (Brenner, 1974).

An aliquot (50 µL) of the anti-fungal Nystatin was supplemented to the agar mix and a volume of 20, 10, 5 and 4 mL of NGM agar was dispensed into 90, 55, 35 mm and 12-multiwell plates, respectively. Plates were left to dry for at least 24 hours at room temperature and stored for up to four weeks at 4°C. *E. coli* OP50 is a commonly used food source for nematode cultures as it is Uracil auxotroph derived from *E. coli* B (Brenner, 1974). Aseptically, a few colonies of OP50 were picked with a pipette tip and incubated in sterilized LB medium at 37°C in a shaking incubator (Stuart, Orbital incubator st1500, UK) for a period of 8 to 18 hours. An aliquot of 200 µL

OP50 was dispensed onto the agar of 90 mm plates, 100 µL OP50 on 55 mm dishes and 50 µL on 35 mm plates. Using a disposable sterilized spreader the bacterial droplet was evenly distributed on NGM agar plates. OP50 seeded plates were left at room temperature overnight allowing the bacteria to grow. Seeded plates can be kept at 4°C for about 2-3 weeks if not contaminated (Stiernagle, 2006).

#### *2.3.1.2 Age synchronization and decontamination of* C. elegans

All experiments were carried out using age-synchronized nematodes (i.e., L1 stage) generated by treating day-1 gravid nematodes with hypochlorite solution. The bleaching method also removes both bacterial and yeast contaminations. Bleaching kills all worms except the eggs that are protected by their shell. Once the NGM agar plates were full of gravid hermaphrodites, the plates were washed with M9 buffer solution (Table 2.3), the worms were collected into 15 mL centrifuge tubes (Alpha Laboratories, UK) and allowed to settle for approximately 10 minutes. Each strain of nematode was washed into a separate tube to minimize the chance of cross contamination. Animals were centrifuged at 2500X g for two minutes, and the supernatant was discarded leaving about 2 mL of the worm pellet. Worms were then re-suspended in 10 mL of freshly prepared bleaching solution (20% alkaline hypochlorite and 5% of 10M NaOH prepared in $dH_2O$). The mixture was shaken vigorously for 2.5 minutes and then immediately pelleted by centrifugation (1 minute, 2500X g). The supernatant was discarded leaving a 2 mL worm pellet and the tubes were filled up with M9 solution, mixed by inverting and centrifuged for

one minute. This washing step was repeated two more times. After the last wash, worm pellets were re-suspended in a total volume of 9 mL M9 buffer solution. Tubes containing worm debris and eggs were rotated (ROTATOR SB3, UK) overnight at room temperature to allow progenies to hatch (it takes about 9-11 hours for the larvae to hatch). During embryogenesis the embryos use the yolk as their food source to develop but once hatched, the L1 larvae arrest at L1 stage due to the lack of food, this results in the age synchronization (Stiernagle, 2006). The following day, tubes were centrifuged for one minute (2500X g) and the M9 was discarded leaving about 1 mL of the worm mixture. A 3-µL droplet of this mixture was dispensed on a glass slide to count the number of successfully hatched larvae and to determine the titer of worms per microliter. Based on the type of assay a maximum volume of 25 µL of worm mixture was transferred onto designated plates as higher volumes of worm mixture can dilute the drug/compound concentrations in exposure experiments.

| **M9 buffer solution** | **Amount needed** |
|---|---|
| **$KH_2PO_4$** | 3 g |
| **$Na_2PO_4$** | 6 g |
| **NaCl** | 5 g |
| **$dH_2O$** | Up to 1000 mL |

**Table 2.3 Composition of M9 Buffer solution (total volume of 1 Liter).** Once prepared, the solution was autoclaved and allowed to cool down overnight. Prior to use 1 mL of $MgSO_4$ was added (Brenner, 1974).

### *2.3.1.3 Freezing and long-term storage of* C. elegans *stocks*

One of the benefits of working with *C. elegans* as a model organism is that worms can be preserved in a glycerol-based freezing solution (Table 2.4) and stored indefinitely at -80°C. Age-synchronized L1 larva is the best stage for preparing frozen stocks as they suffer least from cell membrane changes during the gradual freeze. L1 hatchlings were re-suspended in 3 mL of fresh M9 solution, an equal volume of freezing solution was dispensed into the tube and the mixture was pipetted up and down for several times. Thereafter, 1 mL of the worm mixture was added into six Cryo-vials (Alpha Laboratories, UK), the tubes placed in a polystyrene box and transferred to an -80 freezer to allow the nematodes to cool down slowly and preserve the cells from bursting. After 48 hours one vial was defrosted and the success of freezing procedure was checked by plating the worms onto a seeded plate and subject to successful reproduction. The remaining vials were kept for long-term storage.

| Component | Amount |
|---|---|
| NaCl | 5.8 g |
| $KH_2PO_4$ (1 M) | 50 mL |
| Glycerol | 240 mL |
| $dH_2O$ | Up to 1000 mL |
| $MgSO_4$ (1M) | 30 µL added after autoclaving |

**Table 2.4 Freezing solution ingredients for a total volume of one Liter.** The autoclaved solution could be stored at room temperature for future use.

### 2.3.2 Total RNA extraction

A phenol-based total RNA extraction method modified from the Chomczynski and Sacchi's Single Step RNA Isolation (Chomczynski and Sacchi, 1987) was applied for different assays including, microarray and real-time quantitative PCR (qPCR). The original method was adjusted to improve the efficiency of RNA extraction in the nematodes.

L4 nematodes were washed off 90 mm NGM agar plates using the M9 buffer and collected into 15mL centrifuge tubes. Worms were centrifuged at low speed (700X g), the supernatant was discarded leaving about 2 mL of the worm mixture. Tubes were topped up with M9 buffer and spun again. The washing step was repeated three times, after the last wash, the supernatant was aspirated completely. Sterilized acid-washed glass beads were added to the worm pellet (1:1) with the addition of 500 µL Tri-Reagent. The worms/beads/Tri-Reagent mixture was vortexed (IKA VORTEX GENIUS 3, Germany) for four minutes. Glass beads help to break up the worms and released RNA from the cells while Tri-Reagent inhibited RNase activity. In the next step, the liquid phase was removed and transferred to a 1.5 mL micro-centrifuge tube and incubated for five minutes at room temperature. Chloroform (200 µL) was added to each tube and the mixture was shaken vigorously for 30 seconds. This was followed by a 12-minute incubation at room temperature. Afterwards, the mixture was centrifuged in a bench top cold centrifuge (Eppendorf 5415R, Germany) for 15 minutes at 12000X g. Three layers were formed, a clear color-less aqueous top phase containing the RNA, a thin white layer containing debris, protein and genomic DNA and a phenol phase. The clear phase was transferred into fresh 1.5 micro-centrifuge

tubes containing 500 µL 100% Propan-2-ol, the tube was inverted for 5-7 times and incubated at room temperature for 12 minutes then centrifuged for 10 minutes at 12000X g (4°C). The supernatant was discarded and the pellet was washed with 1 mL of 75% Ethanol, shaking for 30 seconds followed by a 5-minute spin at 12000X g (4°C). The supernatant was discarded and the RNA pellet was left to air-dry for approximately 15 minutes. The RNA sample was then dissolved in a minimum volume of 30 µL Nuclease-Free water. Then, 7 µL of each RNA sample was transferred to a new 0.5 mL micro-centrifuge tube and the remaining sample stored at -80°C until further use. 1.5 µL of the aliquot was used to analyze the quantity of RNA yield (NanoDrop spectrophotometer ND1000, Thermo Scientific) and the rest was run on a 1% TAE Agarose gel for quality checks.

### 2.3.3 Reverse Transcription using total RNA

After defrosting the RNA sample on ice, 1000 ng total RNA was used to synthesize complementary DNA (cDNA), which was then used for downstream applications. M-MLV Reverse Transcription (Moloney Murine Leukemia Virus, Promega), was used throughout the study as this reverse transcriptase has weaker RNase H activity compared to the Avian Myeloblastosis Virus (AMV) reverse transcriptase. Following ingredients were added to a 0.2 mL PCR micro-tube for a final volume of 20 µL (Table 2.5).

Deoxynucleotide Triphosphates dNTPs were made up from dATPs, dTTPs, dCTPs and dGTPs (each 100 mM, Promega) to reach a final concentration of 10 mM in Nuclease Free water.

| **Component** | **Volume** |
|---|---|
| RT Buffer X5 (250 mM Tris-HCl, 375 mM KCl, 15 mM $MgCl_2$) | 4 µL |
| dNTPs (10mM) | 2 µL |
| Oligo (dT) (5'-$(T)_{20}$VN-3') (100 pmole/µL) | 1 µL |
| M-MLV RT Enzyme (200 u/µL) | 1 µL |
| RNA template (1000 ng) | Maximum 12 µL |
| $dH_2O$ | Up to 20 µL |

**Table 2.5 Ingredients used to synthesize complementary DNA from total RNA isolated from nematodes.**

The mixture was incubated in a PCR machine (Applied Biosystems (AB) 2720 Thermal cycler) programmed to incubate the samples at 42°C for 60 minutes, followed by 10 minutes at 72°C. The resulting cDNA product was quantified using a NanoDrop spectrophotometer (ND1000, Thermo Scientific).

### 2.3.4 Quantitative real-time PCR (qPCR)

Throughout this project all gene expressions were normalized to *rla-1*, an invariant acidic ribosomal subunit protein-coding housekeeping gene (Qabazard et al., 2013, Pfaffl, 2001). Once the cDNAs were synthesized, samples were prepared using an adapted qPCR method (Table 2.6). Note that a maximum of 500 ng cDNA was used throughout all real-time PCR experiments in the project.

| Component | 1X Reaction Volume |
|---|---|
| ROX Mastermix | 12.5 µL |
| $dH_2O$ | 7.25 µL |
| cDNA template (1:10) | 3 µL |
| Forward Primer (0.4 µM) | 1 µL |
| Reverse Primer (0.4 µM) | 1 µL |
| Probe (0.2 µM) | 0.25 µL |

**Table 2.6 Components used for qPCR experiments adapted for *C. elegans* assays.** Amounts are for a total volume of 25 µL.

For every quantitative real-time PCR experiment 3-4 technical repeats were loaded on the designated 96-well qPCR plate. Relative gene expression of each sample was determined using three different biological replicates by means of a real-time PCR machine (ABI Prism 7000) (Figure 2.1). Data were primarily analyzed using the 7000-Sequence Detection Software (SDS) version 1.2.3.

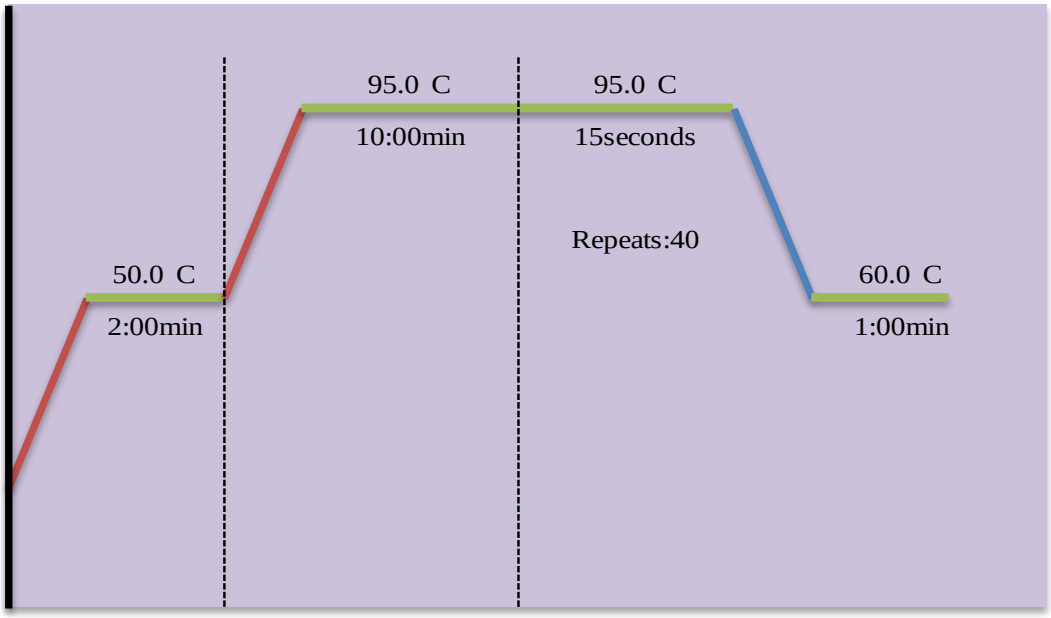


**Figure 2.1 An overview of the thermal cycler program adapted for *C. elegans* gene expression analyses.** The DNA was amplified for a total of 40 cycles.

### 2.3.5 Compound exposure

In general, three different methods of exposure can be utilized, NGM agar plate exposure, *E. coli* OP50 exposure or both NGM agar and *E. coli* OP50 exposures (dual treatment). This project applied two of the exposure approaches, for the *Hoodia gordonii* treatments, the plant extract was mixed with both the melted NGM agar prior to pouring plates and also was added to the *E. coli* OP50 bacteria. In P57 exposure assays, the compound was only added to the OP50 food source (to reduce the amount of material needed, thereby increasing the cost-efficiency).

### 2.3.6 Growth studies (surface area and length)

Nematodes grow from a hatchling into a fully developed adult within three days when maintained in optimal conditions at 20°C (Altun and Hall, 2009).The growth was followed for six days (144 hours post-hatch) and photos were taken every 24 hours for analyses. For each condition 20-30 worms were imaged and data was analysed using the Image Pro-Express software (Media Cybernetic, Buckinghamshire UK). Surface area and length of nematodes was traced by manually drawing lines around the worms via Image Pro-Express software.

### 2.3.7 Lipid staining methods

#### *2.3.7.1 Nile Red staining*

As nematodes are transparent, different techniques can be performed to visualize cellular compartments. In order to evaluate the lipid droplets in *C. elegans*, fixative and vital staining methods can be applied of which the easiest and most rapid is the vital dye Nile Red staining (Ashrafi, 2007). A stock solution of 0.5 mg/mL of Nile Red in acetone was prepared (6.2 µM) and stored at -20°C until further use. Prior to application, Nile Red was diluted 1:250 in *E. coli* OP50. NGM plates were inoculated with the mixture of the dye and OP50 and left at room temperature to grow overnight. The following day, age-matched L1 nematodes were transferred to plates and the dye entered the body of the worms via ingestion of *E. coli* OP50.

Worms were allowed to grow on Nile Red/OP50 plates for 72 hours and then individual nematodes were imaged using an inverted microscope (Nikon Eclipse TE2000-S, Japan) with attached camera. Exposure time and the magnification were consistent throughout imaging (20X magnification) and the background fluorescence was subtracted prior to any further analysis. Data were analyzed using the Image Pro-Express software (Media Cybernetics, Buckinghamshire UK) or ImageJ (ImageJ 1.46 r, NIH, USA).

#### *2.3.7.2 Oil Red O fixative staining method*

About 200-300 of day-1 adult nematodes (72 hours post hatch) were washed with PBS buffer, transferred into 1.5 mL micro-centrifuge tubes and allowed to settle by gravity for approximately 10 minutes. The supernatant was aspirated and worms were re-suspended and washed twice with PBS[5]. Animals were then suspended in 120 µL of PBS to which an equal volume of 2X MRWB[6] buffer (160 mM KCl, 40 mM NaCl, 14 mM $Na_2EDTA$, 1 mM spermidine-HCl, 30 mM NaPIPES pH=7.4, 0.4 mM spermine and 0.2% beta-mercaptoethanole in water) containing 2% PFA[7] were added. Nematode samples were gently rocked for 1 hour on a bench top horizontal rotator (Grant-bio, UK) at room temperature. Thereafter, worms were allowed to settle by gravity, the buffer was discarded and worms were re-suspended and washed with PBS buffer to remove PFA. Following the last wash, the entire

[5] Phosphate Buffered Saline
[6] Modified Ruvkun's Witches Brew
[7] Paraformaldehyde

supernatant was aspirated and the animals were suspended in 60% Propan-2-ol and incubated at room temperature for dehydration (O'Rourke et al., 2009).

Oil Red O solution was made by dissolving 0.5 g of Oil Red O powder in 100 mL Propan-2-ol as a stock solution. The stock solution was allowed to equilibrate for several days before use. A working solution was prepared by diluting the stock solution to 60% with water prior to application. Then the working solution was rocked for at least 1 hour, and filtered using a 0.2 micron sterilized filter. Thereafter, 1 mL was added to a 1.5 mL micro-tube containing the fixed worms and incubated at room temperature on a bench top rocker (Grant-bio, UK) overnight. The following day, the dye was removed after allowing the worms to settle. 200 µL PBS mixed with 0.01% TritonX-100 was added to the tubes and individual nematodes were mounted on 2% Agarose pads and visualized using an inverted microscope (Nikon Eclipse TE2000-S, Japan).

#### *2.3.7.3 Sudan Black fixative technique*

Sudan Black staining is a classic lipid visualization method however, the procedure is invasive as it requires the permeabilization of the cuticle in order for the dye to be able to reach the fat droplets. In order to allow the lipophilic dye, Sudan Black to penetrate through the cuticle, a previously established method of freeze/thaw was utilized adapted from Kimura et al. 1997. To enhance the cuticle permeability, the MRWB method was also applied (O'Rourke et al., 2009, Jones and Ashrafi, 2009,

Kimura et al., 1997). Stained nematodes were visualized using a standard microscope (Nikon, SMZ800).

### 2.3.8 Lifespan studies

Fully age-synchronized nematodes were plated at L1 stage on NGM agar plates using the standard techniques. After 48 hours, when the worms reached L4 stage, nematodes were distributed to four 90 mm plates with 100 worms on each plate. From day three onwards worms were transferred daily to separate adults from their progenies. Every day the total number of viable nematodes was counted and recorded during transfers. If a worm failed to respond to head pokes using a platinum wire it was scored as "dead". Occasionally, worms crawl underneath the agar and therefore are "lost", in such situations the worm was censored from the population. Daily transfers were continued until day 13, thereafter every second day. The experiment was terminated once the last worm died in order to record the maximum lifespan of the animals. Statistical analysis was performed using the Log-rank (Mantel-Cox) test scoring each dead animal as "1" and each lost nematode as "0" using the GraphPad Prism v5 software (GraphPad Software Inc., La Jolla USA). Kaplan-Meier survival curves were plotted that each presented the mean of three biologically independent experiments and all lifespan studies were performed at 20°C.

### 2.3.9 Brood Size assay

It is essential to fully synchronize nematodes before the brood size is quantified. L1 nematodes were allowed to grow to L4 stage on NGM plates seeded with OP50 (approximately 48 hours), and then worms were transferred to individual 12-well plates. Each *C. elegans* was allowed to grow and lay egg for a period of 24 hours. The next day each worm was transferred to a new well, these daily transfers were continued until the $6^{th}$ day when the individual parent nematode was removed. The number of hatchlings was counted two days after the transfer (L2/3 stage). Each experiment utilized 36 individual nematodes per condition and worms that failed to survive (when transferred to the new plate) were censored from the analysis. The total number of successful progenies and daily output of individual *C. elegans* were determined.

### 2.3.10 Neuromuscular assays (pharyngeal pumping and defecation)

Changes in the rate of pharyngeal pumping can be visualized because of the transparency feature of nematodes. Applying, high-resolution microscopy allows the quantification of these movements and recording the number of pumps per minute or 30 seconds. Interestingly, pharyngeal contraction can also serve as a biomarker in nematodes because the worm continuously consumes bacteria throughout its life, therefore if the animal displays no pharyngeal pumping movement then it is possible to conclude that the animal is dead.

Similar to other assays, age-matched L1 *C. elegans* were transferred to NGM agar plates seeded with *E. coli* OP50 and allowed to grow until the L4 stage when the worms were large enough to trace their pharyngeal contractions. Using a high magnifying microscope (Leica M205C-X16, Germany) set at 16X, pharyngeal muscle contractions were counted twice, each for 30 seconds and 30 nematodes per condition.

### 2.3.11 Microarray

#### *2.3.11.1 General overview*

In accordance to the Ambion MessageAmp™ Premier RNA Amplification Kit, the RNA quantity should be between 20-500 ng. In this specific study all RNA samples were normalized to 400 ng. The quantity was determined using a Nanodrop spectrophotometer (ND-1000, Thermo Scientific). In addition, further qualitative analysis was performed using a 2100 BioAnalyzer (Agilent Technologies Inc., UK). As stated in the Agilent RNA 6000 Nano Assay Protocol, an aliquot of 1 µL RNA sample was loaded onto the Bioanalyzer chip and RNA quality was assessed to assure both the purity and integrity of the extracted total RNA samples. Once the RNA quality was confirmed, the next steps were performed as indicated in the instructions of the Ambion MessageAmp™ Premier RNA Amplification Kit (sections 2.3.11.2 to 2.3.11.5).

#### *2.3.11.2 Reverse Transcription to synthesize first-strand cDNA*

Throughout the entire procedure all reagents were kept on ice unless otherwise stated. First-Strand Master Mix was prepared by combining the First Strand Buffer Mix with the First Strand Enzyme Mix (4:1 ratio). Once mixed and vortexed well, 5 µL aliquots were added to 5 µL of each RNA sample (400 ng diluted in Nuclease-Free water). The mixtures were then incubated at 42°C for two hours using a Thermal Cycler (MJ Research Tetrad PTC-225 Thermal Cycler).

#### *2.3.11.3 Second-strand cDNA synthesis*

The First-Strand cDNAs were transferred on ice and the Second-Strand cDNA synthesis immediately initiated by adding 13 µL of Nuclease-Free water, 5 µL of Second Strand Buffer Mix and 2 µL Second Strand Enzyme Mix to the 10 µL First-Strand cDNA, which was then transferred to the Thermal cycler for the Second-Strand cDNA synthesis (16°C for one hour, followed by 10 minutes incubation at 65°C). The Thermal cycler was pre-cooled to 16°C as higher temperature would compromise the aRNA yield.

#### *2.3.11.4 In vitro transcription to synthesize Biotin-modified aRNA*

Double-stranded cDNAs were kept on ice prior to the In Vitro Transcription of Biotin-modified aRNA (IVT). The T7 IVT master mix preparation was performed at room temperature. For a single reaction with the total volume of 30 µL, 4 µL Nuclease-Free water, 20 µL T7 Biotin IVT mix and 6 µL of T7 Enzyme mix were added together. The IVT mixture was combined with the 30 µL double-stranded

cDNA samples. These samples were incubated in a PCR machine for the IVT process for two hours at 40°C.

### *2.3.11.5 aRNA purification*

It was essential to remove any remaining salts, enzymes and unincorporated nucleotides after aRNA synthesis. The aRNA Elution Solution was preheated at 50-60°C for about 10 minutes. The aRNA Binding Mix was prepared at room temperature using 10 µL aRNA Binding Beads and 50 µL Binding Buffer Concentrate (60 µL for each reaction). Samples were distributed into wells of a U-Bottom Plate and 120 µL 100% Ethanol was added to each well and placed on a plate-shaker (Heidolph TITRAMAX 100, Germany) for 3 minutes (90 rpm). This allowed the aRNA samples to bind to the RNA Binding Beads. The plate was placed on a magnetic stand and beads were captured for approximately 5 minutes. In the following step, the liquid was aspirated and discarded carefully, and the plate was taken off the magnetic stand. 100 µL of aRNA Wash Solution (+ Ethanol) was added to the sample of each well and placed on the plate-shaker for one minute at 1200 rpm. Thereafter, the plate was moved back to the magnetic stand to capture the RNA Binding Beads. The supernatant was removed and the washing step was repeated. After the second wash and aspirating the supernatant, the plate was vigorously shaken (1350 rpm, three minutes) in order to evaporate any Ethanol residues.

Finally, purified aRNA samples were eluted in 50 μL of preheated (55°C) aRNA Elution Solution. The plate was shaken vigorously for another three minutes to disperse the Binding Beads completely before capturing them. The supernatant containing the eluted aRNA samples were transferred to a fresh nuclease-free multi-well plate. Once aRNA was purified, the yield was quantified spectrophotometrically (NanoDrop ND-1000). In addition, an aliquot was analyzed using the Agilent bioanalyzer (Agilent Technologies UK Limited). The expected aRNA profile contains different sizes varying from 250 to 5500 nucleotides, with the majority distributed between 850-1500 nucleotides.

#### *2.3.11.6 Fragmentation of Biotinylated aRNA for GeneChip® Arrays*

Prior to array hybridization, samples were fragmented using the Message Amp™ Premier Amplification Kit containing the 5X Array Fragmentation Buffer compatible with the Affymetric GeneChip® array platform. The fragmentation reaction is based on metal-induced hydrolysis for aRNA fragmentation, a process which consists of a 35-minute incubation at 94°C and then transferring onto ice. The fragmented aRNA samples were quantified using the Nanodrop spectrophotometer (ND-1000) and a 300 ng sample of each fragmented aRNA was analyzed on an Agilent bioanalyzer using an Agilent RNA 6000 Nano Kit. Immediately after this step, hybridization was initiated.

### *2.3.11.7 Hybridization*

The hybridization cocktail was prepared following the Affymetrix GeneChip Expression Analysis Technical Manual (www.affymetrix.com). Components and respective target concentrations for each sample reaction was modified for the Affymetrix GeneChip Arrays (Table 2.7).

| Component | Volume | Final concentration |
|---|---|---|
| Fragmented and labeled DNA target | 30 µL | ˜25 ng/µL |
| Control Oligonucleotide B2 (3 nM) | 5.03 µL | 50 pM |
| 20X Eukaryotic Hybridization controls (*bioB, bioC, bioD, cre*) | 14.96 µL | 1.5, 5, 25 and 100 pM respectively |
| 2X Hybridization mix | 149.6 µL | 1X |
| DMSO[8] | 20.94 µL | 7% |
| Nuclease-free water | 79.47 µL | |
| Total volume | 300 µL | |

**Table 2.7 Hybridization cocktail components and their volumes, extracted from the Affymetrix GeneChip Expression Analysis Technical Manual.**

[8] Dimethyl sulfoxide

The hybridization Cocktail was heated at 95°C for five minutes then cooled down to 45°C for another five minutes. A 270 µL aliquot of the Cocktail and 30 µL of the cRNA sample reactions was heat/denatured at 99°C for five minutes and then loaded into the septa of the probe array cartridge. Arrays were placed in a 45°C hybridization oven, and incubated (at 60 rpm) for 16 hours. The following day GeneChip ST Arrays were washed, stained and scanned to analyze the gene expression profile of *C. elegans* samples exposed to *H. gordonii* extract.

### 2.3.12 Crossing single knockout nematodes to create double mutants

Double Knockouts were created using a method adapted from David Fay's procedure described in Worm Methods (Fay, 2006). Before employing any experiments single mutants were backcrossed at least for three generation in order to remove any undesired lesions. This is due to the use of mutagens therefore the knockout strain contains many mutations as well as the deletion of interest. Briefly, the recovered mutant is backcrossed to the wild-type worms to clean up. During the process, nematodes are monitored by genotyping to ascertain that they carry the correct deletion and to isolate the homozygous counterparts. Genotyping was carried out by single worm lysis and nested PCRs (sections 2.3.13 and 2.3.14).

Once single mutants are backcrossed and homozygous of the desired gene, firstly, a population of male *C. elegans* was created from one of the mutant strains. As mentioned earlier the frequency of male *C. elegans* is about 0.2% and they are the

result of X chromosome nondisjunction. In order to increase the proportion of male worms, a standard method was tailored based on Michael Koelle's "heat shock" procedure. Six sets of five hermaphrodite worms (L4) stage were placed on separate 90 mm NGM agar plates seeded with *E. coli* OP50 and incubated at 30°C for 5.5, 6 and 6.5 hours. After each time period, two plates were removed and transferred to a 20°C incubator (SANYO MIR-253). Nematodes were allowed to reproduce and each plate was searched for male nematodes based on their distinct characteristics (size and the fan-shaped tail). Male nematodes were isolated for crossing with the second mutant strain. Five males of the first mutation and one L4 hermaphrodite of the second mutant were transferred to a multi-well plate (three replicates). The parent nematodes were removed from the wells after they laid few eggs. The $F_1$ generation was searched for the presence of male nematodes. Thereafter male worms were isolated and transferred to a new multi-well plate and crossed with L4 hermaphrodites of the first mutant strain (5:1 ratio). Once the hermaphrodites became gravid and laid eggs (approximately 20-30 eggs) the parent nematodes were removed from the plates. At least, 24 hermaphrodite trans-heterozygous worms were isolated onto separate wells on 12-well plates and allowed to reproduce. Progenies were screened using the genomic DNA (gDNA) extraction technique (section 2.3.13), followed by genomic nested PCR (section 2.3.14).

### 2.3.13 Genomic DNA isolation (for single worms)

Because worms have less than 1000 cells, it is easy to lyse and isolate the genomic DNA using lysis buffer and proteinase K. Lysis buffer (25 mM KCl, 25 mM Tris

PH=8.2, 1.25 mM $MgCl_2$, 0.1% (v/v) $NP_4O$, 0.1% (v/v) Tween-20 and 0.005% gelatin) was stored in aliquots at -20°C. Prior to the experiment, 25% (w/v) proteinase K (for degrading proteins) was added (for every 25 µL of lysis buffer 1.5 µL of proteinase K). With the aid of a pipette tip, 2.5 µL of this mixture was used to pick and transfer single nematodes, into a 0.2 mL PCR tube. The isolated nematode was stored at -80°C for at least 30 minutes. Immediately afterwards, the worm was lysed in a PCR machine (Applied Biosystems (AB) Thermal cycler) by incubating at 65°C for 60 minutes followed by 10 minutes at 95°C to deactivate the enzyme. The lysed mixture was then used as the template for a nested PCR. A nested PCR consists of two PCRs, an external and internal amplifications by which a first set of primers is designed to amplify a relatively large fragment of DNA. In the internal PCR, the external amplicon serves as the template and, the resultant PCR products were separated by electrophoresis.

### 2.3.14 Polymerase Chain Reaction (PCR)

The components for a standard PCR protocol were prepared, primers were designed to ideally have a 50%-GC content, an average length of 20bp and C or G anchoring 3′ end.

All sample preparations were performed on ice and the DNA amplified utilizing a PCR machine (Applied Biosystems (AB) Thermal cycler) programmed to take into account the melting point of each primer set and the amplicon size. Extension time is usually one minute per kilo-basepair and annealing temperature is based on the $T_m$ of the designed primer pairs.

| Component | Final concentration |
|---|---|
| 5X Green GoTaq® Flexi Buffer | 1X |
| Magnesium Chloride Solution 25 mM | 2.5 mM or 3.75 mM |
| Upstream primer (10 μM) | 0.1-1 μM |
| Downstream primer (10 μM) | 0.1-1 μM |
| dNTPs (10 mM) | 0.25 mM each dNTP |
| Template DNA | < 10 ng/μL |
| GoTaq® Polymerase (5 u/μL) | 1.25 units |
| Nuclease Free $H_2O$ | Up to 10 μL |

**Table 2.8 PCR components for a final volume of 10 μL are listed in accordance to the Promega GoTaq Flexi manual (Promega, 2013).**

### 2.3.15 Gene silencing via RNA interference (RNAi) by feeding

RNAi by feeding is a procedure in which bacteria expressing the dsRNA of the target gene replace the *E. coli* OP50 food source of the nematodes. In comparison to the other two methods (soaking and injecting), RNAi by feeding is the least expensive and the most rapid method however the efficiency of the knockdown can vary. The bacterial strain that is used for the feeding gene silencing is *E. coli* HT115, the host for the RNAi plasmids. The HT115 has an IPTG[9] inducible T7 polymerase

[9]Isopropyl β-D-1-thiogalactopyranoside

and the RNase III gene. Additionally, an Ampicillin resistance sequence is also engineered to minimize the chance of false positive results (Ahringer, 2006).

NGM agar was prepared as described previously (section 2.3.1.1) which was allowed to cool down to 48°C before adding IPTG and Ampicillin. A stock of 50 mg/mL Ampicillin was prepared in water and filter sterilized through a 0.2-micron filter. IPTG was dissolved in water for making a 1 Molar stock concentration. Final concentrations of Ampicillin and IPTG were targeted to be 100 μg/mL and 1 mM, respectively. Plates were stored up to four weeks at 4°C.

In the first step, specific bacterial strains were picked from the glycerol stock library and allowed to grow overnight in 5 mL LB medium containing 100 μg/mL Ampicillin using a shaking incubator (Stuart, Orbital incubator st1500, UK) set at 37°C.

IPTG/Amp NGM plates were seeded with the bacteria prior to the experiment and the bacteria were left to grow at room temperature overnight. Nematodes were age synchronized using the bleaching protocol and plated on the NGM agar seeded with *E. coli* OP50 for approximately 48 hours. Afterward, animals were transferred to IPTG/Amp plates. In every assay a control (HT115 bacteria carrying the empty vector) was set up along with the bacterial strain of the target gene. L4 nematodes were washed with M9 buffer three times and a small aliquot of 15 μl worm suspension was plated (about 200 nematodes per plate). Animals were allowed to grow for a period of 24 hours to lay about 20-30 eggs, and then parents were discarded from the plates. The eggs were left to hatch and grow ($F_1$), once $F_1$ worms

became gravid, they were age synchronized and prepared for targeted assays including exposures to different compounds (Ahringer, 2006).

### 2.3.16 Fluorescence Lifetime Imaging Microscopy technique (FLIM)

A novel technique was applied to compare lipid content in mutant strains as well as conditions with different concentrations of cholesterol supplementation. Firstly, nematodes were age matched using the previously described bleaching method (section 2.3.1.2). The staining procedure was performed as specified in section 2.3.7.1. In parallel non-stained wild-type worms were also used to normalize/subtract the auto-fluorescence. Lipid droplets were visualized at 72 hours post-hatch. Using a confocal microscopy, the dye-labeled areas were recognized throughout the body of animals. Furthermore, a section of "head to gut cells" was cropped and 50-70 slices were imaged to analyze red fluorescent lifetime.

# Chapter Three

## *Visualization of lipids in*

## C. elegans

# 3 Visualization of lipids in *C. elegans*

## 3.1 Introduction

As introduced in Chapter One, *C. elegans* are transparent, which allows the visualization of physiological changes within the intact body of the animals. Despite the lack of specific adipocytes, it is relatively easy to stain and explore lipid droplets in nematodes. One of the main shortcomings of lipid studies in *C. elegans* is the lack of a robust and reproducible staining approach, possibly due to the fact that the nature and biophysical properties of fat droplets are not fully understood (Zhang et al., 2010). Papers refer to lipid energy reservoirs as being gut granules, Lysosome-Related Organelles (LROs), vesicles distinctive from LROs or just lipid droplets (Zhang et al., 2010).

There are several vital and fixative-lipid staining procedures that have been in use for years with each approach having distinct advantages or disadvantages (Klapper et al., 2011, Ashrafi, 2007, Lemieux et al., 2011). For instance, traditionally Sudan Black has been used to visualize fat droplets in the body of fixed animals. However, this method requires an ethanol-based washing step that is characteristically prone to error (Klapper et al., 2011). It was also stated that the Sudan Black fixative method gives consistent results (Yen et al., 2010) where in other studies, including the work of O'Rourke et al., no reliable outcome was gathered as the staining was significantly variable (O'Rourke et al., 2009). More recently, dye-labeled applications such as BODIPY, or fixative Oil Red O procedures have been applied. Some studies have reported contradicting results about these visualization techniques, declaring that vital dye staining using BODIPY does not necessarily targets the lipid droplets (Yen et al., 2011, O'Rourke et al., 2009).

Most researchers use the Nile Red vital/fixative technique as it is relatively rapid and cheap but also provides high quality data (Lemieux et al., 2011, Mullaney and Ashrafi,

2009, Charan et al., 2011). However, over the last five years, the reliability of certain dye-labeled techniques has been challenged. Whilst interrogating the localization of Nile Red within the body of animals, O'Rourke et al. observed that Nile Red is quarantined in the lysosome-related organelles (LROs) as a foreign material rather than staining the lipid droplets (O'Rourke et al., 2009). It was proposed that Nile Red accumulates in LROs because it is administrated to the nematodes via the *E. coli* OP50 food source. Therefore, the dye is endocytosed and is later recycled in lysosomes. Zhang et al. reported that BODIPY dye is structurally different from Nile Red and is able to conjugate to fatty acid moieties. In mammals, both fatty acids and fatty acid moieties are secreted from lysosomes and constitute a part of the lipid droplet stores (Zhang et al., 2010). This report contradicts several other papers including the O'Rourke's study. In addition, LROs are not simple organelles with lysosomal activity, in *C. elegans* LROs are auto-fluorescent and store excess zinc (Soukas et al., 2013).

In brief, it is worth mentioning that the chemical properties of Nile Red and Oil Red O differ from each other, where Nile Red is composed of boiling a mixture of Nile Blue with sulphuric acid, upon which an iminium group is replaced by a carbonyl counterpart. An advantage of Nile Red is that, it does not fluoresce under polar conditions therefore making it a good candidate for the study of intracellular lipids. Oil Red O does not truly stain, as it cannot bind lipid compartments. The dye pigments the oil-soluable areas and therefore is a physical approach towards visualizing fat droplets (Greenspan et al., 1985, Fowler and Greenspan, 1985).

New advanced technologies have emerged including label-free methods such as Coherent Anti-stokes Raman Scattering (CARS) and Stimulated Raman Scattering (SRS) (Yen et al., 2011, Klapper et al., 2011). CARS microscopy offers an alternative approach in lipid studies where no pre/post-labeling is required. The CARS method allows a direct visualization of the droplets because of the abundance of $CH_2$ groups.

Both chemical and fluorescent analyses can be performed using CARS, but most importantly, it allows the differentiation between auto-fluorescence and neutral lipid particles. Analyzing saturated and unsaturated fatty acid content is also possible through CARS. Unlike many other methods of fluorescent microscopy CARS allows the separation of excitation beams therefore making it more convenient for excluding the linear scattering from a heterogenous biological tissue/sample. It is because the CARS signal is created at a shorter wavelength in comparison to the excitation wavelength and is usually in the visible spectrum where detectors of high quantum capability are available. As a result a CARS image is therefore produced via scanning the sample or the laser beams that allows the 3D sectioning ability as well as several other advantages. Apart from the label-free characteristic of CARS imaging, it is a non-invasive approach, which is essential for analysing small molecules such as lipids or drugs (as labelling such molecules may affect their molecular characteristics) (Cheng, 2007). Furthermore, CARS signals are generated as a quadratic signal due to the coherent addition whereas in SRS imaging the signal is linear. The coherent addition has a highly directional output hence making the signal collection easier. In addition, CARS signals benefit from high-speed vibrational imaging in comparison to Raman microscopy (Cheng, 2007). However, CARS is very labor and cost-intensive, therefore it has not replaced the rapid and inexpensive and dye-labeling methods (Yen et al., 2011). Moreover, CARS techniques cannot be very sensitive to detect weak Raman bands which is due to the nonresonant background properties which are mixed with the resonant signals (Cheng, 2007).

The BODIPY emission wavelength overlaps significantly with the auto-fluorescence signals whereas Nile Red staining has a distinctive emission from the auto-fluorescence and reaches a peak at around 650 nm, yet subject to the solvent in which Nile Red is dissolved (Figure 3.1).

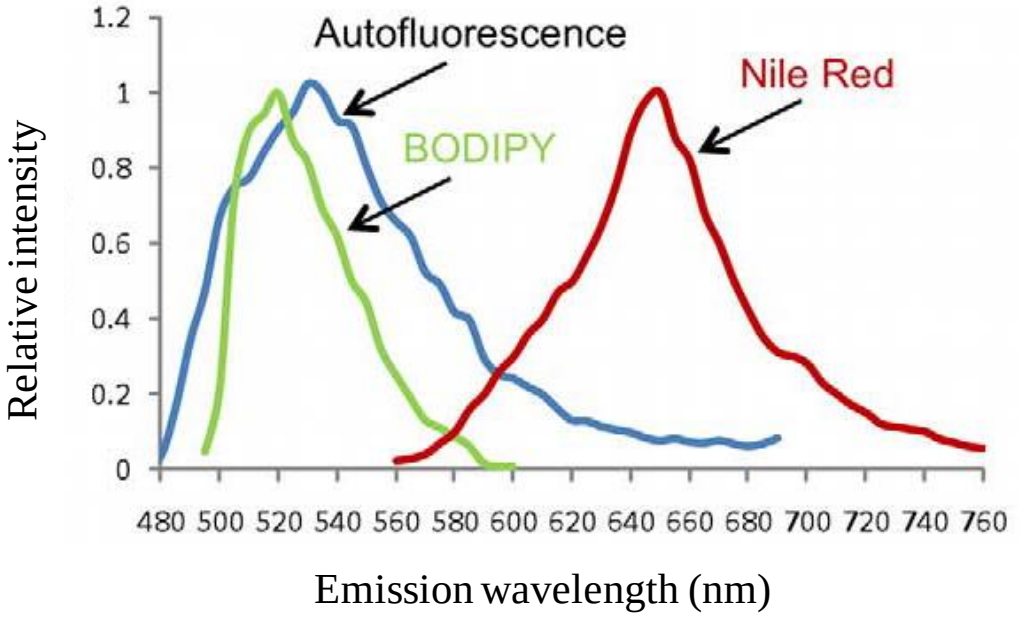


**Figure 3.1 Emission wavelengths of auto-fluorescence, BODIPY and Nile Red.** The overlap between the emission wavelength of BODIPY, Nile Red and the auto-fluorescence reveal that there is a noticeable overlap between BODIPY and auto-fluorescent signals that makes it difficult to distinguish between a real signal and the auto-fluorescence. However, Nile Red has a distinctive emission wavelength which, based on its solvent, varies between 620 to 670 nm (information adapted from (Yen et al., 2010)).

A recent review has summarized different techniques as well as the pros and cons of each method. As well as the dye-based methods, there are analytical approaches such as TLC [10] and GC/MS [11], by which the former allows quantifying triacylglycerols, phospoholipids and free fatty acids and the latter unravels the abundance of single fatty acid chains (Lemieux and Ashrafi, 2014).

Fluorescence Lifetime Imaging Microscopy (FLIM), a less invasive technique can be conducted to image cells and tissues to assess fluorescent intensity, lifetime,

[10] Thin Layer Chromatography
[11] Gas Chromatography- Mass Spectrometry

wavelength and/or polarization. In detail, FLIM analyzes the contrast of an image using spatial variations in fluorescence lifetime of the probe. The contrast is mainly affected by the environment surrounding the fluorophore rather than concentration or intensity. FLIM has been used in cell biology studies to assess protein-protein interactions through Föster Resonance Energy Transfer (FRET) once molecules are labeled with suitable dyes or fluorescent proteins (Levitt et al., 2009).

FLIM relies on the excitation of individual or multiple photons using a laser beam (such as Ti:Sapphire lasers or light-emitting diodes) (Oida et al., 1993). The laser is typically attached to a microscope capable of scanning several slices across the sample for confocal detection with a photomultiplier tube (PMT) linked to a time-resolved single photon counting card. The FLIM data cannot be presented immediately, nevertheless it is derived from a recorded fluorescence decay histogram, which is generated by means of separate software such as TRI2 (Li et al., 2010). Lifetime is measured pixel-by-pixel and an arbitrary color/contour map is created based on the spatial variations (Oida et al., 1993).

To date, FLIM has only been performed with single cells from different sources, rather than a whole organism, such as *C. elegans*. However there has been evidence of the use of FLIM in nematodes in a study by Kuo et al., in 2013, where FLIM was utilized to investigate lipid droplets by conjugated GFP[12] and FND[13]. It was proposed that a combination of FND-FLIM allows a better visualization of LDL-related lipids in worms. FND is a fluorescent nanomaterial, which is mainly carbon-based and contains a high-density ensemble with a nitrogen-vacancy color center that is negatively charged and act as the fluorophore in the diamond matrix. Despite which, no other groups have reported the use of FLIM in whole animal studies (Kuo et al., 2013). Our study still

[12] Green Fluorescent Protein
[13] Fluorescent NanoDiamond

takes the credit of the novelty of targetingthe debate of Nile Red in lipid studies in nematodes.

Measuring lipids is an essential step by which one could be able to analyze alteration in lipid profile of *C. elegans*. It is worth employing diverse approaches to quantify lipid droplets in worms and not to draw conclusion only by applying one certain technique. Not only the overall lipid content but also the distribution of fat must be taken into account when choosing a lipid visualization and/or quantification method. Two mutants with the same fat levels may have significantly different lipid distribution within tissues and cells resulting in the need for conducting a range of approaches to target lipid droplets in these strains (Lemieux and Ashrafi, 2014).

## 3.2 Aims

The work described in this chapter aims to explore approaches to visualize lipid droplet stores in the body of nematodes. It was deemed important to investigate the reliability and efficiency of different techniques and pinpoint a robust procedure that can be utilized in lipid metabolism research. By applying, vital dye Nile Red and LysoTracker® staining, fixative Nile Red, Oil Red O and Sudan Black staining in *C. elegans,* different approaches will be compared and contrasted.

Furthermore, the application of the FLIM technique was developed to localize the vital dye Nile Red in the body of worms to investigate whether the debate surrounding the efficiency and specificity of this staining procedure can be unraveled. In addition, because certain cells and structures auto-fluorescence, it was essential to distinguish the dye induced fluorescence from the auto-fluorescence. The FLIM analysis was made possible through collaboration with the Physics department at King's College London.

## 3.3 Results

### 3.3.1 Fixative approaches

#### *3.3.1.1 The Oil Red O staining technique fails to provide uniformly stained regions*

The cuticle of wild-type nematodes was permeabilized utilizing the MRWB[14]-fixation procedure (section 2.3.7.2) and stained with the non-fluorescent dye Oil Red O to explore lipid droplets. Once stained and visualized with an inverted microscope (Nikon Eclipse TE2000-S, Japan) the dye was not uniformly distributed in the body of the animals and some nematodes failed to take up the dye completely (Figure 3.2). Oil Red O appeared to mainly stain the eggs inside the body of the animals. Results were inconclusive, as the fixing step appeared to be not very successful despite applying the modified fixative technique (i.e., MRWB) described in O'Rourke et al., 2009 (Figure 3.2).

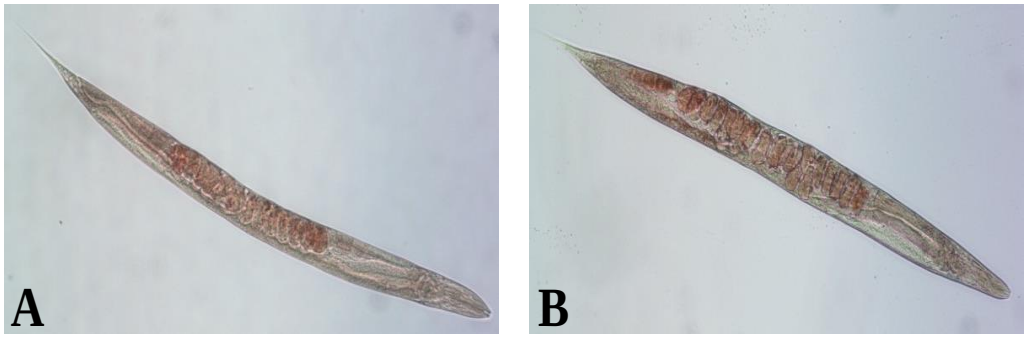


**Figure 3.2 Oil Red O stained wild-type nematodes.** When fat droplets were visualized using the fixative Oil Red O approach, the dye accommodated an orange/brown color in intestine, gonads and eggs. The intensity varied between individuals of the same strain (A and B), (nematodes were visualized using an inverted microscope Nikon Eclipse TE2000-S, Japan, magnification 20X).

[14] Modified Ruvkun's Witches Brew

#### *3.3.1.2 Fixative Nile Red staining of the nematodes is inconclusive*

Wild-type nematodes were fixed using the MRWB-fixing method to allow the dye to enter the cuticle. The body of fixed-worms became particularly fragile therefore at the time of picking and visualization the majority of samples burst. Only few worms could be further assessed under the microscope however, the dye was saturated in the body of nematodes, therefore no quantitative analyses could be performed (data not shown).

#### *3.3.1.3 Sudan Black staining does not target lipid droplets in nematodes*

Due to the on going debate about the variation in Sudan Black staining, the newly introduced MRWB fixation method was applied to permeabilize the cuticle of the nematodes, thus facilitating dye penetration. However, following the fixation step, the wild-type worms failed to take up the dye. Thereafter, the freeze-thaw fixative technique was performed, deemed to be a more invasive approach towards permeabilizing the cuticle, yet this also did not appear to be successful and aligns to observations made by others (Jones and Ashrafi, 2009).

### 3.3.2 Vital staining

#### *3.3.2.1 Nile Red staining targets intestinal vesicles in a reproducible manner*

To optimize the staining procedure, age-matched L1 wild-type nematodes were plated on Nile Red infused *E. coli* OP50 lawn and allowed to grow for 72 hours. At this point, individual nematodes were picked and mounted on 2% Agarose pads in a mixture of M9 buffer and Sodium Azide (a neurotoxin which paralyzes the animals, 50 mM) and photographed using UV-microscopy technique utilizing a Nikon Eclipse TE2000-S

microscope with an attached camera (Figure 3.3). The stained areas were similar to what had been reported in other studies (Ashrafi, 2007, Watts, 2009), Nile Red targeted the spherical compartments in the intestine that were believed to be lipid reservoirs (Ashrafi, 2007). The intensity of Nile Red stained areas was more pronounced in the first intestinal cells just after the pharynx of the nematodes (Figure 3.3). Due to the controversy surrounding the reliability of vital dye staining, it is important to define whether Nile Red distribution targets the lipid droplets or as O'Rourke et al. suggests the lysosome-related organelles (section 3.3.2.2).

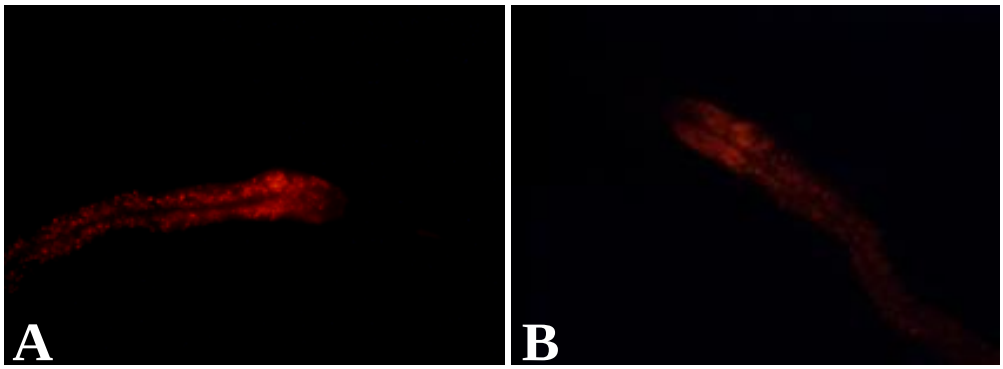


**Figure 3.3 Nile Red staining of wild-type nematodes**. Qualitative analyses of two nematodes of the same strain (N2), revealed a consistent dye distribution in the body of the nematodes (Panels A and B). The outcome confirmed the reliability of Nile Red over Oil Red O staining (X20).

### *3.3.2.2 LysoTracker® and Nile Red staining overlap, however not entirely*

The LysoTracker® (Invitrogen) staining utilized the same protocol as used for the vital dye Nile Red staining (section 2.3.7.1). To compare the staining patterns of LysoTracker® (final concentration of 1 μM) and Nile Red (final concentration 1 μM), three experimental conditions were tested on age-matched nematodes. The first group

of nematodes was stained exclusively with Nile Red, the second group was stained only with LysoTracker® Green and the third group was exposed to a mixture of Nile Red and LysoTracker® Green. Nematodes of each group were incubated for a period of 72 hours before further assessment. As the emission spectra are different for LysoTracker® (approximately 510 nm) and Nile Red (solvent-dependent, in acetone 620-650 nm), the staining pattern of each dye was followed using relevant filters on an inverted microscope. LysoTracker® is believed to specifically stain lysosomes and lysosome-related organelles (O'Rourke et al., 2009), therefore occurrence of any overlap could be studied. Although, co-stained areas were identified, large areas of red staining did not overlap with the lysosome-specific dye. Furthermore, the staining of the lysosome-related organelles was not as sharp and spherical in shape as the lipid droplets (Figure 3.4).

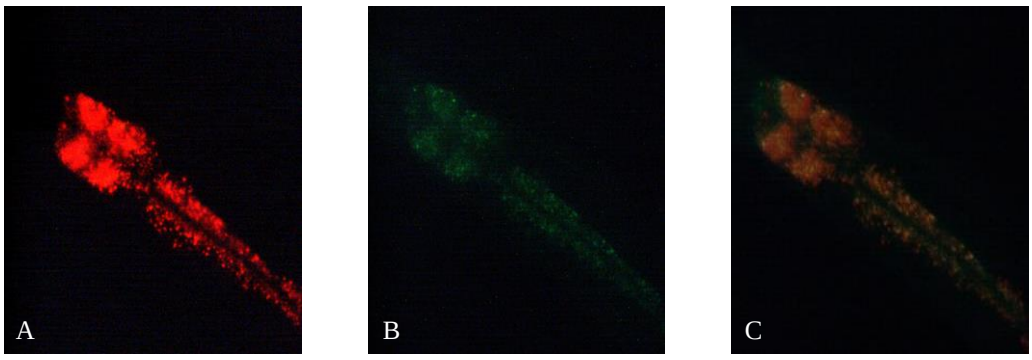


**Figure 3.4 Co-staining of Nile Red and LysoTracker® Green in a wild-type nematode, followed by the overlaid image.** (A) Nile Red stained compartments mainly stain spherical areas. (B) In comparison, LysoTracker® Green appeared to stain less defined areas with a significantly lower fluorescent intensity. (C) The yellow areas in the overlaid image indicated the overlap between Nile Red and LysoTracker® however, these regions were significantly less than the exclusively red stained areas. As the relative intensity of red fluorescence was more pronounced than yellow or green fluorescence, suggesting that Nile Red is at least to some degree valuable for a preliminarily analysis of lipid reservoirs in nematodes (Each image is magnified x20).

### 3.3.2.3 *Confocal microscopy and FLIM can be used to explore the nature of fat droplets*

Wild-type and lipid impaired mutant strains (*eat-1(ad427)* and *sbp-1(ep79)*) were assessed at 72 hours post-hatch. These animals were fed on a mixture of *E. coli* OP50/Nile Red (section 2.3.7.1). Thereafter, individual nematodes of each designated strain were placed on glass slides containing 40 µL of M9 and Sodium Azide 50mM (1:1) to visualize the lipid droplets.

Utilizing a confocal microscope the distribution of Nile Red dye within the intact body of wild-type nematodes was explored in fine details. Furthermore, the peak wavelength of several individual lipid droplets in wild-type was determined (Appendix One) to retain fluorescent signals (specific to Nile Red) which was distinct from the auto-fluorescence (Figures 3.5 and 3.6).

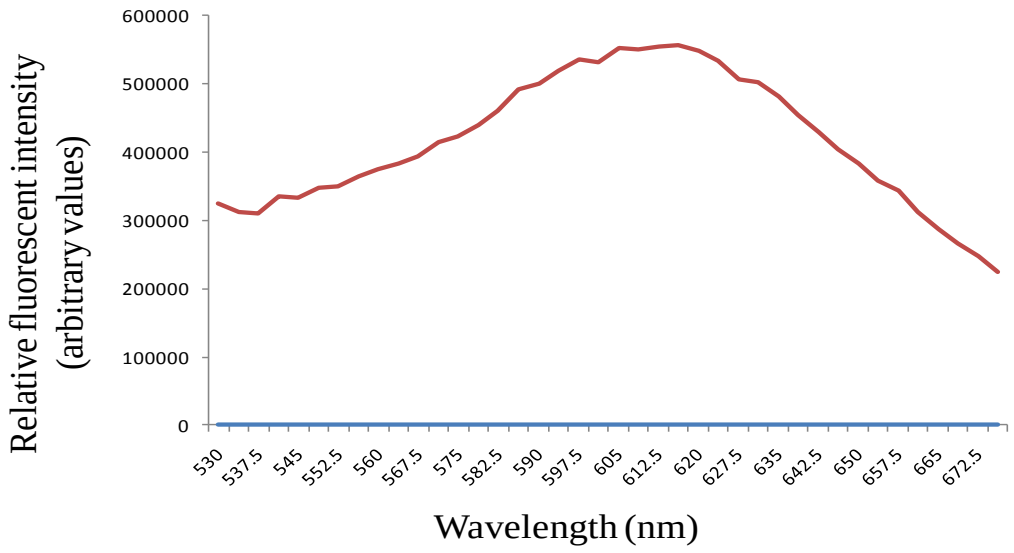


**Figure 3.5 Peak Nile Red fluorescent intensity versus the background auto-fluorescence.** The auto-fluorescence was measured in non-stained wild-type worms and the value was subtracted from the Nile Red fluorescent intensity in worms. The peak of red fluorescence was determined to be at approximately 620 nm in acetone as the dye solvent. The red line presents the average fluorescent intensity quantified in

30 droplets assessed in five individual nematodes and the blue line is the average from five randomly selected areas in five non-stained nematodes.

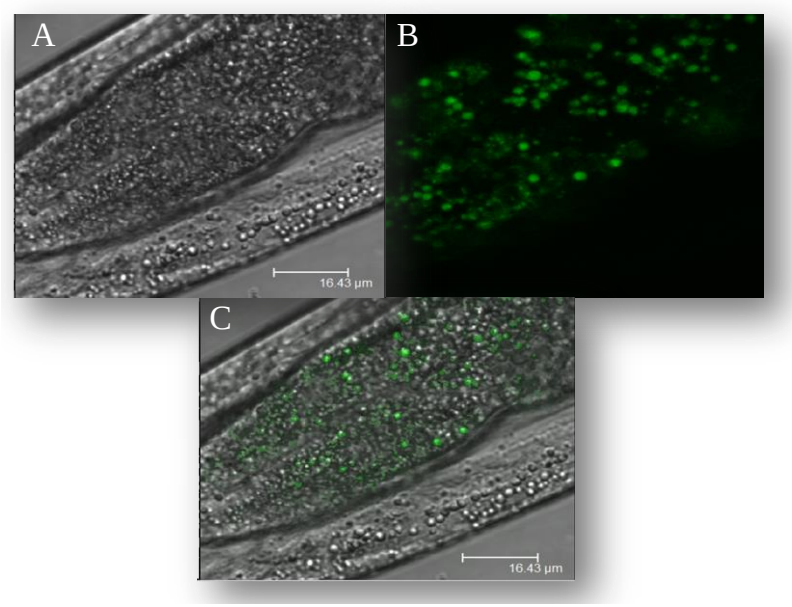


**Figure 3.6 An overlay of Nile Red stained droplets using a confocal microscope.** A selected wild-type nematode image (63X magnification) showing intestinal region (Panel A) and Nile Red stained intestinal droplets (Panel B) were visualized using a Leica TCS SP2 inverted laser scanning confocal microscope. The two images were overlaid (Panel C), thereby revealing the distribution of Nile Red profile droplets. Note that the confocal facility used the pseudo-coloring and demonstrated red as green. The stained droplets are Nile Red positive compartments that are a combination of lipid droplets as well as LROs. The nematode section demonstrates both intestinal and hypodermis droplets.

It was previously reported that *eat-1(ad427)* is characterized by a disrupted pharyngeal feeding behavior resulting in lipid deficiency (Avery, 1993, Lakowski and Hekimi, 1998), similar to *sbp-1(ep79),* which also has a disrupted lipid metabolism (Gonczy et al., 2000, Kamath et al., 2003, Ashrafi et al., 2003). Confocal images (256x256 pixels) as well as the lifetime fluorescent decay were explored using wild-type and lipid metabolism defective mutants (Figures 3.7 and 3.8).

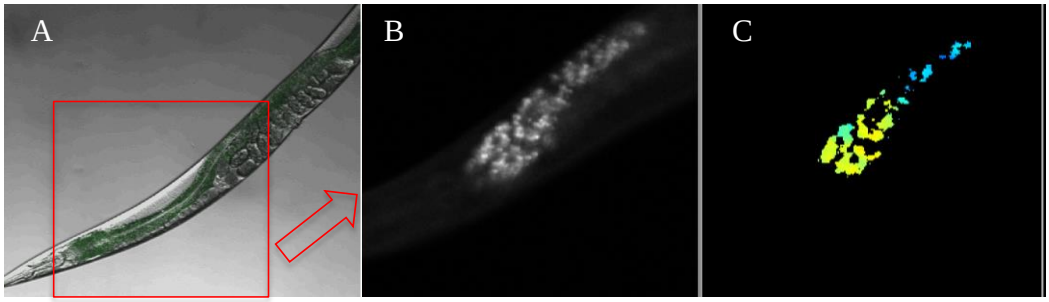


**Figure 3.7 A representative wild-type nematode analyzed by FLIM technology**. An overlay confocal image of a nematode (Panel A) showing the Nile Red stained regions. The lifetime of fluorescent intensity was determined (Panel B) the brighter the region is the more dye is concentrated perhaps correlating to a denser lipid content and a heat map was created (Panel C) showing the possible environment in which the dye resided. Yellow color means closer to acidic regions whereas blue corresponds to more neutral areas. The lifetime was fairly short, and not necessarily within the neutral spectrum. The FLIM image was recorded using a 470 nm pulsed picosecond diode laser (Hamamatsu PLP) with detection using a time correlated single photo counting (TCSPC) card from Becker & Hickl (SPC 830). Data were analyzed using the TRI2 software (Physics department, King's College London). Note that the red fluorescent was shown as pseudo-color green by the software.

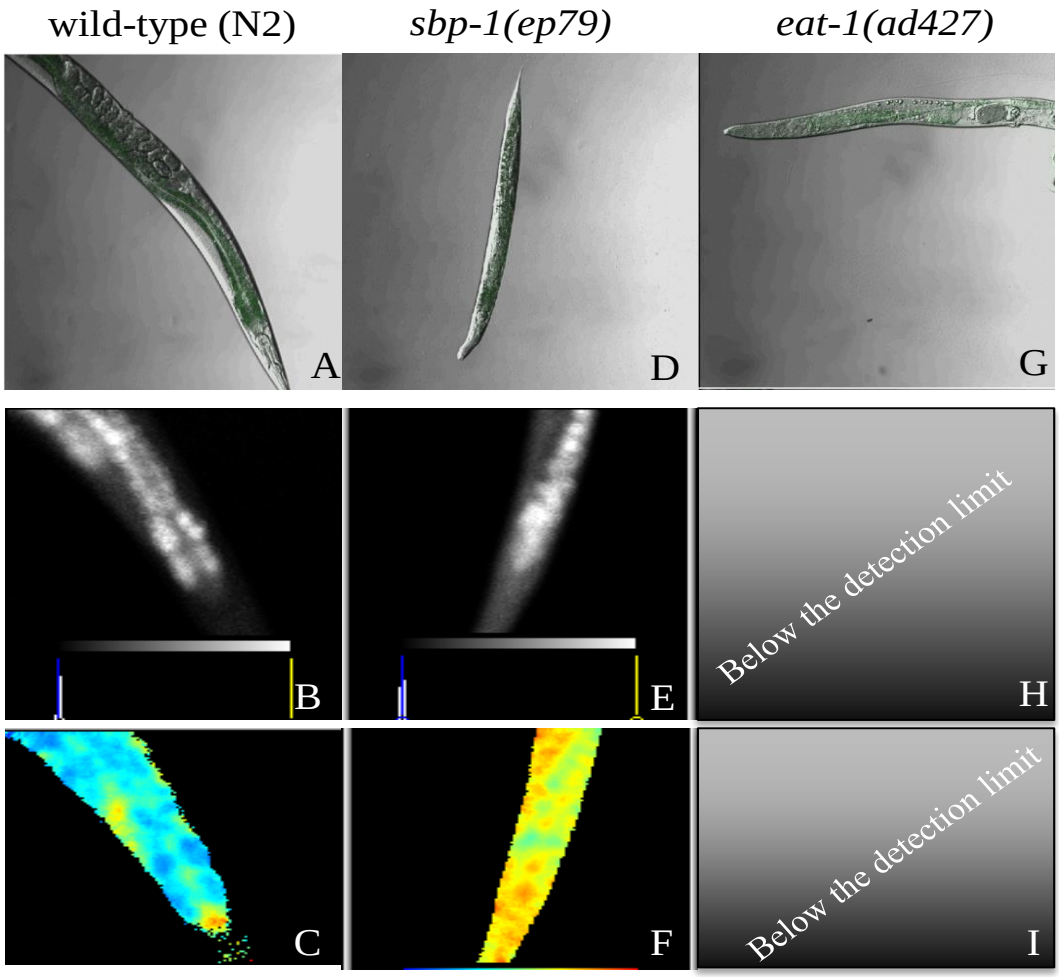


**Figure 3.8 Confocal microscopy and FLIM analyses on individual mutants, *sbp-1(ep79)* and *eat-1(ad427)* compared to wild-type.** Confocal images were generated for all three strains, Nile Red distribution in wild-type (A) followed by the FLIM visualization (B) and the heatmap, where the blue color indicated close to neutral areas. However, the fluorescent intensity was significantly lower in *sbp-1(ep79)* nematodes (D) therefore the lifetime pattern was different from the wild-type (E). The heatmap of *sbp-1(ep79)* was strikingly different from the wild-type indicating that fat profile had changed (Figure 3.7). Nile Red fluorescence was traceable in *eat-1(ad427)* (G) however, the software was not able to analyze/calculate the FLIM (H) and (I). The FLIM images were recorded using a 470 nm pulsed picosecond diode laser (Hamamatsu PLP) with detection using a time correlated single photo counting (TCSPC) card from Becker & Hickl (SPC 830). Data were analyzed using the TRI2 software (Physics department, King's College London). Images were magnified x20.

In addition, the effect of a change in the diet was assessed by feeding nematodes either a high level of cholesterol or starving them (Figure 3.9). This assessment confirmed that food availability affects the Nile Red staining patterns and intensities (Figure 3.9).

When treated with high doses of cholesterol, the relative red fluorescent intensity (defined as green by the confocal microscope) was higher than in nematodes fed the standard diet. In contrast, nematodes that had undergone food deprivation (the nematodes were transferred to NGM Agar plates without *E. coli* OP50 for a period of 24 hours) were characterized by significantly fewer Nile Red stained regions (Figure 3.9), which contained smaller positively stained droplets.

It was demonstrated through this study that the FLIM facility could be applied to whole organism studies such as *C. elegans*. Once the individual animals were mounted on glass slides and visualized using the confocal microscopy. The peak wavelength of red fluorescent stained regions was analyzed by ImageJ (version 1.46r, Wayne Rasband, NIH USA), which confirmed that the peak Nile Red intensity (dissolved in acetone or methanol) was at 620-660 nm regardless of the nematode strain (wild-type or mutant) or the diet of the animal (data not shown).

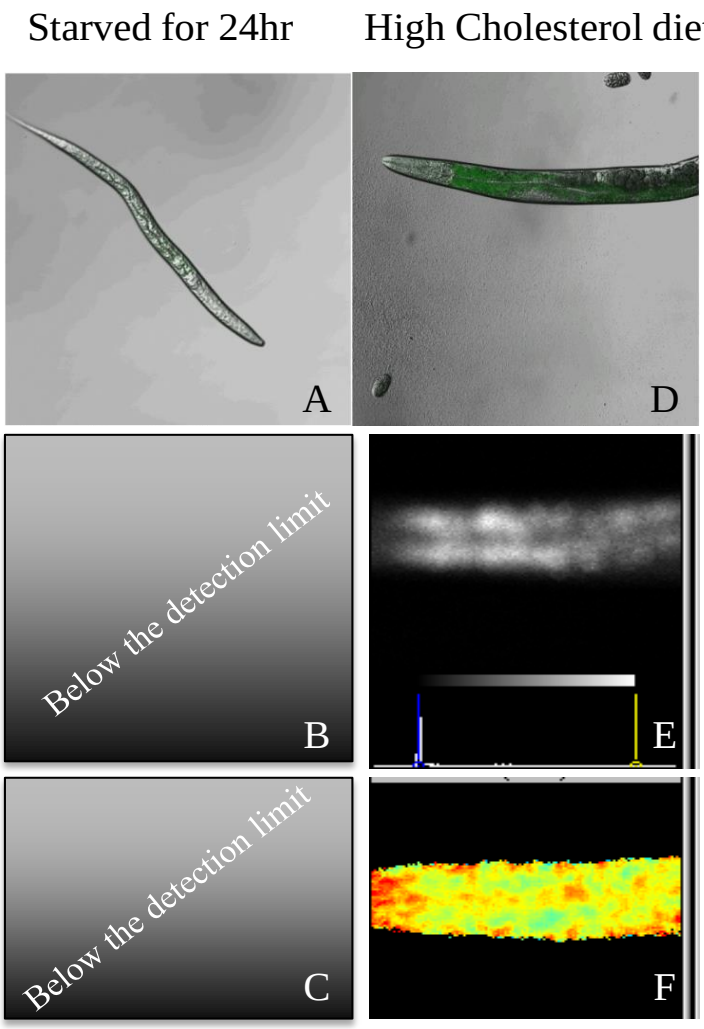


**Figure 3.9 Confocal and FLIM exploration of starved and high fat diet wild-type nematodes.** Panels A, B and C correspond to starved animals where Nile Red pattern is demonstrated (A) however, no detectable FLIM signal was generated perhaps as the technique was not optimized enough to trace the Nile Red labelled compartments (B) and (C). The high cholesterol fed wild-type worms had a high intensity of stained regions (D) followed by FLIM analysis (E) with significantly higher bright areas contributing to a higher lipid profile. The high-cholesterol diet appeared to produce a heatmap (F) which was similar to *sbp-1(ep79)* (Figure 3.8). The FLIM image was recorded using a 470 nm pulsed picosecond diode laser (Hamamatsu PLP) with detection using a time correlated single photo counting (TCSPC) card from Becker & Hickl (SPC 830). Data were analyzed using the TRI2 software (Physics department, King's College London). Nematodes were magnified x20.

Furthermore, the fluorescence decay time was determined by FLIM analyses which defined the decay time in wild-type nematodes and the two mutant strains *eat-1(ad427)* and *sbp-1(ep79)*. All three groups of nematodes the average fluorescence lifetime of Nile Red was approximately 3 nanoseconds, which is considered to be short and synonymous of an acidic environment (Levitt et al., 2009, Tregidgo et al., 2008). However, the Becker & Hickl SPCImage software could not pick up any variation in the fluorescence lifetime of Nile Red stained regions.

## 3.4 Discussion and Conclusions

A wide range of techniques are employed to explore lipid composition in *C. elegans* (Klapper et al., 2011) which can further unravel the functionality of fat-regulatory pathways in higher organisms. Having said that, nematodes lack dedicated adipocytes and only possess lipid droplets located in two major sites, namely the intestinal cells and the skin-like epidermal cells. Another limitation within the contest of exploring the fat regulatory system is that the dynamic nature of lipid droplets and the exact developmental stage of the nematode are crucial (Almeida Barros et al., 2011). This limitation stems from the rapid life cycle of the worms and therefore a highly sophisticated and tailored system is needed to define metabolic and physiological changes.

Vital and fixative staining methods have been in use to study lipid droplets in nematodes. To date, no single method has allowed the uniform and non-biased assessment of all types of fatty acids in nematodes. Throughout this chapter, several methods were utilized to investigate the storage and distribution of putative lipids in nematodes and in doing so address the ongoing debate whether Nile Red staining is a reliable and informative method. The debate was started in 2009 by O'Rourke et al. arguing that Nile Red is accumulated in lysosome-related organelles (LROs) rather than intestinal lipid droplets.

In the previous experiments, Sudan Black staining of the fat droplets was not successful, which was perhaps because of the insufficient permeability of the cuticle, a notion also reported by O'Rourke et al. in 2009, and others have reported that even extensive permeabilization does not help in improving the staining efficiency (Jones and Ashrafi, 2009, Mak, 2012, O'Rourke et al., 2009). Indeed, two fixative techniques (freeze-thaw and MRWB) both failed to permeabilize the cuticle sufficiently to allow Sudan Black

dye to enter the lipid droplets. The extensive permeabilization approach induced severe damage resulting in the bursting of the body.

O'Rourke and colleagues introduced the Oil Red O staining method in nematodes, and claimed the procedure to be superior, more reliable and comparable to advanced microscopy techniques, such as CARS. However, Oil Red O staining involves a considerably long fixation period to allow the penetration of the dye into the nematodes body. In this study, Oil Red O mainly stained the eggs inside the body of the nematodes (a phenomenon that was not reported by O'Rourke et al., although in published images it was clear that eggs were mainly stained) perhaps due to the high vitellogenin levels in the eggs, which might have high affinity for the fatty acids accumulated in eggs whereas Nile Red binds to diverse fatty acids. Alternatively, Oil Red O may also be a selective dye and stain only certain types of fatty acids. Further analyses are required to explore this in more detail. The fixative Nile Red staining procedure suggested in some studies (O'Rourke et al., 2009, Yen et al., 2010) returned only saturated levels of the dye in the body of fixed animals thus failing to generate any conclusive results. This inadequacy can possibly be addressed by a de-staining step or by lowering the concentration of the dye. The main disadvantage of the fixative method is that it requires an alcohol-based dehydration step, which can act as a solvent of certain types of fatty acids therefore changing the lipid profile within the nematode and generate misleading results.

The most widely utilized vital dye is Nile Red, which allows the rapid visualization of areas believed (by some) to be the major sites of lipid accumulation. In order to probe this controversy, two independent approaches were utilized, firstly by co-staining with LysoTracker® Green a lysosomes specific dye and secondly by applying FLIM, a method which to date has not been applied to whole animals. Despite the fact that Nile Red and LysoTracker® Green co-localized to some extent, distinct areas were

exclusively Nile Red positive. It is also worth mentioning that the lysosome-related organelles were shown to be less defined, whereas the Nile Red stained droplets were sharp and well defined. This can be potentially a preliminary identifier of lipid droplets in comparison to the LROs. On the other hand, since Nile Red is delivered to the nematodes via the food source (Nile Red treated *E. coli* OP50), the dye might be handled as a foreign particle (O'Rourke et al., 2009). Indeed, the long (72 hours) exposure time might affect the dye localization, if Nile Red is recognized as a xenobiotic and hence sent to LROs (Klapper et al., 2011). One way to overcome this may be by adapting a modified technique upon which the exposure is shortened, however issues surrounding the potential lack of signal intensity would need to be resolved.

The FLIM analysis was modified to explore the technique in multicellular organisms. Although the fluorescent decay time did not return conclusive results, the stained droplets could be studied in fine detail.

The Nile Red fluorescent peak is approximately at 620 nm when quantified in cell cultures (Greenspan et al., 1985, Levitt et al., 2009). In this study, a similar value was observed in Nile Red exposed worms regardless of genotype or change in diet. One advantage of applying FLIM to whole animal studies is that potential cell-cell interactions can be explored by following the dye location as well as measuring the fluorephore decay time, a phenomenon that cannot be investigated in cell culture approaches.

Through this study, it has become evident that applying FLIM to nematodes is a feasible technique and provides detailed information regarding the characteristics of lipid reservoirs, and the differentiation of signal from auto-fluorescence. Yet, FLIM is, at this stage, unable to provide in depth analysis about the nature of the Nile Red

stained compartments and whether the dye is residing in acidic, basic or neutral environments.

One of the main aims of this study was to assess the reliability of Nile Red staining, given that O'Rourke and colleagues challenge but Ashrafi et al. on the other hand strongly support the method (Yen et al., 2010, Ashrafi, 2007, O'Rourke et al., 2009). The modified FLIM methodology tailored to work in nematodes revealed that the fluorescent decay of Nile Red dye does not differ between mutant strains. The quantified lifetime was consistently short, suggesting that the environment surrounding the dye is slightly acidic and certainly not neutral, an outcome which could explain why Nile Red and LysoTracker® co-localize. This finding provides further support that LROs contain lipids and are not exclusively a site for metabolizing toxic materials. However, as FLIM was not fully optimized, it was not possible to define the exact location of the dye within the body of the nematodes based on the pH of the environment surrounding the dye. Several aspects of lipid droplets can be studied through confocal and FLIM analyses in worms and although the technique it is labor-intensive, FLIM is less complicated than CARS.

In conclusion, the investigation described in this chapter suggests that the vital dye Nile Red can still be utilized as a preliminarily platform for investigating differences in staining intensities of intestinal droplets, which are likely to be a component of the lipid pathway.

# Chapter Four

## *Life history traits following*

## Hoodia gordonii *extract treatment*

# 4 Life history traits following *Hoodia gordonii* extract treatment

## 4.1 Introduction

### *4.1.1 Hoodia gordonii* (MASSON) Sweet ex Decne, a South African plant

In recent years herbal medication has gained popularity as Western manufactured drugs have struggled to fulfill the primary aim of tackling certain diseases. As a result, pharmaceutical industry has invested resources to explore whether herbal remedies can be exploited in order to meet the public demand. Unfortunately, there is not sufficient knowledge on the long-term effects and post-consumption studies have failed to provide detailed information about drug delivery and absorption. It has been reported that herbal medication may modulate the expression of specific genes or alter the activity of certain proteins, however the underlying mechanisms remain elusive (Devinsky et al., 2005). *Hoodia gordonii* is a South African succulent plant that has been in use for hundreds of years by Xhomani bushmen. It is believed that *H. gordonii* extract has both thirst and appetite quenching qualities. When re-discovered by the scientific world and pharmaceutical companies, *H. gordonii* became popular in the nutraceutical market. Although *H. gordonii* and similar herbal medicines are globally marketed, their effectiveness and safety have not been fully determined (Dall'Acqua and Innocenti, 2007). Despite this, at least 20 international patent applications/registrations have been filed regarding predicted anorectic, anti-diabetic and gastro-intestinal effects of *H. gordonii* extract (Tucci, 2010). It was Van Heerden who further investigated the chemical properties and appetite-suppressant characteristics of *H. gordonii* extract (Van Heerden, 2008). Analysis of the chemical properties of the extract has revealed a family of secondary metabolites, namely

pregnane glycosides that contain 6-deoxy- and 2,6-dideoxy sugars (Steyn et al., 1989, Deng et al., 2005). Phytochemical analyses on *H. gordonii* extract have also confirmed the presence of these metabolites. Van Heerden and colleagues discovered appetite suppressant activity of *H. gordonii* extracts and that the appetite suppressing effect was linked to the presence of a tryglycoside (12β-triglyoxy-14β-hydroxypregn-5-en-20-one) in the plant (Van Heerden et al., 2002, Van Heerden et al., 2007). This component is also referred to as P57A53 or P57. Chapter Four focuses on phenotypic and molecular genetic effects of *C. elegans* exposed to *H. gordonii* extract.

## 4.2 Aims

This part of the study explores the potential anorectic properties of the commercially marketed *H. gordonii* extract using the nematode *C. elegans* as a model organism. Given that nematodes and mammalian organisms share many of the fundamental pathways of life implies that, results of *H. gordonii* extract treatment in the *C. elegans* might offer valuable cues that can be extrapolated to higher organisms. This chapter firstly investigates the effects of *H. gordonii* extract exposure on *E. coli* OP50, the standard food source for the worms, as a part of a pilot study. Thereafter life history traits (such as pharyngeal pumping/defecation, developmental changes, reproduction and lifespan) are studied in nematodes treated with different concentrations of *H. gordonii* extract. Finally, upon performing a genome-wide microarray assay, the transcriptional response of genes involved in *H. gordonii* extract treatment will be identified and investigated further. Selected genes are then classified based on the GO term to unravel the metabolic pathways linked to the extract exposure.

## 4.3 Results

### 4.3.1 Growth of *E. coli* OP50 is affected by the supplementation of *H. gordonii* extract

Food or other compounds enter the nematode *C. elegans* via different paths including ingestion, absorption through the skin-like cuticle and sensory cilia (Kaletta and Hengartner, 2006). The contents of *H. gordonii* capsules were soluble in water and the solution was freshly prepared prior to each assay. Each capsule was stated (by RedRose, the manufacturing company) to contain dried extract equivalent to10,000 mg of *H. gordonii* plant. For each assay the contents of one capsule was dissolved in 5 mL of filter-sterilized dd$H_2O$ resulting in a nominal stock solution equivalent to 2,000 mg/mL plant. The solution was then vortexed for approximately 10 minutes and passed through a 0.2-micron filter to obtain a homogenous solution.

To study whether the addition of *H. gordonii* extract affects the growth of the bacterial food source, different concentrations of *H. gordonii* extract (equivalent to 100, 10 and 1 mg/mL) were added to a starter culture of *E. coli* OP50. Data collected from the bacterial growth, using the OD measurements at 600 nm, revealed that the *H. gordonii* extract induces the growth characteristics of *E. coli* OP50 (data not shown). A richer and denser bacterial culture may potentially influence the life history traits as well as metabolic and energy pathways in nematodes. Initially these concentrations of 0, 1, 10 and 100 mg/mL *H. gordonii* extract were utilized to explore the growth parameters of the nematodes and if the extract exert any lethal or growth inducing effect on the worms.

### 4.3.2 The development of wild-type *C. elegans* is altered by exposure to *H. gordonii* extract

Having established that the addition of *H. gordonii* extract affects the growth of *E. coli* OP50, it was deemed important to also explore the potential effect on key lifecycle indices of the extract exposure in nematodes. Age-synchronized L1 wild-type (N2, Bristol) nematodes were exposed to *H. gordonii* extract (0, 1 and 10 mg/mL) and development was followed until 120 hours post-hatch. Changes in the growth parameters of length and surface area were assessed at five time points (every 24 hours), commencing at 48 hours post-hatch. Under control conditions, body volume plateaued within 72 hours post-hatch, thereafter only slightly increasing as a result of aging (Figure 4.1 Panel A). When treated with *H. gordonii* extract, a significant dose-dependent reduction in the surface area was observed. Following the exposure to 10 mg/mL of *H. gordonii* extract, the surface area growth of wild-type was marginally delayed hence reached the final volume at 96 hours post-hatch rather than 72 hours. This trend was not observed with the lower dose of *H. gordonii* extract treatment (Figure 4.1, Panel A).

Body length was also influenced significantly when treated with different concentrations of the *H. gordonii* extract (Figure 4.1 Panel B). During different larval stages, wild-type nematodes expand in their length and reach an approximate length of 1 mm. In this study, wild-type worms grew to a maximum length of slightly over 1000 microns. The, addition of the *H. gordonii* extract attenuated the length of animals treated with 1 and 10 mg/mL of the plant extract (Figure 4.1 Panel B).

It was noted that some 25% of *C. elegans* exposed to 10 mg/mL of the extract failed to survive for 120 hours post-hatch, therefore they were excluded from further investigations. A two-way ANOVA statistical analysis followed by a *post hoc* (Bonferroni multiple comparisons) test suggested that treatment with *H. gordonii*

extract significantly affected the overall volume of the animals with the highest significance being observed at an exposure to 10 mg/mL ($p$ *<0.0001*). Further information is provided in Appendix Two.

Because of the influence of high concentrations of *H. gordonii* extract on the growth parameters of the nematodes, a maximum of 0.5 mg/mL of the extract was administrated to the worms for further studies.

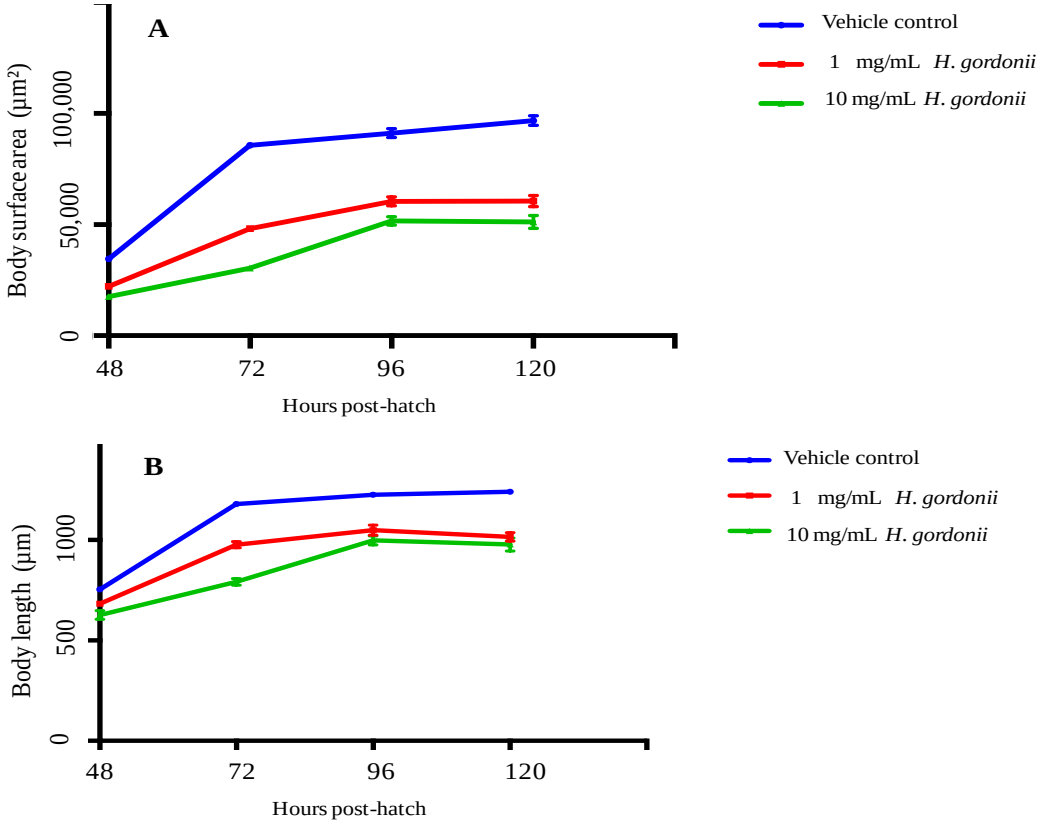


**Figure 4.1 Developmental changes in wild-type nematodes exposed to *H. gordonii* extract (0, 1 and 10 mg/mL).** (A) The body surface area changes from L4 stage (48hrs post-hatch) showed a significant reduction in 1 and 10 mg/mL exposures (**** $p$ *<0.0001*). Moreover, 10 mg/mL of the extract delayed the growth of nematodes marginally. (B) The body length changes upon treatment with *H. gordonii* extract were determined, a significant reduction was observed in the length of the worms (**** $p$ *<0.0001*) in 1 and 10 mg/mL exposures. Each data point in Panels A and B represents the average value of either length or surface area parameter from 20 individual *C. elegans* ± standard error of the mean (SEM). Statistical analyses were performed using a two-way ANOVA followed by a Bonferroni multiple comparisons test.

### 4.3.3 Pharyngeal pumping is decreased upon exposure to the plant extract

In rodents treatment with *H. gordonii* extract resulted in weight-loss, mainly by suppressing the appetite through hypothalamic pathways (MacLean and Luo, 2004). It is known that nematodes consume food continuously throughout their lives. Indeed, environmental and physiological changes influence the rate of pharyngeal pumping which is tightly regulated by a mechanism, that shares a significant similarity with the mammalian serotonin and TGF-β pathways (Srinivasan et al., 2008).

Toxic and/or lethal concentrations of *H. gordonii* extract were excluded from further studies (as explained in section 4.3.1), therefore applying a maximum concentration of 0.5 mg/mL the extract throughout the present project. In order to explore the effect of *H. gordonii* extract on the feeding rate of the wild-type nematodes, a pharyngeal pumping assay was performed on untreated and *H. gordonii* extract-treated worms. Pharyngeal pumping rate typically increases in wild-type nematodes during development, then reaches a peak at day-1 of adulthood (72 hours post-hatch) and subsequently declines during the aging process. The control group of the nematodes as well as the *H. gordonii* extract exposed groups followed this trend regardless of the exposure dose, where the peak of pharyngeal pumping was determined to be at 72 hours post-hatch. However, an overall 81% reduction in the pharyngeal muscle contractions was observed (at 48 hours post-hatch) in animals exposed to 0.5 mg/mL *H. gordonii* extract. Doses of 0.1 and 0.01 mg/mL extract resulted in nematodes exhibiting a 73% and 10% decrease in pharyngeal pumps, respectively. The reduction in the number of pharyngeal muscle concentrations was therefore most pronounced at an exposure to the highest concentration of *H. gordonii* extract. Nevertheless, the animals appeared to recover from the reduction in the feeding rate after 72 hours post-hatch (Figure 4.2). Overall, *H. gordonii* extract had a dose-dependent influence on the pharyngeal pumping rate.

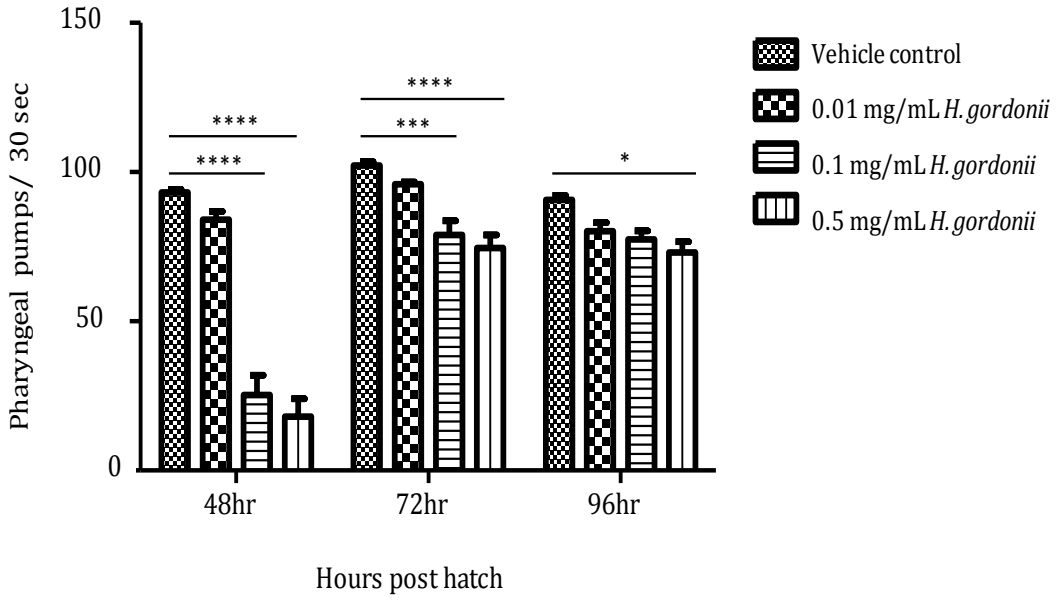


**Figure 4.2 Neuromuscular behavior, pharyngeal pumping assessment in the wild-type nematodes upon *H. gordonii* extract-treatment.** The pharyngeal pumping rate peaks at 72 hours post-hatch, after which the animal starts aging and the pumping frequency, declines. The pharyngeal pumping rate decreased in nematodes exposed to *H. gordonii* extract (0.01, 0.1 and 0.5 mg/mL). Each column represents the average pumping rate of 30 nematodes performed in three independent biological populations ± the standard error of the mean (SEM), two-way ANOVA (* $p < 0.05$, *** $p < 0.001$, **** $p < 0.0001$).

### 4.3.4 The defecation rate is not affected by *H. gordonii* extract-treatment

Defecation intervals in nematodes are activated via sequential muscular contractions (Croll and Smith, 1978, Riddle et al., 1997). In the presence of food, the animal excretes approximately every 45 seconds, this process is under neuronal control, is temperature independent but may vary based on the food availability, the feeding behavior or other environmental changes. Moreover, there are several mutations that are known to result in a "constipated" phenotype such as *aex-1(sa9)* (Thomas, 1990, Jorgensen et al., 1995).

Given the observed alteration in pharyngeal pumping, it was deemed to be important to determine the defecation rate in response to *H. gordonii* extract-exposure in worms. In

this present study, untreated wild-type nematodes defecated every 41 seconds at L4 stage with a progressive extension in the intervals as worms aged (Figure 4.3).

When compared with the *H. gordonii* extract-exposed animals, defecation intervals were marginally extended at 48 hours post-hatch, however this change was statistically insignificant when analyzed by two-way ANOVA followed by Bonferroni multiple comparisons *post hoc* test.

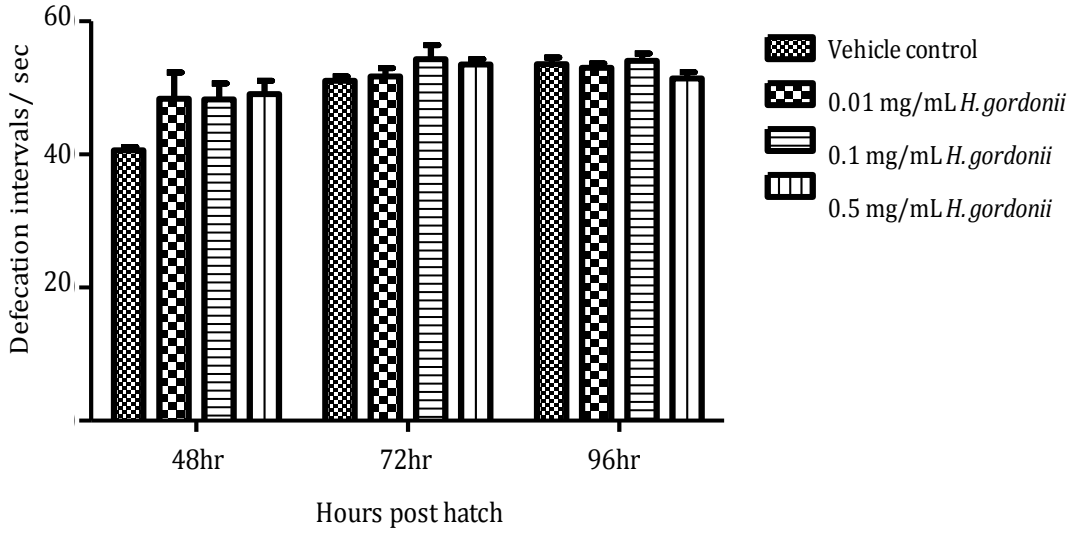


**Figure 4.3 Defecation rate of wild-type nematodes when treated with *H. gordonii* extract.** Based on an ANOVA statistical test, there were no significant changes in the defecation of worms exposed to *H. gordonii* extract. Each graph represents the average defecation intervals of 30 nematodes with the standard error of the mean (±SEM).

### 4.3.5 The volumetric surface area of *C. elegans* is attenuated by *H. gordonii* extract treatment

A growth assay was performed to explore the potential connection between the changes in feeding behavior and the normal developmental stages of wild-type nematodes.

Under optimal conditions (i.e., 20°C and *ad labitum* supply of *E. coli* OP50 food) developmental changes were measured with and without the addition of *H. gordonii* extract. Growth parameters of body surface area as well as the length of the animals revealed that volumetric size and length were overall reduced (Figures 4.4 and 4.5). Growth characteristics were assessed by taking daily photographs of the non-exposed and exposed worms, on a daily base from 24 hours post-hatch until the 6th day of life (144 hours post-hatch). Thereafter, the perimeter of each worm was traced using the Image-Pro Express® software (Media Cybernetics, Buckinghamshire, UK).

The effect of *H. gordonii* extract treatment was not significant until 72 hours post-hatch, with the exception of the highest dose (0.5 mg/mL) (Figures 4.4 and 4.5). Interestingly, growth retardation was more pronounced in worms exposed to 0.05 mg/mL *H. gordonii* extract rather than at the higher concentration (0.5 mg/mL) (Figures 4.4 and 4.5).

The body surface area of wild-type increases during larval stages and nematodes become gravid adults within three days (72 hours post-hatch). Regardless of *H. gordonii* extract-treatment, nematodes developed into adults (no larval arrest) however, a robust dose-dependent reduction in the body surface area was observed in the extract-treated groups in comparison to the control group (Figure 4.4). The effect of *H. gordonii* extract on volumetric growth was most pronounced in worms challenged with 0.05 mg/mL, in which equated to a 22% reduction in size (compared to the vehicle control). At 0.1 and 0.5 mg/mL of *H. gordonii* extract, the body surface area was overall 12% and 11% reduced, respectively (Figure 4.4).

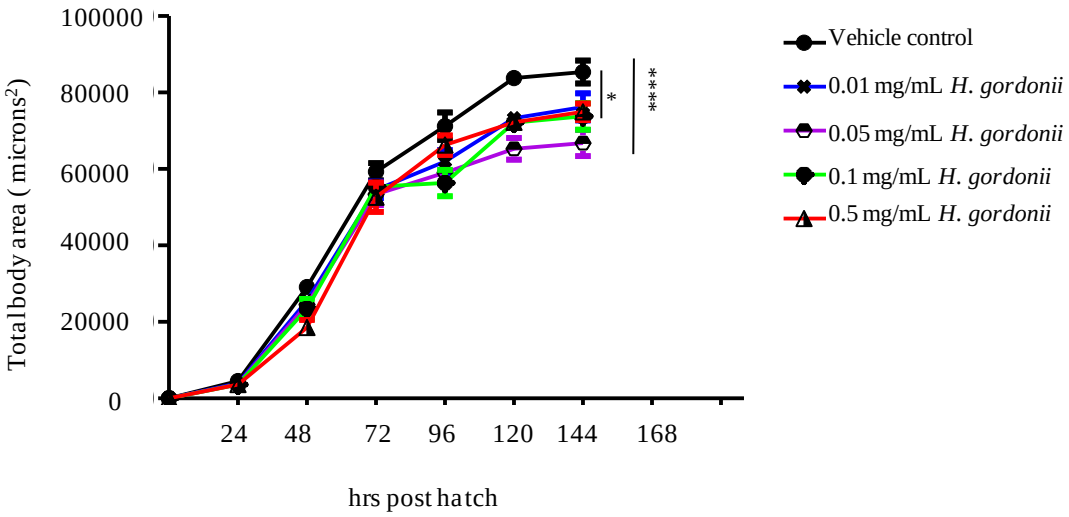


**Figure 4.4 Developmental changes (body surface area) in wild-type *C. elegans* in response to *H. gordonii* extract-spiked OP50 fed *ad libitum*.** *H. gordonii* extract exposed animals reached a smaller size in comparison to the untreated worms. The highest reduction was determined at 0.05 mg/mL. Each data point corresponds to the average body surface area measured from 20 individual nematodes ± standard error of the mean (SEM), two-way ANOVA analyses pinpointed the statistical differences (* *p <0.05*, **** *p <0.0001).*

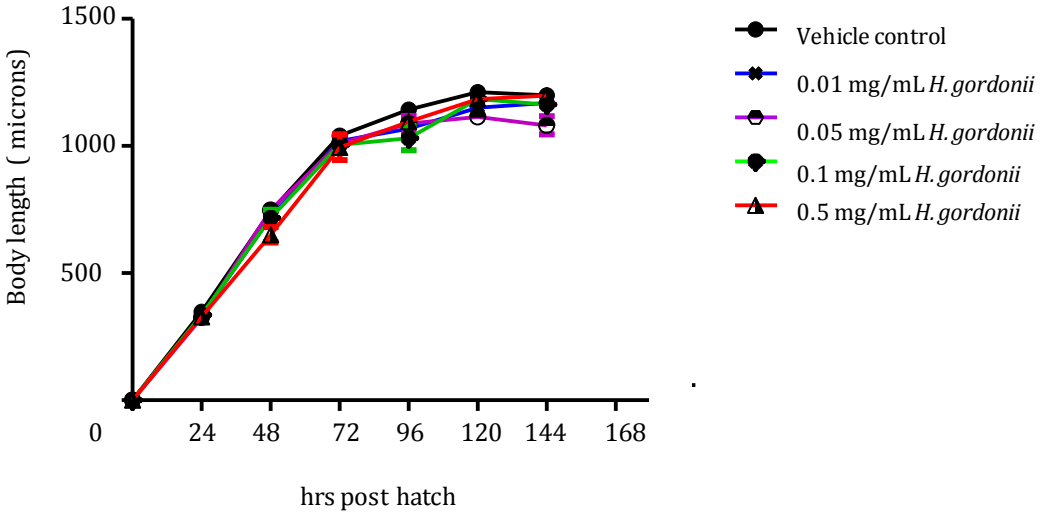


**Figure 4.5 The body length changes over time upon treatment with *H. gordonii* extract.** The length of wild-type nematodes was assessed for a period of six days. There was a significant reduction in the length of animals (* *p <0.05*) when exposed to 0.05 mg/mL of the plant extract. Data points represent the mean length of 20 individual worms and error bars are ± the standard error of the mean (SEM).

The body length of the nematodes was assessed and quantified using Image Pro Express®. Similar to the body surface area, length of the wild-type nematodes also increases during the four larval stages. *H. gordonii* extract-treatment modestly but robustly decreased the length of the nematodes (Figure 4.5). The influence of the extract was mostly pronounced in 0.05 mg/mL, a similar trend as observed when assessing the body surface area changes (Figure 4.5). The length retardation was proportional to the volumetric reduction meaning that the effect did not result in dauer formation. Tables S. 3 and S. 4 in Appendix Three provide further data in regards to volumetric and length changes of these nematodes.

### 4.3.6 A reduction in the Nile Red stained compartments is observed in *H. gordonii* extract-exposed nematodes

As feeding rate and the growth parameters were reduced in *H. gordonii* extract-exposed wild-type animals, it was hypothesized that such effects could influence the lipid content of the treated animals. To examine this hypothesis, lipid droplets were visualized using an *in vivo* approach.

Due to the hydrophobic properties of lipid droplets, the lipophilic fluorescent dye Nile Red was used to stain intact body fat in *C. elegans*. Exposure and staining were performed as explained in section 2.3.7.1. Ten individual nematodes per condition were picked and mounted on 2% Agarose pads thereafter visualized using a wide-field inverted microscope (Nikon Eclipse TE2000-S, Japan) with a green filter (Nile Red's excitation range is 400-600 nm) (Greenspan et al., 1985). Nematodes were photographed from the anterior region to the vulva and subsequently analyzed to quantify the red fluorescent intensity of the stained droplets normalizing to fluorescent

intensity of unexposed animals. A qualitative analysis revealed a remarkable reduction in the relative red fluorescent intensity in *H. gordonii* exposed nematodes in droplets likely to be the main sites of fat droplets (intestinal cells and under the hypodermis) (Figure 4.6).

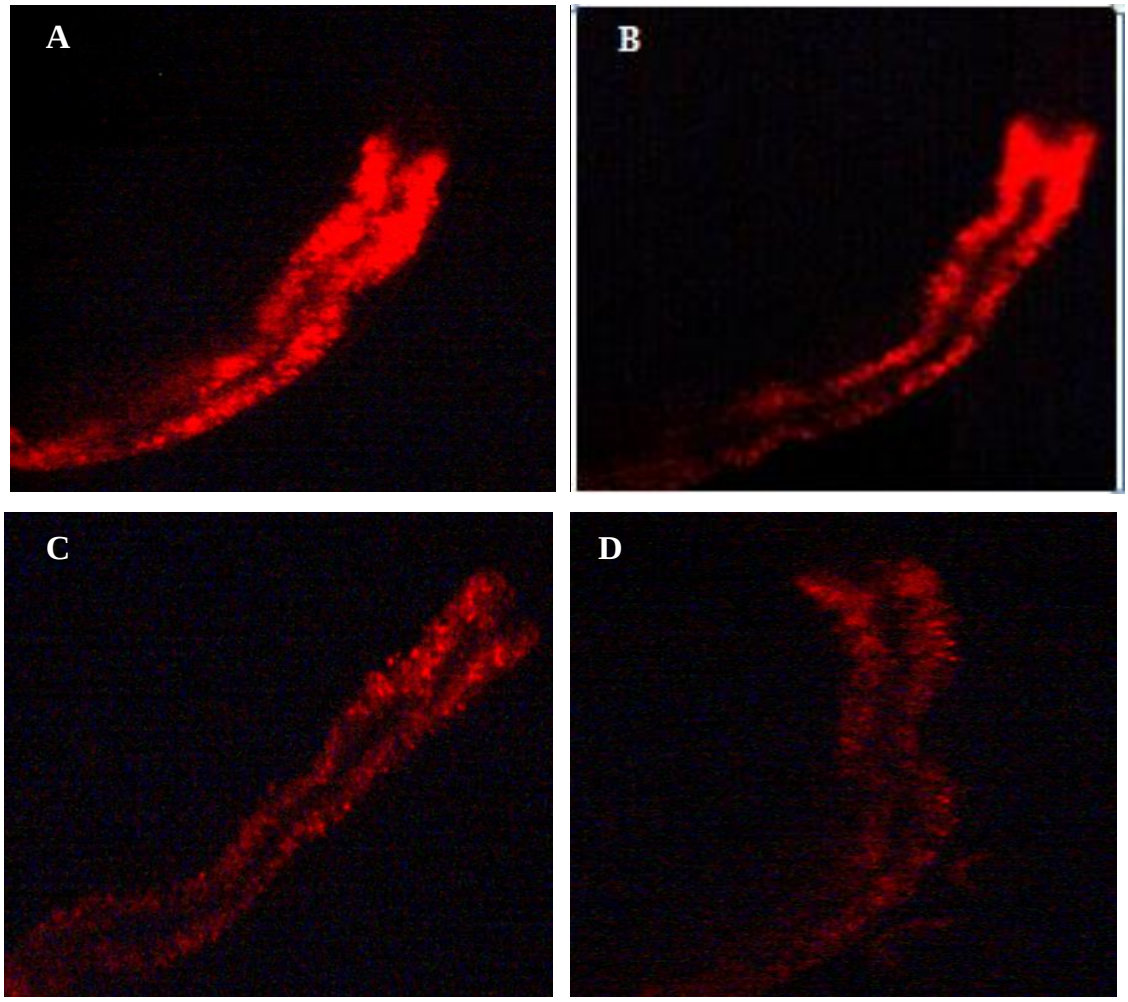


**Figure 4.6 Lipophilic dye Nile Red staining in wild-type nematodes treated with *H. gordonii* extract.** Images used were acquired with the same exposure time to allow a direct comparison between all conditions. Magnification was set at 20X for all conditions. The UV visualization of Nile Red stained lipid droplets under control conditions (A). Note that the staining was mostly pronounced in the first two intestinal cells. Images of *H. gordonii* extract-exposed nematodes stained with Nile Red (0.01, 0.05 and 0.1 mg/mL corresponding to B, C and D, respectively) display the staining pattern upon treatment where an overall reduction of red fluorescent intensity was observed.

*H. gordonii* extract treatment resulted in a reduction in the Nile Red stained compartments (both the number and size of the stained organelles), therefore the relative red fluorescent intensity was compared in *C. elegans* treated with different concentrations of the extract. A one-way ANOVA followed by Tukey's multiple comparisons test was applied to define the statistical significance of the relative fluorescent intensity between different exposures. Red fluorescent intensity under control conditions (no *H. gordonii* extract added) was used as the reference therefore, changes in the relative red fluorescent intensity upon treatment with *H. gordonii* extract were compared to the control (Figure 4.7). There was a 58% reduction in red fluorescent intensity in the animals treated with 0.5 mg/mL extract followed by a 25% and 13% decrease in the 0.1 and 0.01 mg/mL treatment groups, respectively.

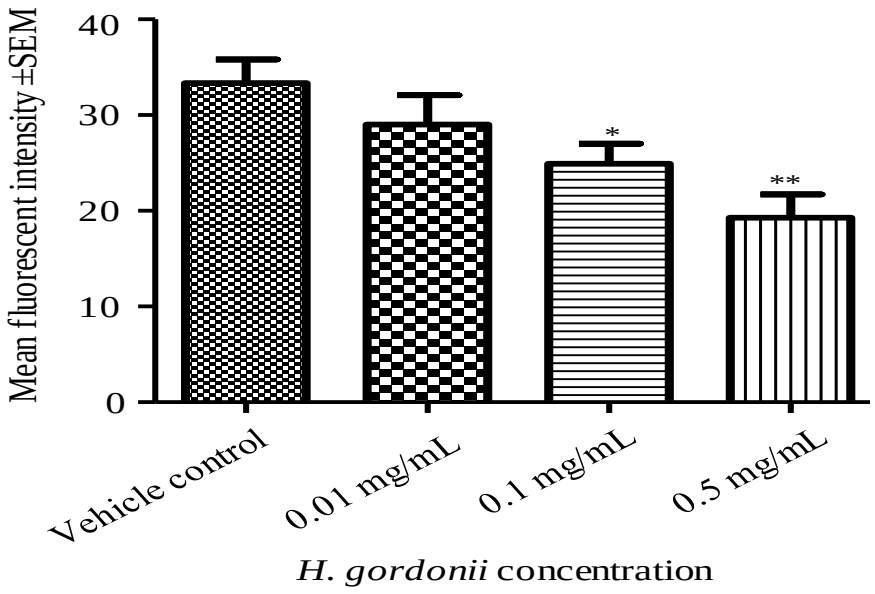


**Figure 4.7 Quantitative analyses of the Nile Red stained compartments in wild-type nematodes exposed to *H. gordonii.*** The Nile Red positive organelles were quantified by measuring absorbance at 620 nm when dissolved in acetone. *H. gordonii* extract-exposed nematodes were compared to the nematodes under control conditions. Statistical analyses revealed that the mean fluorescent intensity significantly declined in worms treated with 0.1 or 0.5 mg/mL of the extract. Each bar graph represents the mean fluorescent intensity from 10 individual nematodes ± standard error of the mean (SEM). Tukey's multiple comparisons test: (* $p < 0.05$, ** $p < 0.01$).

### 4.3.7 Fecundity is modulated by *H. gordonii* extract treatment

Hermaphrodite nematodes mainly reproduce by self-fertilization. Over approximately five days, wild-type nematodes under normal conditions can lay up to 300 eggs, however the number of total progenies varies based on environmental changes (such as the temperature or food availability) and genetic mutations (Fraser et al., 2000).

To this point, developmental analyses, neuromuscular behavior of pharyngeal pumping and Nile Red dye assessment confirmed that *H. gordonii* extract treatment modulates several life history traits including a significant retardation of growth parameters (the body surface area and the length), a substantial reduction in the relative intensity of red fluorescent intensity correlating to the granules likely to be of fat reservoirs and a decline in the pharyngeal pumping rate.

In order to evaluate the influence of *H. gordonii* extract treatment on the reproduction of wild-type nematodes, an assay was performed to quantify the total progeny number and the brood period. The total number of viable hatchlings was decreased robustly in animals exposed to the extract (Figure 4.8). In control worms (not treated with the plant extract) the total progeny number was approximately 200 viable larvae. In contrast, *H. gordonii* exposure resulted in a significantly smaller brood size with the most pronounced reduction being observed in nematodes challenged with 0.5 mg/mL *H. gordonii* extract, equating to a 42% drop compared to the control (Figure 4.8).

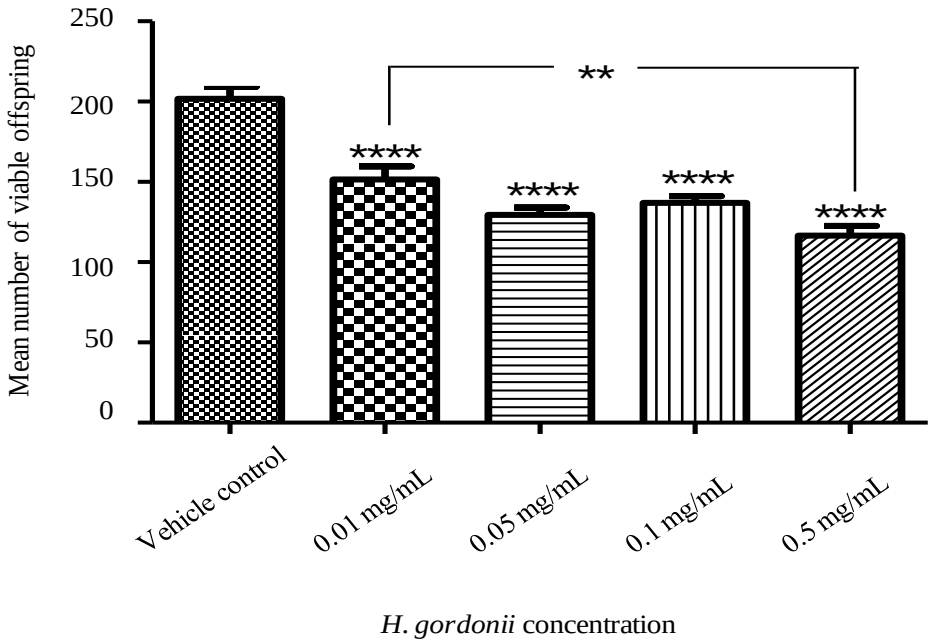


**Figure 4.8 The total number of viable progenies in wild-type nematodes treated with *H. gordonii* extract**. A robust and dose-dependent reduction in the number of progenies was observed when animals were treated with *H. gordonii* extract. Under control conditions, the total progeny number was approximately 200 whereas, exposure to the extract resulted in a reduced brood size. The effect was most significant at the highest dose (0.5 mg/mL). Each bar graph represents the average progeny number quantified from 30 individual worms and error bars show the standard error of the mean (±SEM) (** *p <0.01,* **** *p <0.0001).*

The reduction in the progeny number upon *H. gordonii* extract treatment was approximately 35% in animals exposed to 0.05 and 0.1 mg/mL *H. gordonii* extract, and a 25% at 0.01 mg/mL of the plant extract (Figure 4.8).

Genetic alterations in addition to environmental stress can influence the reproduction profile by either enforcing "early or delayed" reproduction. As mentioned earlier, the brood period is approximately five days in wild-type worms. The daily reproductive output has a Gaussian distribution, however this pattern can vary upon exposure to certain chemicals or environmental changes including an imbalanced diet, stress,

infections or temperature variations. These alterations can be studied by scrutinizing the daily brood output for each animal over a period of six days (Figure 4.9).

Under control conditions, the peak day of reproduction was at 96 hours post-hatch, which shifted to a later time point when worms were treated with 0.1 and 0.5 mg/mL *H. gordonii* extract (Figure 4.9). A marginal but robust influence was observed in the brood period, where brood period started earlier in nematodes exposed to two higher doses (0.1 and 0.5 mg/mL) of the extract (Figure 4.9). Therefore, despite the fact that *H. gordonii* extract significantly attenuates the fecundity in wild-type nematodes, the daily output is not modulated significantly.

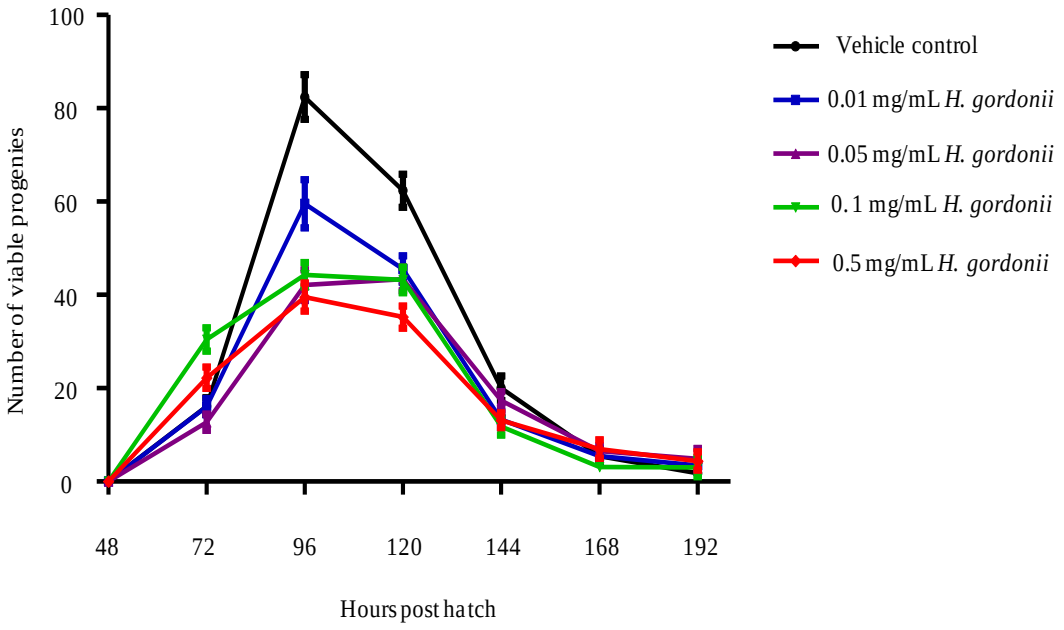


**Figure 4.9 Daily output of the wild-type treated with *H. gordonii* extract.** The Gaussian distribution of fecundity was studied in response to the plant extract exposure for a period of six days after the L4 stage. *C. elegans* worms started laying eggs from 72 hours post-hatch and reached a peak at 96 hours in the absence of the extract. At 72 hours post-hatch more progenies were produced by worms exposed to 0.1 and 0.5 mg/mL *H. gordonii* extract, whereas at lower concentrations (0.01 and 0.05 mg/mL) reproduction was similar to the (vehicle) control. Each data point represents the average daily output from 36 nematodes and the standard error of the mean (±SEM). Statistical analyses were performed by applying a two-way ANOVA following a Bonferroni multiple comparisons test.

### 4.3.8 Survival of the wild-type nematodes is not modulated by exposure to *H. gordonii* extract

Calorie restriction (also known as dietary restriction) has offered a possible lead towards life extension and longevity (Cohen et al., 2004). In nematodes, mutants such as *eat-2* with a significantly lower feeding rate are calorie restricted and long-lived. It is because once energy uptake is decreased by means of less food intake, survival rate increases to its maximum level however, severe food scarcity results in a rapid drop in the lifespan of the animal (Piper and Partridge, 2007). In addition, bacterial dilution (live or dead) also contributes to life extension as an outcome of calorie restriction (Fontana et al., 2010). Dauer nematodes have a higher fat content and are long-lived, or *daf-2* mutants that exhibit an elevated amount of stored fat in the body of the adult worm tend to live long (Guarente and Kenyon, 2000, Ashrafi, 2007, Kenyon, 2010). On the other hand, some mutations result in phenotypes with a lower fat content, which are also associated with long-lived animals. These emphasize the complexity of aging and lipid pathways even in a simple metazoan animal such as *C. elegans* (Ashrafi, 2007).

Because earlier in this chapter it was shown that wild-type nematodes that were treated with *H. gordonii* extract had a reduced pharyngeal pumping rate, the possibility of CR and longevity was then explored. The experiment was set up to compare the lifespan of nematodes treated with 0, 0.01, 0.05, 0.1 and 0.5 mg/mL *H. gordonii* extract. In detail, the survival curves were plotted from 400 nematodes per condition. Data analyses revealed that the median lifespan was not different in any of the extract-treated groups and animals reached a median lifespan of 15 days regardless of exposure conditions (Figure 4.10). Moreover, the maximum survival rate also remained unchanged and wild-type worms lived up to 22 days in the presence or absence of the *H. gordonii* extract (Figure 4.10). A more detailed list including the number of censored worms

from analysis, median survival and the statistical significance (p-values) are provided in Appendix Four.

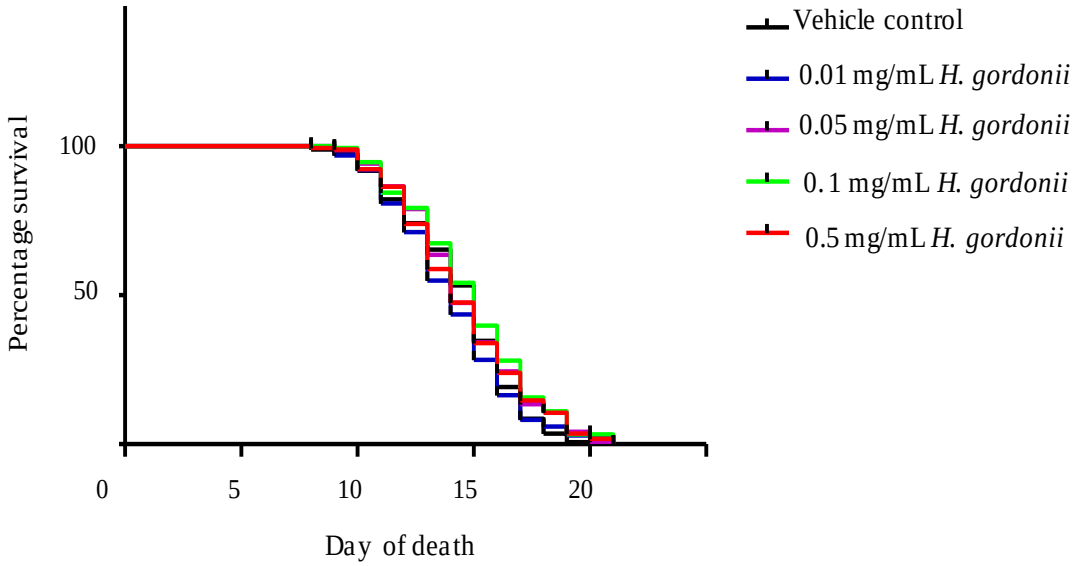


**Figure 4.10 Survival curves of wild-type nematodes upon treatment with *H. gordonii* extract.** The mean lifespan value was 15 days ± 0.5 (n=400 per experimental condition), regardless of exposure condition. Comparison of the data using the Log-rank (Mantel-Cox) test identified no statistical difference between the means. The maximum survival was also not affected in animals. Each Kaplan-Meier survival curve is the average of three biologically independent replicate and all experiments were carried out at 20°C.

### 4.3.9 A genome-wide microarray identifies several pathways that are involved in respond to *H. gordonii* extract exposure

#### *4.3.9.1 Overview*

The microarray can be used to explore several areas of genomics including SNP genotyping and the genome-wide analysis of gene expression. Importantly, whole

genome studies allow researchers to gain an overview of global gene expression patterns and to obtain a better understanding of the link between mRNA levels and biological functions (Dalma-Weiszhausz et al., 2006). Moreover, genome-wide arrays have offered new leads when studying the genetic basis of diseases, such as cancer (Armstrong et al., 2002, Huang et al., 2004, Yeoh et al., 2002). Understanding the state of a disease and achieving more promising therapeutic options have become more defined with the microarray technology (Dalma-Weiszhausz et al., 2006). In this study, a global approach was performed via the Affymatrix GeneChip® Arrays to unravel the molecular fingerprints of *H. gordonii* extract exposure in the nematode *C. elegans*.

#### *4.3.9.2 Data interpretation and statistical analysis*

The molecular-genetic impact of *H. gordonii* extract on staged L4 *C. elegans* exposed to different concentrations (0, 0.01, 0.05 and 0.1 mg/mL) of the plant extract for approximately 44 hours, was determined using a whole-genome microarray approach. The processing of each RNA sample was carried out by means of a MessageAmp™Premier RNA Amplification Kit (Ambion, Austin, TX, USA) (details in section 2.3.11), and each array represented 22,548 different transcripts of *C. elegans*. The scans were conducted with a GeneChip® scanner 7G (Affymetrix), thereafter raw data from Affymatrix GeneChip® Array were launched onto the AGCC[15] portal for initial quantification. Because of the lack of true biological repeats, a linear normalization via MAS5.0 was chosen and responsive gene IDs were identified. The MAS5.0 Expression Report provides intensity values and the presence/absence call for each transcript and is therefore a rather qualitative procedure (Harr and Schlotterer, 2006, Lim et al., 2007). In order to obtain a better overview of the number of

[15] GeneChip® Command Console® software

transcriptional dynamics in response to *H. gordonii* extract exposure, a heatmap was generated (Figure 4.11).

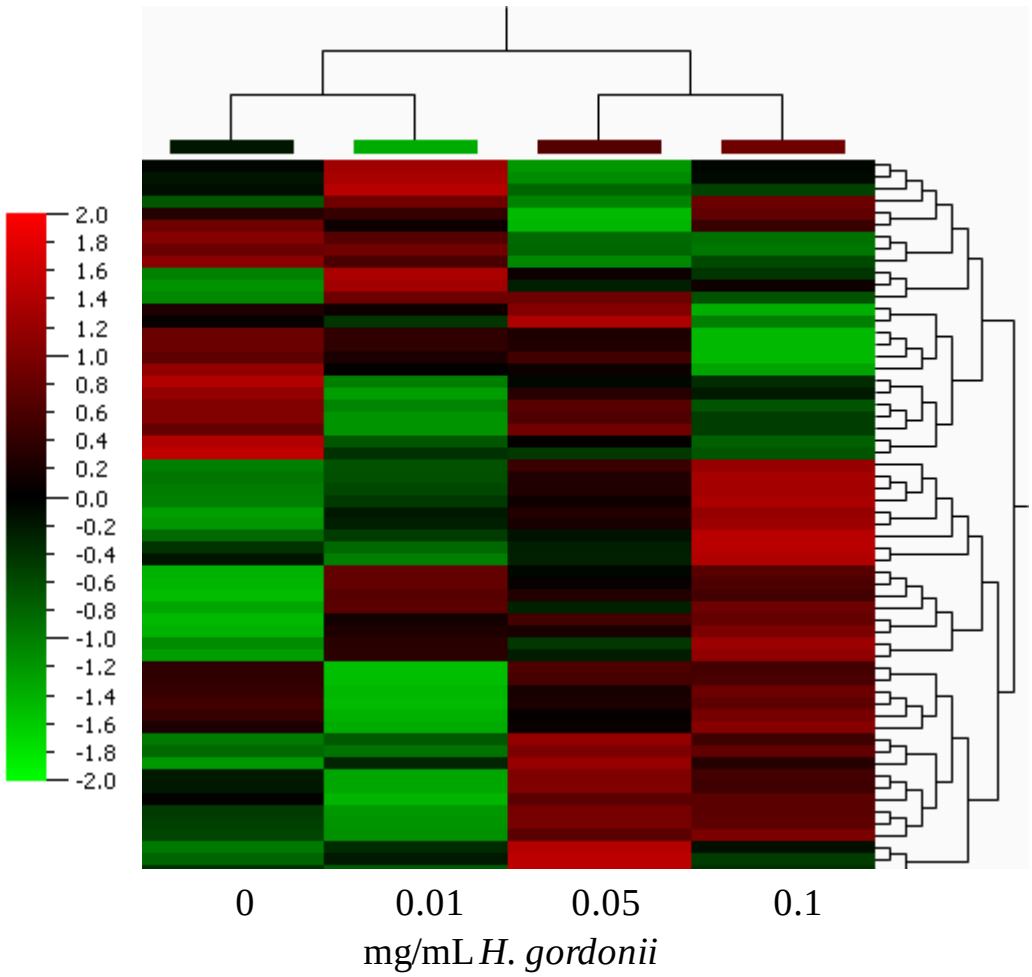


**Figure 4.11 The heatmap of genes that were transcriptionally modulated in *C. elegans* exposed to *H. gordonii* extract.** Note that the severity of the response is marked by the color red whereas down-regulated or suppressed genes are shown as green. Black denotes a transcript that did not change upon treatment with the extract. The heatmap was generated by Qlucore platform and an arbitrary scale was set where the most significant down regulation was scored as -2 and the highest up-regulation as 2 (compared to the control sample group i.e. non-exposed nematodes). Note that not necessarily all changes were statistically meaningful. The heatmap only represents an overview of transcriptional changes in response to *H. gordonii* treatment.

Furthermore, a cutoff point was applied to genes with fold change below 1.4 (up/down-regulation). At 0.01 mg/mL of *H. gordonii* extract exposure, 402 genes were found to be either induced or suppressed 1.4 fold. In contrast, the intermediate dose (0.05 mg/mL) affected only 176 genes and exposure to 0.1 mg/mL extract modulated the expression of 1266 genes. To define the level of overlap between *H. gordonii* extract doses, Venn diagrams of the three concentrations were generated (Figure 4.12).

A Fisher's Exact Test was used to pinpoint the significance of overlap between the responsive genes within dose groups. Responsive genes within each concentration group were divided into two groups of either up- or down-regulated categories and each group was then compared to the corresponding counterpart from the other two doses. Appendix Five presents the data used for the Fisher's Exact Test based on the Venn diagrams. Overall, the overlap between genes that were up/down-regulated in response to three doses of *H. gordonii* extract appeared to be highly significant and that the data were not of random appearance of the genes. In detail, the Affymatrix GeneChip® Array contains a total of 16917 genes on each chip, out of which 166 were shown to be up-regulated in 0.01 mg/mL and 122 genes in 0.05 mg/mL, having said that, the observed overelap (Figure 4.12) was determined to be 37 genes whereas the expected random appearance of genes in two doses was 2. The outcome suggested that the overlap was statistically meaningful. Among 0.05 and 0.1 mg/mL doses, the occurrence of any random data was 5 genes, whereas the actual observed overlap was 100 genes (Figure 4.12). Furthermore, between the 0.01 and 0.1 mg/mL concentrations it was expected to find a chance of 7 genes being up-regulated, in which the microarray data returned 105 genes to be over-expressed in both doses, excluding the chance of random appearance of the genes (refer to Appendix Five).

Moreover, a similar statistical significance was observed among down-regulated genes when doses were compared. The trend was mostly pronounced between 0.1 and 0.05 and further confirmed by the Fisher's Exact Test (Appendix Five).

In total, 42 genes were responsive at all three conditions of *H. gordonii* extract exposure (Table 4.1), however this did not take into account the level of response or direction of changes (up- or down-regulation). To address this, the expression data were re-sorted by fold change (significantly up/down-regulated). From each *H. gordonii* extract-exposed condition, the 60 most responsive transcripts were selected (Tables 4.2 to 4.7) and subjected to the bioinformatics platform DAVID (the Database for Annotation, Visualization and Integrated Discover) Bioinformatics Resource "version 6.7", (Huang da et al., 2009) to define significant Gene Onthology (GO) terms. Based on the data obtained from the Venn diagram (Figure 4.12) and the most responsive genes (Tables 4.2 to 4.7), 11 genes were selected for further analysis via quantitative real-time PCR. These 11 genes were positioned in different categories of the molecular function GO terms, and thus helped to unravel metabolic pathways involved in mRNA expression of *H. gordonii* extract-treated nematodes (Table 4.8).

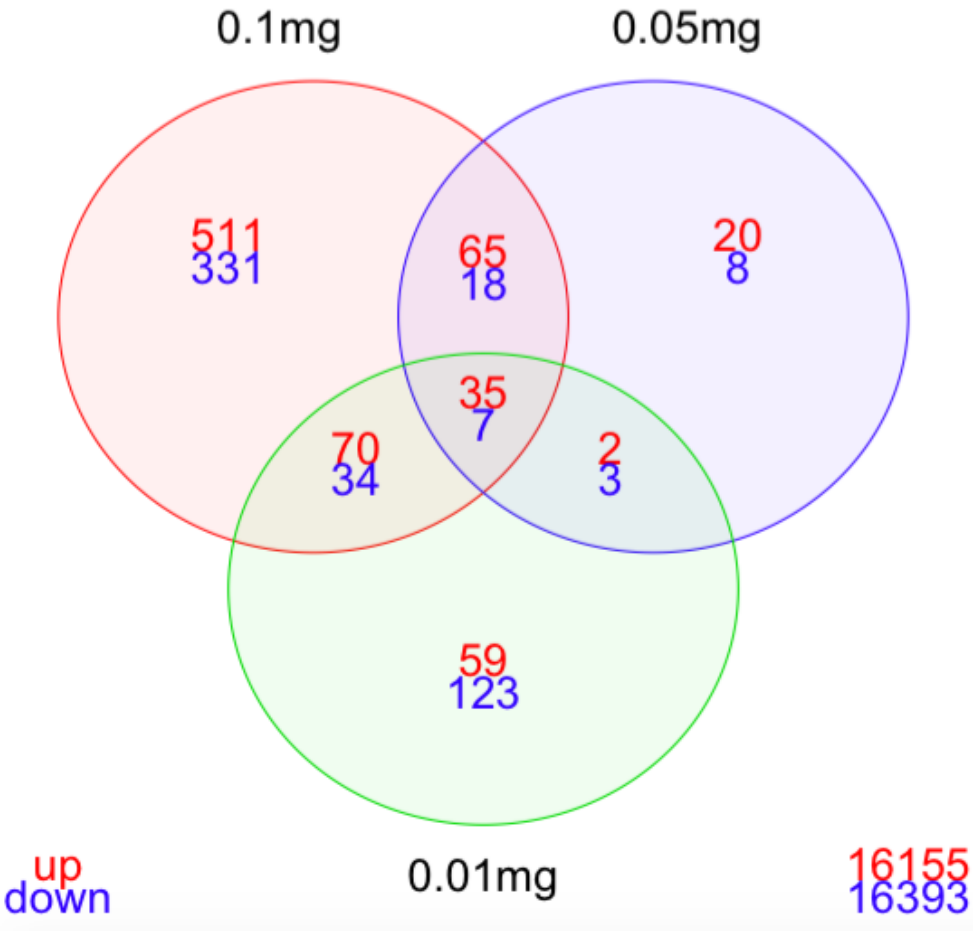


**Figure 4.12 Venn diagram to identify transcripts that were shown to be significantly affected by *H. gordonii* extract treatment**. Note that 42 transcripts were found to be common to all three dosing regimes. Significance of the plant extract exposure was determined the Fisher's Exact Test, http://research.microsoft.com/en-us/um/redmond/projects/mscompbio/fisherexacttest/.

| Gene name | Description | Molecular Function |
|---|---|---|
| C54D10.10 | Unknown | Serine-type endopeptidase inhibitor activity |
| K07A1.4 | Unknown | Unknown |
| *col-120* | A member of collagen super family | Structural constituent of cuticle |
| T12B5.10 | Coding a protein containing F-box, a motif predicted to mediate protein-protein interactions | Protein binding |
| K07F5.5 | *nspd-2*, nematode specific peptide family, group D | Unknown |
| Y75B12B.3 | Unknown | Unknown |
| F40H6.1 | Unknown | Unknown |
| Y54E2A.9 | Unknown | Unknown |
| *col-131* | A member of collagen super family | Unknown |
| ZC239.16 | Unknown | Protein binding |
| M60.2 | Unknown | Hydrolase activity, acting on ester bonds |
| Y51A2D.9 | *ttr-24,* Trans Thyretin-Related family domain | Unknown |
| W06D12.3 | *fat-5,* fatty acid desaturase | Oxidoreductase activity by acting on paired donors with addition of a pair of donors resulting in the reduction of molecular oxygen to two molecules of water, Stearoyl-CoA 9-desaturase activity |
| H10E21.4 | Unknown | Calcium ion binding |
| *mlt-10* | Encodes a nematode-specific protein that contains a domain of unknown function, DUF644, and tandem proline- and hydroxy amino acid-rich repeats. | Unknown |
| *cdh-12* | Encodes a cadherin, predicted to function in cellular adhesion | Calcium ion binding |
| K04H4.2A | Required for larval growth and locomotion | Chitin binding |
| *col-41* | Encodes a cuticle collagen | Structural constituent to cuticle |
| F49E10.2 | Unknown | Unknown |
| F58D5.2 | Unknown | Unknown |

| Gene name | Description | Molecular Function |
|---|---|---|
| Y37D8A.19 | Unknown | Unknown |
| Y62H9A.5 | Unknown | Unknown |
| ZK813.1 | Unknown | Unknown |
| C04H5.7 | Unknown | Unknown |
| C45B2.1 | Unknown | Unknown |
| F57C2.4 | Unknown | Unknown |
| Y62H9A.6 | Unknown | Unknown |
| *decr-1.1* | DiEnoyl-CoA Reductase (mitochondria) | Unknown |
| *col-19* | A member of collagen super family | Structural constituent of cuticle |
| D1054.10 | Unknown | Unknown |
| EEED8.3 | Similar to fatty acid binding protein | Unknown |
| T04G9.7 | Unknown | Unknown |
| *col-62* | A member of collagen super family | Structural constituent of cuticle |
| *col-81* | A member of collagen super family | Structural constituent of cuticle |
| F54F7.3 | Unknown | Unknown |
| *col-106* | A member of collagen super family | Structural constituent of cuticle |
| Y75B8A.23 | Unknown | Unknown |
| C43G2.3 | Unknown | Unknown |
| F21H7.2 | Unknown | Unknown |
| F36A4.2 | Unknown | Unknown |

**Table 4.1 The 40 overlapped genes derived from Venn diagrams after excluding two pseudo genes (*nhr-191* and K01C8.4).** Gene IDs were pinpointed using DAVID Bioinformatics platform and checked by wormbase portal, http://www.wormbase.org.

| MAS5.0 ID | Signal Log Ratio (0.01 mg/mL) | Wormbase name | Description |
|---|---|---|---|
| 180098_s_at | 4.6 | F49E2.5F | Unknown |
| 180065_s_at | 4.4 | Y62H9A.5 | Unknown |
| 174502_s_at | 4.4 | C32E12.4 | Unknown |
| 193558_at | 4.4 | F26A1.14 | Unknown |
| 173177_s_at | 3.8 | F21H7.2 | Unknown |
| 173156_s_at | 3.7 | AU115064_rc | Unknown |
| 181968_s_at | 3.4 | Y48C3A.7 */mac-1* | Essential for proper regulation of fat storage and for normal larval developmen |
| 185964_at | 3.3 | Y37D8A.19 | Unknown |
| 177200_at | 3.2 | Y39A3CL.4 | Uncharacterized conserved protein with TLDc domain |
| 189061_at | 3.1 | F26A1.4 | Casein kinase (serine/threonine/tyrosine protein kinase) |
| 173392_s_at | 3 | AU114057_rc | Unknown |
| 189781_at | 2.8 | F26A3.2 */ncbp-2* | Involves in reproduction, vulval morphogenesis and mRNA decay |
| 194234_x_at | 2.7 | Y62H9A.5 | Unknown |
| 179587_at | 2.7 | F44F4.3 | Unknown |
| 174925_s_at | 2.7 | CEK121B5R_rc. | Serine-Threonine phosphotase |
| 192282_at | 2.6 | R11G11.2 */nhr-58* | Zinc finger protein |
| 173599_s_at | 2.5 | Y48G10A.3 | Differentiation-related gene 1 protein (NDR1 protein) |
| 194189_x_at | 2.3 | AU115826_rc | Unknown |
| 187213_at | 2.2 | EEED8.3 | Simialr to fatty acid binding protein (FABP family) |
| 186554_s_at | 2.2 | Y116A8C.26 | Intermediate filament-like protein, sorting nexins, and related proteins containing PX domain(s) |
| 190902_at | 2.2 | R10D12.10 | Lipid storage |
| 193896_s_at | 2.2 | F23B2.5_rc */flp-1* | FMRFamide-related peptides (FaRPs), required for movement and egg-laying |
| 173767_s_at | 2.1 | CEK058GZF */col-7* | A member of collagene super-family |
| 173195_s_at | 2.1 | AV185121_rc */smu-2* | Affects the accumulation of alternatively spliced unc-52 transcripts |
| 180677_s_at | 2.1 | ZK813.1 | Unknown |
| 173149_at | 2 | AU113969_rc | Unknown |
| 176691_at | 2 | C45B2.1 | Unknown |
| 186337_at | 1.9 | F43C11.3 | Unknown |
| 171767_x_at | 1.9 | AU116500_rc | Unknown |

**Table 4.2 The 30 most up-regulated transcripts in nematodes exposed to 0.01 mg/mL *H. gordonii* extract as defined by the Affymetrix® microarray platform.**

| MAS5.0 ID | Signal Log Ratio (0.01 mg/mL) | Wormbase name | Description |
|---|---|---|---|
| 176985_at | -2 | Y54G2A.A | Unknown |
| 184411_at | -2 | C12D12.1 | Unknown |
| 187941_at | -2 | W01G7.1 /*daf-5* | May regulate chemosensation via AWC neurons, and may regulate egg laying |
| 174819_at | -2 | CEC7393_rc | Unknown |
| 186302_s_at | -2 | Y105C5A.1 | Reproduction |
| 183094_at | -2 | F15A4.13 /*Rfbxb-102* | F-box B protein |
| 179385_s_at | -2 | F14H3.3 | Unknown |
| 182743_at | -2.1 | Y47D3B.6 | Unknown |
| 194064_at | -2.1 | ZK666.3 /*clec-58* | C-type LECtin |
| 182170_at | -2.2 | C14E2.1 | Unknown |
| 191419_at | -2.2 | C24A8.4 /*cst-2* | STE20-like serine-threonine kinase |
| 174258_at | -2.2 | F09F7.5 | Regulator of growth, lifespan and large broodsize |
| 176532_at | -2.3 | Y55B1BR.3/*cec-8* | *C. elegans* Chromodomain protein |
| 184556_at | -2.4 | C18B10.2 /*srbc-10* | Serpentine Receptor, class BC (class B-like) |
| 182632_at | -2.4 | R03H4.4 /*srt-18* | Serpentine Receptor, class T |
| 182651_at | -2.5 | C50E3.2 | Unknown |
| 172294_x_at | -2.5 | Y9D1A.2 | Unknown |
| 183008_at | -2.6 | K01A2.6 | Unknown |
| 192624_at | -2.7 | F55D12.3 /*nhr-191* | pseudogene |
| 191293_at | -2.7 | T04A8.1 /*srg-10* | Serpentine Receptor, class G (gamma) |
| 191500_at | -2.7 | F37B4.5 /*srh-270* | Serpentine Receptor, class H |
| 181675_at | -2.9 | R03G5.6 | Unknown |
| 177388_at | -2.9 | K05C4.3 | Unknown |
| 172780_x_at | -3 | C25A8.1 | Unknown |
| 185366_at | -3 | T06C10.2 /*srt-73* | Serpentine Receptor, class T |
| 179008_at | -3.3 | C09G1.2 | Unknown |
| 174331_at | -3.6 | C59659_rc | Unknown |
| 182818_at | -3.9 | T05G11.7 /*srw-53* | Serpentine Receptor, class W |
| 185860_s_at | -3.9 | F22E5.12 | Unknown |
| 190408_s_at | -4.6 | K09H9.4 | Unknown |

**Table 4.3 The 30 most down-regulated transcripts in nematodes exposed to 0.01 mg/mL *H. gordonii* extract as defined by the Affymetrix® microarray platform.**

| MAS5.0 ID | Signal Log Ratio (0.05 mg/mL) | Wormbase name | Description |
|---|---|---|---|
| 180065_s_at | 5.5 | Y62H9A.5 | Unknown |
| 185964_at | 4.6 | Y37D8A.19 | Unknown |
| 175377_at | 4.4 | ZK813.7 | Unknown |
| 173177_s_at | 4 | F21H7.2 | Unknown |
| 194234_x_at | 3.7 | Y62H9A.5 | Unknown |
| 179470_at | 3.2 | K08E7.4 | Unknown |
| 173767_s_at | 3.1 | COLlagen/*col-7* | A member of collagene superfamily |
| 180677_s_at | 2.8 | ZK813.1 | Unknown |
| 177820_at | 2.6 | ZC373.2 | Unknown |
| 183721_at | 2.6 | F17E9.4 | Unknown |
| 192869_at | 2.5 | T01G5.7 | Unknown |
| 187964_at | 2.5 | F54F3.3 */lipl-1* | LIPase Like |
| 186519_at | 2.5 | F15E11.12/*pud-4* | Unknown |
| 192134_at | 2.4 | T05A10.4/*scl-22* | SCP-Like extracellular protein |
| 173316_s_at | 2.4 | Y62H9A.6 | Unknown |
| 192163_at | 2.4 | ZK1193.1 */col-19* | A member of collagene superfamily, required for alae normal structure |
| 189221_at | 2.4 | F28G4.1 */cyp-37B1* | Cytochrome P450 family member |
| 176691_at | 2.4 | C45B2.1 | Unknown |
| 175102_at | 2.4 | C04H5.7 | Unknown |
| 192509_at | 2.3 | ZK666.6 */clec-60* | A role in innate immune response |
| 186337_at | 2.3 | F43C11.3/*decr-1.1* | DiEnoyl-CoA Reductase, mitochondria |
| 180752_s_at | 2.3 | D1054.10 | Unknown |
| 183841_at | 2.3 | C50F7.9 | Unknown |
| 188281_s_at | 2.2 | F38A3.1 | Unknown |
| 189545_s_at | 2.1 | F41F3.4 / *col-139* | A member of collagene superfamily |
| 188078_at | 2.1 | F46B6.8 */lipl-2* | LIPase Like |
| 187213_at | 2.1 | EEED8.3 | Simialr to fatty acid binding protein (FABP family) |
| 177131_s_at | 2.1 | Y19D10B.A | Unknown |
| 178304_at | 2 | K08D8.1 | Unknown |
| 172998_s_at | 2 | W06D12.3/*fat-5* | a delta-9 fatty acid desaturase |

**Table 4.4 The 30 most up-regulated transcripts in nematodes exposed to 0.05 mg/mL *H. gordonii* extract as defined by the Affymetrix® microarray platform.**

| MAS5.0 ID | Signal Log Ratio (0.05 mg/mL) | Wormbase name | Description |
|---|---|---|---|
| 174175_at | -1.4 | *lam-2* | A laminin gamma subunit; lam-2 activity is required for embryonic development |
| 174044_at | -1.4 | K04H4.2 | Required for larval growth and locomotion |
| 172248_x_at | -1.4 | T20G5.8 | Unknown |
| 193156_s_at | -1.4 | K10D3.4 | Unknown |
| 186202_s_at | -1.4 | F39H12.4/*igcm-1* | a protein containing immunoglobulin and fibronectin repeats |
| 179187_s_at | -1.4 | F46F2.3 | Unknown |
| 178497_at | -1.4 | C13G3.1 | Unknown |
| 171855_x_at | -1.4 | Y59A8A.3 | Unknown |
| 185450_s_at | -1.5 | Y106G6G.2 /T20F10.5 | Unknown |
| 179208_at | -1.5 | B0399.1 /*kcnl-1* | Encodes a small-conductance calcium-activated potassium channel subunit |
| 188870_s_at | -1.5 | ZC416.8B /*cha-1* | Synthesizes acetylcholine, and is required for viability, normal growth and locomotion |
| 175122_at | -1.6 | C16D9.1 | Unknown |
| 190966_at | -1.6 | C11E4.2/*gpx-3* | Glutathione PeroXidase |
| 190901_s_at | -1.6 | K04H4.2A /RK04H4.2 | Required for larval growth and locomotion |
| 182280_at | -1.6 | F13C5.5 | Unknown |
| 178671_at | -1.6 | F56D5.4 | Unknown |
| 175701_at | -1.6 | *ceh-22* | Required for normal pharyngeal development |
| 173138_s_at | -1.6 | C53B7.3 | Unknown |
| 192487_at | -1.7 | Y43F8C.14 /*ani-3* | Encodes one of three C. elegans anillins. |
| 182573_at | -1.7 | T05B4.3 /*phat-4* | PHAryngeal gland Toxin-related |
| 180889_at | -1.7 | T17H7.1 | Unknown |
| 190134_s_at | -1.8 | T10B10.1 /*col-41* | A member of collagene superfamily |
| 180628_at | -1.8 | C53B7.3 | Unknown |
| 176026_at | -1.8 | C06E1.3 | Unknown |
| 172088_x_at | -2.1 | Y73B3B.C | Unknown |
| 171890_x_at | -2.3 | *klp-4* | Neuronal development (predicted role) |
| 184881_s_at | -2.5 | T23E7.2C | Unknown |
| 187242_at | -3 | F59B10.6 | Unknown |
| 185933_at | -3.1 | F49E10.2 | Unknown |
| 190527_at | -3.5 | H36L18.1 | Unknown |

**Table 4.5 The 30 most down-regulated transcripts in nematodes exposed to 0.05 mg/mL *H. gordonii* extract as defined by the Affymetrix® microarray platform.**

| MAS5.0 ID | Signal Log Ratio (0.1 mg/mL) | Wormbase name | Description |
|---|---|---|---|
| 185964_at | 7 | Y37D8A.19 | Unknown |
| 180065_s_at | 7 | Y62H9A.5 | Unknown |
| 194234_x_at | 6.5 | Y62H9A.5 | Unknown |
| 175377_at | 6.4 | ZK813.7 | Unknown |
| 178411_s_at | 5.9 | W02D9.7 | Unknown |
| 180677_s_at | 5.8 | ZK813.1 | Unknown |
| 178079_at | 5.7 | C11E4.7 | Unknown |
| 175102_at | 5.3 | C04H5.7 | Unknown |
| 183721_at | 4.9 | F17E9.4 | Unknown |
| 177820_at | 4.6 | ZC373.2 | Unknown |
| 174121_at | 4.6 | C30770_rc | Unknown |
| 176691_at | 4.5 | C45B2.1 | Unknown |
| 186281_s_at | 4.4 | Y45F10C.2 | Unknown |
| 175010_s_at | 4.4 | F57C2. | Unknown |
| 180534_at | 4.4 | Y62H9A.6 | Unknown |
| 180069_s_at | 4.3 | F44F1.6A | Unknown |
| 180369_at | 4.3 | C17E7.4 | Unknown |
| 180173_at | 4.3 | Y62H9A.4 | Unknown |
| 181468_s_at | 4.2 | ZK813.3 | Unknown |
| 173316_s_at | 4.2 | Y62H9A.6 | Unknown |
| 186337_at | 4.2 | F43C11.3 | Unknown |
| 188406_s_at | 4.1 | F11H8.3 /*col-8* | A member of collagene superfamily |
| 173110_at | 4.1 | AV182332_rc | Unknown |
| 192163_at | 4.1 | ZK1193.1/*col-19* | A member of collagene superfamily, required for alae normal structure |
| 185184_at | 4.1 | Y57G11B.5 | Unknown |
| 180752_s_at | 4.1 | D1054.10 | Unknown |
| 181958_at | 4 | T06D4.1 | Unknown |
| 174222_at | 4 | F19B10.1 | Unknown |
| 187213_at | 4 | EEED8.3 | Simialr to fatty acid binding protein (FABP family) |

**Table 4.6 The 30 most up-regulated transcripts in nematodes exposed to 0.1 mg/mL *H. gordonii* extract as defined by the Affymetrix® microarray platform.**

| MAS5.0 ID | Signal Log Ratio (0.1 mg/mL) | Wormbase name | Description |
|---|---|---|---|
| 189705_s_at | -2.4 | M88.6A */pan-1* | Required for normal molting |
| 185608_at | -2.4 | H03E18.1 | Unknown |
| 178695_at | -2.4 | F53B3.6 | Unknown |
| 178194_at | -2.4 | R07E3.6 | Unknown |
| 178776_at | -2.5 | ZC334.2 / *ins-30* | Encodes an insulin-like peptide |
| 176188_at | -2.5 | Y119D3B.L */cdh-12* | Predicted to function in cellular adhesion |
| 193344_at | -2.5 | C44H4.3 /*sym-1* | Embryonic viability and attachment of body muscle to the extracellular cuticle |
| 190901_s_at | -2.5 | K04H4.2A | Required for larval growth and locomotion |
| 184175_at | -2.5 | F58E10.7 | Unknown |
| 190134_s_at | -2.6 | T10B10.1 */col-41* | A member of collagene superfamily |
| 177650_at | -2.6 | W04G3.8 */lpr-3* | Related to lipocalin family, binds and transports lipophilic molecules/intercellular signaling |
| 193246_s_at | -2.7 | B0272.5A */fln-2* | FiLamiN (actin binding protein) homolog |
| 191064_at | -2.7 | Y47H9C.5 / *dnj-27* | Encodes a protein containing a DnaJ ('J') domain. |
| 177724_at | -2.8 | W04G3.1 */lpr-6* | Related to lipocalin family, binds and transports lipophilic molecules/intercellular signaling |
| 173579_s_at | -2.8 | l*pr-5* | Related to lipocalin family, binds and transports lipophilic molecules/intercellular signaling |
| 193156_s_at | -2.9 | K10D3.4 | Unknown |
| 180628_at | -2.9 | C53B7.3 | Unknown |
| 182280_at | -3 | F13C5.5 | Unknown |
| 174238_at | -3 | *nsy-7* | A protein with distant similarity to homeodomain transcription factors, neuronal symmetry |
| 185064_at | -3.1 | C17H11.2 | Unknown |
| 172037_x_at | -3.2 | *unc-17/cha-1* | A choline acetyltransferase synthesizes acetylcholine. Viability, normal growth and locomotion |
| 186744_at | -3.3 | Y116F11B.1 */daf-28* | Homolog of human insulin, inhibits dauer formation |
| 187722_at | -3.5 | K01C8.4 | Dead gene |
| 180861_at | -3.9 | C08G9.2 | Unknown |
| 174892_at | -4.3 | *lin-66* | Expressed in body wall, vulval muscles, intestine, neurons, and probably the hypodermis |
| 180889_at | -4.6 | T17H7.1 | Unknown |
| 186220_at | -4.7 | R03H10.2 | Unknown |
| 181248_s_at | -4.7 | F16F9.2 */dpy-6* | Involved in normal body morphology |
| 185933_at | -6 | F49E10.2 | Unknown |

**Table 4.7 The 30 most down-regulated transcripts in nematodes exposed to 0.1 mg/mL *H. gordonii* extract as defined by the Affymetrix® microarray platform.**

| Gene name | Biological process | Cellular Component |
|---|---|---|
| **W06D12.3 (*fat-5*)** | Lipid metabolic process | Integral to membrane |
| | Long-chain fatty acid biosynthesis process | |
| | Multi-cellular organismal development | |
| | Oxidation reduction | |
| | Positive regulator of growth rate | |
| | Positive regulator of multicellular organism growth | |
| **ZK1193.1 (*col-19*)** | Unknown | Alae of collagen and cuticulin-based cuticle extra cellular matrix |
| | | Annuli extracellular matrix |
| **C01C10.3 (*acl-12*)** | Lipid storage | Integral to membrane |
| | Metabolic process | |
| **T10B10.1 (*col-41*)** | Unknown | Integral to membrane |
| **EEED8.3** | Embryonic development ending in birth or egg hatching | Unknown |
| | Hatching | |
| | Similar to fatty acid binding proteins | |
| **Y71D11A.1 (*cdh-12*)** | Determination of adult lifespan | Unknown |
| **ZK813.1** | Unknown | Chorion |
| **K07F5.5 (*nspd-2*)** | Unknown | Unknown |
| **Y62H9A.5** | Unknown | Unknown |
| **Y62H9A.6** | Unknown | Unknown |
| **F49E10.2** | Unknown | Unknown |

**Table 4.8 GO terms of selected *H. gordonii* extract responsive genes from the microarray data.** Biological processes and where available, the cellular organelle to which the gene belongs to is presented (information adapted from www.wormbase.org).

#### *4.3.9.3 Verification of transcriptional responses of selected genes utilizing the quantitative real-time PCR platform*

The Roche Universal Probe Library (UPL) offers a platform for real-time PCR analysis. The FastStart UPL master mix (which contains ROX, a novel reference dye) and probe both contain fluorescent components. In addition, Roche provides online software that defines the most compatible probe and primer set for the targeted amplification within specific organisms including *C. elegans*. The Roche website is linked to wormbase portal, http://www.wormbase.org, therefore by selecting the gene of interest, the Roche software suggests the best probe and primer match for the chosen gene. The probe is usually a short complementary DNA sequence (8 to 9-mer), a hydrolysis probe with a fluorescent tag. These probes are made up of locked nucleic acids (LNA), which are often inaccessible RNA sequences and ideal for detecting short fragments of DNA or RNA, therefore being specifically designed for the real-time PCR analyses (Kaur et al., 2006).

The invariant house-keeping gene *rla-1* was chosen throughout this project to normalize the target genes, since it has been shown to be unaffected by experimental conditions (Qabazard et al., 2013, Pfaffl, 2001). The *rla-1* encodes an acidic ribosomal subunit protein P1 with 63% homology to the *H. sapiens* RPLP1 60S acidic protein P1 alpha, which is involved in the interaction of translational elongation factors with the ribosome (information adapted from BLASTP, http://www.ensembl.org). A list of utilized UPL probe and primer sets is provided (Appendix Six).

Initially, the same RNA that was used for the microarray experiment was also utilized to perform a real-time PCR in order to assess the reliability of the

microarray data (Appendix Seven). In addition, at least two further biological repeats were generated to reconfirm the results (Table 4.9).

The transcriptional responses of the 11 genes from the microarray were quantified of which 10 exhibited a similar expression pattern to the fold changes determined by the microarray analysis (Appendix Seven). Quantifying the relative mRNA expression of these genes via two platforms (microarray and RT-PCR) verified the general validating of global microarray experiment. Three genes were down-regulated upon exposure of the worms to *H. gordonii* extract and the response was most significant in F49E10.2, a nematode protein of unknown function. The suppression levels of *cdh-12*, which encodes a cadherin predicted to be involved in cellular adhesion, was similar to *col-41*, a cuticle collagen gene (Appendix Seven).

Regarding the induced genes, the expression of Y62H9A.5 exhibited the highest fold change, however to date no studies have further analyzed this nematode-specific protein of unknown identity. Furthermore, *fat-5*, a gene involved in lipid and fatty acid pathways, was modestly but robustly induced and was chosen for further studies, mainly due to its involvement in lipid metabolism as well as sharing homology with mammalian SCD-1. The expression of *acl-12*, an ACyLtransferase-like gene involved in lipid storage and metabolic processes, was moderately up-regulated in nematodes treated with *H. gordonii* extract (Table 4.9).

Moreover, several collagen-related genes were up/down regulated as displayed earlier (Tables 4.1 to 4.7), genes that are mainly activated during the development of the animal (larvae to adulthood). Here, the transcriptional response of *col-19* was assessed and it was shown to be induced significantly

(Table 4.9). In addition, EEED8.3, which encodes a protein with similarities to fatty acid binding protein (Piano et al., 2002), was observed to be strongly up-regulated in response to *H. gordonii* extract treatment (Table 4.9). As explained previously, the gene expression profiles of biological repeats followed the same general trend as the microarray outcome however, the quantification (in absolute terms) was not the same, perhaps because of different sensitivities of each platform.

| | ***H. gordonii* treatment (mg/mL)** | | | | | |
|---|---|---|---|---|---|---|
| | **Microarray** | | **RT-PCR the same RNA as for the microarray** | | **RT-PCR using Biological repeats** | |
| **Gene** | **0.01** | **0.1** | **0.01** | **0.1** | **0.01** | **0.1** |
| Y62H9A.5 | 4.4 | 7.0 | 1.8 ± 0.3 | 7.8 ± 0.6 | 2.9 ± 0.4 | 4.9 ± 0.4 |
| *fat-5* | 1.1 | 1.7 | 1.1 ± 0.1 | 1.7 ± 0.2 | 2.6 ± 0.3 | 3.6 ± 0.6 |
| *col-19* | 1.1 | 4.1 | 1.2 ± 0.2 | 4.8 ± 1.1 | 4.1 ± 0.8 | 4.7 ± 1.0 |
| *acl-12* | 1 | 1.4 | 0.8 ± 0.0 | 1.5 ± 0.1 | 0.4 ± 0.0 | 0.7 ± 0.0 |
| EEED8.3 | 2.2 | 4.0 | 2.2 ± 0.6 | 4.0 ± 0.6 | 0.2 ± 0.0 | 0.3 ± 0.0 |

**Table 4.9 Relative expression levels of selected genes from the microarray data compared to RT-PCR analyses in response to *H. gordonii* extract.** The transcriptional responses of five genes was quantified by RT-PCR in response to the extract, using two biological populations and at least three technical repeats. Each data point is the average fold change of the gene ± the standard error of the mean (SEM) except for the microarray values.

## 4.4 Discussion and Conclusions

*Hoodia gordonii* extract was previously suggested to have appetite suppressant and thirst-quenching effects on African hunters of the Kalahari Desert (Dall'Acqua and Innocenti, 2007, Van Heerden, 2008). The flood of media attention towards the weight-loss property of this plant extract also attracted the scientific community to unravel the mechanisms by which *H. gordonii* extract alters the normal physiology and metabolism of mammalian organisms. However, the possible side effects and cross activity of the extract have, to date, not been fully explored. To address this need, life history traits were assessed in wild-type nematodes exposed to extracts of the *H. gordonii* plant.

*E. coli* OP50 is the standard food source for the nematodes and since *H. gordonii* extract was supplemented via the bacterial food source, it was of interest to assess whether the plant extract affects bacterial growth, in order to rule out the presence of harmful secondary metabolites and/or indirect triggers. Concentrations above 1 mg/mL extract affected the growth of *E. coli* OP50 moderately. Thereafter, developmental changes of wild-type worms treated with the same doses of *H. gordonii* extract were studied by which effects became distinct after 72 hours of the exposure in 10 and 100 mg/mL groups and extended exposure also increased lethality on nematodes. Because of the influence of *H. gordonii* extract on *E. coli* OP50 growth and the toxic consequences on the worms, the maximum administrated concentration of the extract was set at 0.5 mg/mL throughout this project.

Several phenotypic properties of the nematodes were investigated including feeding/defecation rates, growth, lipid storage, reproduction and survival. The pharyngeal pumping rate was reduced in nematodes exposed to *H. gordonii*

extract. However in contrast, the defecation cycle did not change in animals upon the extract treatment. A reduced pumping rate could be due to *H. gordonii* extract directly affecting the food sensory neurons of the worms, the hypothalamic neurons, or perhaps by influencing the serotonergic responses. Alternatively, the reduced pharyngeal phenotype could be due to changes in food quality as the *H. gordonii* extract was mixed with the OP50 and incubated overnight to generate the food lawn. In consequence, *H. gordonii* may have altered the taste, smell or the consistency and quality of the bacterial food, resulting in the production of a less desirable food source (Hills et al., 2004).

The overall size of the wild-type animals was also significantly influenced by *H. gordonii* extract exposure. The treated *C. elegans* exhibited a reduced body surface area and since the body length of the nematodes did not increase upon exposure to the plant extract, it could be concluded that nematodes did not enter the dauer stage, the defense pathway to avoid undesired conditions (Wood, 1988b, Wood, 1988a).Therefore, the designated concentrations of *H. gordonii* extract were sufficiently effective to alter physiological responses yet did not induce severe stress.

Wild-type nematodes exposed to *H. gordonii* extract also exhibited reduced Nile Red fluorescent staining within the areas believed to be fat reservoirs (intestine and under the skin-like epidermal cells). The reduction in relative fluorescent intensity has been compared to lower lipid content similar to weight reduction in mammalian studies (Vermaak et al., 2011a, Vermaak et al., 2011b). The obtained data is consistent with other findings including the Lemieux et al., 2011 study where the Nile Red staining procedure was utilized to identify lipid regulatory genes in response to a variety of chemical compounds. However, the vertebrate

and invertebrate respond to *H. gordonii* extract by means of distinctive physiological and behavioral pathways (Lemieux et al., 2011, Brohard et al., 2012).

Nematodes overcome stress-inducers by physiological and phenotypic modulations that reduce the potential side effects. Upon application of *H. gordonii* extract, the fecundity progressively decreased, at a concentration of 0.5 mg/mL the number of viable progenies was reduced to 58% of untreated control. This outcome was perhaps due to the fact that the nematodes exhibited significantly reduced number of Nile Red stained compartments (likely to be the major fat reservoirs), therefore limiting the stored energy to be spent on reproduction until conditions improved. This hypothesis is also supported by other studies, where it is believed that reproduction is regulated by an adaptation strategy during dietary restriction. Upon which energy becomes re-allocated to maintain somatic cells, in some cases an extended survival and delaying/extending reproduction period until survival conditions improve (Shanley and Kirkwood, 2000, Vilchez et al., 2012). Moreover, eggs contain a large amount of fat to supply energy for the next generation until the larvae hatch, hence a reduced fat content means less available energy for the progenies, resulting in a compromized reproductive output (Heine and Blumenthal, 1986).

It was of interest to assess whether the proposed anorectic effects of *H. gordonii* extract would lead to longevity in nematodes. Some mammalian studies have already proven a correlation between life extension and calorie restriction, however this hypothesis needs to be studied in more detail. In *H. gordonii* extract-treated animals, the median lifespan of the worms was not affected and although the nematodes displayed some calorie restriction mimetic features, such

as the reduced pharyngeal pumping rate, no extension was observed in the survival of *H. gordonii* extract-treated nematodes. This suggested that the calorie restriction did not necessarily result in an extended lifespan and the mechanisms are more complex than a simple direct correlation between fat regulatory pathways and longevity.

Genome-wide approaches such as microarray and RNAi have facilitated reverse genetic studies over the last two decades. Large scale transcriptomics have offered a non-biased assessment of molecular genetic pathways involved in response to different chemicals, pollutants, natural compounds and etc. (Pietsch et al., 2012). In the past it has been stated that microarray studies rely on the use of replicates (Groen, 2001). Due to the financial restrictions, this project did not utilize technical replicates but instead used replicates of several doses of *H. gordonii* extract exposed nematodes. The assessment of molecular responses was performed on the raw signals generated by the GeneChips arrays using MAS5.0 linear data processing. Once GO terms were explored, it revealed that *H. gordonii* extract treatment mainly targets the development, fecundity and lipid metabolism, lipid regulation/transport and cuticle-related molecular processes.
Further scrutinized genes included *fat-5, acl-12* and EEED8.3, which are involved in lipid storage, lipid metabolic processes or fatty-acid modulations. As the prime aim of the research was to study lipid-regulatory genes with mammalian homologs, the nematode-specific genes were excluded to simplify the approach.

The RT-PCR platform confirmed, at large, that the results obtained from the Affymetrix® arrays were reliable and reproducible. Nevertheless, the absolute levels of transcriptions differed.

Transcriptional response of *H. gordonii* extract-induced genes that are involved in metabolism, such as EEED8.3 is responsible for encoding a protein with similarity to fatty acid binding proteins (FABPs) and has several *H. sapiens* orthologs (FABPs) that are listed in the wormbase. Previous RNAi studies had resulted in 20-30% embryonic lethality when EEED8.3 was knocked down (Piano et al., 2002). Furthermore, *col-19* was also significantly induced upon exposure to different doses of the *H. gordonii* extract. This COLlagen gene belongs to the superfamily of *col-* genes, which has 165 members, and is essential for the normal structure of the alae (GO terms information adapted from the wormbase). An ACyLtransferase-like protein coding gene, *acl-12*, is approximately 26% orthologue to the human LPGAT1 (Information adapted from Ensembl) , an Acyl-CoA lysophosphatidylglycerol acyltransferase 1 that catalyzes the reacylation of phosphatidylglycerol and is a membrane phospholipid responsible for the synthesis of cardiolipin (Yang et al., 2004). Moreover, one of the CaDHerin family members, namely *cdh-12* is predicted to have cellular adhesion function that is modulated upon *H. gordonii* extract exposure.

A key metabolic-related gene selected for the follow up studies was *fat-5*, a delta-9 fatty acid desaturase that has 39% homology with the *H. sapiens* Acyl-CoA desaturase (Shanklin et al., 1994, Watts and Browse, 2000). The following chapters will discuss in detail *fat-5*'s in response to pure P57 treatment (the

active compound from *H. gordonii* extract). Thereafter, the *fat-5* genetic network is explored with the aim to find putative links between metabolic and nutrient-sensing pathways.

It could be argued that results obtained were either due to direct effects of the *H. gordonii* extract or because the dried plant extract purchased contained other ingredients including lubricants and sugar-based additives (Cellulose, Magnesium Stearate and Silican Dioxide). Since others have confirmed Van Heerden's work (Steyn et al., 1989, Deng et al., 2005, Van Heerden, 2008) that there is one major active compound in the plant extract, namely P57, it was important to compare and contrast the outcomes of *H. gordonii* extract treatment with those of the pure P57 exposure. The following chapter discusses the characteristics of P57 exposure both on life history traits and molecular responses of the nematodes.

# Chapter Five

*Life history traits and genetic responses of P57 treatment*

# 5 Life history traits and genetic responses of P57 treatment

## 5.1 Introduction

From 1990 to 2000 *Hoodia* species received a significant amount of commercial attention mainly due to the proclaimed anorectic properties of the plant from the pharmaceutical industry (Phytopharm, Unilever and Pfizer), (Vermaak et al., 2011b). However, further investigations were needed to pinpoint the active phytochemical compounds. Data obtained from analytical studies was dependent upon the species of *Hoodia* being tested hence here only the *Hoodia gordonii* species will be discussed (MacLean and Luo, 2004). Lyophilized aerial parts of *H. gordonii* were tested and NMR[16] and HPLC[17] methods were applied to isolate and characterize the major active compound as a steroid glycoside, named P57 (Van Heerden et al., 2007, Vermaak et al., 2011a, Vermaak et al., 2011b). The structure was determined by HR-MS[18] and 1D- and 2D-NMR spectroscopy (Figure 5.1).

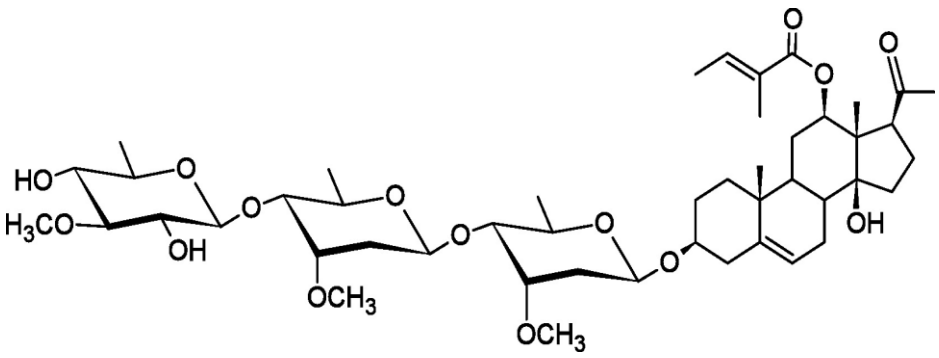


**Figure 5. 1 Pure P57.** The image is adapted from (Vermaak et al., 2011b).

[16] Nuclear Magnetic Resonance spectroscopy
[17] High-performance liquid chromatography
[18] High Resolution Mass Spectrometry

Rodent studies have suggested that P57's major site of action is the Central Nervous System (CNS). The appetite suppressant effects are induced via hypothalamic neurons, which increase ATP content by 50-150% in the hypothalamus. When P57 is injected to the ventricle, food consumption is reduced for a period of 24 hour (40-60%) and the ATP content is subsequently increased in return (MacLean and Luo, 2004).

## 5.2 Aims

Experiments of this chapter were designed to study the effects of P57 exposure on several life history parameters such as growth, reproduction, survival and neuromuscular properties including the pharyngeal pumping rate. Moreover, to compare and contrast the concentration-dependent effects between *H. gordonii* extract exposures (Chapter Four) and the treatment with the purified P57. Furthermore, it was deemed important to explore whether the dietary restriction mimetic imposed by P57 treatment result in longevity in *C. elegans*.

## 5.3 Results

### 5.3.1 *H. gordonii* extract

Following LC-MS [19] studies performed by Vermaak and colleagues, it was reported that 0.304% of the plant material is the active compound P57 (Vermaak et al., 2011a, Vermaak et al., 2011b).

The approximate amount of P57 present in each *H. gordonii* capsule was determined based upon the information provided by the RedRose manufacturing company (UK). Each capsule contained the equivalent of 10,000 mg of *H. gordonii* plant, and contained 500 mg extract of which 0.3% was taken to be P57 (Vermaak et al., 2011a, Vermaak et al., 2011b). Hence, the stock solution of *H. gordonii* extract prepared as in Chapter Four (equivalent to 2000 mg/mL) was estimated to contain 6 mg/mL P57.

### 5.3.2 Pure P57 compound

Pure P57 was dissolved in 5% methanol (MeOH) as the vehicle. One mg of P57 was dissolved in 50 µL of methanol and diluted in dd$H_2O$ to a final concentration of 1 mg/mL (stock solution). For each assay, in order to reach the designated final working solutions, P57 was diluted in *E. coli* OP50 and NGM agar plates were seeded with the mixture of OP50/P57 and allowed to grow overnight before putting the nematodes on the plates. Concentrations of P57 were 0.03 and 0.3 µg/mL to correlate with the *H. gordonii* extract doses utilized in Chapter Four. To exclude the potential effects of MeOH on P57-dependent responses, the amount of MeOH in the highest concentration was determined and added to

[19] Liquid Chromatography/Mass Spectrometry

control as well as the lower dose exposures to have a normalized amount of MeOH within all three experimental groups (0.0015% MeOH). Previous studies had confirmed that an exposure to 5% MeOH is not toxic to nematodes (Thomson and Pomerai, 2005), and in these experiments all treatments contained MeOH concentrations of 0.0015%, i.e., well below the toxic threshold.

### 5.3.3 Neuromuscular pharyngeal pumping rate is modulated by P57 and *H. gordonii* extract exposures

An initial experiment was performed to explore the pharyngeal pumping rate when wild-type nematodes were exposed to either P57 or *H. gordonii* extract to determine equivalence between the two test samples.

The pharyngeal pumping assay was performed by exposing nematodes to 0.1 mg/mL *H. gordonii* extract or pure P57 at 0.3 μg/mL (as the theoretically calculated concentration of P57 in the plant extract) and 0.0015% MeOH as the control. In detail, the pharyngeal pumping of 30 age-synchronized nematodes were determined at the 96 hours post-hatch being exposed to either P57 or *H. gordonii* extract. In both cases of *H. gordonii* extract and P57 compound treatments, animals experienced a significantly reduced pharyngeal pumping rate when compared to the control (Figure 5.2).

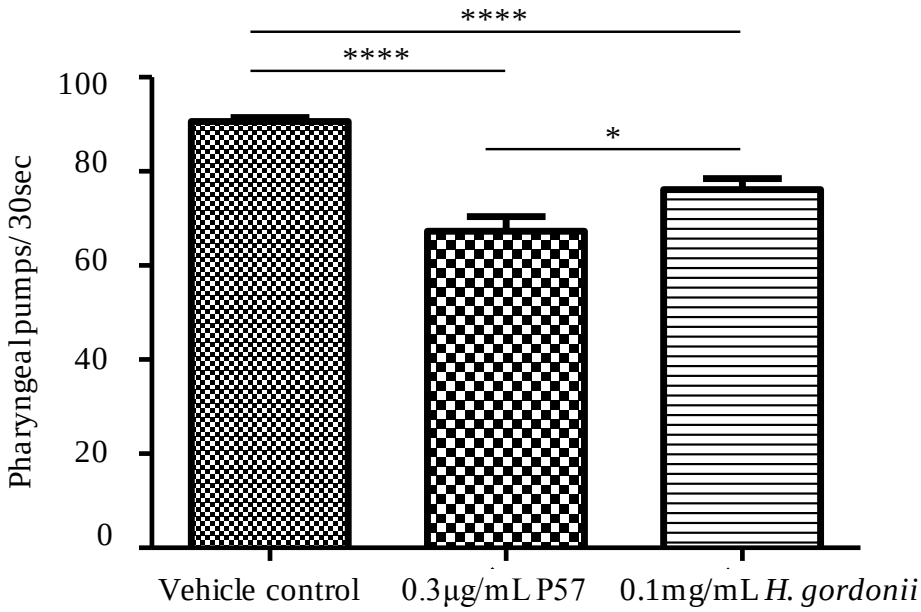


**Figure 5.2 Pharyngeal pumping rate comparison between *H. gordonii* extract and P57 exposures.** The concentrations used were chosen assuming 0.3% of the *H. gordonii* extract was pure P57 (Vermaak et al., 2011a, Vermaak et al., 2011b). Wild-type nematodes were characterized by a significantly reduced pharyngeal pumping rate upon P57 or *H. gordonii* extract exposure, however the response was more pronounced in the P57-exposed nematodes. This assay was performed for one time point (96 hours post-hatch). Each bar graph represents the average pharyngeal pumps of 30 nematodes ± the standard error of the mean (SEM). Data were analyzed using a one-way ANOVA and revealed that the statistical differences were more pronounced in P57 exposure (* $p \leq 0.05$, **** $p < 0.0001$).

### 5.3.4 Pharyngeal pumping is regulated by exposure to P57 in wild-type nematodes

The preliminarily screen to assess the nominal P57 concentration in the *H. gordonii* extract by pharyngeal pumping rate confirmed the notional P57 percentage in the extract (as explained in 5.3.3). Thereafter, pharyngeal pumping rate was determined upon P57 treatment in wild-type nematodes for a period of four days. In total, 30 age-synchronized nematodes were observed per exposure condition (three biological replicates of 30 worms). P57 treatment resulted in a severe reduction in the number of pumps per 30 seconds. A vehicle control

(OP50 supplemented with 0.0015% MeOH) was prepared in addition to two doses of P57 (0.03 and 0.3 μg/mL). In general, the pharyngeal pumping rate increases during the larval stages and reaches a peak at day-1 adulthood and subsequently decreases as the animals age (Riddle et al., 1997).

In this study, the pharyngeal pumping was assessed from 48 hours post-hatch until 120 hours and a significant decrease in the pumping rate was observed in nematodes exposed to P57 compound (Figure 5.3). When data were statistically analyzed, assessed using a two-way ANOVA and Bonferroni multiple comparisons test, it was concluded that treatment with 0.03 μg/mL of P57 the pumping rate was reduced progressively in comparison to the vehicle control, with the most significant reduction (25%) being observed at 48 hours post-hatch. A similar trend was apparent in nematodes challenged with 0.3 μg/mL P57, effects being most pronounced at L4 stage. Once animals started aging the influence of P57 on pharyngeal pumping rate became less significant (Figure 5.3) especially at the lower concentration of P57. There was a 10% and 14% reduction in the feeding rate of 0.03 and 0.3 μg/mL P57-treated animals, respectively when analyzed at 72 hours post-hatch, with similar results observed at 96 hours post-hatch animals. However, at 120 hours post-hatch only the higher P57 dose (0.3 μg/mL) induced a statistically significant reduction in pharyngeal muscle contractions (compared to control worms).

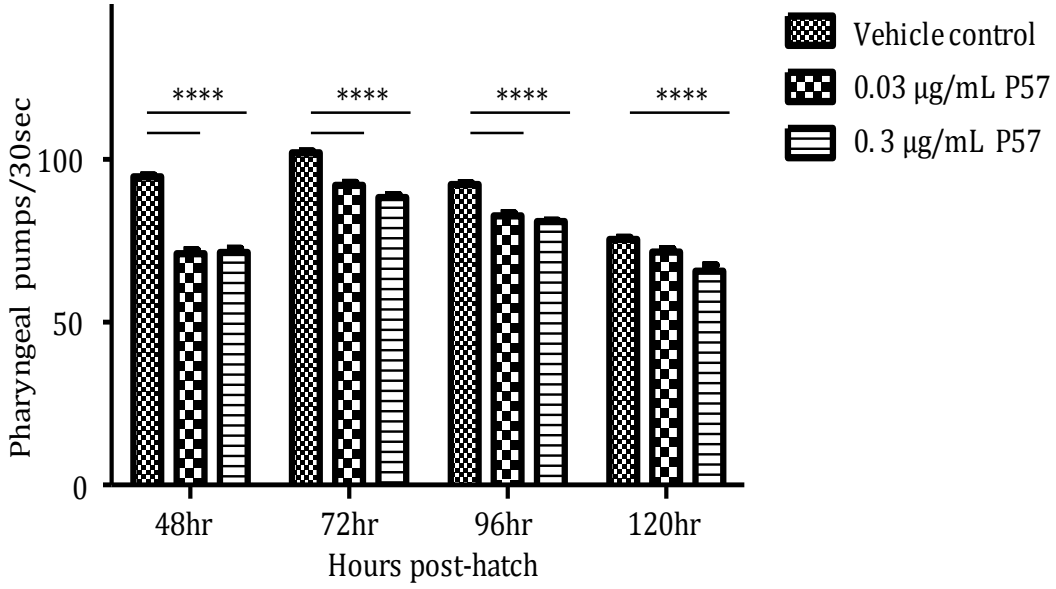


**Figure 5.3 Pharyngeal pumping in wild-type nematodes treated with P57.** The neuromuscular pharyngeal pumping rate was determined over a period of four time points (48, 72, 96 and 120 hrs post-hatch). P57 treatment significantly reduced the pharyngeal pumping rate in nematodes. A two-way ANOVA followed by Bonferroni post-test was performed on the data to pinpoint the significance levels compared to the untreated controls. Each bar is the average feeding rate measured in 30 individual worms ± the standard error of the mean (SEM) *(**** $p < 0.0001$).*

### 5.3.5 Exposure duration affects the P57-dependent pharyngeal pumping response in wild-type nematodes

The responses towards environmental changes can vary in animals of different developmental stages. To assess whether the duration of exposure affected pharyngeal pumping rate, worms were exposed to P57 after reaching the L4 stage as well as exposure from the L1 stage (stated as chronic exposure). In order to have an acute effect, the selected concentration of P57 was 10 fold higher than what had been used throughout the other assays (i.e., 3 µg/mL). The pharyngeal pumping rate was measured daily starting from L4 stage (48 hours post-hatch) for four days. Both the controls and P57-exposed nematodes followed the normal

pharyngeal pumping pattern by which the pharyngeal muscle contractions increased during the development of the nematodes, reached a peak at 72 hours post-hatch (day-1 adulthood), the trend was followed by a reduction in the pharyngeal pumping rate upon aging (Figure 5.4). The chronic exposure group was treated with 3 μg/mL P57 from L1 stage and served as a positive control. In comparison, the acute P57 exposure nematodes were maintained on control plates until L4 stage and then treated with P57. Nematodes that were exposed to the compound from L1, had the most significant reduction in the pharyngeal pumping rate at 48 hours post-hatch (as observed in section 5.3.4), however the effect was reverted at 72 hours post-hatch and nematodes of this group had a considerably higher pharyngeal pumping rate in comparison to the control group, an effect that could be due to a compensation mechanism.

When the L4 exposure group of worms was compared to the control group, there were no significant changes observed in the number of pharyngeal pumps per 30 seconds until the 120 hours post-hatch (Figure 5.4). The statistical analysis was performed by a two-way ANOVA following Bonferroni *post hoc* test and the difference was determined to be significant ($p < 0.05$). However, at day-1 adulthood the acutely P57-treated nematodes (L4 exposure) reached a higher pharyngeal pumping rate in comparison to the controls (statistically insignificant) (Figure 5.4).

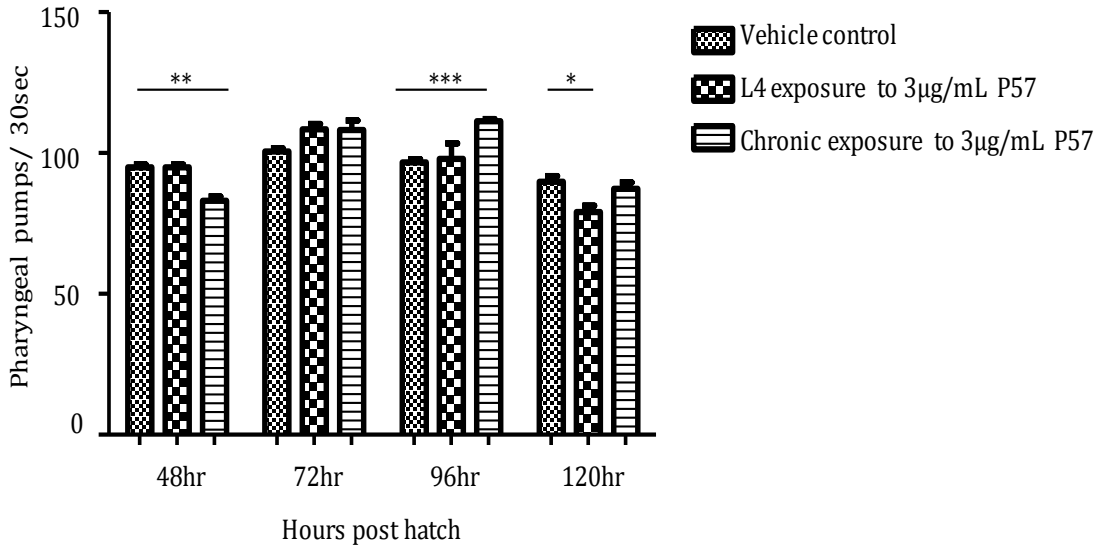


**Figure 5.4 The effects of exposure period on the feeding rate of P57-treated nematodes.** Pharyngeal pumping rate was measured for the duration of four days from the L4 stage under three experimental conditions, a control group, a chronic exposure group (L1 exposure), as well as an acute dose of P57 starting the exposure from the L4 stage. When the pumping rate was quantified in the L4 exposure group the average rate did not differ from the untreated group until the 120 hours post-hatch. Whereas, the positive control group (chronic exposure) had a significant reduction at 48 hours post-hatch, however the effect was reverted from the 72 hours post-hatch. Each bar graph represents the mean pharyngeal pumping of 30 individual nematodes and the standard error of the mean (±SEM), statistical analysis was performed using a two-way ANOVA with Bonferroni *post hoc* test *(* $p < 0.05$, ** $p < 0.001$, *** $p < 0.0001$*).

Conclusively, P57 influences the neuromuscular pharyngeal pumping rate in wild-type nematodes in a duration-dependent manner. Because when the pharyngeal muscle contractions were measured for a period of four days, results indicated that the exposure time and the stage in which nematodes are exposed to P57 are both important factors. This phenomenon is because of the observed evidence upon treatment with P57 at the end of larval stages (L4 stage) stimulated no immediate reduction in the pharyngeal pumping.

### 5.3.6 Development is affected in wild-type nematodes treated with P57

To assess the potential effects of the appetite suppression on the development of *C. elegans*, a six-day growth assay was performed on nematodes maintained in the presence and absence of P57.

Nematodes were age matched, plated on designated P57 plates (control, 0.03 and 0.3 μg/mL P57) and 20 individual nematodes were photographed from 24 hours post-hatch until 144 hours. The body length and body area of each worm was traced at the different stages using the Image Pro-Express® software. Data were assessed by means of two-way ANOVA statistical analyses with Bonferroni multiple comparisons (Figures 5.5 and 5.6 and Appendix Eight).

#### *5.3.6.1 The length of the nematodes decreases upon treatment with P57*

As nematodes develop, length and volumetric surface area increase until they reach adulthood. The control nematode group grew into adults and reached the plateau length within three days (72 hours post-hatch), when length was determined in P57-treated nematodes despite the overall significant decrease there was neither a delay nor any noticeable dauer formation witnessed in the treatment groups (Figure 5.5). A continuous effect was observed in the two doses of P57 with the most pronounced statistical difference in 0.3 μg/mL P57-exposed samples ($p < 0.001$) at 144 hours post-hatch.

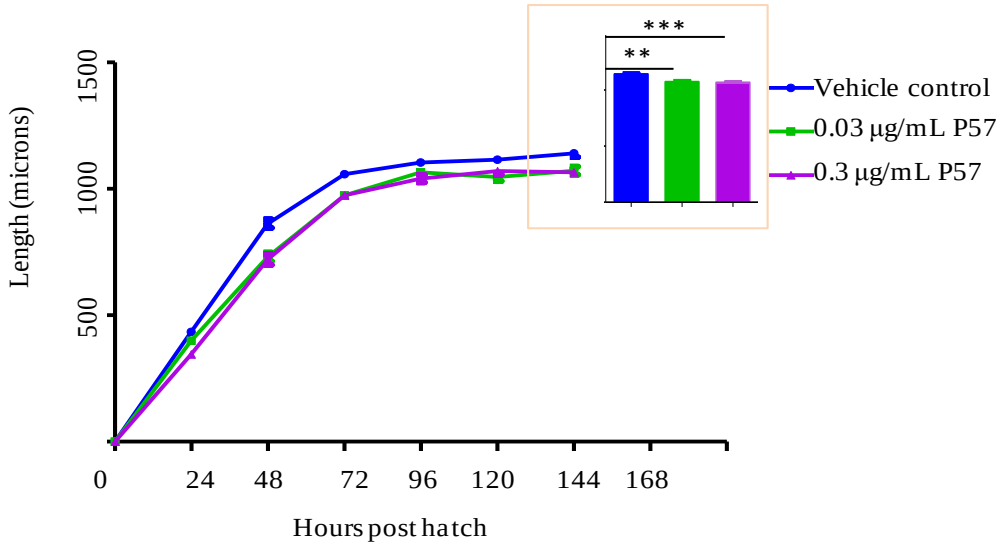


**Figure 5.5 Developmental change (body length) of *C. elegans* maintained in the presence or absence of P57.** Animals were studied for a period of six days and the length was traced using Image Pro-Express® software. Data were assessed for statistical differences using a two-way ANOVA (** $p < 0.01$, *** $p < 0.001$) and the length of P57-exposed animals was reduced progressively in comparison to the unexposed controls. Each data point represents the average length of 20 worms ± the standard error of the mean (SEM) of three independent biological repeats.

### *5.3.6.2 Surface area of the nematodes is progressively reduced in response to P57*

As well as the length of the nematodes, body area changes (i.e., volumetric surface) were also quantified following an exposure to P57. Similar to the length, the body area of wild-type animals increases from L1 stage until the animals reach day-1 adulthood. Untreated nematodes reached the final body area within approximately 96 hours post-hatch (Figure 5.6). In 0.03 and 0.3 µg/mL P57 treatment groups, a significant reduction in the overall body area of the worms was observed. The body surface area was reduced by 14% upon treatment with P57, although there was no significant dose-dependency between 0.03 and 0.3

µg/mL P57. Bonferroni multiple comparisons revealed that the observed reduction was statistically robust ($p < 0.0001$) thus confirming the significant modulation of volumetric size upon P57 treatment.

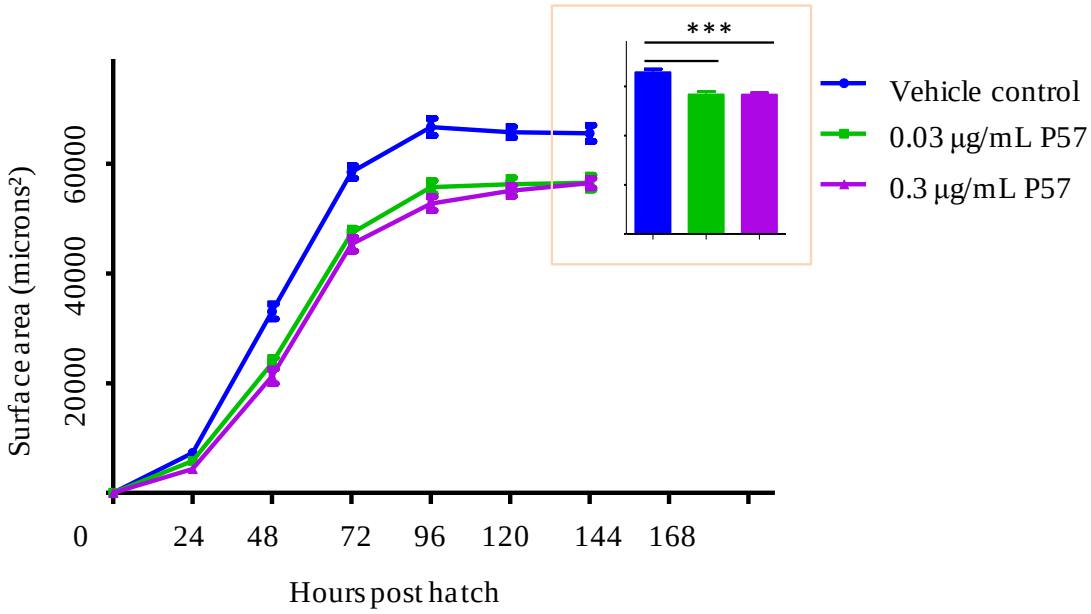


**Figure 5.6 Changes in volumetric surface area over time.** The body area was traced for six days after hatching (144 hours). P57-treated nematodes exhibited a significant reduction in overall body volume however this was not dose-dependent. Each data point represents the average surface area of 20 individual nematodes ± standard error of the mean (SEM) from three independent biological trials. A two-way ANOVA statistical analysis was performed on the data to pinpoint the difference between conditions (*** $p < 0.001$).

### 5.3.7 Nile Red dye uptake is reduced in P57-treated wild-type nematodes

Exposure to P57 resulted in a reduced rate of pharyngeal pumping and an overall reduction in the length and volume of the body. To observe the influence of P57 exposure on the Nile Red staining pattern of the nematodes, wild-type worms

were treated with P57 and Nile Red in addition to the untreated counterparts (section 2.3.7.1). As addressed in Chapter Three, there are several debates in regards to the accuracy of the Nile Red vital dye in targeting the lipid droplets. However, it was confirmed that Nile Red is capable of targeting certain types of fatty acids yet it is not a universal dye for lipid droplets.

The animals were treated with both the dye and P57 and the relative intensity of red fluorescence was assessed after 72 hours via a wide-field microscope (Nikon Eclipse TE2000-S, Japan). All images were taken from the anterior end of the animals to the vulva. The staining procedure was applied on two biological repeats, yet the data were neither reproducible nor comparable to the *H. gordonii* extract exposure (Appendix Nine). Under control conditions, nematodes exhibited a normal distribution of Nile Red positive compartments whereas in P57-treated nematodes there was a significant inconsistency observed within the worms of the same treatment concentration making it impossible for further quantification.

### 5.3.8 Reproduction of the wild-type *C. elegans* is influenced by P57 application

When nematodes were exposed to *H. gordonii* extract, the total number of viable progeny was affected with a statistical significance in comparison to the untreated group. To ascertain whether P57 had a similar influence on the progeny number of the exposed animals, brood size was determined within a period of six days after the worms had reached the L4 stage.

Nematodes were treated with two doses of P57 equivalent to the previously applied *H. gordonii* extract concentrations as well as a control. The daily reproduction was determined for all conditions and the untreated group exhibited a normal Gaussian distribution in which the egg-laying peak was defined between days three and four (Figure 5.7). When P57-treated nematodes were compared to the untreated group, in the low concentration of P57 (0.03 µg/mL) the Gaussian distribution of the egg laying period was not affected and the peak was as determined in the control group (Figure 5.7). However, when exposed to 0.3 µg/mL of P57, the peak was more shifted to the 120 hours post-hatch (Figure 5.7). After 120 hours in all three conditions reproduction was declined at the same pace.

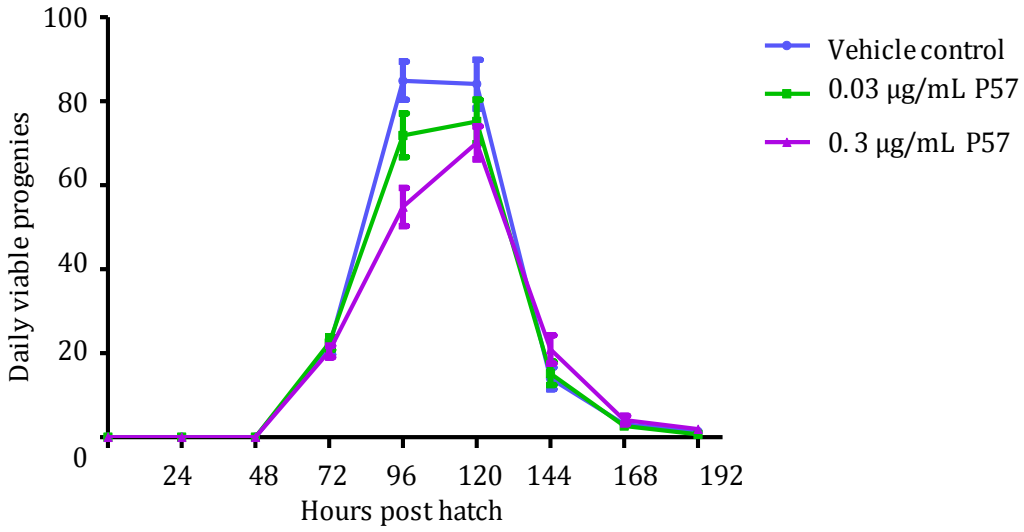


**Figure 5.7 Daily reproduction of P57-treated wild-type nematodes in comparison to untreated controls.** Egg production peaked at 96 hours post-hatch for the vehicle control worms. Upon treatment with the high dose of P57 the peak day was shifted to 120 hours whereas no significant difference was observed in the lower dose of P57 treatment. The difference was most pronounced at 96 hours post-hatch of P57-exposed nematodes. Each data point represents the average daily reproduction output of 26-36 individual nematodes ± the standard error of the mean (SEM).

A single hermaphrodite *C. elegans* nematode (wild-type) is capable of producing up to 300 eggs over a six-day period when kept under optimum laboratory conditions and most eggs are laid between 72 to 120 hours post-hatch (Figure 5.7).

The total number of viable progeny was determined in nematodes raised in the presence and absence of P57 (Figure 5.8). The total progeny number of control nematodes was 212 ± 9, however P57 treatment significantly decreased the fecundity in *C. elegans*. A low dose of P57 (0.03 μg/mL) reduced the total progeny output by 13% and the 0.3 μg/mL P57 exposure resulted in an 18% drop in reproductive performance, suggesting that the influence was dose responsive (Figure 5.8). Statistical analyses were carried out by employing Bonferroni multiple comparison *post hoc* test to quantify the degree of significance and showed that P57 exposure decreases the fecundity in nematodes with $p < 0.01$ and $p < 0.001$ in 0.03 and 0.3 μg/mL, respectively (Figure 5.8).

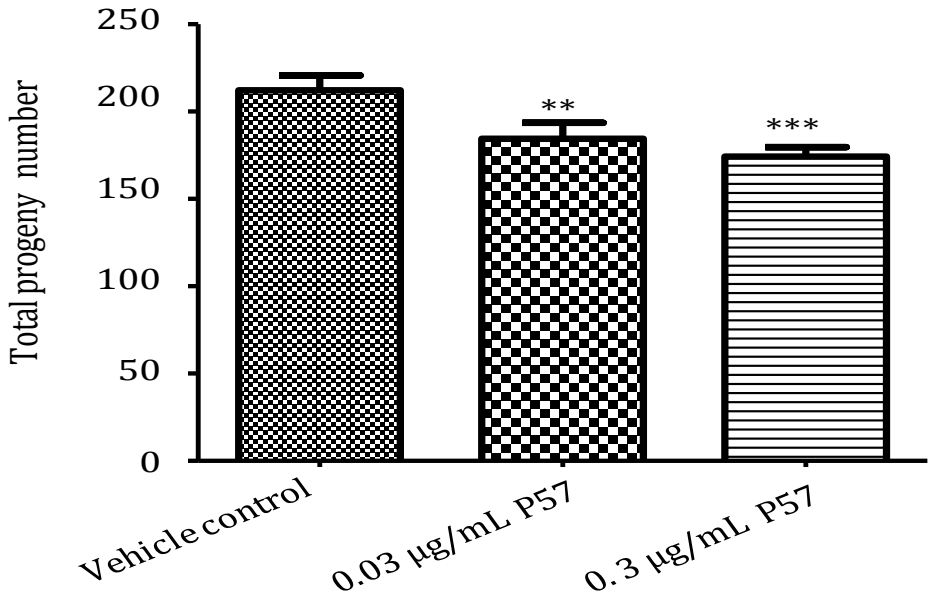


**Figure 5.8 Total progeny number of wild-type nematodes raised in the presence and absence of P57.** Untreated worms produced approximately 210 progeny whereas the total progeny number of P57-exposed animals was affected significantly. Each bar chart displays the mean brood size ± standard error of the mean (SEM). Bonferroni multiple comparisons confirmed the statistical significance in comparison to the vehicle control worms (** $p < 0.01$, *** $p < 0.001$).

### 5.3.9 Lifespan is extended in wild-type nematodes treated with P57

As changes in the diet of *C. elegans* can influence aging, it was deemed important to assess the effect of P57 treatment on lifespan. Untreated Wild-type nematodes had a median lifespan of 12 days whereas median lifespan was extended by 24 hours as worms exposed to 0.03 µg/mL P57. The 0.3 µg/mL P57-treated group was marked by a 48-hour extension in the median survival (Figure 5.9), nevertheless P57 application did not influence the maximum survival of the nematodes. Statistical analysis utilizing the Log-rank (Mantel-Cox) method (Prism GraphPad v5 Software Inc., La Jolla USA) determined the difference

observed in the lifespan of the P57-treated *C. elegans* with a *p*- value of *0.001* (Figure 5.9). A table including the number of censored nematodes from analysis, median lifespan of worms under different conditions as well as p-values, is provided in Appendix Ten.

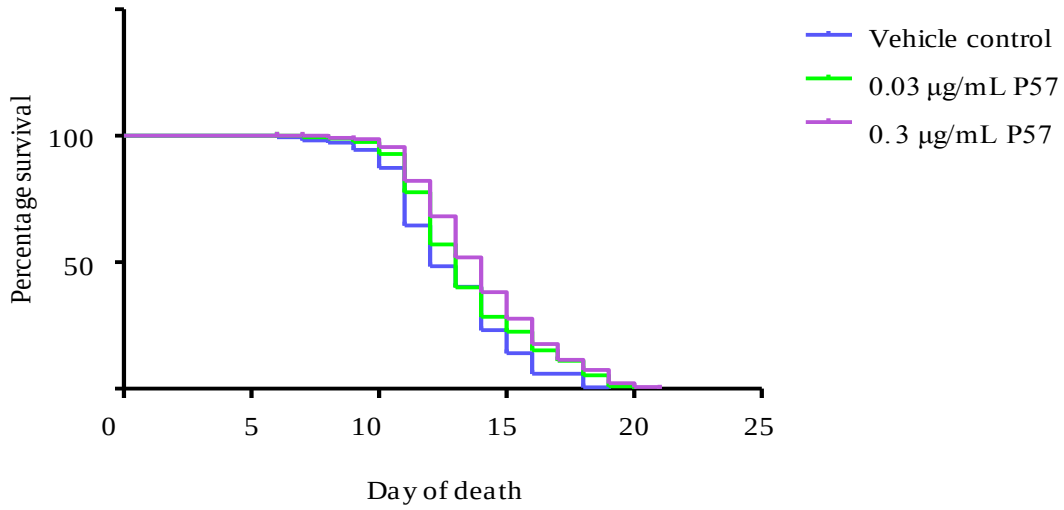


**Figure 5.9 Survival of the P57-treated wild-type animals in comparison to control nematodes.** The median lifespan (the time point at which 50% of the animals are alive) was extended in P57-treated worms. The treatment with P57 resulted in a 24 and 48 hours extension in the median survival of the animals with 0.03 and 0.3 µg/mL, respectively. The experiment was initiated with 400 nematodes and the death was scored daily ("lost" animals were censored) (*** $p < 0.001$). Note: there was no change in the maximum survival of the nematodes upon treatment with P57.

### 5.3.10 Impacts of P57 exposure on gene expression profile in nematodes

#### *5.3.10.1 Several genes are modulated in wild-type* C. elegans *upon treatment with P57*

Data obtained from experiments, which analyzed various phenotypic characteristics (pharyngeal bulb contractions, development, brood size and

lifespan) confirmed the correlation between *H. gordonii* extract and pure P57 exposures. The next step involved the assessment of the molecular level effects upon P57 treatment to provide an understanding of some underlying pathways involved in the metabolism of P57. To address this, wild-type worms were treated with 0.03 and 0.3 μg/mL P57 and the transcriptional responses of some genes were determined utilizing the real-time qPCR platform. Five genes, previously identified from the microarray study, were chosen namely Y62H9A.5, *fat-5*, *col-19*, EEED8.3 and *acl-12*. Nematodes were collected at L4 stage and the total RNA was extracted and complementary DNA (cDNA) synthesized. Thereafter, relative expression of selected genes was quantified after normalizing the data to the expression of *rla-1,* the invariant housekeeping gene. Each bar chart represents the average of three independent biological repeats. Expression levels were normalized to "1" under control condition for all assessed genes and the two doses of P57 were compared to the vehicle control of each gene (Figure 5.10). The expression of Y62H9A.5 exhibited a significant up-regulation by exposure to the P57 compound in a dose-dependent manner. When *fat-5* transcriptional response was quantified upon treatment with P57, the relative expression of the gene was marginally increased in the 0.03 μg/mL P57 group in comparison to a significant increase at the 0.3 μg/mL dose. Furthermore, the expression level of *col-19* was determined in P57-treated groups and the gene was strikingly induced in both concentrations. Nevertheless, a considerably high variation was observed amongst biological populations (Figure 5.10).

Moreover, the transcriptional level of EEED8.3, which shares similarities to fatty acid-binding elements, was also affected by P57 (Figure 5.10). However the effect was only observed in the low concentration (0.03 μg/mL P57). The

expression pattern of *acl-12* was investigated in the presence and absence of P57 that did not show any statistically significant changes from the control group. Although the gene was up-regulated in the presence of *H. gordonii* extract, there was no response to pure P57 therefore the gene was excluded from further studies (Figure 5.10).

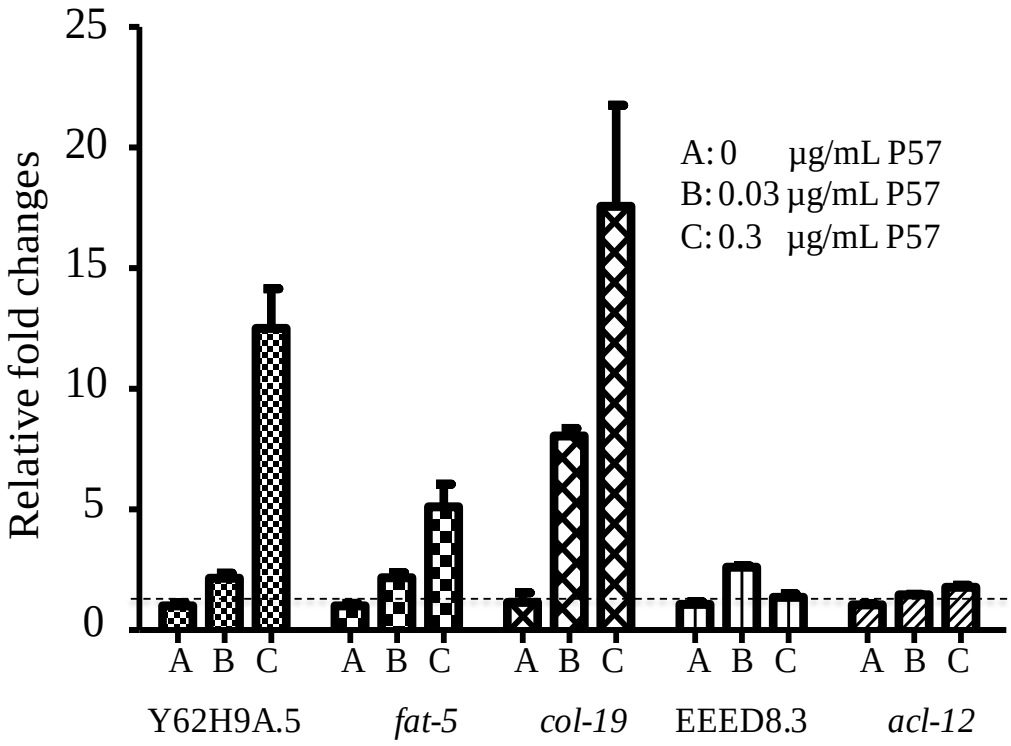


**Figure 5.10 Relative fold changes of selected genes quantified by RT-PCR in wild-type nematodes treated with P57.** The relative expression of five nominated genes that were previously confirmed to be responsive to *H. gordonii* extract (microarray and RT-PCR platforms) were assessed in P57-exposed animals. (A) The first bar chart of each set represents the expression of the designated gene under control condition (0 µg/mL P57), whereas (B and C) following bar charts display the expression of the gene exposed to 0.03 and 0.3 µg/mL P57, respectively. Each chart represents an average expression of the gene determined in three biologically independent populations with at least three technical repeats per condition ± the standard error of the mean (SEM).

## 5.4 Discussion and Conclusions

To date, P57 has been the only main active compound isolated from the *H. gordonii* extracts having anorectic effects (Van Heerden et al., 2007). As discussed previously, the study of bioactive compounds in *C. elegans* has returned useful information in regards to pinpointing effective pharmacological therapies. However it has also been shown that nematodes may not respond to pharmacologically active molecules under some circumstances (Gosai et al., 2010, Burns et al., 2010, Aitlhadj and Sturzenbaum, 2013). It was deemed to investigate whether P57, the active compound derived from *H. gordonii* plant extract, is capable of inducing similar dietary restriction mimetic effects in nematodes (as observed in mice model) and also if the nominated P57 concentration within the *H. gordonii* extract is equivalent to the directly applied pure P57 doses. The neuromuscular behavior, pharyngeal pumping, in *C. elegans* increases from the L1 stage to adulthood where the pharyngeal muscle contractions reach a peak in the day-1 adults (72 hours post-hatch). This pumping rate declines once the worms start the aging process upon which not only the number of pumps reduces but also the consumption of *E. coli* OP50 is affected as it has previously been shown to accumulate in the intestine without being digested (Riddle et al., 1997). When pharyngeal pumping of either *H. gordonii* extract or pure P57-exposed animals were determined, either treatment group of the nematodes exhibit anorectic effects with a significantly lower number of pharyngeal pumps. Direct exposure of P57 results in a progressively more severe reduction in the pharyngeal pumping rate of the wild-type animals in comparison to the *H. gordonii* extract treatment. The observed difference within P57 and *H. gordonii* extract exposures could be due to the fact that P57 is

a pure active compound whereas *H. gordonii* although is believed to be a purified extract, potentially contains additives that may decrease the efficiency of the active compound. Despite the variability in the effectiveness of pure P57 versus *H. gordonii* extract exposures, both applications induce similar dietary restriction mimetic effects on the pharyngeal pumping rate of the worms.

Moreover, the stage-specific P57 exposure reveals that the time point of exposure within the nematodes life cycle is important. A significant reduction in the pharyngeal bulb contractions rate is observed in nematodes that are exposed to the compound P57 at post-L4 stage. It becomes evident that the influence of P57 is most pronounced when animals are chronically exposed to the compound from the L1 stage onwards.

Another phenotypic property of P57-exposed wild-type nematodes is an overall reduction in the volumetric body area size by 14%. Since the length of the animals is also reduced proportionally upon P57 exposure hence the compound does not seem to induce dauer formation. Reductions in volumetric surface area as well as a substantially lower pharyngeal pumping rate suggest that P57 treatment might decrease the lipid metabolism in wild-type nematodes. This hypothesis was further studied through the Nile Red staining of the animals. As previously explained in details in Chapter Three, Nile Red vital staining may return contradicting results due to an overlap between some lysosome related organelles and lipid droplets. Yet, there is no universal dye that can stain fat droplets in the intact body of the nematodes, each staining procedure seems to target only certain types of fatty acids. Having said that, one hypothesis that may explain the observed inconsistency amongst the P57/Nile Red stained nematodes could be that, P57 does not necessarily target the intestinal lipid droplets. Instead

P57 exposure may affect the hypodermic fat stores, further analyses such as determining the triglyceride levels can be applied. This idea also sheds light on debates regarding the reliability of the vital dye Nile Red staining as utilizing only one method of staining may not be sufficient for visualizing all types of fatty acids and lipid droplets.

Reproduction is essential for passing the genetic information on to the next generation. Gravid hermaphrodite *C. elegans* start laying eggs from 72 hours post-hatch once an egg is laid it undergoes embryogenesis for approximately 10-14 hours until the larva hatches. Reproduction can be affected by several factors both environmentally and genetically, for instance pleiotropic mutations usually influence survival rate as well as changes in the metabolism, stress responsiveness and reproduction (Friedman and Johnson, 1988, Kennedy et al., 1995, Vanfleteren and De Vreese, 1994, Tissenbaum and Ruvkun, 1998). The brood size of nematodes is affected by changes in temperature and may result in sterility. It has been shown, via other studies such as Tissenbaum and Ruvkun (1998), that incubating the animals at non-favorable temperatures for a short period and later transferring them to optimum conditions results in their progeny numbers being affected. Exploring *C. elegans* reproduction serves as a sensitive tool for acute toxicity analyses without the need for sexual impregnation. The process of reproduction can highlight any effects caused by potential toxins directly on development and indirectly on the neuromuscular activity i.e., by egg laying (Boyd et al., 2010, Aitlhadj and Sturzenbaum, 2013).

Fecundity is a complex process that is in harmony with a variety of other motor programs and is shown to be regulated by feedback from motor-neurons to

interneurons in the head, which are responsible for forward movement (Aitlhadj and Sturzenbaum, 2013).

When the reproduction of P57-treated animals is assessed, the total number of viable progeny is significantly reduced however the Gaussian distribution of daily output as well as the length of the brood period of the worms are not influenced except of the highest P57-treated dose (0.3 µg/ml) where a delay in the start of reproduction period is observed. This influence on fecundity of P57-exposed nematodes suggests a toxic or stress inducer effect of the compound on wild-type nematodes.

More importantly, reproduction requires energy and that is provided mainly in the form of fat and vitellogenin proteins. Therefore, if certain fatty acids are reduced in P57-exposed worms, they may attempt to balance their physiology to compensate for the lack of stored energy and in turn reduce the energy allocation to generate offspring thus explaining the reduced number of brood. Unlike the *H. gordonii* extract-exposed samples where no lifespan change is observed, P57 alters and extends the survival rate by 24 and 48 hours at the low and high concentrations, respectively. Previously, several mammalian studies, specifically in rats and mice, reported a correlation between energy metabolism and the lifespan by which a dietary restriction resulted in an extended survival rate in test subjects (Finch and Morgan, 1990, Masoro et al., 1991), however to date, there is not sufficient supporting evidence in regards to a direct link between calorie restriction and longevity. Nonetheless, a small number of nutrient-sensing cells present in *C. elegans* (ASI neurons) and *Drosophila* (NMC cells) are partially or completely responsible for modulating the protective effects of calorie restriction to extend the survival of the animals. Yet a similar mechanism has not been

established in mammals, it has been shown that the mammalian hypothalamic neurons regulate several responses to food availability and deprivation resulting in dietary restriction mimetic effects (Broughton et al., 2010, Dacks et al., 2013). Nevertheless, in nematodes some high fat containing mutants such as *daf-2*, tend to live longer, and *daf-16* mutants which have a lower lipid profile tend to be longer lived (Tissenbaum and Ruvkun, 1998). Notably, the long-lived dauer form accumulates additional lipid droplets in the body. This study provides *in vivo* evidence that P57 exposure results in an extension of adult lifespan possibly linked to a dietary restriction mimetic pathway. However the longevity induced by calorie restriction is not fully understood and requires additional investigations.

Screening of the lifespan assays reveals that the median lifespan of control wild-type nematodes was determined to be 12 days whereas in previous experiments (Chapter Four), median lifespan was 15 days. This discrepancy within the same strain of nematodes (i.e., wild-type) observed under control conditions has already been discussed by Gems and Riddle (2000) and could be due to several reasons. Spontaneous mutations occur within the population of nematodes as well as environmental changes, handling and maintenance differences can result in differences within the same strain of the worms (Gems and Riddle, 2000, Qabazard et al., 2013). The experiments described in Chapters Four and Five were performed at different times and seasonal changes might have influenced the temperature in the laboratory during worm counting and transfers, then possibly accounting for the observed differences. Despite such variability, each experimental procedure was performed to include a vehicle control hence the observed effects of P57 treatment were deemed to be directly attributed to the

compound exposure. To date it remains to be seen whether any P57-derived *C. elegans* fat regulatory effects will exert similar results in other species despite some studies in rodents (MacLean and Luo, 2004). However due to the high level of conservation of the chemical structures of most enzymatic cofactors, metabolic intermediates, neurotransmitters and lipid-based signaling intermediates between organisms ranging from nematodes to humans any observations made in studies which utilize a single organism, such as the worm, could also be applicable to more complex organisms such as mammals and even humans.

Several gene and protein pathways are conserved between mammals and *C. elegans* including the serotonergic system linked to lipid metabolism (Aitlhadj and Sturzenbaum, 2013). Following the microarray analyses of control and *H. gordonii* extract-exposed nematodes, over 300 genes were shown to be transcriptionally modulated. From which five genes were selected for further studies. Extending this to P57-treated animals, data reveal that this molecule induces analogous responses. Notably, the fold changes in gene expression were more pronounced in the P57-treated animals in comparison to *H. gordonii* extract. This could be due to the fact that the crude plant extract capsule contains the active compound but also other additives that might potentially reduce its effectiveness. Key genes identified from the microarray experiment are involved in fat-regulation or are cuticle-related genes linked to lipid storage. The induction of *col-19* may be a consequence of lowered lipid content that can result in the development of a fragile hypodermis. In response the worm might over-express cuticle-related genes to protect its body from the environmental damage. Furthermore, EEED8.3 and *acl-12* are genes reportedly involved in the

regulation of fatty acids although *acl-12* is not statistically changed in P57-exposed animals, even though it is observed to be up-regulated by the *H. gordonii* extract treatment. The mechanisms by which pure P57 and the crude plant extract modulate the lipid metabolism may therefore differ in certain pathways.

The gene, *fat-5* has a human homolog allowing this fat regulatory gene to be preliminarily studied in a lower organism, such as *C. elegans*, before being further investigated in a more complex system such as mammalian. The up-regulation of *fat-5* in the presence of P57 can be explained by the notion that the animal can switch to the *de novo* production of certain fatty acids rather than obtaining them from a food source. As shown, P57 treatment results in the suppression of pharyngeal bulb contractions and therefore food consumption is likely reduced, an analogous of fasting. This in turn restricts the amount of essential fatty acids obtained via the food source. It is conceivable that via the activity of FAT-5 more unsaturated fatty acids are provided, and by doing so the metabolism is kept balanced. The statistically significant transcriptional induction of *fat-5* is confirmed throughout the project utilizing several biological repeats and thus warrants closer inspection, which will be covered in the following chapters.

# Chapter Six

## *Putative association between*

## fat-5 *and* cyp-35A2

# 6 Putative association between *fat-5* and *cyp-35A2*

## 6.1 Introduction

### 6.1.1 The delta-9 desaturase, *fat-5*

In previous chapters, *fat-5* gene was introduced, which is a member of the fatty acid desaturase family involved in converting palmitic acid into palimtoyl-CoA. Throughout this study it was observed that *fat-5* expression is influenced by treatment with P57 and therefore a good candidate for lipid metabolism studies.

### 6.1.2 The cytochrome P450 superfamily

Cytochrome P450 mono-oxygenases are biocatalysts that add oxygen to their target molecule. These enzymes catalyze a wide range of reactions and have been studied in drug development, assessment of new compounds and in bioremediation (Urlacher and Eiben, 2006, Aarnio et al., 2011).

Cytochrome P450a are divided into different groups based on their amino acid sequence identity. By which, proteins with ≥ 40% identity are in the same family such as CYP1, CYP2, etc., within each family, if members share ≥ 55% identity they fall into the same subfamily (CYP1A1, CYP1A2, etc.,). P450s are involved in catalysis activity where they receive electrons by reduced pyridine nucleotides through NAD(P)H and NADH. They require auxillary redox proteins cooperating with them to obtain electrons on the haem site (Fe). Eukaryotic P450a utilize membrane-bound flavin mononucleotide (FMN)/FAD-containing NADH cytochrome P450 oxidoreductase (CPR) whereas the mitochondrial P450s are reduced by adrenodoxin (Adx) and adrenodoxin reductase (ADR)

(Lamb and Waterman, 2013). The *C. elegans* genome encodes more than 80 members of the cytochrome family. Similar to their mammalian counterparts, nematode CYP- members are involved in detoxifying cellular compartments from exogenous and endogenous xenobiotics (especially the CYP-35A/C family) (Menzel et al., 2005, Menzel et al., 2001).

Prior to this project other studies such as Aarnio et al., had confirmed a link between lipid pathways and some of the cytochrome P450 family members. Although the gene was not highly up/down regulated in the microarray experiment that was carried out in this study, we chose the gene based on literature indicating the involvement of the gene in lipid regulatory pathways.

### 6.1.3 Gene size and location

Gene expression can be influenced greatly by the location of the target gene (Hazelrigg and Petersen, 1992). The genome position of *fat-5* and *cyp-35A2* and their neighboring genes were identified using the *C. elegans* portal wormbase (www.wormbase.org) and schematically annotated. The coding region for *fat-5* is 3070 bp (this includes the two introns, the 5'UTR[20] and 3'UTR) that when spliced and translated encodes for a FAT-5 protein consisting of 333 amino acids. The *fat-5* gene is localized between positions 17723756 and 17726825 bp on the forward strand of chromosome V (Figure 6.1). The two genes flanking *fat-5* are *str-77* (W06D12.4) and *twk-42* (W06D12.2). The *str-77* is 7TM Receptor (7 trans-membrane receptor), also known as G-protein-coupled receptors that are integral membrane proteins, and contain seven membrane-spanning helices. The

[20] UnTranslated Region

*twk-42* is one of 44 members of the TWik family of potassium channels, which are defined as two-P domain $K^+$ (Menzel et al., 2001, Ashrafi et al., 2003, Menzel et al., 2005, Chakrapani et al., 2008). These neighboring genes do not seem to be directly involved in lipid regulatory pathways and were therefore not studied further.

The location of *cyp-35A2* is also chromosome V, positioned between 7362316 and 7364204 bp on the reverse strand. The gene *cyp-35A2* (C03G6.15) consists of seven exons (Figure 6.1). The length of the *cyp-35A2* transcript is 1889 nucleotides with a coding sequence of 1485 nucleotides. The neighboring genes are C03G6.5 and C03G6.14, the former is an uncharacterized protein in the *C. elegans* genome and the latter a further cytochrome P450 family member namely, *cyp-35A1* (information adapted from http://www.wormbase.org).

Only one mutant *fat-5*(*tm420*) targets exclusively the *fat-5* gene. This allele has a deletion of 779 bp located at 19998/19999 to 20777/20778 which spans a small part of exon 1, intron 1, exon 2 and over half of intron 2 (information adapted from http://www.wormbase.org). There are two mutants corresponding to a *cyp-35A2* deletion, namely *cyp-35A2(gk317)* and *cyp-35A2*(*gk326)*. The *cyp-35A2(gk317)* allele is characterized by a deletion of 1245 bp whereas *cyp-35A2*(*gk326)* contains a deletion/insertion of 1256 bp (www.wormbase.org). Most published studies have utilized *cyp-35A2*(*gk317)* to explore the effects of *cyp-35A2* knockout on lipid regulation of the nematodes.

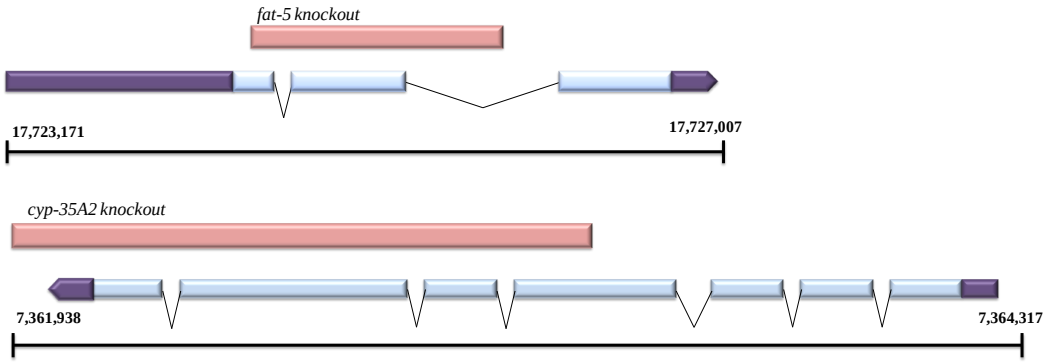


**Figure 6.1 Schematic overview of *fat-5* and *cyp-35A2*: genomic locations and deletions.** The genomic location of *fat-5* on chromosome V, the three exons (light blue bars) are separated by two introns (black lines). The promoter and 3'-UTR sequences are shown in purple, the pink bar above the gene sequence indicates the region of the deletion in *fat-5*(*tm420*). The *cyp-35A2* gene on chromosome V, is made up of seven exons (light blue bars) and six introns (black lines). The promoter sequence and the 3'-UTR are both shown in purple. The pink bar above the *cyp-35A2* gene sequence annotates the approximate position of deletion in *cyp-35A2*(*gk317*) utilized in this project.

## 6.2 Aims

The purpose of this chapter is to acquire information about a putative link between *fat-5* and *cyp-35A2* by studying respective mutant strains corresponding to these genes. Since others have already suggested a relationship between members of the cytochrome P450 family and lipid regulatory pathways in *C. elegans* (Aarnio et al., 2011, Ashrafi et al., 2003, Menzel et al., 2007), it is deemed to be of interest to explore the potential interactions between *cyp-35A2* and *fat-5*. This hypothesis will be explored by utilizing reverse genetics techniques such as RNAi.

## 6.3 Results

### 6.3.1 Life history traits and genetic aspects of *fat-5* and *cyp-35A2* mutants

#### *6.3.1.1 Pharyngeal pumping rate is not influenced by P57 treatment in a* fat-5 *knockout strain*

The *fat-5* gene was selected for further investigations, as it is believed to be involved in fatty acid metabolism of the nematodes (Watts, 2009). In order to explore the possible anorectic effects of the P57 compound in a *fat-5*(*tm420*) mutant, the nematode strain was obtained from CGC[21] and several life history characteristics were studied.

As shown in previous chapters, the pharyngeal pumping rate increases during the developmental stages in wild-type nematodes and peaks at 72 hours post-hatch (day-1 adults) thereafter decreases as the animals age. The pharyngeal pumping in *fat-5*(*tm420*) was similar to the wild-type under control conditions where the pharyngeal muscle contractions increased until the nematodes reached adulthood (Figure 6.2). P57 exposure did not initially affect the pharyngeal pumping characteristics of the *fat-5*(*tm420*) mutant. However, there was a statistically insignificant decrease in the pharyngeal pumping rate in nematodes treated with 0.03 and 0.3 μg/mL P57 at 96 hours post-hatch (Figure 6.2).

[21] *Caenorhabditis* Genetics Center, University of Minnesota, USA.

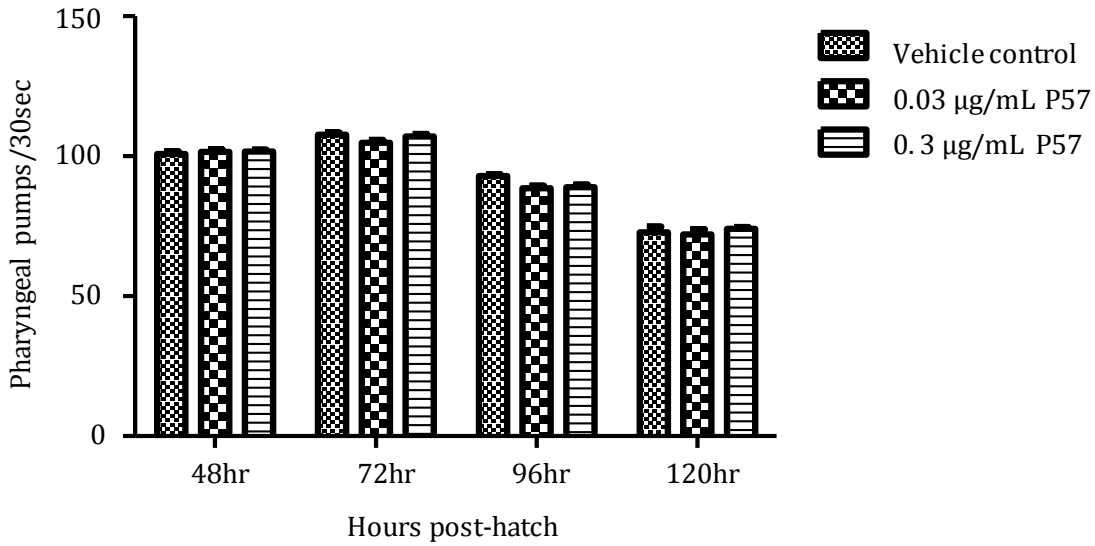


**Figure 6.2 Pharyngeal pumping rate in *fat-5*(*tm420*) in response to P57.** The pharyngeal muscle contractions were measured for 30-second intervals, the trend followed a similar pattern as the wild-type nematodes (Chapter Five, Figure 5.3). Data were analyzed by a two-way ANOVA statistical analysis, which identified that P57 treatment induced no statistically meaningful differences. Each bar chart expresses the average pharyngeal pumping rate of 30 individual *fat-5(tm420)* in three biologically independent populations ± the standard error of the mean (SEM).

#### *6.3.1.2 The body size of* fat-5(tm420) *is not affected by P57 exposure*

The development of the *fat-5(tm420)* mutants was followed by assessing length and the overall surface body area over time (Figure 6.3). The treatment of *fat-5(tm420)* nematodes with P57 did not result in any changes in growth, and nematodes reached the final body size within the expected period of 96 hours (Figure 6.3). Moreover, the overall size of *fat-5(tm420)* was not different of the wild-type nematodes (personal observation), however no direct comparison was made against wild-type counterparts.

In the previous section (6.3.1.1) it was demonstrated that when *fat-5* is knocked out the neuromuscular behavior of pharyngeal bulb contractions is not influenced by P57 exposure. Likewise, no P57-mediated changes in volumetric body area were observed (Figure 6.3 Panel A). Although the length of P57-treated *fat-5(tm420)* worms decreased at 120 hours post-hatch, this change was deemed to be statistically insignificant (Figure 6.3 Panel B). Therefore, P57 exposure did not affect the growth parameters in *fat-5(tm420)* mutants (Figure 6.3). Tables S. 12 and S. 13 in Appendix Eleven present the data corresponding to growth measurements of *fat-5(tm420)* mutant in response to P57 exposure.

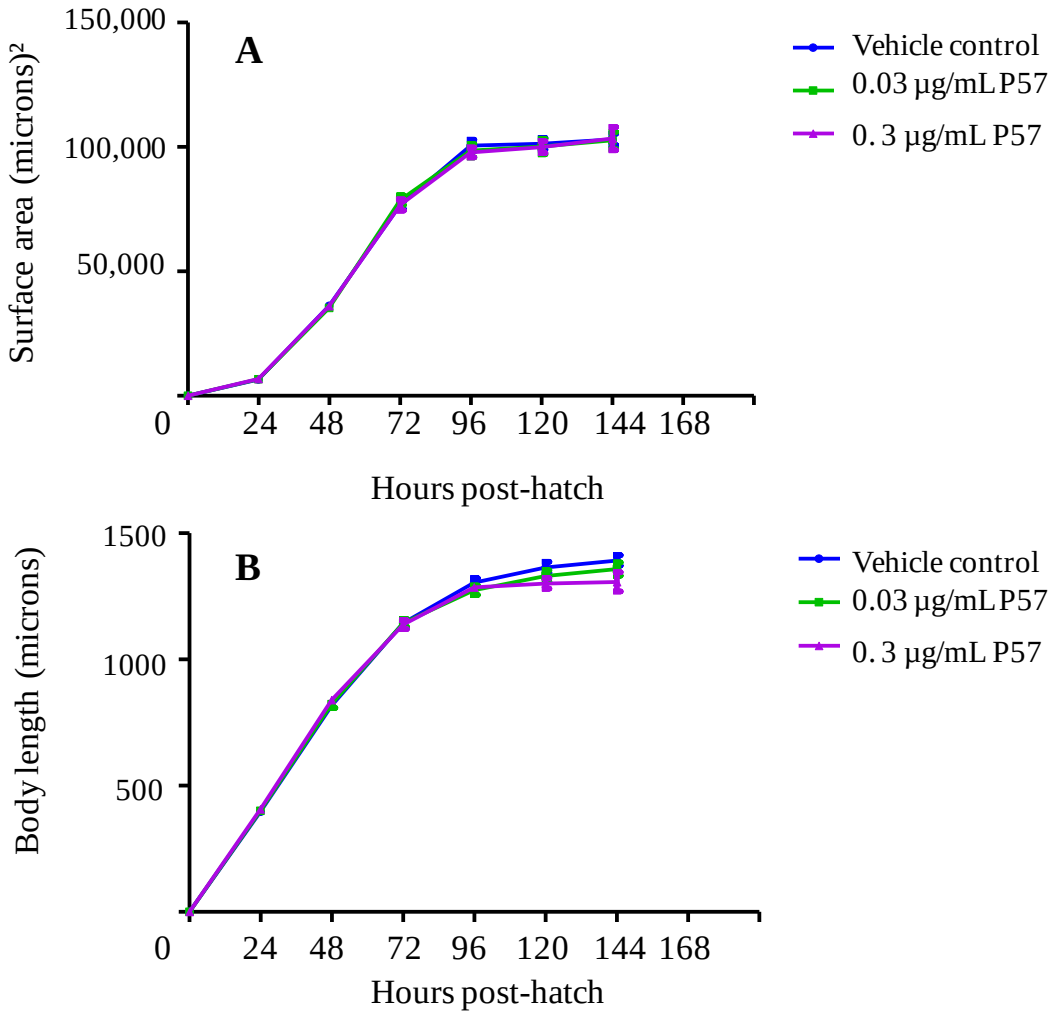


**Figure 6.3 Developmental changes of *fat-5*(*tm420)* nematodes upon treatment with P57.** The changes in the volumetric body area (A) and length (B) of *fat-5(tm420)* were not affected by P57 exposure. Statistical analysis was performed by a two-way ANOVA and Bonferroni post-test multiple comparisons and revealed an insignificance reduction the surface body area (B) of P57-treated animals at 144 hours post-hatch. Each data point is the average body area or length of 20 nematodes explored in three biological repeats ± the standard error of the mean (SEM).

### *6.3.1.3 Survival rate of the* fat-5(tm420) *is modulated by P57 exposure*

Given that neither pharyngeal pumping nor development of *fat-5(tm420)* was affected by P57 treatment (Figures 6.2 and 6.3), it was deemed important to assess the lifespan of *fat-5(tm420).*

The untreated *fat-5(tm420)* had a median survival of 11 days and exposure to 0.03 and 0.3 µg/mL P57 shortened the median lifespan by 24 hours (Figure 6.4). There was no dose-dependency in the lifespan reductions observed between P57 doses, however the one-day decrease of median lifespan in P57-exposed *fat-5*(*tm420*) was statistically significant ($p$ <0.01, Log-rank statistical analysis). Nevertheless, the maximum lifespan of *fat-5(tm420)* nematodes challenged with P57 was not affected (Figure 6.4, Appendix Twelve).

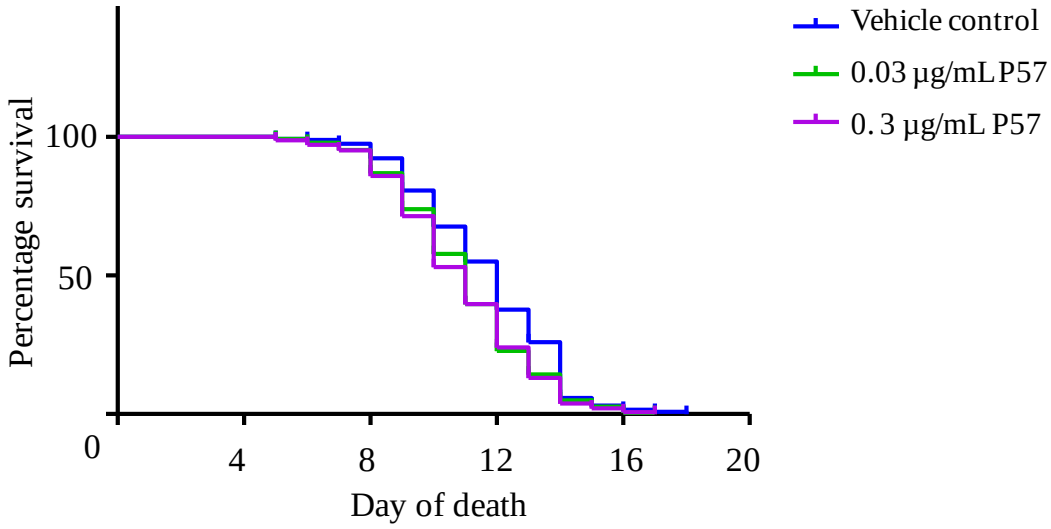


**Figure 6.4 Survival rate of *fat-5*(*tm420*) upon treatment with P57.** Under control condition, *fat-5(tm420)* mutants had a median lifespan of 11 days whereas once treated with 0.03 and 0.3 µg/mL P57 there was a significant reduction in the median lifespan of the nematodes. A one-day reduction was observed in P57-exposed *fat-5(tm420)*. The maximum survival was not affected by P57 treatment. Each condition was started with a population of 400 worms and death was scored daily ("lost" animals were censored from the cohort studies).

#### *6.3.1.4 The development of* cyp-35A2(gk317) *is not modulated by P57*

The growth parameters of body surface area and length were assessed in *cyp-35A2(gk317)* over time for a period of 144 hours post-hatch (six days). Within the first four days after hatching, *cyp-35A2(gk317)* grew normally (Figure 6.5) i.e., analogous to wild-type nematodes (Chapter Five, Figures 5.4 and 5.5). When *cyp-35A2(gk317)* were treated with 0.03 and 0.3 μg/mL P57, growth parameters were not affected, namely length and the body surface area were similar to the untreated nematodes (Figure 6.5). It is worth mentioning that the overall size of *cyp-35A2(gk317)* nematodes was not different from the wild-type worms (personal observation). Further information in regards to growth measurement is provided in Appendix Thirteen.

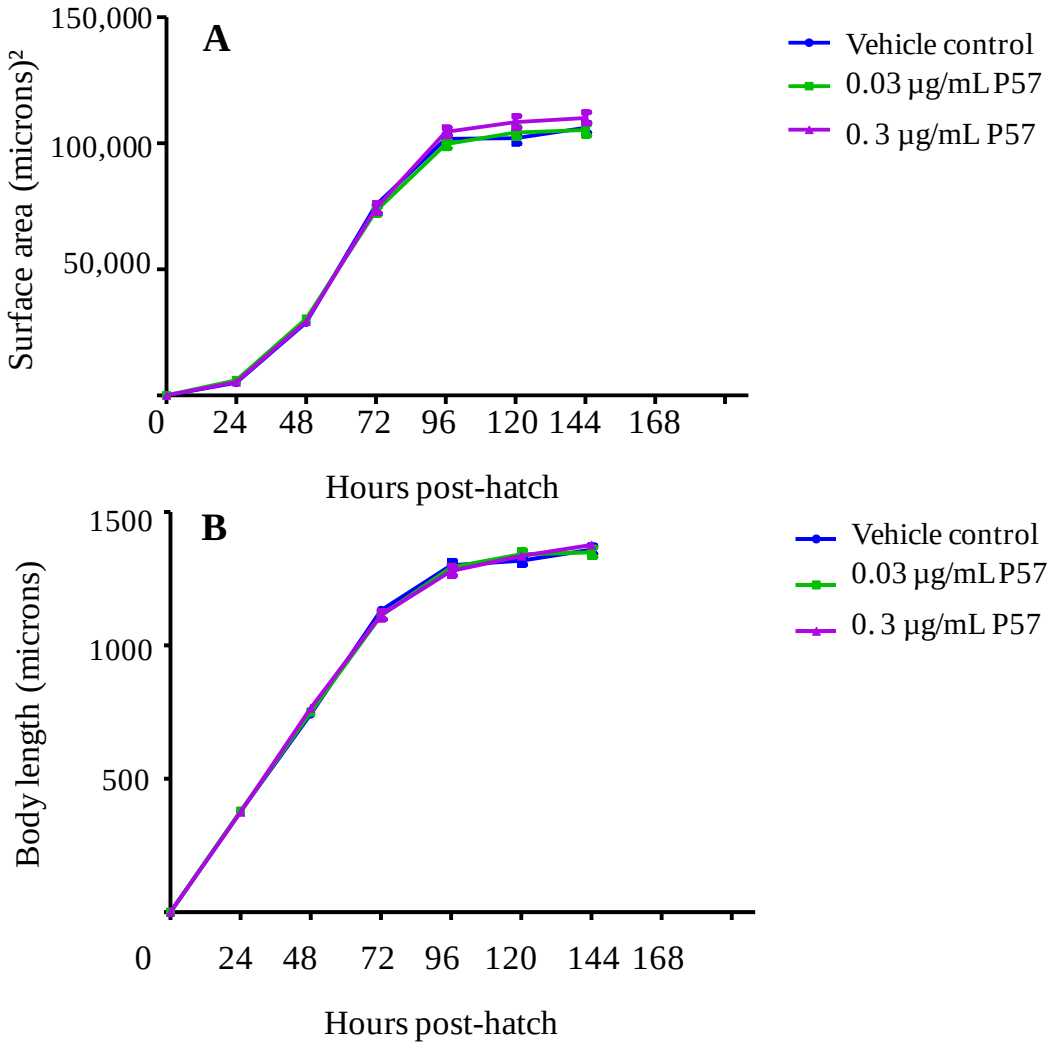


**Figure 6.5 Growth parameters in the *cyp-35A2*(*gk317*) maintained in the presence or absence of P57.** The volumetric surface area (A) and length (B) were not modulated by P57. The marginal reduction in the volumteric surface area at 120 and 144 hours post-hatch in P57-treated nematodes, was statistically insignificant. Each data point is the average size of 20 nematodes explored in three independet biological repeats ± the standard error of the mean (SEM).

### *6.3.1.5 Lifespan of* cyp-35A2(gk317) *is not affected by P57 exposure*

Changes in the survival rate of the *cyp-35A2(gk317)* was explored in response to the P57 treatment. A lifespan assay was performed and the median survival, as well as the maximum lifespan was determined (Figure 6.6). Treatment with P57

did not affect the survival of *cyp-35A2(gk317)*. Under control conditions the median lifespan of *cyp-35A2(gk317)* was 12 days, which did not alter in response to exposure to 0.03 and 0.3 µg/mL P57 (Figure 6.6). Moreover, no difference was observed in the maximum survival rate within the three experimental conditions (control and the two doses of P57), maximum lifespan was 19 days regardless of the P57 treatment (Figure 6.6, Appendix Fourteen).

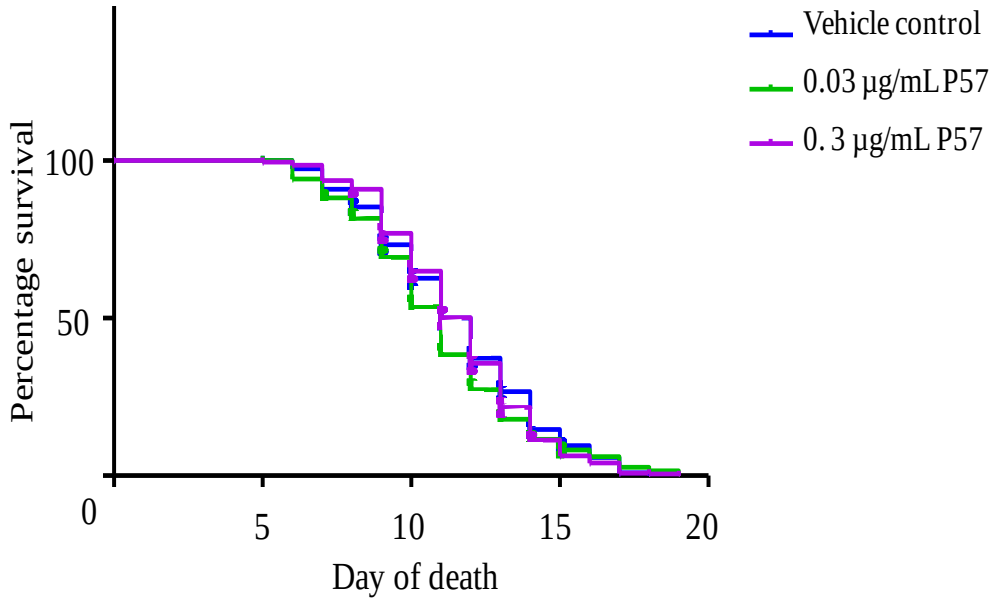


**Figure 6.6 Survival rate of *cyp-35A2(gk317)* in response to P57 exposure.** The median lifespan of *cyp-35A2(gk317)* was 12 days, which was not influenced by exposing the nematodes to P57. Data were analyzed via the Log-rank (Mantel-Cox) statistical test (GraphPad Software Inc., La Jolla USA). The maximum lifespan was determined to be 19 days in all three conditions. Each experimental group started with a population of 400 nematodes and death was scored daily, "lost" animals were censored.

### 6.3.2 Gene silencing

#### *6.3.2.1 General aspects and strategies*

RNAi clones (from the Ahringer RNAi library) were utilized to silence genes via the feeding method. *E. coli* HT115(DE3) was used for all RNAi assays, which is derived from the *E. coli* K12 strain and is RNase III deficient (Kamath et al., 2001). Initially Timmons and Fire introduced the RNAi feeding method and since then it has been the method of choice for most reverse genetics studies (Timmons and Fire, 1998, Ahringer, 2006). When utilizing the feeding technique, the effects of the RNAi become evident after the L4 stage and directly target the germline and gonads. The parent population and progenies were both continuously exposed to the bacteria expressing the dsRNA of the gene of interest to maximize the efficiency of the knockdown.

The gene silencing procedure was performed as previously stated (Section 2.3.15) where nematodes were maintained for one generation, fed on the HT115 bacteria containing the designated dsRNAs and the resultant progenies ($F_2$) were used for downstream analyses. Since RNAi via feeding can yield variable results, the efficiency of gene knockdown was quantified by real-time qPCR prior to each assay.

To investigate the putative interaction between *fat-5* and *cyp-35A2*, the latter gene was silenced in the wild-type strain (N2) and the *fat-5(tm420)* knockout strain. Four experimental conditions were designed for each assay as well as a positive control (*dpy-10* RNAi results in a "short and fat" (dumpy) phenotype) to visually assess the success of the RNAi procedure. The four conditions consisted of two controls (grown on HT115 bacteria expressing the empty vector) that will be referred to as wild-type and *fat-5(tm420)*, unless otherwise stated. In addition,

wild-type and *fat-5(tm420)* nematodes that were fed with the bacteria containing dsRNA of *cyp-35A2*, here referred to as wild-type (*cyp-35A2* RNAi) and *fat-5* (*cyp-35A2* RNAi), respectively. The age-matched $F_2$ generation of each condition (wild-type, *fat-5(tm420)*, wild-type (*cyp-35A2* RNAi) and *fat-5* (*cyp-35A2* RNAi)) was placed on the designated plates with the corresponding bacterial lawn and nematodes were allowed to grow to the L4 stage (approximately 40 hours post-hatch). At this stage, RNA was extracted from each sample group and reverse transcribed to cDNA utilizing the standard RNA extraction and cDNA making techniques (Sections 2.3.2 and 2.3.3).

Quantitative RT-PCR was performed on cDNA synthesized from the four different populations – wild-type, wild-type (*cyp-35A2* RNAi), *fat-5(tm420)* and *fat-5* (*cyp-35A2* RNAi). The efficiency of the gene silencing was examined via three biological repeats to quantify the percentage of the knockdown. The reproducibility and reliability of the gene knockdown was deemed to be statistically significant with an overall silencing effect of 94-98% (Figure 6.7).

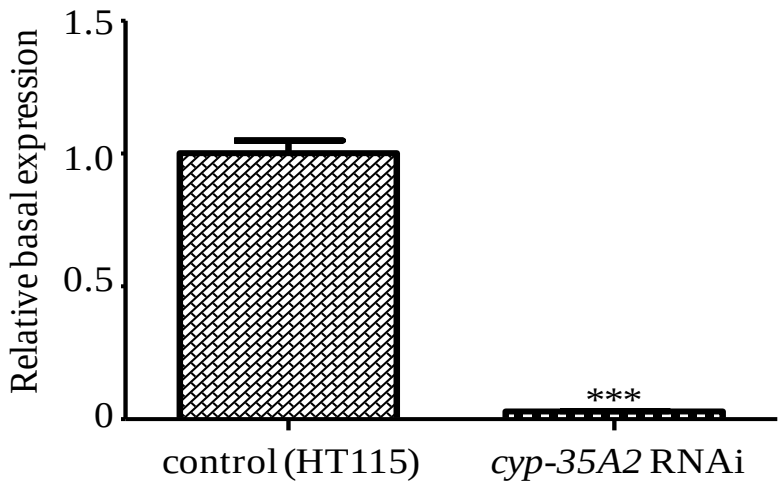


**Figure 6.7 Relative expression of *cyp-35A2* quantified by RT-PCR technique in control and RNAi silenced nematodes.** Wild-type worms were fed either control RNAi bacteria (HT115) or bacteria expressing *cyp-35A2* dsRNA. The efficiency of RNAi was found to vary between 94-98% (based on three biologically independent populations). Statistical analysis confirmed the reduction in the expression level of the *cyp-35A2* gene to be significant (*** $p < 0.001$). Each bar graph is the relative expression of *cyp-35A2* in wild-type nematodes either in controls or the RNAi groups ± the standard error of the mean (SEM).

### 6.3.3 Phenotypic analysis upon *cyp-35A2* gene silencing

#### *6.3.3.1 Growth parameters are affected by* cyp-35A2 *silencing in wild-type and* fat-5(tm420)

After determining the gene silencing efficiency, downstream experiments were performed to explore potential phenotypic influences upon the knockdown of *cyp-35A2*. In principal, feeding the worms with the *E. coli* HT115(DE3) strain (regardless of the nematode background) resulted in animals to grow larger in size when compared to the *E. coli* OP50 fed counterparts (personal observation, data not shown). Between 20-25 nematodes of each experimental group were

photographed, from L1 stage every 24 hours for a six-day period. Images of individual nematodes were traced to determine growth parameters including the surface area and length (Figure 6.8). Each group of nematodes was compared to wild-type animals that were fed on HT115. In all four conditions, wild-type, *fat-5(tm420)*, wild-type (*cyp-35A2* RNAi) and *fat-5* (*cyp-35A2* RNAi), the four larval stages were completed within 72 hours post-hatch, nevertheless *cyp-35A2* silencing introduced different phenotypic responses in wild-type and the *fat-5(tm420)* background (Figure 6.8).

The length of nematodes was traced over a period of six days and *fat-5(tm420)*, wild-type (*cyp-35A2* RNAi) and *fat-5* (*cyp-35A2* RNAi) were compared to the wild-type group of nematodes (Figure 6.8, Panel A). There was an overall marginal increase in the length of the three conditions versus the wild-type, observed mainly from the third day of life (72 hours post-hatch). However, the increased length of these nematodes was statistically insignificant when analyzed by a two-way ANOVA (GraphPad Prism v5).

Furthermore, the knock down of *cyp-35A2* by RNAi in the *fat-5(tm420)* background significantly reduced the overall volumetric growth of the nematodes (Figure 6.8, Panel B). Changes in the surface area became significant from 72 hours post-hatch, when compared to the wild-type. In contrast, in the wild-type (*cyp-35A2* RNAi) group the final body surface area was induced by 7% at 144 hours post-hatch, whereas *fat-5(tm420)* mutants were 4% smaller than the wild-type counterparts, a phenotypic characteristic that was not observed in *fat-5(tm420)* nematodes when fed on *E. coli* OP50 (Figure 6.8, Panel B). In addition, a statistically significant 11% reduction was observed in the *fat-5* (*cyp-35A2* RNAi) group (versus the wild-type) (Figure 6.8, Panel B). A table with extended

data on growth analysis upon knockdown of *cyp-35A2* is presented in Appendix Fifteen.

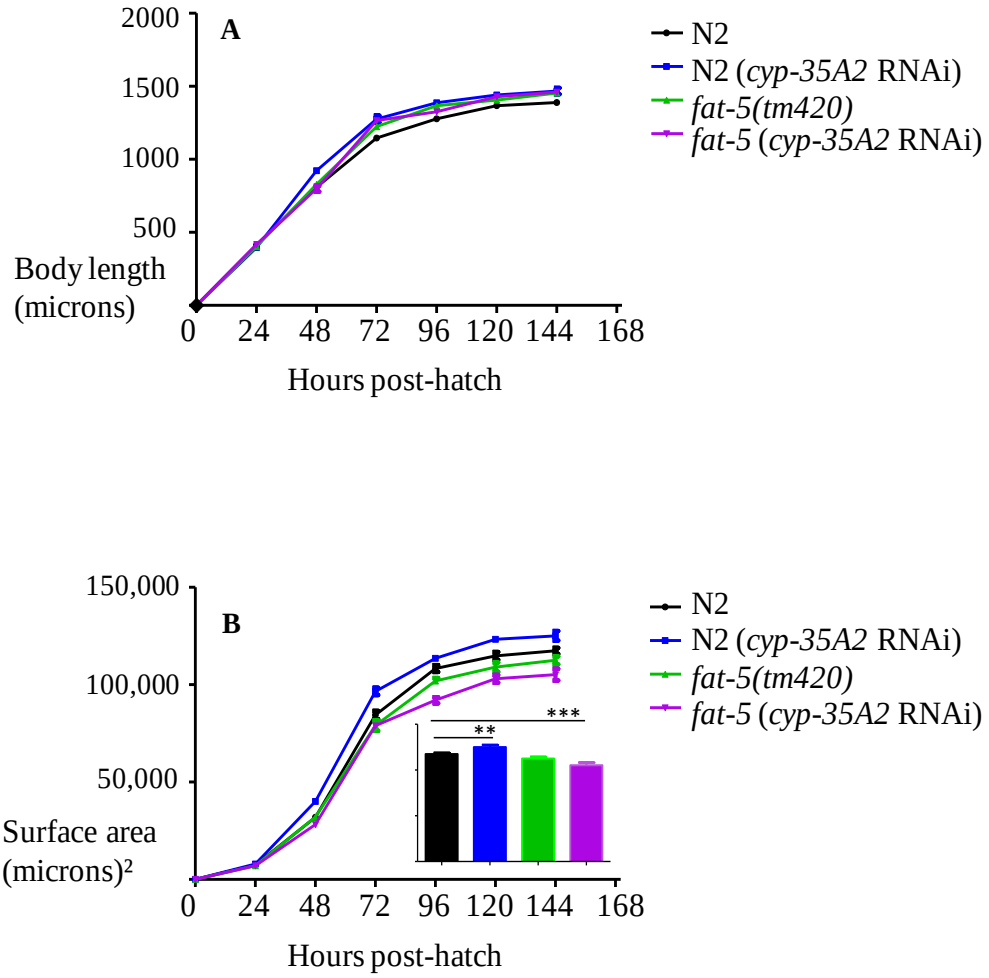


**Figure 6.8 Growth (body length and surface area) of nematodes upon *cyp-35A2* gene silencing via RNAi.** Developmental changes were followed from 24 hour post-hatch until 144 hours. Length (A) and body surface area (B) were measured every 24 hours, in wild-type, *fat-5(tm420)*, wild-type (*cyp-35A2* RNAi) and *fat-5* (*cyp-35A2* RNAi) nematodes. The average length of 20 nematodes is presented for each time point repeated in two biologically independent populations ± the standard error of mean (SEM). The surface area was significantly affected by *cyp-35A2* silencing and resulted in a considerable reduction ($p < 0.001$) in the overall volumetric growth of *fat-5 (cyp-35A2* RNAi) as well as a significant induction ($p < 0.01$) in the surface area of wild-type (*cyp-35A2* RNAi) mutants. Each data set is the average surface area of 20 individual nematodes taken from two biological repeats ± the standard error of mean (SEM). Bar charts present the final volumetric body area of the worms at 144 hours post-hatch

#### *6.3.3.2 Lifespan is influenced by* cyp-35A2 *gene silencing in a wild-type and* fat-5(tm420) *background*

Volumetric surface area was significantly reduced when the *cyp-35A2* gene was knocked down in the *fat-5(tm420)* mutant background, in contrast *cyp-35A2* silencing in the wild-type background resulted in larger nematodes, yet the length of animals was not affected by the *cyp-35A2* RNAi regardless of the background strain (Figure 6.8).

In order to explore whether the simultaneous deletion of *cyp-35A2* and *fat-5* influence the survival of nematodes, a lifespan assay was performed to determine both the median lifespan and the maximum survival of the age-matched nematodes under four RNAi conditions, namely wild-type, *fat-5(tm420)*, wild-type (*cyp-35A2* RNAi) and *fat-5 (cyp-35A2* RNAi). The dead nematodes were scored daily as well as censoring the number of "lost" worms to determine the survival rate. The median survival of wild-type animals was 12 days (Figure 6.9 and Table 6.1), whereas silencing of *cyp-35A2* in the wild-type background, i.e., wild-type (*cyp-35A2* RNAi), resulted in a considerably reduced median lifespan of 10 days. In comparison to the wild-type nematodes, the *fat-5(tm420)* mutants had a significantly extended median survival of 15 days and the lifespan was extended by two days in *fat-5* (*cyp-35A2* RNAi) (Figure 6.9 and Table 6.1).

The maximum survival was also affected by *cyp-35A2* silencing in wild-type and *fat-5(tm420)*. The wild-type (control) nematodes lived up to 19 days, whereas wild-type (*cyp-35A2* RNAi) had a reduced survival rate of 17 days (Figure 6.9). Moreover, the maximum survival of *fat-5(tm420)* was extended to 22 days, and the *cyp-35A2* gene knockdown on *fat-5(tm420)* mutants resulted in a similar increase (Figure 6.9, Appendix Sixteen).

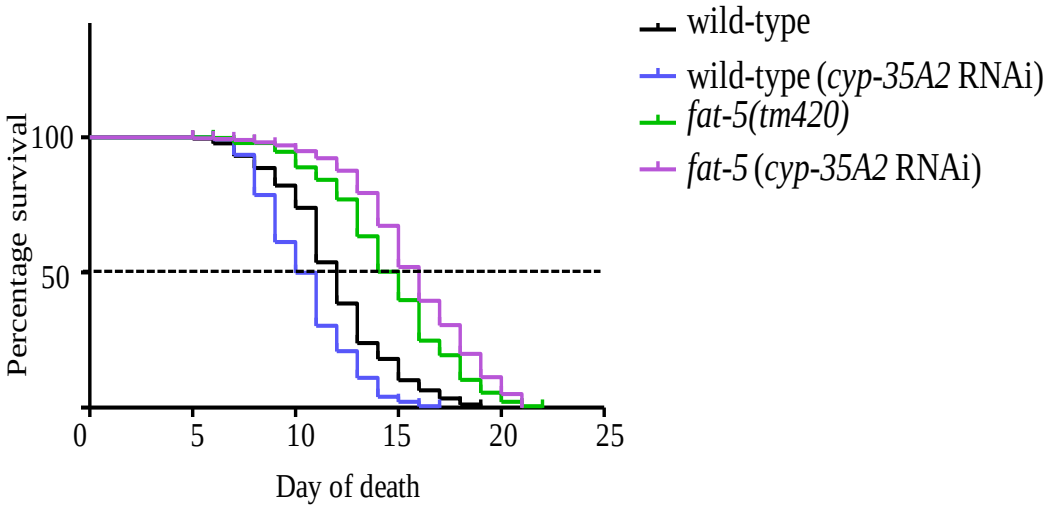


**Figure 6.9 Survival of nematodes upon *cyp-35A2* gene silencing in a wild-type or *fat-5(tm420)* background.** Lifespan of wild-type nematodes was shorter in comparison to the *fat-5(tm420)* mutants, whilst *cyp-35A2* RNAi on wild-type nematodes reduced the median and the maximum survival of these worms. The silencing of *cyp-35A2* extended the median survival rate of a *fat-5*(*tm420)* background and induced the maximum lifespan. Each experimental condition started with a population of 400 nematodes and death was scored daily and "lost" nematodes were censored. The median lifespan values were determined and statistically analyzed (refer to Table 6.1). Each Kaplan-Meier survival curve is the mean of three independently performed biological repeats at 20°C.

| **wild-type** | **wild-type (*cyp-35A2* RNAi)** | ***fat-5(tm420)*** | ***fat-5* (*cyp-35A2* RNAi)** |
|---|---|---|---|
| 12 | 10 | 15 | 17 |
| N/A | *p <0.0001* | *p <0.0001* | *p <0.0001* |

**Table 6.1 Median lifespan of wild-type and the *fat-5(tm420)* strains upon *cyp-35A2* gene silencing.** The statistical difference in the median lifespan of designated nematodes was determined using the Log-rank (Mantel-Cox) test with 95% significance using GraphPad Prism v5 software.

### 6.3.4 *A putative feedback is observed in the expression of* fat-5 *and* cyp-35A2

As explained earlier in this chapter, the gene silencing efficiency via feeding RNAi was confirmed utilizing real-time qPCR (Figure 6.7) and further phenotypic analyses including size determination and lifespan studies (Figures 6.8 and 6.9) suggested a relationship between *fat-5* and *cyp-35A2*. Thereafter, gene expression analyses were performed to investigate the presence of a possible regulatory and feedback mechanism between *fat-5* and *cyp-35A2* expression, in response to P57 exposure.

Designated RNAi bacterial strains were mixed with P57 (0, 0.03 or 0.3 μg/mL) prior to being spread on the RNAi NGM plates. Animals were maintained on the RNAi bacteria/P57 mixture plates until they reached the L4 stage, total RNA subsequently extracted (section 2.3.2) followed by cDNA synthesis (section 2.3.3). Real-time qPCR was performed using the standard ABI7000 protocol (section 2.3.4). Relative expressions of the *fat-5* and *cyp-35A2* genes were determined after the normalization to the invariant house-keeping gene *rla-1* (Figures 6.10 and 6.11). For each sample group two biological populations were assessed to determine the standard error of the mean (±SEM). Under control conditions in wild-type nematodes the expression of *fat-5* was defined to be one (basal expression normalized to one) therefore the relative transcriptional response of the gene could be quantified upon gene knock down/out. Accordingly, when nematodes were not exposed to P57, the basal expression of *fat-5* in wild-type was different from that of the wild-type (*cyp-35A2* RNAi) as the latter showed an approximate 44% decrease in the expression level of *fat-5* (Figure 6.10). In *fat-5*(*tm420*), there was no expression of the *fat-5* gene (serving as a negative control). A significant and statistically robust transcriptional

induction of *fat-5* was observed in wild-type and wild-type (*cyp-35A2* RNAi) when treated with 0.03 or 0.3 µg/mL P57 (Figure 6.10). Although, the expression of *fat-5* was notably low in wild-type (*cyp-35A2* RNAi), the general up-regulation upon P57 exposure was similar to wild-type nematodes (Figure 6.10).

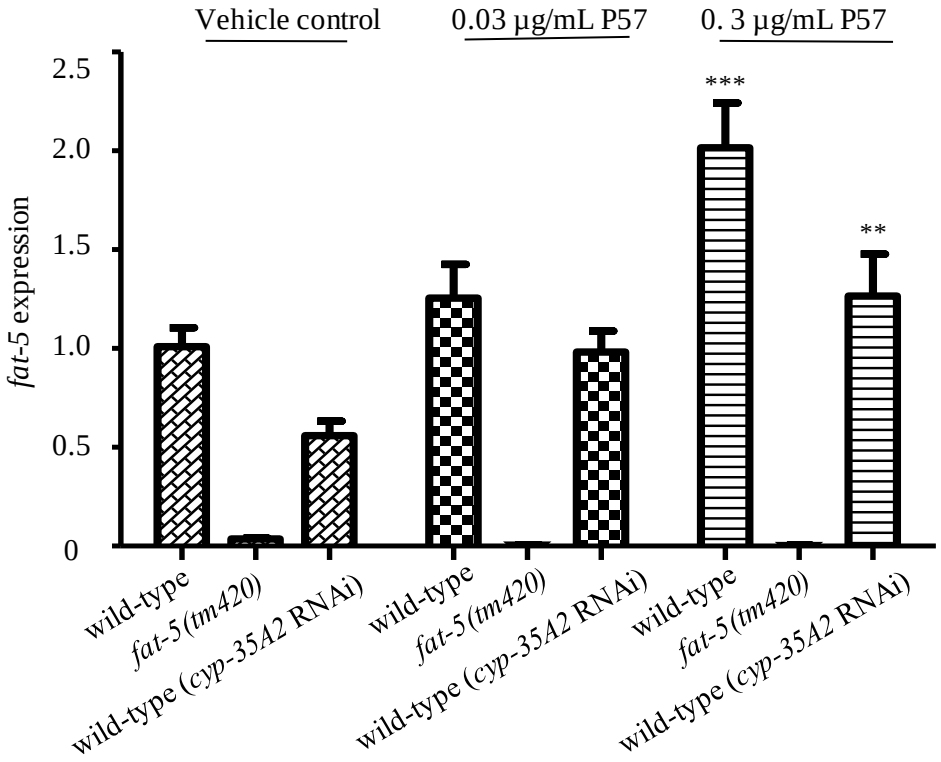


**Figure 6.10 The transcriptional response of *fat-5* in wild-type, wild-type (*cyp-35A2* RNAi) and in *fat-5(tm420)* exposed to P57.** Expression changes of *fat-5* associated with P57 (0, 0.03 or 0.3 µg/mL) treatment were determined under three experimental conditions. The basal expression of *fat-5* was normalized to 1 under control conditions in wild-type worms whereas in *fat-5*(*tm420)* nematodes the expression of *fat-5* was essentially abolished (thereby confirming the specificity of the probe and the null deletion of *fat-5(tm420*)). Importantly, when *cyp-35A2* was silenced in wild-type worms the basal expression of *fat-5* was reduced to approximately half of the level observed in the wild-type. Upon exposure to P57, the expression of *fat-5* was up-regulated in a dose responsive manner. In wild-type (*cyp-35A2* RNAi) nematodes *fat-5* expression was modest but statistically robust. Each bar graph is the average from two individual repeats with at least three technical repeats ± the standard error of the mean (SEM) (** $p < 0.01$, *** $p < 0.001$).

The relative expression of *cyp-35A2* was further determined upon treatment with P57 in wild-type, *fat-5(tm420)* and wild-type (*cyp-35A2* RNAi) (Figure 6.11). Under control conditions (P57 untreated) the *cyp-35A2* expression was normalized to 1 for the wild-type, whereas in untreated *fat-5(tm420)* mutants the expression of *cyp-35A2* was reduced by 81% (Figure 6.11). In wild-type (*cyp-35A2* RNAi) group the expression of *cyp-35A2* was negligible (thus served as the negative control). Treatment with P57 (0.03 and 0.3 µg/mL) down-regulated the *cyp-35A2* expression in wild-type and *fat-5(tm420)* nematodes (Figure 6.11), although the P57 effect was more pronounced in wild-type nematodes where *cyp-35A2* suppression was determined to be 84%.

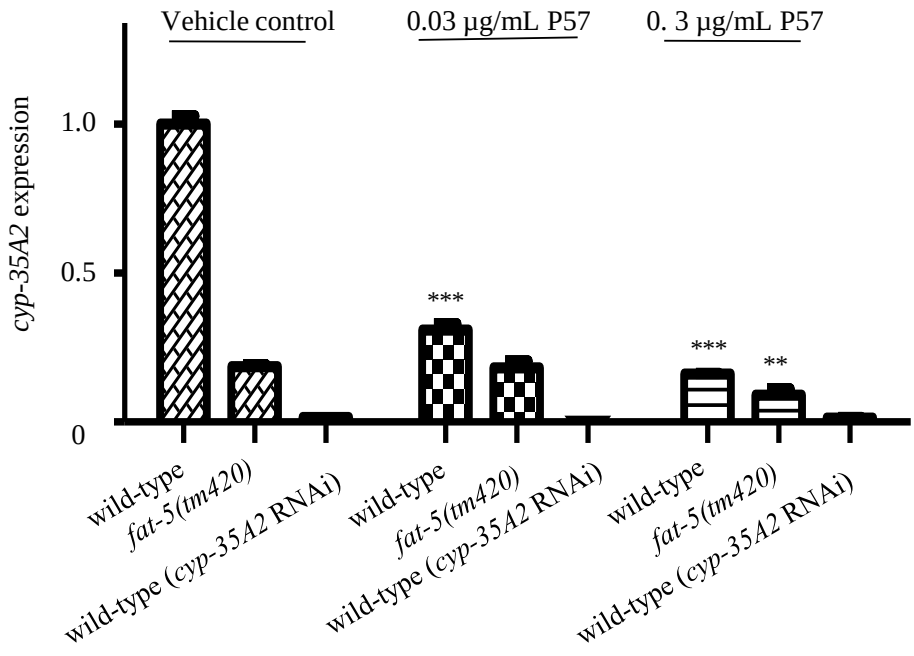


**Figure 6.11 Relative fold changes of *cyp-35A2* in P57-exposed nematodes of wild-type, *fat-5(tm420)* and wild-type (*cyp-35A2* RNAi).** The expression level of *cyp-35A2* was normalized to one in untreated wild-type nematodes. The untreated *fat-5(tm420)* nematodes had a significantly reduced transcriptional level of *cyp-35A2*. In wild-type (*cyp-35A2* RNAi) as was confirmed previously (Figure 6.7) the expression of *cyp-35A2* was almost abolished. Exposing the nematodes to P57 significantly reduced the transcriptional response of *cyp-35A2* in wild-type (control) and *fat-5(tm420)* (control) nematodes. Each bar chart is the average fold change in two biologically independent populations with at least three technical repeats ± the standard error of the mean (SEM) (** $p < 0.01$, *** $p < 0.001$).

## 6.4 Discussion and Conclusions

The *C. elegans* genome contains a wide range of fat-regulatory genes with mammalian homologs including *fat-5*, a fatty acid desaturase with a human homolog known as SCD-1 "stearoyl-CoA desaturase-1". These genes are responsible for the production of polyunsaturated fatty acids from the saturated forms. The homology between *fat-5* and *H. sapiens* SDC-1 is approximately 39% protein identity. Furthermore, *cyp-35A2* belongs to the cytochrome P450 family of mono-oxygenases in nematodes and has between 19%-22% homology with CYP1B1, CYP1A1, CYP1A2, CYP17A1 and CYP21A2. However, the closest mammalian counterpart is found to be CYP2C8. There is some evidence that the *C. elegans cyp-35A2* is involved in lipid regulatory pathways (Aarnio et al., 2011, Menzel et al., 2007).

Life history traits such as development, pharyngeal bulb contractions and survival in single mutant strains of *fat-5*(*tm420*) and *cyp-35A2*(*gk317*) were assessed in response to P57 treatment. It was revealed that pharyngeal pumping is not affected in the absence of *fat-5*, a modest increase was observed in the pharyngeal pumping rate of P57-exposed *fat-5(tm420)* in comparison to the wild-type (Chapter Five, Figure 5.8). This observation suggests that there may be a connection between *fat-5* and the P57-mediated changes in pharyngeal pumping. As the mean number of pumps was marginally elevated in the presence of P57, it could be argued that *fat-5(tm420)* mutants utilize a compensation feedback mechanism triggered by the lack of certain essential fatty acids as a result of *fat-5* deletion. As mentioned earlier, *fat-5* is predicted to encode a mitochondrial Δ9 fatty acid desaturase involved in the conversion of saturated fatty acids into the unsaturated forms, specifically Palmitic Acid (16:0) to its unsaturated

counterpart Palmitoyl-CoA. There is also some evidence that FAT-5 may be involved in the desaturation of other medium chain fatty acids, including 14:0 and 15:0 (Watts and Browse, 2002, Marcotte et al., 2000, Strittmatter et al., 1974). Furthermore, there is a possibility that FAT-5 plays a role in synthesizing *cis* vaccenic acid, which is involved in metabolizing hypolipidemic drugs and fatty acids (Knox et al., 2011). This notion may explain why *fat-5* was over-expressed in nematodes exposed to the *H. gordonii* extract or P57.

P57 treatment did not influence the growth parameters of *fat-5*(*tm420)*, neither the overall body area nor the length, in comparison to wild-type nematodes, in which a significant decrease was observed in growth parameters. Moreover, P57 exposure resulted in a longevity phenotype in wild-type (Chapter Five, Figure 5.9), it was of interest to see whether a similar tend happens in the survival rate of *fat-5*(*tm420)* to find a potential link between this life history trait and presence or absence of *fat-5*. However, *fat-5(tm420)* had a significantly shorter median lifespan upon treatment with P57, a phenomenon that could possibly be due to toxic effects.

The reduction in the median lifespan of *fat-5(tm420)* mutants in response to P57 treatment observed in this study could be explained by a reduced level of specific fatty acids. Furthermore, exposure to a compound, which is believed to have anorectic features, may eventually decrease the lifespan in the absence of a fatty acid desaturase.

Cytochrome P450s are mainly involved in the response to xenobiotics (Chakrapani et al., 2008, Menzel et al., 2005, Menzel et al., 2001). A study by Aarnio et al. in 2011 clearly demonstrated the involvement of the cytochrome P450s superfamily, specifically *cyp35A*- members, in lipid metabolism and fatty

acid regulation (Aarnio et al., 2011). Menzel et al. also investigated the responses of *cyp-35A2(gk317)* knockout nematodes to xenobiotics and identified reduced Nile Red staining in these mutants (Menzel et al., 2007).

In this project, a *cyp-35A2(gk317)* mutant was chosen to investigate phenotypic and molecular pathways which are mediated by an exposure to P57. Growth parameters, length and body surface area, were not affected by P57 treatment. An outcome that was also observed in *fat-5(tm420)* nematodes whilst wild-type worms exhibit a significantly decreased body area size and length upon P57 exposure. One explanation could be that the concentrations used did not induce any responses in *fat-5* or *cyp-35A2* deletion strains. Moreover, it could be due to the molecular modulations in response to *fat-5* or *cyp-35A2* deletion upon P57 treatment. Furthermore, the lifespan did not change in P57-exposed *cyp-35A2(gk317)*. This outcome suggests a possible link between *cyp-35A2* deletion and exposure to P57, which in turn may protect the animals from premature death.

To explore the relationship between the expression of *fat-5* and *cyp-35A2*, and their possible interactions, reverse genetic techniques were applied utilizing RNAi by feeding and the efficiency of the RNAi knockdown was assessed via the real-time qPCR platform. Using RT-PCR one can examine the success of the mRNA knockdown in the absence of a distinct knockdown phenotype. In addition, the wild-type (*dpy-10* RNAi) was utilized as the positive control to visually assess the success of RNAi by feeding method. Although the quantification of mRNA levels is a tool for assessing the knockdown success, the protein product may still exist despite the undetectable amount of the mRNA. This is due to the stability of certain proteins over the days. Nevertheless, with a

knockdown efficiency of 94-98% the RNAi of *cyp-35A2* can be considered to be very high and likely similar to a chromosomal knockout.

Detailed phenotype analysis of wild-type and *fat-5(tm420)* nematodes in response to *cyp-35A2* silencing revealed certain changes in developmental growth, lifespan and molecular basis of the nematodes. One phenotypic characteristic observed in all four conditions of wild-type, wild-type (*cyp-35A2* RNAi), *fat-5(tm420)* and *fat-5* (*cyp-35A2* RNAi) was an increase in length and surface area (personal observation). This phenomenon could be due to the change in the diet of nematodes since the animals are fed on *E. coli* HT115 rather than *E. coli* OP50. Indeed, it was reported that when nematodes are maintained on different *E. coli* strains such as OP50, HB101, HT115 or DA837, the percentage of certain fatty acids change, as well as an alteration between protein and lipid composition (Brooks et al., 2009). Therefore, the size induction in HT115 fed nematodes might be a direct consequence of a change in bacterial food. Having said that, the pro-longevity and reduced body area size of the *fat-5* (*cyp-35A2* RNAi) nematodes may also be because of a reduction or a change in the lipid composition of these nematodes. It is worth mentioning that although median survival determination is a sensitive endpoint, *C. elegans* is indeed highly susceptible to the changes in developmental conditions. As a result, even wild-type nematodes may differ between laboratories, therefore causing the median lifespan to vary from 11.8 to 20 days (Gems and Riddle, 2000, Qabazard et al., 2013). Moreover, inter-laboratory changes such as temperature may also affect the survival rate of the animals, resulting in a difference in median lifespan of the same strain if assessed at different time points throughout the year. This could explain why the median lifespan of wild-type nematodes was 12 days in

this particular assay, which was considerably shorter than what was previously determined in other chapters.

The 70% induction in the longevity of *fat-5* (*cyp-35A2* RNAi) in comparison to wild-type (*cyp-35A2* RNAi) may indicate a putative correlation between *fat-5* and *cyp-35A2*. To further investigate the possible link between *fat-5* and *cyp-35A2* and to explore the molecular basis of P57 action upon *cyp-35A2* silencing, quantitative real-time PCR was utilized. However, the expression level of *cyp-35A2* was only modestly affected in the absence of *fat-5*. The appetite suppressing properties of the active compound P57 from *H. gordonii* has been reported previously (MacLean and Luo, 2004), and here via the genome-wide microarray analyses *fat-5* was confirmed to be responsive towards P57. The transcriptional induction of *fat-5* in response to P57 concentrations was deemed not to be directly related to *cyp-35A2*, nevertheless, the expression of *cyp-35A2* was almost diminished in the absence of *fat-5*. In contrast to the *fat-5* response, *cyp-35A2* expression was suppressed in wild-type nematodes exposed to P57. Yet, the insignificant down-regulation of *cyp-35A2* in *fat-5(tm420)* suggests they are linked at the molecular level. Moreover, transcriptional analyses propose a putative interaction between *fat-5* and *cyp-35A2* in response to P57 treatment of the worms.

Thereafter, to compare and contrast the phenotypic properties exhibited in the *fat-5* (*cyp-35A2* RNAi), it was deemed important to create a double mutant from single mutants of *fat-5(tm420)* and *cyp-35A2(gk317)*. Furthermore, to define life history traits and explore the molecular pathways involved in response to the simultaneous deletion of *fat-5* and *cyp-35A2*.

# Chapter Seven

*Characterization of the*

fat-5(tm420);cyp-35A2(gk317)

*double knockout*

# 7 Characterization of the *fat-5(tm420);cyp-35A2(gk317)* double knockout

## 7.1 Introduction

The previous Chapter suggested that the expression of *fat-5* and *cyp-35A2* are correlated. Furthermore, RNAi of *cyp-35A2* in a *fat-5* knockout background resulted in an extended lifespan phenotype of worms, which notably were also marked by a reduced body surface area. It was therefore deemed to be of interest to create a double knockout strain using single mutants of each gene.

It is reported that *fat-5(tm420)* mutants do not exhibit the normal fat stores(Watts, 2009). In addition, some studies (Menzel et al., 2005, Ashrafi et al., 2003) have already reported that the lipid profile of *cyp-35A2(gk317)* is significantly impaired. In a more recent paper (Aarnio et al., 2011) at least four members of the cytochrome P450 family were shown to be involved in lipid pathways.

### 7.1.1 Many transcription factors in the lipid regulatory pathway are involved in responses to *fat-5* and *cyp-35A2* deletion

#### *7.1.1.1 Sterol-Regulatory-Element-Binding Protein (SREBPs)*

The Δ9 desaturase, *fat-5*, interacts with several key fat regulatory genes such as *sbp-1*, which is the *C. elegans* homolog of the sterol-regulatory-element-binding protein (SREBP) family of basic helix-zipper transcription factors. SREBPs are essential for the regulation of cholesterol levels and fatty acid homeostasis in mammals. The inactive form of SREBP is located outside the endoplasmic reticulum (ER) membrane. If the level of specific cellular lipids drops, certain

proteins are transported into the Golgi apparatus and proteases that are released from the N-terminal of SREBP bind to certain proteins. Thereafter, SREBP is translocated to the nucleus and induces the transcription of lipogenic genes. Once bound to the target sequence of specific promoters, SREBP and nuclear hormone receptors (NHRs) build multi-protein co-regulator machinery systems which contain both transcriptional cofactors responsible for connecting the transcriptional activators and the transcription initiation MDT-15 which binds specifically to both NHR-49 and SREBP (Watts, 2009).

When *sbp-1* is either knocked out or knocked down via RNAi, the resultant nematodes display significantly fewer stored fat droplets, diminished growth and a significantly lower expression of lipogenic genes, including *fat-5* and *fat-7* (Ashrafi et al., 2003, McKay et al., 2003, Kniazeva et al., 2004, Yang et al., 2006, Watts, 2009).

#### *7.1.1.2 Nuclear Hormone Receptors (NHRs)*

Small hydrophobic molecules act as ligands for nuclear hormone receptors (NHRs) and the resultant dimerized NHRs enter the nucleus to target promoter sequences containing hormone response elements. Both NHR-49 and NHR-80 are important for the expression of *fat-5* and *fat-7*. When *nhr-49* is deleted, the expression of *fat-5* and *fat-7* decreases dramatically (Watts, 2009). Moreover, NHR-49 is involved in the regulation of β-oxidation as well as the expression of several other essential genes linked to the dietary input. The closest structurally similar mammalian counterpart to the *C. elegans* NHR-49 is the hepatocyte nuclear factor 4 (HNF-4). However, functionally NHR-49 is also related to the mammalian peroxisome proliferator-activated receptors (PPARs) (Watts, 2009).

It has been confirmed by several studies such as, Van Gilst and colleagues, that *nhr-49* is essential for a normal lifespan. Deletion in the ligand-binding domain of the *nhr-49* sequence results in the generation of short-lived mutants (6-8 days in comparison to the normal lifespan of 12-18 days in *C. elegans* at 20-23°C). Additionally, mutations in *nhr-49* lead to an accumulation of excessive fat levels due to the reduced expression of mitochondrial β-oxidation genes (Van Gilst et al., 2005b).

#### *7.1.1.3 DAF-16, the* C. elegans *fork head box O (FOXO)*

The *C. elegans* homolog of FOXO, namely DAF-16 (abnormal DAuer Formation), is a transcription factor involved in the insulin/IGF-1 signaling-mediated pathway (IIS). The IIS is responsible for several diverse pathways including dauer formation, aging, fat metabolism, stress responses and innate immunity. An increase in the nematode's lifespan can be related to dietary restrictions or a reduction in IIS pathways (Gems and Riddle, 2000, Lin et al., 2001). In fact, longevity is not a simple concept and unlikely reliant only on ROS[22] formation, which was previously reported to be a major cause. It has been shown that a healthy lipid status promotes longevity, however the precise mechanisms are yet to be defined. Several fat-regulatory genes are involved in response to an extended lifespan such as *lips-4*, *lips-7*, *fat-6*, *lips-17*, *fard-1*, *fat-5* and *hacd-1*. These genes are involved in lipase activity, desaturation mechanism, dehydrogenizing and fatty acid reductase activity. *C. elegans daf-16* has been studied in great detail including its involvement in several metabolic activities such as lifespan, sugar metabolism and lipid pathways. DAF-16 extends the

[22] Reactive Oxygen Species

lifespan of nematodes by regulating the expression of several genes that are involved in anti-oxidant, anti-microbial and metabolic activities (Lee et al., 2003, Murphy et al., 2003, Oh et al., 2006, Boulias and Horvitz, 2012).

The link between transcription factor DAF-16 and its regulatory effects on the lipid composition of the nematodes have been studied to some extent (Shmookler Reis et al., 2011). Though, structural properties of fatty acids (features such as number of branches, chain length and saturated/unsaturated ratio) have never been studied in depth, and may well play a role in the lifespan of nematodes (Shmookler Reis et al., 2011).

#### *7.1.1.4 Cytochrome P450 family members (CYPs)*

Cytochrome P450s (CYP-) are a large family of diverse NADPH-dependent mono-oxygenases mainly involved in the metabolism of endogenous compounds, including fatty acids and lipid signaling molecules, as well as a role in oxidation. CYP- family members have been mostly studied from a toxicological point of view, where have been linked to some xenobiotics such as atrazine, PCB52 and fluoranthene (Aarnio et al., 2011, Menzel et al., 2005, Menzel et al., 2007).

Gene silencing by RNAi has revealed that the CYP-35A family members target the lipid metabolism of the worms (Ashrafi et al., 2003). It was also reported that mutations in *cyp-35A1* and *A5* results in a significantly decreased intestinal fat accumulation (Aarnio et al., 2011). Nonetheless this study showed no changes in the lipid composition of *cyp-35A2,* which contradicts Ashrafi's work (Menzel et al., 2001, Aarnio et al., 2011, Ashrafi et al., 2003).

## 7.2 Aim

In order to assess the observed characteristics of the knockout/down mutant, *fat-5* (*cyp-35A2* RNAi), a *fat-5(tm420)* and *cyp-35A2(gk317)* knockout will be created to enable the study of life history traits in a double mutant background. Furthermore, as both *fat-5* and *cyp-35A2* have mammalian homologous (human homologs are SCD-1 and CYP2C8, respectively) it may be possible in the future to extend the research into the higher organisms and find potential leads to tackle hereditary obesity.

## 7.3 Results

### 7.3.1 Creating a *fat-5(tm420);cyp35A2(gk317)* double knockout

A new strain was created by mating the *fat-5(tm420)* and *cyp-35A2(gk317)* mutants (section 2.3.12). Thereafter, individual progenies were isolated and cultured on 12-well plates allowing them to reach adulthood. Once the animals had started to lay eggs, the parent nematodes were lyzed using the single worm lysis technique and genomic DNA was extracted to screen for homozygous mutants via nested PCR (Figure 7.1). These double mutants were used for further investigations.

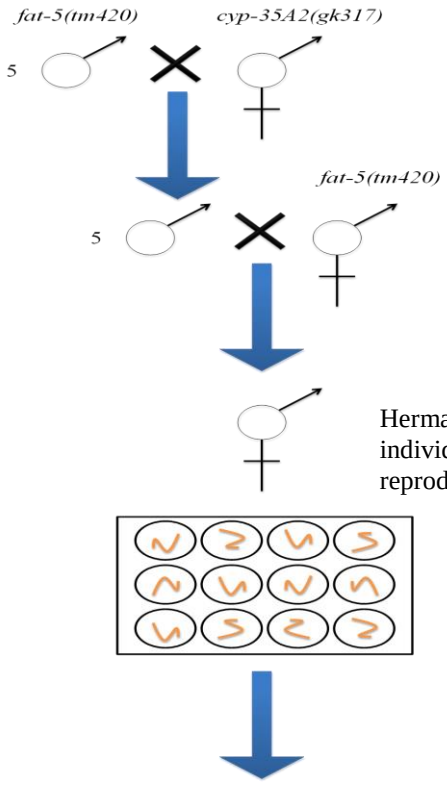


Hermaphrodite nematodes were singled out into individual wells of 12-well NGM plates and allowed to reproduce (4-5 sets of 12-well plates were maintained).

Single worm PCRs on the gravid adults after the first few hours of reproduction.

**Figure 7.1 Generation of double knockout nematodes.** Once the hermaphrodites were isolated, their offspring were screened using single worm lysis followed by a nested PCR to confirm the homozygous double mutants.

### 7.3.2 Nile Red staining is significantly reduced in the *fat-5(tm420);cyp-35A2(gk317)* double mutant

As discussed in Chapter Three, the value of vital dye Nile Red in visualizing lipid droplets has been challenged, however it can still be utilized in preliminary studies. In addition, Nile Red might stain certain fatty acids selectively, therefore if no change in the red fluorescent intensity of the Nile Red stained samples are observed, might indicate that the level of those fatty acids are not changed.

Nile Red staining was performed on four strains of wild-type, *fat-5*(*tm420*), *cyp-35A2*(*gk317*) and the double mutant *fat-5(tm420);cyp-35A2*(*gk317*). Age-synchronized nematodes of each strain were incubated with Nile Red infused *E. coli* OP50 for 72 hours. Thereafter, individual worms were mounted on 2% Agarose pads with a mixture of 1:1 M9 and Sodium Azide (50 mM) to paralyze the nematodes before capturing images using a wide-field microscope (Nikon Eclipse TE2000-S, Japan). The Nile Red staining pattern of 10 individual *C. elegans* was visualized in each strain and the red fluorescence intensity was analyzed using the ImageJ software (version 1.46, Wayne Rasband, NIH, USA). Nile Red positive organelles were assessed for determining their shape and the number of stained droplets.

Interestingly, Nile Red positive compartments in *fat-5(tm420)* displayed a similar pattern to the wild-type nematodes, however the relative red fluorescent intensity was lower than the wild-type (Figure 7.2). In contrast, the staining pattern of *cyp-35A2*(*gk317*) and the *fat-5(tm420);cyp-35A2(gk317)* double knockout were visually different from the wild-type and *fat-5*(*tm420*). In *cyp-35A2*(*gk317)* and *fat-5(tm420);cyp-35A2(gk317)* the red fluorescent intensity of Nile Red positive organelles was strikingly low and the shape of the stained droplets was not

defined clearly (Figure 7.2). In *cyp-35A2(gk317)* the number of Nile Red positive compartments was significantly reduced in comparison to the wild-type and the red fluorescent signal was marginally above the background auto-fluorescence (Figure 7.2). The *fat-5(tm420);cyp-35A2(gk317)* mutant exhibited a dramatic reduction in the number of Nile Red stained areas and droplets were not well-defined nor spherical in shape as seen in wild-type and *fat-5(tm420)* (Figure 7.2). Furthermore, the relative fluorescent intensity of Nile Red stained areas was quantified in all four strains. The average red fluorescent intensity of wild-type was normalized to 100% and compared to *fat-5(tm420)*, *cyp-35A2(gk317)* and the *fat-5(tm420);cyp-35A2(gk317)* (Figure 7.3). Quantitative analyses revealed that Nile Red staining of *fat-5(tm420)* was 19% reduced in comparison to the wild-type, however this change was statistically not significant (Figure 7.3). The fluorescent intensity of *cyp-35A2(gk317)* was decreased by 24%, which was a statistically significant reduction (Figure 7.3). The double deletion of *fat-5* and *cyp-35A2* resulted in a severe reduction of Nile Red stained compartments, manifested by a 57% reduction in the relative red fluorescent intensity within main areas of staining (the anterior to the gut) in comparison to the wild-type (Figure 7.3).

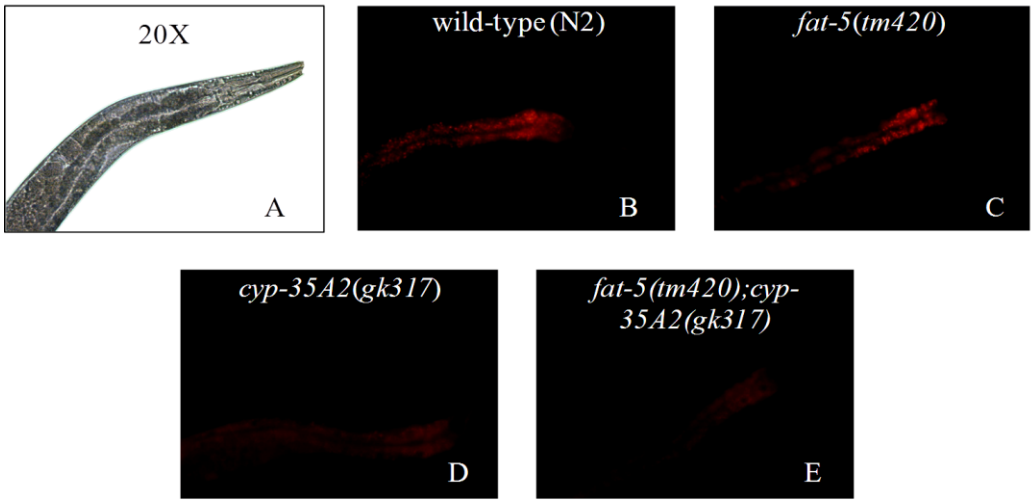


**Figure 7.2 Nile Red distribution in *fat-5(tm420);cyp-35A2(gk317)* double mutants compared to the wild-type, *fat-5(tm420)* and *cyp-35A2(gk317).*** All four strains were age-matched and incubated with the vital dye Nile Red and photographed after 72 hours. The image of a wild-type nematode (20X) is presented (A) to demonstrate the photographed area. Nile Red stained organelles in mutant strains were compared to the staining pattern in wild-type animals (B). *fat-5(tm420)* was marked by a reduction in the red fluorescent intensity (C) however the Nile Red stained organelles had a similar shape to the wild-type counterparts. In *cyp-35A2(gk317)* the Nile Red stained compartments (D) were significantly reduced in the overall number and the signal was close to the background auto-fluorescence. The *fat-5(tm420);cyp-35A2(gk317)* double mutant (E) displayed the same phenotype as the *cyp-35A2(gk317)*.

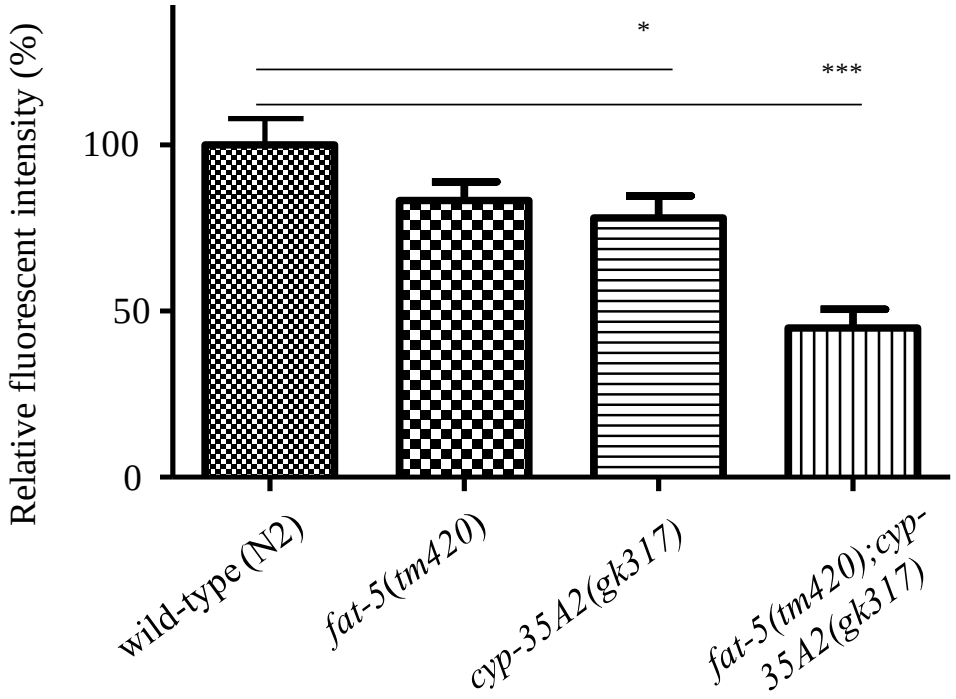


**Figure 7.3 Nile Red intensity of mutant nematodes compared to the wild-type (normalized to 100%).** Quantitative analyses using ImageJ software revealed that the red fluorescent intensity was lower in *fat-5(tm420)* in comparison to the wild-type, yet this reduction was insignificant. In *cyp-35A2(gk317)* the relative fluorescent intensity was decreased with a statistical significance. The *fat-5(tm420);cyp-35A2(gk317)* double knockout exhibited a strikingly significant reduction in the relative fluorescent intensity. Each bar graph represents the mean Nile Red intensity measured from 10 worms ± the standard error of the mean (SEM). A one-way ANOVA was applied to define the statistical significance. The reduction was mostly pronounced in *cyp-35A2(gk317)* and the *fat-5(tm420);cyp-35A2(gk317)* double mutant (* $p < 0.05$, *** $p < 0.001$).

### *7.3.3* Survival rate is extended in the *fat-5(tm420);cyp-35A2(gk317)* mutant

When *cyp-35A2* was knocked down by RNAi in the *fat-5(tm420)* background, lifespan and maximum survival were extended. To confirm this phenotype, a lifespan assay was performed using wild-type, *fat-5(tm420)* and *cyp-35A2(gk317)* and the *fat-5(tm420);cyp-35A2(gk317)* double mutant. The median

survival rate of wild-type nematodes was 13 days, which was reduced in the *fat-5(tm420)* and *cyp-35A2(gk317)* mutants to 11 and 12 days, respectively (Figure 7.4). Interestingly, the median lifespan of the *fat-5(tm420);cyp-35A2(gk317)* was 17 days. The extension in median survival of the double knockout was statistically highly significant when compared to the single mutants (Figure 7.4). The maximum lifespan was also considerably increased in the *fat-5(tm420);cyp-35A2(gk317)* mutant, these animals lived up to 28 days whereas wild-type nematodes reached a maximum survival of 21 days and the single mutants each lived up to 17 and 18 days (Figure 7.4, Appendix Seventeen).

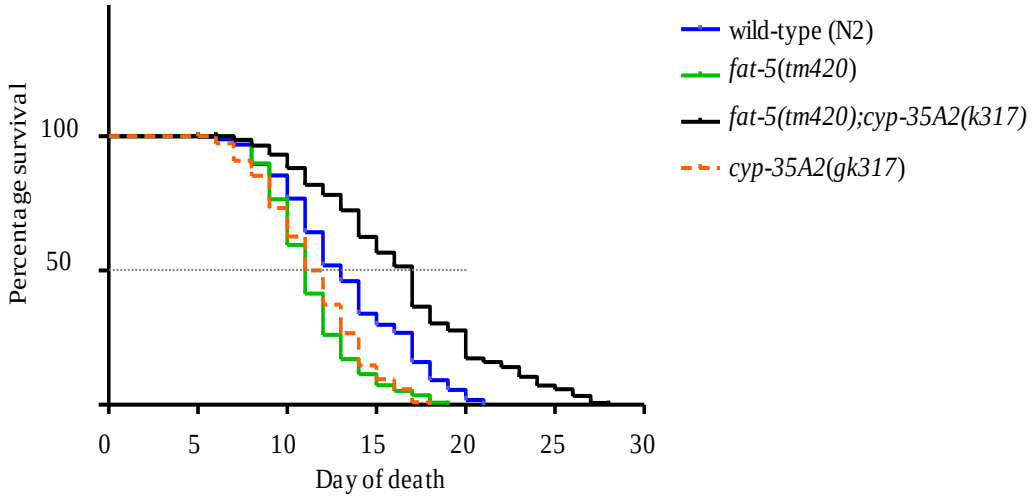


**Figure 7.4 Effect of *fat-5* and/or *cyp-35A2* mutation on lifespan.** Survival rate of wild-type, *fat-5(tm420), cyp-35A2(gk317)* and the double mutant were compared. Median lifespan and the maximum survival of each strain were determined, and graphs were plotted by the Kaplan-Meier method followed by a Log-Rank (Mantel-Cox) test with 95% significance (GraphPad Prism v5 software). The median lifespan (50% alive) and maximum lifespan in the double knockout nematodes was significantly extended in comparison to the wild-type as well as the corresponding single knockout strains. The median survival rate of wild-type was 13 days, but notably reduced in the *fat-5(tm420)* and *cyp-35A2(gk317)*, each experimental group of the nematodes was started with a population of 400 age-matched worms.

### 7.3.4 P57 treatment increases the body size of *fat-5(tm420);cyp-35A2(gk317)* mutant

Age-synchronized nematodes (L1) of the *fat-5(tm420);cyp-35A2(gk317)* were plated on designated NGM Agar plates seeded with *E. coli* OP50 supplemented with P57 (0, 0.03 or 0.3 μg/mL). Nematodes were maintained and photographed every 24 hours over six days (144 hours post-hatch). Thereafter, two growth parameters (length and volumetric surface area) of each worm were determined using the Image Pro-Express software (Media Cybernetic, Buckinghamshire UK). P57 exposure started to affect the development after 48 hours post-hatch. In the absence of P57, the *fat-5(tm420);cyp-35A2(gk317)* reached the final body surface area within four days (96 hours post-hatch) (Figure 7.5). The double mutant reached, when treated with the P57 (0.03 and 0.3 μg/mL), a significantly increased overall body surface area (i.e., volumetric expansion), with an approximate 20% increase at 144 hours post-hatch (Figure 7.5). A two-way ANOVA statistical analysis followed by Bonferroni post-test multiple comparisons revealed that despite the significant increase in the overall volumetric body size of P57-treated nematodes, there was no dose-dependency amongst the two dosing regimes (Figure 7.5).

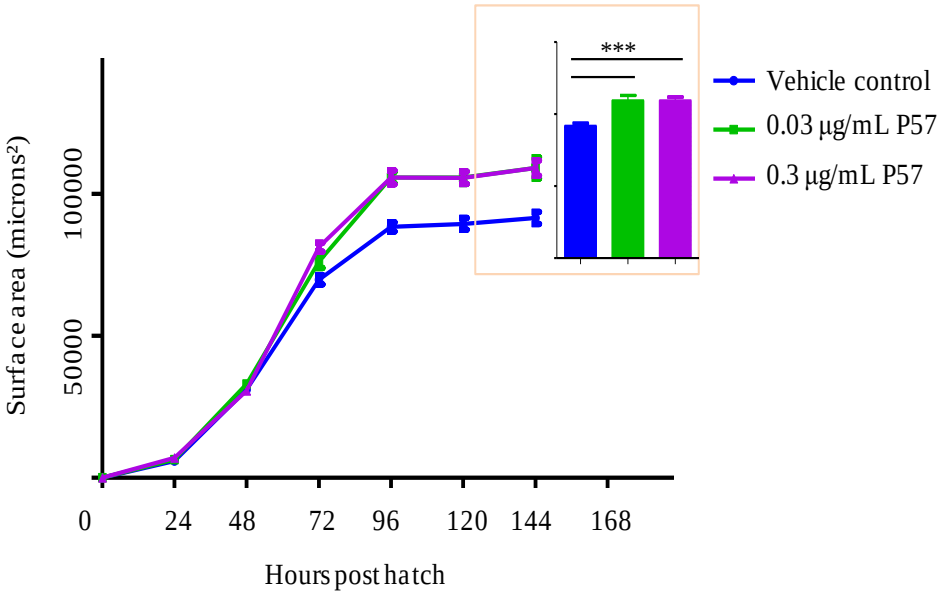


**Figure 7.5 Body surface area of the *fat-5(tm420);cyp-35A2(gk317)* mutant in response to P57 exposure.** Volumetric changes of the double mutant were analyzed by tracing the surface area of individual worms every 24 hours for a period of six days after hatching. Regardless of P57 exposure, all three conditions reached a plateau within 4 days. Treatment with two doses of P57 resulted in significantly larger animals in comparison to the vehicle control group. A two-way ANOVA confirmed the variation to be significant, however with no dose dependency between the P57 concentrations. Each data point is the average body surface area from 20 nematodes ± standard error of the mean (SEM). Bar graphs present the final surface area at 144 hours post-hatch (*** $p < 0.001$).

The changes in length over time were also assessed. P57 treatment of *fat-5(tm420);cyp-35A2(gk317)* resulted in a marginal increase in the final length of the animals and no significant variations between the two concentrations of P57 applied were observed (Figure 7.6). Since the P57-exposed animals were larger in volume but their length remained, at large, unaffected by P57 treatment, exposed nematodes resembled a mild "dumpy" phenotype. In addition Table S. 21 in Appendix Eighteen displays data corresponding to the growth changes in double mutant nematodes upon P57 treatment.

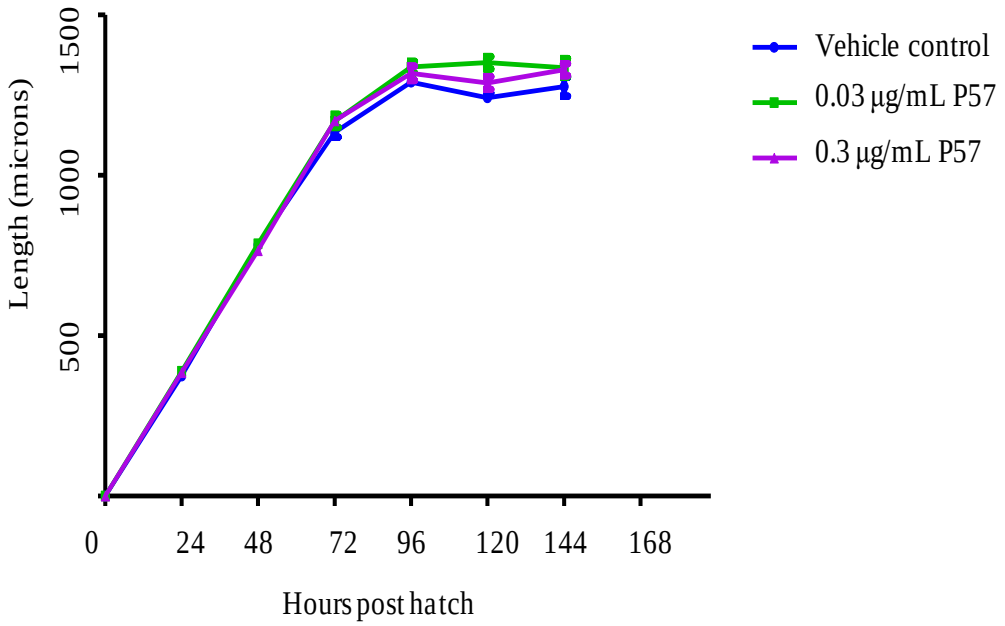


**Figure 7.6 P57 effects on the length of the double knockout mutant during and after larval development.** The length of the *fat-5(tm420);cyp-35A2(gk317)* double knockout was traced over a period of six days. Overall P57 exposure did not influence the length of the animals. Statistical analyses using a two-way ANOVA with Bonferroni *post hoc* test returned no statistical difference among groups.

### 7.3.5 Longevity in *fat-5(tm420);cyp-35A2(gk317)* is reversed upon P57 treatment

Lifespan was also investigated in the *fat-5(tm420);cyp-35A2(gk317)* in response to P57 exposure. The lifespan assay was performed as explained (section 2.3.8) and daily death was counted to determine the median lifespan and also the maximum survival rate at each condition. Throughout the egg-laying period the nematodes were transferred onto new plates to separate the adults from the progenies (Figure 7.7).

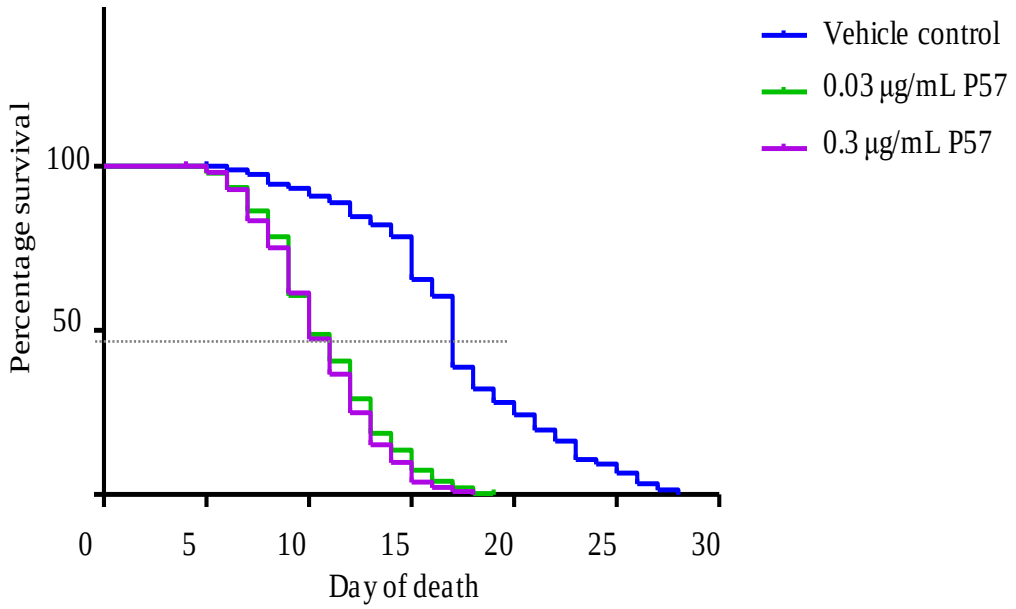


**Figure 7.7 Influence of P57 on the survival rate of the *fat-5(tm420);cyp-35A2(gk317)* double mutant.** Lifespan of *fat-5(tm420);cyp-35A2(gk317)* was analyzed following the exposure to 0, 0.03 and 0.3 µg/mL P57. The median lifespan as well as the maximum survival of the nematodes were quantified. Under control conditions, the median survival rate (50% alive) and maximum survival rate of *fat-5(tm420);cyp-35A2(gk317)* reached 17 days whereas upon treatment to P57, the median lifespan reduced significantly to 10 days in both exposure groups. Graphs were plotted by the Kaplan-Meier method and Log-rank (Mantel-Cox) statistical analyses determined the change in the median lifespan to be highly significant (**** $p < 0.0001$). However, there was no dose-dependency observed between the P57 doses. Each experimental condition was started with a population of 400 worms.

The median lifespan of *fat-5(tm420);cyp-35A2(gk317)* was 17 days, however upon treatment with P57 the median survival was shortened by 41% with no dose dependency. The maximum survival of *fat-5(tm420);cyp-35A2(gk317)* was 28 days whereas the P57-exposed worms only lived up to 19 and 18 days at 0.03 and 0.3 µg/mL doses, respectively. The difference in survival rate of the control *fat-5(tm420);cyp-35A2(gk317)* and P57-treated groups was statistically significant with a *p* value of 0.0001 (Figure 7.7, Appendix Nineteen).

### 7.3.6 Transcriptional effects of *fat-5* and *cyp-35A2* deletion

Life history traits such as lifespan and growth parameters were significantly different in the *fat-5(tm420);cyp-35A2(gk317)* mutant, resulting in a long-lived phenotype marked by a smaller overall body surface area. Moreover, the double mutant exhibited smaller and fewer Nile Red stained compartments. It was therefore deemed to be of interest to investigate possible changes at the molecular level.

A series of real-time quantitative PCRs were performed to evaluate the transcriptional response of selected genes in wild-type, *fat-5(tm420), cyp-35A2(gk317)* and the *fat-5(tm420);cyp-35A2(gk317)* double mutant. Primers and probes were designed using the Universal Probe Library Software (available at Roche Diagnostics website http://lifescience.roche.com). Expression of each gene was normalized to the invariant *rla-1* (a ribosomal house keeping gene) and transcriptional changes were compared to the basal expression of the chosen gene in wild-type nematodes. The interaction network of *fat-5* was taken from the nematode portal wormbase (www.wormbase.org) and potential candidates were chosen based on their predicted link to both metabolic changes and lifespan (Watts, 2009). Selected genes were *daf-16, nhr-49, sbp-1, cyp-35A5* and *cyp-35C1*.

Nematodes were age-synchronized to L1 stage and plated on designated NGM Agar plates, incubated at 20°C for a maximum of 40 hours (young L4s), thereafter samples of each strain were collected, followed by the total RNA extraction and reverse transcription to produce the cDNA which served as the template for the quantitative assessment (sections 2.3.2 and 2.3.3). RT-PCR

analyses were performed as described in the methodology section 2.3.4. A list of probe and oligo sets designed by UPL software are provided (Appendix Twenty). The basal expression of each gene was normalized to 1 for the wild-type animals (Figures 7.8, 7.9 and 7.10) and the relative transcriptional copy number of the selected genes was determined in all four strains raised in the presence or absence of P57 (Figures 7.8 and 7.9).

The *C. elegans* FOXO homolog, *daf-16* is involved in several metabolic pathways including longevity. The expression of this gene was quantified in *fat-5(tm420), cyp-35A2(gk317)* and the *fat-5(tm420);cyp-35A2(gk317)* mutant and compared to the expression in wild-type worms. In *fat-5(tm420);cyp-35A2(gk317)* the expression of *daf-1*6 was up-regulated significantly, in contrast *fat-5(tm420)* marginally expressed *daf-16* (Figure 7.8, left Panel). P57 treatment, suppressed the expression of *daf-16* in wild-type and *fat-5(tm420);cyp-35A2(gk317),* but not in *fat-5(tm420)* or *cyp-35A2(gk317)* (Figure 7.8, left Panel).

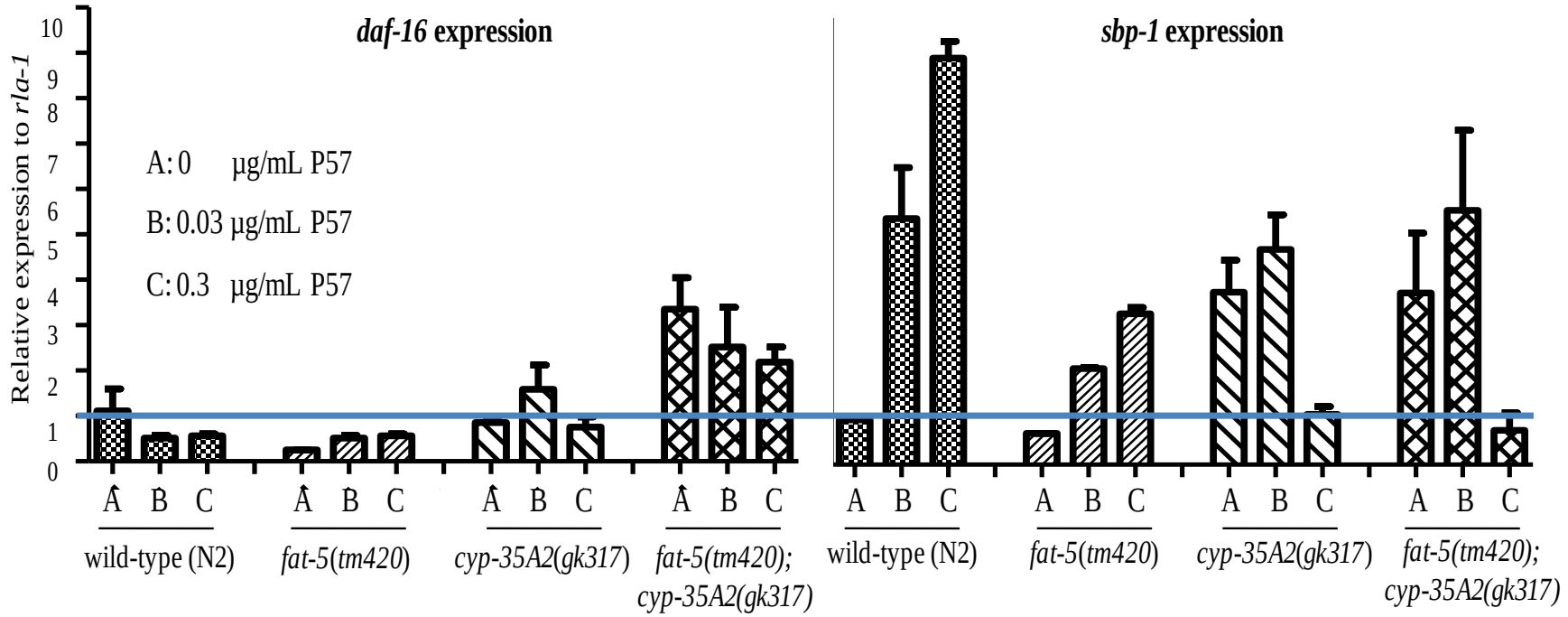


**Figure 7.8 The transcriptional responses of *daf-16* and *sbp-1* in wild-type, *fat-5(tm420), cyp-35A2(gk317)* and *fat-5(tm420);cyp-35A2(gk317)* treated with and without P57.** Genes involved in aging- and lipid-regulatory pathways were selected to evaluate, by qPCR, expression changes associated with P57 treatment (0, 0.03 and 0.3 µg/mL, A, B and C respectively). The expression of *daf-16* (left Panel) and *sbp-1* (right Panel) were quantified in all four strains and the transcriptional response was normalized to 1 in wild-type. Each bar graph presents the average fold changes of the selected gene normalized to the invariant *rla-1* assessed from two independent experiments with at least three technical repeats in each condition ± the standard error of the mean (SEM).

The nematode homolog of sterol-regulatory-element-binding protein (SREBP) is *sbp-1* and is believed to be involved in lipid regulatory pathways. Therefore, the transcriptional response was quantified in wild-type, *fat-5(tm420)*, *cyp-35A2(gk317)* and the *fat-5(tm420);cyp-35A2(gk317)* exposed to P57 (Figure 7.8, right Panel). In control conditions (i.e., the absence of P57) the expression of *sbp-1* was similar in wild-type and *fat-5(tm420),* however *sbp-1* was significantly up-regulated in *cyp-35A2(gk317)* and *fat-5(tm420);cyp-35A2(gk317).*

In the presence of P57, *sbp-1* expression was elevated in wild-type and *fat-5(tm420),* whereas the transcriptional response of the gene was suppressed significantly in *cyp-35A2(gk317)* and the *fat-5(tm420);cyp-35A2(gk317),* at least in the higher dose (0.3 μg/mL P57) (Figure 7.8, right Panel).

The nuclear hormone receptor *nhr-49*, which is also an important regulator of lipid metabolism in *C. elegans*, was also assessed (Figure 7.9, left Panel). The expression of *nhr-49* was normalized to 1 in unexposed wild-type. The transcriptional response of *nhr-49* was suppressed in *fat-5(tm420)* but not in *cyp-35A2(gk317)* and *fat-5(tm420);cyp-35A2(gk317)* (Figure 7.9, left Panel). Upon treatment with P57, a robust transcriptional induction was observed in wild-type. Exposure to P57 induced *nhr-49* levels in *fat-5(tm420)* when applied in a low dose (0.03 μg/mL), though the effect was reverted when treated with 0.3 μg/mL of P57. A highly significant transcriptional suppression of *nhr-49* was observed in *cyp-35A2(gk317)* treated with P57. Overall, P57 did not significantly modulate the expression of *nhr-49* in *fat-5(tm420);cyp-35A2(gk317)* in comparison to the wild-type (Figure 7.9, left Panel).

Quantitative real-time PCR was performed to investigate whether the expression of *cyp-35A5* and *cyp-35C1*, which are believed to be co-expressed with *cyp-35A2*, is affected in a *fat-5* and/or *cyp-35A2* mutant background and in the presence or absence of P57. The expression of *cyp-35C1* was strongly suppressed in *fat-5(tm420)*, but significantly induced in *cyp-35A2(gk317)*. In *fat-5(tm420);cyp-35A2(gk317)* the transcriptional response of *cyp-35C1* was not modulated (compared to wild-type) (Figure 7.9, middle Panel). P57 treatment robustly suppressed the expression of *cyp-35C1* in all four nematode strains, suggesting that the response to P57 exposure was independent from the deletion of *fat-5* and/or *cyp-35A2* (Figure 7.9, middle Panel).

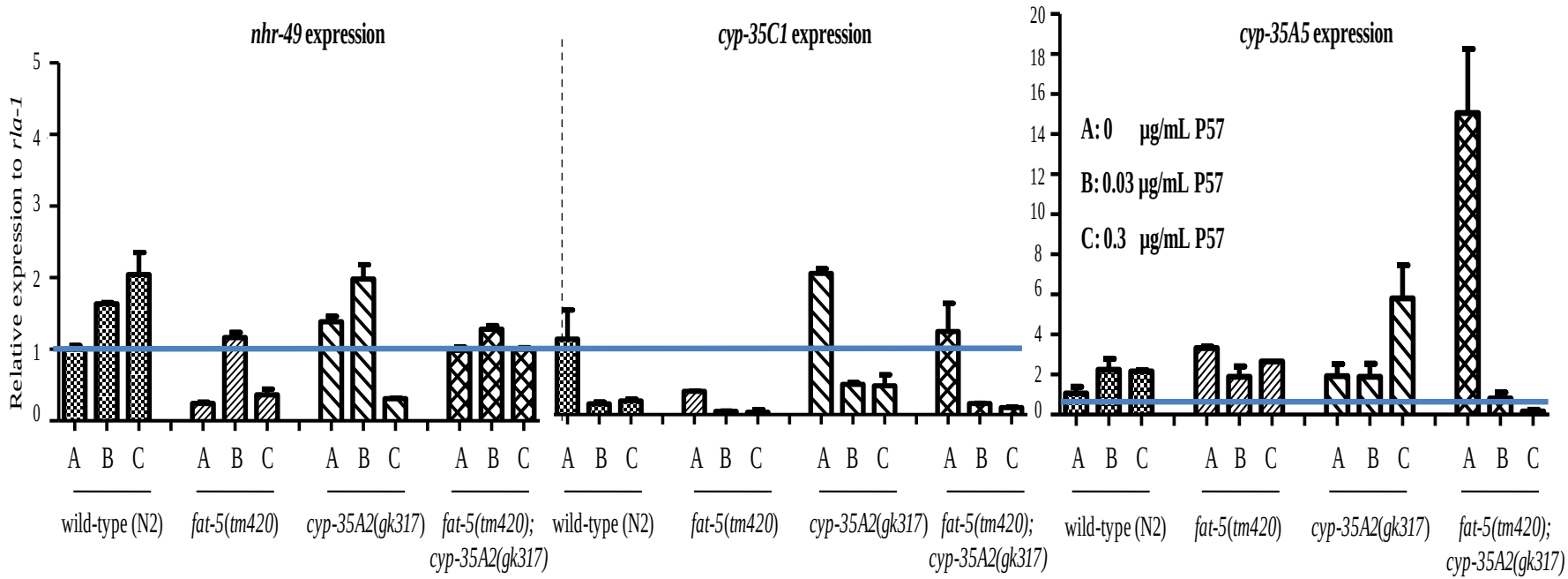


**Figure 7.9 The relative mRNA expression (fold change) of *nhr-49, cyp-35C1* and *cyp-35A5* in wild-type, *fat-5(tm420), cyp-35A2(gk317)* and *fat-5(tm420);cyp-35A2(gk317)* upon P57 treatment.** The transcriptional responses of *nhr-49* (left Panel), *cyp-35C1* (middle Panel) and *cyp-35A5* (right Panel) were selected due to their predicted involvement in fat regulatory pathways. Expression changes associated with P57 were also analyzed in worms exposed to 0, 0.03 and 0.3 µg/mL P57 (A, B and C, respectively). Each bar graph represents the average fold change from two biological experiments with at least three technical repeats in each condition ± the standard error of the mean (SEM).

Thereafter, the expression profile of *cyp-35A5* was quantified in *fat-5(tm420)*, *cyp-35A2(gk317)* and *fat-5(tm420);cyp-35A2(gk317)* and compared to the wild-type (Figure 7.9, right Panel). A modest but statistically robust transcriptional up-regulation was apparent in *fat-5(tm420)* and *cyp-35A2(gk317)*, whereas a striking induction of *cyp-35A5* was observed in the *fat-5(tm420);cyp-35A2(gk317)* double mutant (Figure 7.9, right Panel). Upon treatment with P57 the expression level of *cyp-35A5* was up-regulated in a dose responsive manner in both wild-type and *cyp-35A2(gk317)*, but marginally reduced in *fat-5(tm420)* and eventually completely suppressed in *fat-5(tm420);cyp-35A2(gk317)* (Figure 7.9, right Panel).

## 7.4 Discussion and Conclusions

As pointed out in the previous chapter, in the absence of *fat-5* and *cyp-35A2* (using the *cyp-35A2* RNAi performed in a *fat-5(tm420)* background), nematodes were smaller in size and had an extended lifespan. Because both genes have mammalian homologs, creating a double knockout of *fat-5* and *cyp-35A2* may help in understanding the underlying pathways and mechanisms involved in longevity and developmental growth in nematodes with possible applications in higher organisms. Phenotypic and molecular genetic properties of the created double knockout strain were studied as well as the influence of P57 on life history traits and the genetic profile of these nematodes.

The number and size of the Nile Red stained compartments were significantly reduced in the *fat-5(tm420);cyp-35A2(gk317)* double mutant, in regions that are believed to be dominated by lipid storage organelles. One might argue that, these mutants exhibit a lower lipid content resulting in a reduced red fluorescence within the intact body of the nematodes. The Nile Red controversy should not be discounted, nevertheless given that the Nile Red intensity was reduced by over 50% in the *fat-5(tm420);cyp-35A2(gk317)* nematodes, suggests that even if the triglyceride profile remained unchanged, the ratio of saturated/unsaturated fatty acids must have been affected. There were no defined Nile Red stained organelles in the *cyp-35A2(gk317)* strain utilized in this study, an outcome which is in agreement with a report by (Menzel et al., 2007).

The Nile Red profile of the *fat-5(tm420);cyp-35A2(gk317)* double mutant is similar to *cyp-35A2*(*gk317*) with no defined droplets and poorly visible red fluorescent stained areas. In contrast, where fat visualization was utilized using the tissue fixation technique followed by Oil Red O staining the *cyp-*

*35A2(gk317)* did not display the same pattern, therefore highlighting that there are inconsistencies between different studies (Aarnio et al., 2011). The proposed results by Aarnio et al. did not match with the figures in their paper, emphasizing that the analyses of Oil Red O and Nile Red lipid staining can be biased (details in Chapter Three). Furthermore due to the shift in fatty acid profile, Nile Red may not be able to target all types of fatty acids, therefore different approaches are needed based on the downstream studies. Regardless of all the issues surrounding the Nile Red debate, the double mutation of *fat-5* and *cyp-35A2* results in the formation of relatively pale-looking nematodes compared to the wild-type.

The median lifespan as well as the maximum survival rate of the *fat-5(tm420);cyp-35A2(gk317)* double mutant were comparable to the RNAi of *cyp-35A2* in a *fat-5(tm420)* background. This further confirms the reliability of RNAi by feeding that was performed in the previous chapter (Chapter Six). The extended survival rate of *fat-5(tm420);cyp-35A2(gk317)* could be driven by a reduced level of accumulated fat in the body, perhaps mimicking a dietary restriction, a hypothesis that leads to further investigations.

It is worth mentioning that other studies have reported a median lifespan of wild-type nematodes to be 18-19 days whereas in this chapter the median survival was only 13 days. This is not necessarily unusual, Gems and Riddle demonstrated that wild-type worms maintained by different research groups can vary in median lifespan, possibly due to the handling of the nematodes as well as the seasonal changes in the laboratory temperatures (Gems and Riddle, 2000).

Throughout this project the same wild-type strain of *C. elegans* was utilized therefore it was not possible to exclude the occurrence of spontaneous mutations.

Moreover, it was observed that lifespan assays that were performed during the warmer seasons resulted in a shorter median survival in comparison to the other time periods. Because nematodes have a short lifespan, a 24-hour life extension or reduction can introduce a major impact. The observed 5-day increase in the survival of the double knockout is statistically significant in comparison to the parental strains (the single knockouts). Furthermore, parental single mutants have a shorter median survival compared to the wild-type used in our laboratory, this emphasizes the complex mechanisms involved in longevity and perhaps how different pathways are involved.

The influence of P57 treatment on the *fat-5(tm420);cyp-35A2(gk317)* animals was explored, the data gathered from the developmental changes of the double mutant as well as the shortened lifespan suggests that P57 introduces a toxic effect and possibly speeds up the aging procedure. It is highlighted that P57 exposure results in the formation of considerably larger nematodes. Because during the aging process nematodes expand in the volumetric surface area size, the overall size expansion in P57-treated double mutants could be due to an elevated rate of aging (Croll and Smith, 1978). In addition, for years the theory of ROS formation leading to cellular oxidative damage and aging, was the main focus in aging studies however the oxidative stress levels and their connection to the aging theory were never consistent, experimentally. Perez et al., as well as Van Raamsdonk and Hekimi, have challenged the concept of reactive oxygen species generation through the mitochondrial respiration in aging (Perez et al., 2009, Van Raamsdonk and Hekimi, 2010, Ackerman and Gems, 2012). For instance, in a study by Yang and Hekimi in 2010 it was reported that, an elevated level of oxidative stress could lead to longevity and so were other data backing

up this idea (Schulz et al., 2007, Yang and Hekimi, 2010, Cabreiro et al., 2011). Moreover, in a mammalian study, a tightly controlled evaluation of anti-oxidant enzymes did not show any connection to longevity and the over-expression of these enzymes (Van Raamsdonk and Hekimi, 2010). Having said that, there was no evidence found to explain the aging concept of P57 exposure in the double knockout nematodes and ROS formation.

To address how the double mutation of *fat-5* and *cyp-35A2* influences metabolic pathways and leads to physiologically healthier nematodes, the transcriptional response of genes involved in aging and lipid-related pathways were selected and evaluated by the quantitative real-time PCR. Similar to mammalian species, where the ratio between HDL[23] and LDL[24] accounts for healthy versus unhealthy lipid components, nematodes may alter lipid metabolism by switching into healthier lipid compartments that eventually lead to longevity.

In the absence of *fat-5* the desaturation of palmitic acid is impaired, perhaps resulting in a higher concentration of saturated fatty acids. Consequently, elevated levels of saturated fatty acids can influence the cellular membrane fluidity because changes in the fatty acid composition affect the structure of the lipid bilayer. A tougher cell membrane might also protect the cellular compartments from oxidative stress and free radical formation. Therefore, less toxic material can be transported between cells, delaying the aging process (Ackerman and Gems, 2012). The *C. elegans daf-16* is a transcription factor involved in several metabolic and developmental pathways. In order to find potential links between fat metabolism and survival rate, several factors should be taken into account. For instance, one possibility could be that mutations in fat-

[23] High Density Lipoprotein
[24] Low Density Lipoprotein

regulatory genes, in this project the double mutation of *fat-5* and *cyp-35A2*, generate lipid-signaling molecules that regulate the lifespan of the nematodes. Secondly, an alteration in the fatty acid composition pool leading to the accumulation of more saturated forms potentially renders the membrane more resistance towards peroxidation (Ackerman and Gems, 2012). The mutation of *fat-5* and *cyp-35A2* perhaps modulates the fatty acid profile of the animals whereas the single mutation in *fat-5* may not necessarily change the fatty acid compositions suggesting that other desaturases such as FAT-6 and FAT-7 may compensate for the loss of function of FAT-5 (Watts, 2009). Nonetheless, mutation of *cyp-35A2* enforces significant alteration in the physiological state of the animals with notably extended survival rate.

Several transcription factors, enzymes and regulatory elements work together, which in concert trigger new phenotypic features. Calorie restriction or calorie restriction mimetic conditions and IIS mutants in addition to the germline deficient nematodes that exhibit higher lipid content are also longer lived (Ackerman and Gems, 2012).

We then propose that the double mutation of *fat-5* and *cyp-35A2* produces a strain, which has a possibly low fat content or has a reformed fatty acid composition and benefits from an extended lifespan. P57 extends the lifespan of wild-type nematodes (Chapter Five), but reduces the survival rate of *fat-5(tm420);cyp-35A2(gk317)* suggesting the presence of toxic effects.

To further explore the molecular basis of the *fat-5* and/or *cyp-35A2* link, the underlying metabolic pathways in response to P57 action quantitative real-time PCR was performed. The putative correlation between *fat-5* and *cyp-35A2* in aging and lipid-regulatory pathways was explored using up- and downstream

transcription factors that were reported in a study by (Watts, 2009). Although *nhr-49* was not directly affected by the double mutation of *fat-5* and *cyp-35A2*, it was induced by P57 treatment in a dose-dependent manner in wild-type nematodes. The transcriptional response of DAF-16, that serves as an essential transcription factor upstream of Δ9 desaturases including FAT-5 was induced statistically significant in the *fat-5(tm420);cyp-35A2(gk317)* double mutant. As DAF-16 is believed to be involved in longevity and in some fat regulatory responses, therefore the delayed aging phenotype that is observed in *fat-5(tm420);cyp-35A2(gk317)* may suggest the presence of a causative link between DAF-16 induction and the extended lifespan of the double mutant. In addition to this, over the past few years a link has been discovered between autophagy and longevity, which is further regulated by DAF-16/FoxO pathway. Lepierre *et al.*, reported that, autophagy is required for longevity responses. In addition, once germline is removed from nematodes or flies, they tend to live longer through DAF-16/FoxO (similar to insulin/IGF-1 signaling pathway). In long-live/germline-less mutants, lipid metabolism plays an essential role. Studies have shown that, upon removing of the germline the expression of LIPL-4 up-regulates, which is a lipase that is activated through DAF-16/FoxO transcription factor. It has also been shown that *lipl-4* is essential for lifespan extension in these worms. Interestingly, when *lipl-4* is up-regulated it increases the survival rate of the nematodes significantly, which proves a direct link between lipid metabolism and longevity in nematodes. In addition to this finding is a recently found link between the role of autophagy in hydrolyzing lipids and the effect on extending lifespan, a phenomenon named lipophagy (Lapierre et al., 2012).

The study by Lapierre *et al.,* suggested that the number of autophagic events are increased both in intestinal and hypodermal cells, since they are reported to be the main lipid storage regions. Additionally, *lipl-4* is mainly expressed in these tissues. At molecular level, an overexpression of many genes involved in autophagy were reported in long-lived/germline-less worms, genes such as *unc-51*/ULK1, *bec-1*/BECN1, and *lgg-1*/LC3. The study further implied that autophagy and lipid metabolism are regulated through the common upstream TOR in conjunction with the forkhead transcription factor DAF-16/FoxO and PHA/FoxA. Both transcription factors are involved in lipid metabolism and autophagy (Lapierre et al., 2012). This emphasizes not only the complexity of lipid regulation and aging but also the fact that many abundant pathways are involved in a healthy and extended survival rate in nematodes.

Overall, the transcriptional responses of *sbp-1, daf-16* and *cyp-35A5* are highly induced in the absence of *fat-5* and *cyp-35A2*, a characteristic that is not observed if only one of the genes is mutated. The over-expression of *sbp-1* may be due to a homeostatic mechanism for balancing the ratio between saturated and unsaturated fatty acids in nematodes. The striking overexpression of *cyp-35A5* can be due to a compensatory approach once *cyp-35A2* is mutated, however the response is most pronounced in *fat-5(tm420);cyp-35A2(gk317).* Although DAF-16 has been reported to play a major role in the survival rate of the nematodes, lifespan is not only directly regulated by DAF-16. As mentioned earlier, pathways influencing adiposity in *C. elegans* via DAF-16 activation through a kinase cascade exists upstream of Δ9 desaturases in fat synthesis/ breakdown (Watts, 2009) and our study proposes a role for FAT-5 in the expression of the DAF-16 transcription factor. There seems to exist a negative feedback between

f*at-5* and *daf-16* that, as in the absence of *fat-5* the expression of *daf-16* is significantly reduced. Yet the double mutation of *fat-5* and *cyp-35A2* triggers the expression of *daf-16* leading to a significant over-expression of the *daf-16*.

The *C. elegans* homolog of the sterol-regulatory-element-binding protein, SBP-1, is an essential component for a healthy lipid metabolism as its deletion has been shown to affect the fat accumulation of the animals (Gonczy et al., 2000, Ashrafi et al., 2003). Since *sbp-1* resides directly upstream of *fat-5* and is a regulator of *fat-5* expression (Watts, 2009), the effects of *fat-5* deletion alone, and in conjunction with *cyp-35A2*, revealed that the expression of *sbp-1* is not influenced extensively in the absence of *fat-5*. However *sbp-1* is highly induced in the absence of *cyp-35A2*, implying that *cyp-35A2* is a putative positive regulator of *sbp-1*. Though, in *fat-5(tm420);cyp-35A2(gk317)* the transcriptional response of *sbp-1* is induced which may be due to the absence of *cyp-35A2* rather than *fat-5* mutation. Finally, we suggest that the expression of *sbp-1* and deletion of *cyp-35A2* are inter-linked, as *cyp-35A2* appears to be required for the induction of *sbp-1*. Such regulatory mechanism is perhaps essential for maintaining a balanced and healthy lipid metabolism by monitoring the ratio of saturated to unsaturated fatty acids.

In wild-type and *fat-5(tm420)*, *sbp-1* is up-regulated in response to P57. This may be due to P57's anorectic effects (Chapters Four and Five). As nematodes tend to have a significantly reduced pharyngeal pumping rate when treated with P57, they might lack sufficient amounts of essential fatty acids. To compensate this, nematodes might insinuate the *de-novo* production of specific fatty acids, which normally account for only 7% of fatty acid formation. Therefore, *sbp-1* over-expression may be a molecular feedback to activate transcription factors

and enzymes involved in fatty acid synthesis to maintain the lipid homeostasis as both *nhr-49* and *sbp-1* are believed to co-express with *fat-5* (Watts, 2009, Watts and Browse, 2000, Watts and Browse, 2002).

As demonstrated by others, *fat-5* is not only regulated by *sbp-1* but also by other transcription factors such as *nhr-49* and *nhr-80* (the effects being mainly involved in the regulation of *fat-6* and *fat-7*). Furthermore, *sbp-1* and *nhr-49* are found to have a common co-activator namely *mdt-15* (Yang et al., 2006, Taubert et al., 2006, Nomura et al., 2010). Since *nhr-49* is reported to play an important role in the normal lifespan of the animals (Watts, 2009), its induction in response to P57 may be a possible cause of the extended lifespan in wild-type.

In the absence of P57, wild-type, *cyp-35A2(gk317)* and *fat-5(tm420);cyp-35A2(gk317)* express similar levels of *nhr-49*, suggesting that the expression levels of *nhr-49* and *cyp-35A2* are not correlated. In contrast, the severe suppression of *nhr-49* in *fat-5(tm420)* suggests that there might be a link between these two genes. NHR-49 is responsible for the mitochondrial β-oxidation in addition to fatty acid desaturation, and in the absence of *nhr-49* animals exhibit a higher fat content due to the reduced expression of β-oxidation genes (Watts, 2009).

As upon P57 treatment, *nhr-49* is over-expressed, which may explain the observed longevity in P57-treated wild-type animals. On the other hand, the *nhr-49* expression is not influenced by P57 in *fat-5(tm420);cyp-35A2(gk317)*, suggesting that two different pathways may be involved in the creation of long-lived double knockout animals.

As the *cyp-35A/C* gene members share protein domains and are co-expressed (information adapted from www.wormbase.org), their interaction network is

inter-woven. When studied in this project, the expression levels of two family members, *cyp-35A5* and *cyp-35C1,* were assessed in the presence or absence of *fat-5* and *cyp-35A2*. Ashrafi and colleagues had previously reported that the RNAi of *cyp-35A3* and *cyp-35A5* affect the normal lipid regulatory pathways in *C. elegans* (Ashrafi et al., 2003).

When *cyp-35A1, cyp-35A2, cyp-35A3, cyp-35A4* and/or *cyp-35A5* is knocked down, the resultant nematodes show almost complete fat-storage deficiency (Menzel et al., 2007), as confirmed by Nile Red staining. In contrast, Aarnio et al. (2011) demonstrated that only *cyp-35A1* and *cyp*-35*A5* exhibit a lower fat content phenotype and *cyp-35A2* and *cyp*-35*A4* have normal levels of stained lipid droplets as determined by the Oil Red O technique (Aarnio et al., 2011).

Likewise, mutations in *cyp-35A1* resulted in the over-expression of a certain fatty acid synthesizing genes, such as *fat-2*. By adding oleic or elaidic triglycerides to the normal diet of wild-type animals, *cyp-35A1* had shown to be non-responsive but *cyp-35A2, cyp-35A4* and *cyp-35A5* were significantly down-regulated (Aarnio et al., 2011). The expression of *cyp-* genes is localized in the intestine of the animals where most fat-droplets are also stored. Lipids are mainly accumulated in the form of triacylglycerides in intestinal lysosome-related organelles and in lipid droplets in the gut, in addition to the epidermal skin-like cells (Aarnio et al., 2011). Upon deletion of *cyp-35A2* and *fat-5,* the expression of *cyp-35A5* was strongly induced, although this over-expression was less pronounced in the respective single mutants (*fat-5(tm420)* and *cyp-35A2(gk317)*). Moreover, *cyp-35A5* expression is shown to be similar in wild-type and *cyp-35A2* mutants and when treated with P57, no significant link was observed. In contrast, there seems to be a connection between the deletion of *fat-5* and *cyp-*

*35A2* and expression levels of *cyp-35A5* in response to P57, leading to the notion that *fat-5* could perhaps serve as a precursor of *cyp-35A5* in the absence of *cyp-35A2* (as *cyp-35A5* is not significantly increased in *fat-5(tm420)*).

The transcriptional response of *cyp-35C1* is notably suppressed in the absence of *fat-5* and over-expressed approximately two fold when *cyp-35A2* is knocked out. Regardless of the worm strain, P57-treated animals exhibit a significant decrease in the expression levels of *cyp-35C1*, from this one can concluded that the expression levels of *cyp-35C1* in response to P57 is independent of *fat-5* and/or *cyp-35A2*.

To provide an overview of the putative correlation between selected genes within the *fat-5* and *cyp-35A2* pathways, we propose a network, which extends the lipid regulatory network firstly reported by Watts in 2009. The network consists of several transcriptional factors that reside upstream of FAT-5, FAT-6 and FAT-7. By combining the P57-dependent transcriptional responses of *fat-5* and c*yp-35A2* and their corresponding transcription factors and/or co-expressers, a modified network was suggested to highlight the complexity of lipid regulatory pathways and their connection to longevity and survival mechanisms (Figure 7.10)

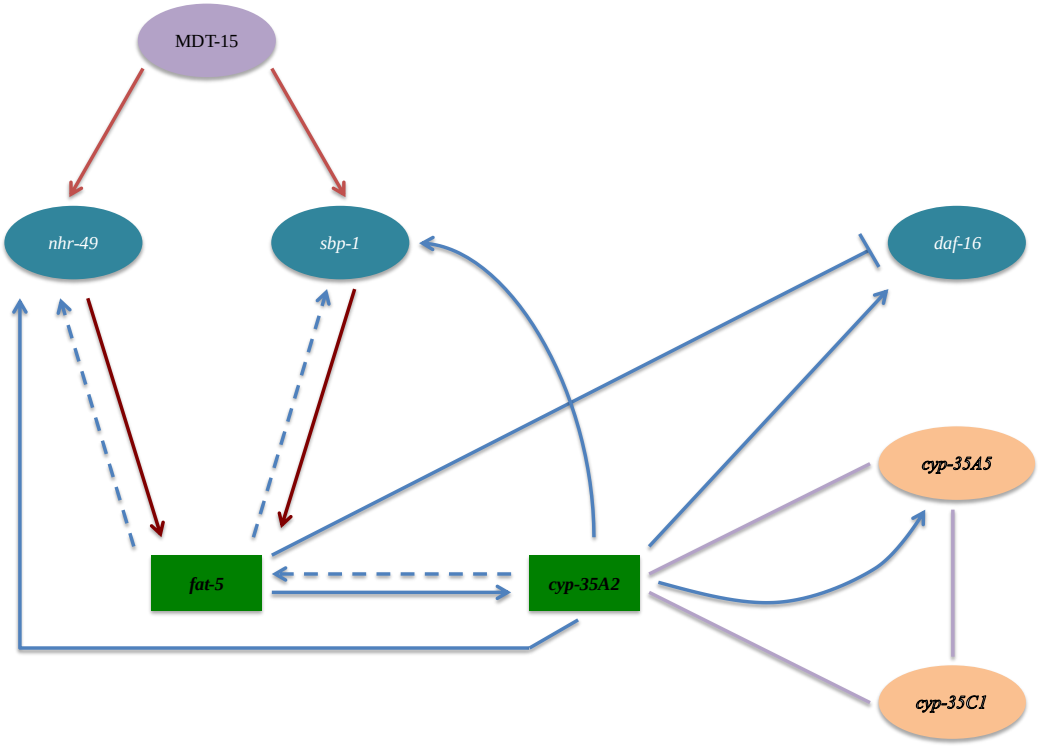


**Figure 7.10 The proposed network, combining lipid regulatory and survival rate influences in *C. elegans* in relation to *fat-5* and *cyp-35A2* deletions.** The model is designed based on the quantitative RT-PCR analyses of the genes in addition to their connection to the P57 compound in the lipid synthesis/breakdown. The red arrows indicate previously published interconnections while the dashed arrows and the blue/purple lines indicate the proposed genetic interactions perceived in this project. The *cyp-35A*- family members are reported to have co-expression yet no significant correlation was observed.

# Chapter Eight

## *Final discussion*

# 8 Final discussion

## 8.1 Obesity and herbal medication

Overweight or obesity are key factors of several fundamental illnesses involved in metabolic diseases, such as diabetes type II, coronary heart problems as well as certain types of digestive tract-related cancers. In principle, the lack of a balanced energy distribution results in an undesirable accumulation of fat (Ashrafi, 2007). Over the past few decades, the prevalence of obesity has increased due to environmental factors, which are an integral part of the modern (caused by single or multiple mutations) can lead to an excess of fat reservoirs (WHO, 2013).

Biochemical and molecular approaches have identified key regulators in lipid metabolism utilizing mammalian and model organisms (Elle et al., 2010). The presence of shared ancestral homologs of key regulators involved in lipid-related pathways suggests that genes found in worms may have a similar role in the human lipid metabolism (Elle et al., 2010). It was therefore deemed important to explore mechanisms underlying metabolic pathways so that hereditary overweight and obesity, which are non-contagious diseases of the 21$^{st}$ century, can be studied in more detail.

## 8.2 Discrepancies in lipid visualization

Several biochemical and microscopy techniques allow the visualization and quantification of fat content in nematodes. However, to date there is no single

approach that can visualize or quantify all different types of fatty acids in the body of worms. Staining lipid droplets by vital or fixative methods does not return consistent results, as fixative approaches usually have an alcohol-wash step that can potentially dissolve certain types of fatty acids (Almeida Barros et al., 2011). Furthermore, the fixation step is usually an invasive approach and leads to the fragility of the hypodermis resulting in a high risk that nematodes can burst before being visualized, especially when staining with Sudan Black.

Despite the literature stating that Oil Red O staining is as reliable as CARS microscopy (O'Rourke et al., 2009), it is a fairly labor-intensive method and in this present study MRWB fixation required an overnight incubation step which had to be followed by de-staining before visualization of the lipid droplets was possible. It was also demonstrated that, the Oil Red O dye mainly stains the eggs inside the body of nematodes, perhaps because of the high levels of vitellogenins and the affinity of the dye for these proteins (Figure 3.2), an observation that was not directly reported in the literature. However, the vital staining via Nile Red may also lead to false-positive results due to the nature of the staining procedure, upon which the long exposure time possibly leads to the accumulation of Nile Red in LROs. This phenomenon might be caused by worms treating the dye as a foreign compound and therefore quarantine the dye in LROs for later degradation. Furthermore, co-staining of the nematodes with Nile Red and LysoTracker® revealed that although there is some co-localization/overlap between Nile Red and the lysosome specific dye, there are still many areas that are exclusively marked by Nile Red, suggesting that the dye is not entirely exclusive to the LROs (Figure 3.4).

To further assess the reliability of Nile Red vital staining, the FLIM technique was modified to be applied to *C. elegans,* a technique that, for the first time, was introduced to whole animals (although a study by Kuo et al., (Kuo et al., 2013) has used the technique, yet not the same approach that we applied). Utilizing confocal microscopy, images were created to assess the Nile Red emission peak and confirm that Nile Red vital staining is a valuable technique for the preliminary investigation of major fat reservoirs in nematodes (Figures 3.5, 3.6, 3.7). Moreover, by applying FLIM, it was possible to stipulate that lipid droplets have a more defined surrounding and are spherical whereas Nile Red stained LROs or auto-fluorescence display unclear and scattered staining patterns, a notion that can be used to distinguish fat organelles from auto-fluorescence in nematodes (Figure 3.3). However, the precise nature of the Nile Red stained organelles could not be defined via the FLIM, as the system is yet to be optimized for whole organism studies. For example, it was not possible to establish whether the environment of Nile Red stained compartments are neutral or acidic.

The observation that results can differ dependent on the staining procedures used might be due to changes in the ratio of fatty acids (such as the conversion of saturated fatty acids to the mono/poly-unsaturated forms), a concept that can explain the inconsistency in the efficiency of visualization methods. Besides, it is worth to assess the fatty acid content and the changes in the ratio of saturated and unsaturated fatty acids via lipid extraction methods or GC-MS, however these analytical techniques are not only labor-intensive and costly but also insensitive, therefore require a large number of nematodes. Overall, a simple comparison between Oil Red O and Nile Red positive compartment can easily demonstrate

that perhaps different fatty acids have a certain affinity for a dye hence upon labelling of the lipid content with Oil Red O mainly lipids accumulated in the eggs can be observed whereas Nile Red mainly binds epidermal fatty acids.

Unfortunately, these shortcomings make it impossible to apply a universal approach to visualize lipid compartments in nematodes and different procedures should be adapted based on the downstream assays that need to be performed.

## 8.3 Pharmacological treatment of obesity

The pharmaceutical industry has invested much in obesity research, as chemical drugs seem to be more desirable than dieting, exercising or liposuction surgery. However, the safety and long-term effects of anti-obesity medication has been challenged. For example, Acomplia (also known as Rimonabant) and Reductil were anti-obesity drugs that were approved by the FDA[25], however, the former was withdrawn from the European market in 2008 and the latter was also discontinued in several Western and Asian counties due to severe side effects including a high risk of cardiovascular diseases and stroke. Due to the negative feedback and lack of alternatives, the demand for herbal anti-obesity remedies has mushroomed. There are several aspects that need to be taken into consideration before releasing an anti-obesity compound of herbal origin, such as identifying the number of active compounds, possible effects by inactive ingredients and the activity of the compound in different solvents or environments (Vermaak et al., 2011a).

[25] Food and Drug Administration

*Hoodia gordonii* a South African succulent has been known among African hunters to have thirst and/or hunger-quenching effects, a feature that received much attention by the anti-obesity drugs market resulting in a patent by Van Heerden and colleagues (Van Heerden et al., 2002).

Throughout the present study, it was deemed important to use the least invasive and non-toxic solvent for dissolving *H. gordonii* crude extract or pure P57. Unlike the plant extract, which was water-soluble, P57 required an organic solvent, such as methanol.

*H. gordonii* assays were performed by adding the plant extract to the bacterial food source (*E. coli* OP50) and NGM agar whereas, for cost reasons P57 was only administrated to OP50. The application of *H. gordonii* extract or P57 returned comparable data. Comparing results of *H. gordonii* extract exposure with P57 treatment was to explore the possibility of cross-activity, as it is possible for the "inactive" ingredients of the plant extract to have an impact on the efficiency of *H. gordonii* extract response in nematodes. Therefore it was essential to apply the active compound directly to pinpoint whether the phenotypic and molecular responses are because of the active compound or are an indirect response to the inactive compounds or additives of the *H. gordonii* extract capsules.

It was previously reported that *H. gordonii* extract is found to have anorectic effects in mammals, leading to weight loss symptoms (MacLean and Luo, 2004). Here, the exposure of *H. gordonii* extract resulted in a significant reduction in pharyngeal pumping rate, progeny number and growth characteristics in wild-type nematodes (Figures 4.2 to 4.9), however the lifespan of the worms was not influenced by the *H. gordonii* extract (Figure 4.10). Moreover, the Nile Red

stained compartments were reduced in *H. gordonii* extract-treated nematodes, suggesting that these animals may have a reduced fat content (Figure 4.6 and 4.7).

A genome-wide microarray was utilized to unravel the molecular pathways involved in the response to *H. gordonii* extract treatment. Selected genes from the microarray were further studied to confirm whether the main mode of action as suggested by the GO term analyses, is linked to the nutrient sensing and lipid pathways (Table 4.5). The key gene of interest belongs a Δ9 desaturase family member of proteins, namely FAT-5.

It is known that P57 is associated with the anorectic features of *H. gordonii* extract and appears to be homologous to the steroidal core of cardiac glycosides (MacLean and Luo, 2004). Moreover, P57 is known to target the central nervous system and in particular the hypothalamus, which is evidently involved in sensing metabolic or/and nutrient cues. Hypothalamus utilizes ATP as the main source of energy, therefore it can be concluded that P57 triggers a response by which body uses the internal ATP content rather than gaining the energy, ATP, by food consumption (MacLean and Luo, 2004). When wild-type nematodes were treated with P57, the pharyngeal pumping rate was reduced at L4 stage (Figure 5.3), a response that is analogous to fasting in mammals. This outcome may be due to appetite suppression as there is evidence that P57 acts via serotonin and TGF-β pathways in mammals (Srinivasan et al., 2008). Having said that, since the pharyngeal muscle contractions are controlled by serotonin (Hobson et al., 2006), P57 may modulate the serotonin pathway leading to

appetite suppression, however the literature has suggested that, in nematodes serotonin induces the rate of pharyngeal pumping, which is in contrast to mammalian organisms where the increased levels of serotonin lead to satiety (Srinivasan et al., 2008). Interestingly, the significant reduction in pharyngeal pumping was mainly observed at L4 stage but increased during adulthood, which is consistent with findings in P57-exposed rodents.

The P57 treatment of wild-type nematodes introduced a dose-dependent reduction in the growth parameters of the nematodes, resulting in the formation of smaller nematodes (Figures 5.5 and 5.6). In addition, the Nile Red intensity of stained compartments was attenuated in response to P57, however, inconsistency in the staining suggested that perhaps Nile Red is not a good candidate for assessing the fatty acid changes followed by P57 exposure (data not shown). Moreover, a significantly reduced progeny number upon P57 treatment may be due to the affected lipid status in the body of nematodes, resulting in the reduction of available energy for reproduction (Figures 5.7 and 5.8). This hypothesis aligns with the microarray data that showed an induction in vitellogenin-related genes (*vit-3, vit-4* and *vit-5*), which might reflect a compensation mechanism in response to the low energy reservoirs. Furthermore, reduced lipid content may induce a switch from reproduction mode to survival mode, by which the animals postpone optimal fecundity until environmental factors improve. The extended survival of P57-treated nematodes suggest that perhaps the compound has a calorie restriction mimetic influence, upon which animals consume less food and therefore have fewer stored lipid compartments followed by an increased lifespan (Figure 5.9). Yet this phenotype was not

observed when the crude extract was applied to the nematodes perhaps because other compounds might mask the possible life extending properties of the plant extract. The fact that both *H. gordonii* extract and its active compound P57 cause reduction in several life history traits, including the growth parameters, progeny number and the pharyngeal pumping rate, is consistent with the anticipated purpose of the medication, namely to decrease fat levels. Lipid reduction might occur through two distinctive paths, either by an increase in the energy expenditure or a decrease in the energy uptake (via eating). Having said that, a reduced energy uptake caused by appetite suppression will indisputably affect the stored energy and fatty acid available for reproduction, development and to some extent introduce results similar to calorie restriction and ultimately an extended median lifespan. An overview of the phenotypic characteristics of wild-type nematodes exposed to *H. gordonii* extract or P57 is summarized in Table 8.1. As mentioned earlier, direct administration of pure P57 introduces a more pronounced effect in comparison to *H. gordonii* extract.

| Life history trait | *H. gordonii* | P57 |
|---|---|---|
| Pharyngeal pumping rate | ↓ | ↓↓ |
| Body length | ↓ | ↓ |
| Surface area | ↓↓ | ↓↓ |
| Reproduction | ↓↓ | ↓↓ |
| Lifespan | ↔ | ↑ |
| Nile Red positive compartments | ↓↓ | ↓ |

**Table 8.1 Life history traits of wild-type nematodes treated with *H. gordonii* extract or P57.** An upwards pointing arrow indicates an increase, a downwards pointing arrow a decrease One arrow means a moderate effect, whereas two arrays a significant effect. Note that the horizontal arrow indicates no change.

Global transcriptomics identified key genes that were modulated in nematodes exposed to *H. gordonii* extract, which were explored further by assessing their response in P57-treated animals (Figure 5.10). Interestingly, there seem to be a more pronounced gene induction in P57-exposed nematodes, an expected outcome as the crude plant extract might have "inactive" compounds resulting in moderating the effect of the active compound. Therefore, although the mRNA level of selected genes determined by qPCR followed the same trend as the *H. gordonii* extract treatment, the fold changes were more significant upon P57 treatment. The top three most responsive genes upon treatment with either *H. gordonii* extract or P57 measured utilizing RT-PCR technique are listed in Table

8.2. The P57 doses are equivalent to the nominated amount of the active compound found in the dried plant extract.

It can be argued whether the observed responses (phenotypic and molecular levels) in regards to *H. gordonii* extract or P57 treatments were a direct influence of the exposure or an indirect effect via the *E. coli* OP50 since compounds were incubated with the bacteria before nematodes were placed, or if the effects were a combination of both. It would be ideal to investigate that by either mixing the compound with dead bacteria to exclude the possible effects of secondary metabolites generated by the bacteria. Another solution would be washing bacteria from the drug before placing the nematodes to examine the hypothesis.

| | ***H. gordonii*** | | **P57** | |
|---|---|---|---|---|
| | 0.01 mg/mL | 0.1 mg/mL | 0.03 µg/mL | 0.3 µg/mL |
| Y62H9A.5 | 2.9 ±0.4 | 5.1 ±1.0 | 2.2 ±0.2 | 12.4 ±1.2 |
| *fat-5* | 2.7 ±0.4 | 3.6±0.4 | 2.2 ±0.1 | 5.2 ±1.2 |
| *col-19* | 4.1 ±0.8 | 4.6 ±1.0 | 5.4 ±1.3 | 12.9±5.5 |

**Table 8.2 The transcriptional responses of three nominal genes measured using RT-PCR platform.** The expression levels of Y62H9A.5, *fat-5* and *col-19* were significantly induced in response to *H. gordonii* extract and P57. Fold changes were normalized to 1 under control conditions in wild-type nematodes and the fold change of three biologically independent replicates is presented as the mean ± the standard error of the mean (SEM).

## 8.4 Pharmacogenomics of lipid regulation and longevity

The nematode, *C. elegans* has been utilized in three main research areas including, genomic, toxicity and disease studies, making it a strong tool for both forward and reverse genetic studies.

A Δ9 desaturase gene, namely *fat-5,* was found to be robustly induced in response to P57 (initially identified through the microarray platform), further studies were performed to explore the phenotypic and genetic responses within a

*fat-5* knockout background. Previous studies have reported that cytochrome P450 family members, in particular *cyp-35A2*, are involved in fat regulation of the nematodes (Aarnio et al., 2011).

Initial investigations utilized RNAi to define the correlation between the knockdown of *fat-5* and *cyp-35A2* at phenotypic and molecular levels. These links include a potential longevity influence (Figure 6.8) and a significantly reduced body size (Figure 6.9) in *fat-5* (*cyp-35A2* RNAi).

In this study, *fat-5* influenced the transcriptional response of *cyp-35A2*, however it was not possible to ascertain that *cyp-35A2* had the same effect on the expression of *fat-5* (Figures 6.10 and 6.11).

## 8.5 Lipids, calorie restriction and aging paradigm

The double mutant *fat-5(tm420);cyp-35A2(gk317)* was long-lived and was characterized by a significantly reduced body size. In addition, the attenuation of the Nile Red staining in *fat-5(tm420);cyp-35A2(gk317)*, supports the notion that longevity and calorie restriction mimetic responses are linked (Figures 7.2, 7.3 and 7.4). The hypothesis was further supported at the molecular level when the transcription responses of selected genes involved in lifespan and lipid pathways were assessed (Figures 7.8 and 7.9). The significant induction of *daf-16* and *sbp-1* transcription factors in *fat-5(tm420);cyp-35A2(gk317)* is consistent with the extended survival rate and the reduction in the overall body size of the animals. DAF-16 has been shown to be involved in metabolic responses such as lipid regulation and longevity and SBP-1 is associated with in the regulation of

cholesterol levels and fatty acid homeostasis (Watts, 2009, Shmookler Reis et al., 2011).

Interestingly, the transcription of *nhr-49* was not affected in the *fat-5* and *cyp-35A2* double mutant, despite the literature stating that NHR-49 is required for a healthy lifespan (Watts, 2009). This outcome highlights the complexity of metabolic pathways as different transcription factors regulate lifespan, development, lipid and nutrient-sensing pathways, and not all of the pathways are necessarily involved in phenotypic and/or physiological responses towards different inducers at the same time.

Surprisingly, P57 introduced responses in *fat-5(tm420);cyp-35A2(gk317)* that reversed the longevity effect as well as resulting in the formation of larger worms, a phenomenon that is best explained by an onset of aging, where the body surface area of the nematodes typically expands, due to the accumulated/undigested *E. coli* OP50 in the intestine and the occurrence of cell necrosis.

Because *cyp-35A2, cyp-35A5* and *cyp-35C1* are co-expressed (information adapted from www.wormbase.org), the absence of *cyp-35A2* results in the transcriptional induction of *cyp-35C1* and *cyp-35A5*. However, upon P57 treatment the general trend for *cyp-35C1* expression was a severe suppression regardless of the nematode strain background. In a similar manner, P57 treatment strongly reduced the expression level of *cyp-35A5* particularly in *fat-5(tm420);cyp-35A2(gk317).* The transcriptional responses of *daf-16, sbp-1, nhr-49, cyp-35A5* and *cyp-35C1* are summarized and fold changes in wild-type, *fat-*

*5(tm420)*, *cyp-35A2(gk317)* and *fat-5(tm420);cyp-35A2(gk317)* are compared (Table 8.3).

| | wild-type | *fat-5(tm420)* | *cyp-35A2(gk317)* | *fat-5(tm420);cyp-35A2(gk317)* |
|---|---|---|---|---|
| *daf-16* | normalized to 1 | ↓↓ | ↔ | ↑↑↑ |
| *sbp-1* | normalized to 1 | ↓ | ↑↑↑ | ↑↑↑ |
| *nhr-49* | normalized to 1 | ↓↓ | ↑ | ↔ |
| *cyp-35A5* | normalized to 1 | ↑↑↑ | ↑ | ↑↑↑↑ |
| *cyp-35C1* | normalized to 1 | ↓↓ | ↑↑ | ↔ |

**Table 8.3 The transcriptional responses of genes involved in lipid- and aging pathways in wild-type, *fat-5(tm420), cyp-35A2(gk317)* and *fat-5(tm420);cyp-35A2(gk317)*.** The fold change of each gene was determined by qPCR technique and normalized to 1 in wild-type nematodes. An upwards-pointing arrow shows gene induction whereas a downwards-pointing arrow indicates down-regulation. The severity of response is presented by number of arrows. In the event of no change in the gene expression, a horizontal arrow is placed.

Furthermore, the comparison of *daf-16, sbp-1, nhr-49, cyp-35A5* and *cyp-35C1* expression upon treatment with P57 reveals that the mechanism of P57 action differs in certain mutant backgrounds, an effect that emphasizes the importance of *fat-5* and/or *cyp-35A2* in their transcriptional response (Table 8.4).

A longevity/lipid regulatory network was originally published in a study by Watts in 2009, in which a nutrient sensing pathway was suggested to be a key player. Here, we introduce a putative link between lipid regulatory responses and three members of the cytochrome P450 family members (Figure 7.10).

| | wild-type | *fat-5(tm420)* | *cyp-35A2(gk317)* | *fat-5(tm420);cyp-35A2(gk317)* |
|---|---|---|---|---|
| *daf-16* | ⇔ | ↑ | ⇔ | ↓ |
| *sbp-1* | ↑↑ | ↑↑↑ | ↓↓ | ↓↓↓ |
| *nhr-49* | ↑↑ | ⇔ | ↓ | ⇔ |
| *cyp-35A5* | ↑ | ↓ | ↑↑ | ↓↓↓↓ |
| *cyp-35C1* | suppressed | suppressed | suppressed | suppressed |

**Table 8.4 The overall transcriptional responses of selected genes involved in lipid- and aging pathways upon P57 treatment explored in wild-type, *fat-5(tm420), cyp-35A2(gk317)* and *fat-5(tm420);cyp-35A2(gk317)*.** The expression levels were assessed by RT-PCR and severity of the response is presented by the number of arrows. Note that P57 exposure essentially suppressed the transcription of *cyp-35C1* regardless of the nematode strain. Horizontal arrows refer to no changes in transcriptional activity.

## 8.6 Data gaps and research needs

One of the challenges encountered during this study was the influence of laboratory temperature specifically on lifespan assays. Interestingly, although laboratory conditions (such as temperature and humidity) were kept supposedly constant throughout the year, there was a significant divergence in the median lifespan of wild-type nematodes when determined in different seasons. A temperature effect may have been magnified because NGM agar plates containing the nematodes were kept outside the controlled temperature (i.e.,

worm incubator) for extended periods whilst transferring and counting the number of viable animals on a daily base.

Furthermore, *H. gordonii* extract and P57 were delivered via ingestion and/or epidermal absorption. There was no direct assessment to determine how much of the treatment was taken up by the nematodes and to what degree the supplemented concentration of the compound was delivered to the body of the nematodes. In addition, living *E. coli* OP50 can also metabolize the plant extract or P57 compound resulting in the generation of secondary metabolites. Certain metabolic assays for *E. coli* could be performed to study the potential influence of the bacterial food source upon treatment with P57 and/or *H. gordonii* extract, such as the bacterial respiration assay or metabolite analysis by LC-MS/MS (Lenaerts et al., 2008, Cabreiro et al., 2013). As well as, the use of dead bacteria over living ones or washing the bacteria before placing the nematodes. However, due to time restrictions performing such assays were not possible. Having said that, the growth rate of *E. coli* OP50 was assessed in response to *H. gordonii* extract, which revealed that high levels of the extract could induce bacterial growth therefore these doses of *H. gordonii* extract were not used in subsequent experiments. Besides, *C. elegans* lack dedicated adipocytes and hepatic enzymes therefore certain pathways and physiological responses are not detectable in worms. Only preliminarily studies can be conducted to nematodes and detailed analyses need to be performed in higher organisms in order to define the clinical relevance.

This project, aimed to identify molecular leads within the area of pharmacogenomics and herbal medicine. Several transcriptional changes were observed that may be relevant to higher organisms, therefore worth exploring

this notion at least in mammalian cell cultures to quantify the expression of homologous and/or orthologous genes.

Moreover, GC-MS or customized fatty acid quantification kits can determine the ratio of saturated and unsaturated fatty acids, as the changes in saturated and unsaturated forms of fatty acids are predicted to be involved in response to P57 treatment. There have been some studies where a newly developed approach has been utilized by using flow cytometry and biochemical assays. This method allows the measurement of fat content per volume at single worm level. It is mainly based on BODIPY 493/503 and COPAS. Interestingly, the fluorescent intensity is quantified in relation to the length of the worm (TOF) and the body volume-dependent reduction in laser light of individual nematodes. Outcomes have been comparable to CARS and therefore emphasizes the reliability of the technique (Klapper et al., 2011). Therefore, the use of vital staining of lipids in combination with TAG measurements have allowed unravelling pitfalls that are on-going in lipid metabolism studies of *C. elegans*.

Nevertheless, these techniques are cost and labor-intensive, as they require the generation of large samples.

An important factor in whole-genome studies is the assessment of data reliability. Because of the nature of genome-wide studies, false positives and negatives are possible and therefore results should be reconfirmed via other platforms. However as demonstrated in this project the results were largely reproducible when assessed by RT-PCR. This emphasized that the output obtained by the Affymetrix® arrays was efficient and reliable.

Lastly, it would be of interest if one could perform a whole-genome approach on the *fat-5(tm420);cyp-35A2(gk317)* mutant and wild-type nematodes in order to

establish which pathways are influenced by the double mutation of *fat-5* and *cyp-35A2*.

## 8.7 Conclusions

The use of nematode *C. elegans* as a disease model has been hailed over the last few decades, including areas such as diabetes, obesity and neurodegenerative disorders. This project revealed a putative link between two distinctive pathways involved in xenobiotic activities and lipid metabolism. Namely that, FAT-5, a member of Δ9 desaturases modulates CYP-35A2, a member of cytochrome P450 family members and that the interaction between *fat-5* and *cyp-35A2* results in the formation of several phenotypic and physiological responses in nematodes. The *fat-5(tm420);cyp-35A2(gk317)* mutants are long-lived and their body size is significantly attenuated, a reduction that is beneficial to the animals as the worms do not form dauers or/and their development is not disrupted. The reduced growth parameters are in conjunction with a significantly diminished Nile Red fluorescent intensity in the compartments that are likely to be lipid droplets. Taken together, this may result in the formation of nematodes that exhibit a healthier fat content due to a putative change in the ratio of saturated and unsaturated fatty acids, a phenomenon similar to the mammalian HDL and LDL ratios. As clinical studies have shown, the imbalance between the ratio of HDL and LDL in the body can lead to obesity and several cardiovascular challenges (Attie et al., 2007, Ackerman and Gems, 2012). Due to the fact that major parts of the nematode and mammalian metabolic pathways overlap, it could be argued that molecular cues involved in hereditary lipid disorders and key regulators of longevity can be extrapolated to higher organisms.

A hypothesis that describes this putative link has been suggested throughout this project, which adjusts well to the nutrient sensing and lipid regulatory pathway reported by Watts in 2009 (Figure 8.1). The proposed pathway identified

transcription factors involved in nutrient sensing responses, upon which the lipid synthesis/breakdown mechanisms change the ratio of saturated to unsaturated fatty acids. In nematodes, the regulation of Δ9 desaturases have mainly been explored at the transcription level, though there is evidence that these enzymes are stable at protein levels (studied in other organisms such as mice) (Flowers and Ntambi, 2008, Watts, 2009). Several transcription factors as well as environmental elements influence the expression of Δ9 desaturase enzymes, which in turn affect the lipid content of the nematodes.

Because the cell membrane is a lipid bilayer, it is essential to keep the membrane fluidity under optimum conditions. This aim is fulfilled by changes in the fatty acid content, Watts pathway clearly states the importance of sensory neurons, which are responsible for the secretion of serotonin and insulin hormones as regulators of adiposity in *C. elegans*. Such hormonal responses are found to be triggered by nutritional signals. Receptors such as MOD-1 or DAF-2 receive and convey the signals to kinases and other signaling pathways resulting in the transcription of fatty acid desaturases.

As a balanced ratio between saturated and unsaturated fatty acids is crucial for *C. elegans*, several transcription factors including NHR-49, NHR-80, SBP-1/SREBP and DAF-16/FOXO as well as the transcriptional mediator MED-15 control the expression of Δ9 desaturase genes such as *fat-5, fat-6* and *fat-7*. Having said that, any environmental and/or molecular changes in upstream transcription factors may affect the expression pattern of Δ9 desaturases, resulting in unhealthy lipid storage or impaired β-oxidation (Watts, 2009).

In the modified pathway that is proposed in this project, the putative link between the nutrition-sensing pathway and the lipid regulatory feature of cytochrome P450 family members are introduced in a P57-dependent manner (Figure 8.1). The presence of *fat-5* and/or *cyp-35A2* modulates the transcriptional responses of aging and lipid regulatory genes such as *daf-16* and *sbp-1* with or without the addition of P57 compound. It was previously established that NHR-49 and SBP-1 are core transcription factors for the expression of FAT-5 and other Δ9 desaturases (Watts, 2009). This study highlighted that the expression of *nhr-49* mRNA is influenced by the deletion of *fat-5* and/or *cyp-35A2*, a similar link has been found between the transcription responses of *fat-5, cyp-35A2* and *daf-16.* In addition, despite the co-expression of *cyp-35A2, cyp-35A5* and *cyp-35C1,* the P57 response of *cyp-35C1* was deemed to be independent of *cyp-35A2* and/or *fat-5.*

Because of the evolutionarily conserved pathways between nematodes and humans, the proposed aging and longevity pathway regulated by P57 may contribute towards uncovering cues leading to study hereditary obesity in mammals and in particular humans.

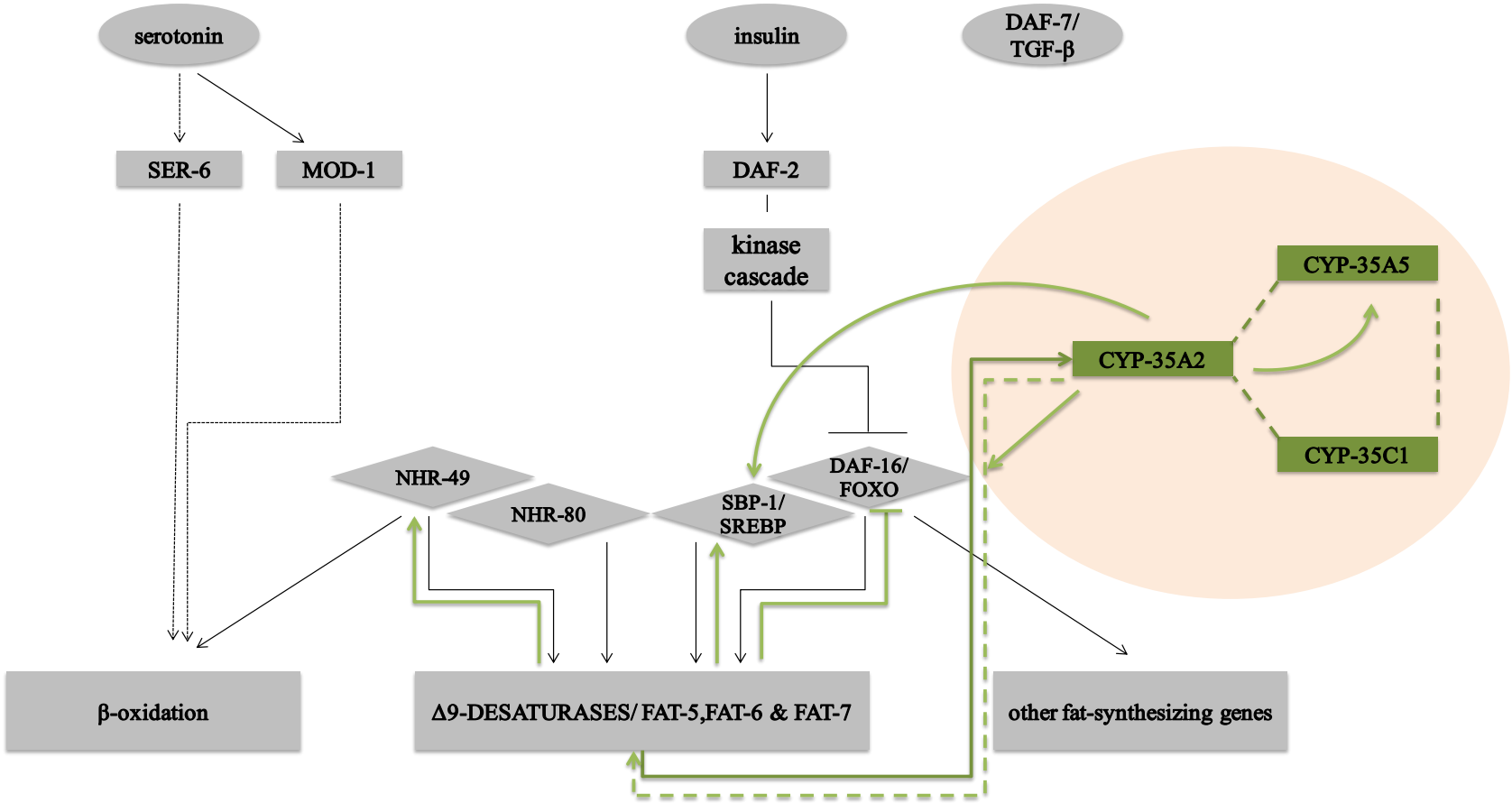


**Figure 8.1 The lipid regulatory/aging pathway based on the nutritional sensing mechanisms, in response to P57.** The original pathway was published by Watts in 2009 and expanded to include the advances uncovered by this study in a P57-dependent manner (shown in green).

# *Bibliography*

# 9 References


AARNIO, V., LEHTONEN, M., STORVIK, M., CALLAWAY, J. C., LAKSO, M. & WONG, G. 2011. Caenorhabditis Elegans Mutants Predict Regulation of Fatty Acids and Endocannabinoids by the CYP-35A Gene Family. *Front Pharmacol,* 2**,** 12.

ACKERMAN, D. & GEMS, D. 2012. The mystery of C. elegans aging: an emerging role for fat. Distant parallels between C. elegans aging and metabolic syndrome? *Bioessays,* 34**,** 466-71.

AHRINGER, J. 2006. reverse genetics. Available: http://www.wormbook.org/chapters/www_introreversegenetics/introreversegenetics.html - d0e2681 [Accessed 2013].

AITLHADJ, L. & STURZENBAUM, S. R. 2013. The toxicological assessment of two anti-obesity drugs in C. elegans. *Toxicology Research,* 2**,** 145-150.

ALMEIDA BARROS, A. G., LIU, J., LEMIEUX, G. A., MULLANEY, B. C. & ASHRAFI, K. 2011. *RE: Analyses of Fat Metabolism.* Type to IMANIKIA, S.

ALTUN, Z. F. & HALL, D. H. 2009. *Hermaphrodite life cycle* [Online]. Available: http://www.wormatlas.org/hermaphrodite/introduction/Introframeset.html [Accessed 21 August 2013].

APFELD, J., O'CONNOR, G., MCDONAGH, T., DISTEFANO, P. S. & CURTIS, R. 2004. The AMP-activated protein kinase AAK-2 links energy levels and insulin-like signals to lifespan in C. elegans. *Genes Dev,* 18**,** 3004-9.

ARMSTRONG, S. A., HSIEH, J. J.-D. & KORSMEYER, S. J. 2002. Genomic approaches to the pathogenesis and treatment of acute lymphoblastic leukemias. *Current Opinion in Hematology,* 9**,** 339-344.

ARNOLD, C., KONKEL, A., FISCHER, R. & SCHUNCK, W. H. 2010. Cytochrome P450-dependent metabolism of omega-6 and omega-3 long-chain polyunsaturated fatty acids. *Pharmacol Rep,* 62**,** 536-47.

ASHRAFI, K. 2007. Obesity and the regulation of fat metabolism. *WormBook***,** 1-20.

ASHRAFI, K., CHANG, F. Y., WATTS, J. L., FRASER, A. G., KAMATH, R. S., AHRINGER, J. & RUVKUN, G. 2003. Genome-wide RNAi analysis of Caenorhabditis elegans fat regulatory genes. *Nature,* 421**,** 268-72.

ATTIE, A. D., FLOWERS, M. T., FLOWERS, J. B., GROEN, A. K., KUIPERS, F. & NTAMBI, J. M. 2007. Stearoyl-CoA desaturase deficiency, hypercholesterolemia, cholestasis, and diabetes. *Nutr Rev,* 65**,** S35-8.

AVERY, L. 1993. The genetics of feeding in Caenorhabditis elegans. *Genetics,* 133**,** 897-917.

AVERY, L. & HORVITZ, H. R. 1990. Effects of starvation and neuroactive drugs on feeding in Caenorhabditis elegans. *J Exp Zool,* 253**,** 263-70.

BAUGH, L. R. & STERNBERG, P. W. 2006. DAF-16/FOXO regulates transcription of cki-1/Cip/Kip and repression of lin-4 during C. elegans L1 arrest. *Curr Biol,* 16**,** 780-5.

BENENATI, G., PENKOV, S., MULLER-REICHERT, T., ENTCHEV, E. V. & KURZCHALIA, T. V. 2009. Two cytochrome P450s in Caenorhabditis elegans are essential for the organization of eggshell, correct execution of meiosis and the polarization of embryo. *Mech Dev,* 126**,** 382-93.

BERG, J., TYMOCZKO, J. & STRYER, L. 2002. The Citric Acid Cycle. *Biochemistry.* 5 ed. New York: WH Freeman.

BONNER, J. & O'CONNOR, T. P. 2000. Semaphorin function in the developing invertebrate peripheral nervous system. *Biochem Cell Biol,* 78**,** 603-11.

BOULIAS, K. & HORVITZ, H. R. 2012. The C. elegans microRNA mir-71 acts in neurons to promote germline-mediated longevity through regulation of DAF-16/FOXO. *Cell Metab,* 15**,** 439-50.

BOYD, W. A., MCBRIDE, S. J., RICE, J. R., SNYDER, D. W. & FREEDMAN, J. H. 2010. A high-throughput method for assessing chemical toxicity using a Caenorhabditis elegans reproduction assay. *Toxicol Appl Pharmacol,* 245**,** 153-9.

BRAECKMAN, B. P., HOUTHOOFD, K. & VANFLETEREN, J. R. 2002. Assessing metabolic activity in aging Caenorhabditis elegans: concepts and controversies. *Aging Cell,* 1**,** 82-8; discussion 102-3.

BRENNER, S. 1974. The genetics of Caenorhabditis elegans. *Genetics,* 77**,** 71-94.

BROHARD, J., ROBERTSON, M. & RAMMELSBERG, A. 2012. Efficacy of Hoodia gordonii Extract as a Weight Loss Supplement: A Comparative Study Between an Invertebrate, Tenebrio molitor (Coleoptera: Tenebrionidae), and a Vertebrate, Rattus norvegicus (Rodentia: Muridae). *Transactions of the Illinois State Academy of Science,* 105.

BROOKS, K. K., LIANG, B. & WATTS, J. L. 2009. The influence of bacterial diet on fat storage in C. elegans. *PLoS One,* 4**,** e7545.

BROUGHTON, S. J., SLACK, C., ALIC, N., METAXAKIS, A., BASS, T. M., DRIEGE, Y. & PARTRIDGE, L. 2010. DILP-producing median neurosecretory cells in the Drosophila brain mediate the response of lifespan to nutrition. *Aging Cell,* 9**,** 336-46.

BROWN, M. S. & GOLDSTEIN, J. L. 1997. The SREBP pathway: regulation of cholesterol metabolism by proteolysis of a membrane-bound transcription factor. *Cell,* 89**,** 331-40.

BURNELL, A. M., HOUTHOOFD, K., O'HANLON, K. & VANFLETEREN, J. R. 2005. Alternate metabolism during the dauer stage of the nematode Caenorhabditis elegans. *Exp Gerontol,* 40**,** 850-6.

BURNS, A. R., WALLACE, I. M., WILDENHAIN, J., TYERS, M., GIAEVER, G., BADER, G. D., NISLOW, C., CUTLER, S. R. & ROY, P. J. 2010. A predictive model for drug bioaccumulation and bioactivity in Caenorhabditis elegans. *Nat Chem Biol,* 6**,** 549-57.

CABREIRO, F., ACKERMAN, D., DOONAN, R., ARAIZ, C., BACK, P., PAPP, D., BRAECKMAN, B. P. & GEMS, D. 2011. Increased life span from overexpression of superoxide dismutase in Caenorhabditis elegans is not caused by decreased oxidative damage. *Free Radic Biol Med,* 51**,** 1575-82.

CABREIRO, F., AU, C., LEUNG, K.-Y., VERGARA-IRIGARAY, N., COCHEMÉ, HELENA M., NOORI, T., WEINKOVE, D., SCHUSTER, E., GREENE, NICHOLAS D. E. & GEMS, D. 2013. Metformin Retards Aging in C. elegans by Altering Microbial Folate and Methionine Metabolism. *Cell,* 153**,** 228-239.

CARRANO, A. C., LIU, Z., DILLIN, A. & HUNTER, T. 2009. A conserved ubiquitination pathway determines longevity in response to diet restriction. *Nature,* 460**,** 396-9.

CARROLL, P. M. & FITZGERALD, K. 2003. *Model Organisms in Drug Discovery,* Wiley.

CASTRO, C., SAR, F., SHAW, W. R., MISHIMA, M., MISKA, E. A. & GRIFFIN, J. L. 2012. A metabolomic strategy defines the regulation of

lipid content and global metabolism by Delta9 desaturases in Caenorhabditis elegans. *BMC Genomics,* 13**,** 36.

CHAKRAPANI, B. P., KUMAR, S. & SUBRAMANIAM, J. R. 2008. Development and evaluation of an in vivo assay in Caenorhabditis elegans for screening of compounds for their effect on cytochrome P450 expression. *J Biosci,* 33**,** 269-77.

CHARAN, S., CHIEN, F. C., SINGH, N., KUO, C. W. & CHEN, P. 2011. Development of lipid targeting Raman probes for in vivo imaging of Caenorhabditis elegans. *Chemistry,* 17**,** 5165-70.

CHENG, J. X. 2007. Coherent anti-Stokes Raman scattering microscopy. *Appl Spectrosc,* 61**,** 197-208.

CHOMCZYNSKI, P. & SACCHI, N. 1987. Single-step method of RNA isolation by acid guanidinium thiocyanate-phenol-chloroform extraction. *Anal Biochem,* 162**,** 156-9.

COHEN, H. Y., MILLER, C., BITTERMAN, K. J., WALL, N. R., HEKKING, B., KESSLER, B., HOWITZ, K. T., GOROSPE, M., DE CABO, R. & SINCLAIR, D. A. 2004. Calorie restriction promotes mammalian cell survival by inducing the SIRT1 deacetylase. *Science,* 305**,** 390-2.

CROLL, N. A. & SMITH, J. M. 1978. Integrated behaviour in the feeding phase of Caenorhabditis elegans (Nematoda). *Journal of Zoology,* 184**,** 507-517.

DACKS, P. A., MORENO, C. L., KIM, E. S., MARCELLINO, B. K. & MOBBS, C. V. 2013. Role of the hypothalamus in mediating protective effects of dietary restriction during aging. *Front Neuroendocrinol,* 34**,** 95-106.

DALL'ACQUA, S. & INNOCENTI, G. 2007. Steroidal glycosides from Hoodia gordonii. *Steroids,* 72**,** 559-68.

DALMA-WEISZHAUSZ, D. D., WARRINGTON, J., TANIMOTO, E. Y. & MIYADA, C. G. 2006. The affymetrix GeneChip platform: an overview. *Methods Enzymol,* 410**,** 3-28.

DE BONO, M. & BARGMANN, C. I. 1998. Natural variation in a neuropeptide Y receptor homolog modifies social behavior and food response in C. elegans. *Cell,* 94**,** 679-89.

DENG, J., LIAO, Z. & CHEN, D. 2005. Marsdenosides A-H, polyoxypregnane glycosides from Marsdenia tenacissima. *Phytochemistry,* 66**,** 1040-51.

DEVINSKY, O., SCHACHTER, S. & PACIA, S. 2005. *Complementary and alternative therapies for epilepsy*, Demos Medical Publishing.

DOBROSOTSKAYA, I. Y., SEEGMILLER, A. C., BROWN, M. S., GOLDSTEIN, J. L. & RAWSON, R. B. 2002. Regulation of SREBP processing and membrane lipid production by phospholipids in Drosophila. *Science,* 296**,** 879-83.

ELLE, I. C., OLSEN, L. C., PULTZ, D., RODKAER, S. V. & FAERGEMAN, N. J. 2010. Something worth dyeing for: molecular tools for the dissection of lipid metabolism in Caenorhabditis elegans. *FEBS Lett,* 584**,** 2183-93.

FAHY, E., SUBRAMANIAM, S., MURPHY, R. C., NISHIJIMA, M., RAETZ, C. R., SHIMIZU, T., SPENER, F., VAN MEER, G., WAKELAM, M. J. & DENNIS, E. A. 2009. Update of the LIPID MAPS comprehensive classification system for lipids. *J Lipid Res,* 50 Suppl**,** S9-14.

FARES, H. & GRANT, B. 2002. Deciphering endocytosis in Caenorhabditis elegans. *Traffic,* 3**,** 11-9.

FAY, D. 2006. Genetic mapping and manipulation: chapter 1--Introduction and basics. *WormBook***,** 1-12.

FER, M., DREANO, Y., LUCAS, D., CORCOS, L., SALAUN, J. P., BERTHOU, F. & AMET, Y. 2008. Metabolism of eicosapentaenoic and docosahexaenoic acids by recombinant human cytochromes P450. *Arch Biochem Biophys,* 471**,** 116-25.

FINCH, C. E. & MORGAN, D. G. 1990. RNA and protein metabolism in the aging brain. *Annu Rev Neurosci,* 13**,** 75-88.

FLOWERS, M. T. & NTAMBI, J. M. 2008. Role of stearoyl-coenzyme A desaturase in regulating lipid metabolism. *Curr Opin Lipidol,* 19**,** 248-56.

FONTANA, L., PARTRIDGE, L. & LONGO, V. D. 2010. Extending healthy life span--from yeast to humans. *Science,* 328**,** 321-6.

FOWLER, S. D. & GREENSPAN, P. 1985. Application of Nile red, a fluorescent hydrophobic probe, for the detection of neutral lipid deposits in tissue sections: comparison with oil red O. *J Histochem Cytochem,* 33**,** 833-6.

FRASER, A. G., KAMATH, R. S., ZIPPERLEN, P., MARTINEZ-CAMPOS, M., SOHRMANN, M. & AHRINGER, J. 2000. Functional genomic analysis of C. elegans chromosome I by systematic RNA interference. *Nature,* 408**,** 325-30.

FRIEDMAN, D. B. & JOHNSON, T. E. 1988. Three mutants that extend both mean and maximum life span of the nematode, Caenorhabditis elegans, define the age-1 gene. *J Gerontol,* 43**,** B102-9.

FUKUYAMA, M., ROUGVIE, A. E. & ROTHMAN, J. H. 2006. C. elegans DAF-18/PTEN mediates nutrient-dependent arrest of cell cycle and growth in the germline. *Curr Biol,* 16**,** 773-9.

GEMS, D. 1999. Nematode ageing: Putting metabolic theories to the test. *Curr Biol,* 9**,** R614-6.

GEMS, D. & RIDDLE, D. L. 2000. Defining wild-type life span in Caenorhabditis elegans. *J Gerontol A Biol Sci Med Sci,* 55**,** B215-9.

GONCZY, P., ECHEVERRI, C., OEGEMA, K., COULSON, A., JONES, S. J., COPLEY, R. R., DUPERON, J., OEGEMA, J., BREHM, M., CASSIN, E., HANNAK, E., KIRKHAM, M., PICHLER, S., FLOHRS, K., GOESSEN, A., LEIDEL, S., ALLEAUME, A. M., MARTIN, C., OZLU, N., BORK, P. & HYMAN, A. A. 2000. Functional genomic analysis of cell division in C. elegans using RNAi of genes on chromosome III. *Nature,* 408**,** 331-6.

GONZALEZ, F. J. 2008. Regulation of hepatocyte nuclear factor 4 alpha-mediated transcription. *Drug Metab Pharmacokinet,* 23**,** 2-7.

GORR, T. A., GASSMANN, M. & WAPPNER, P. 2006. Sensing and responding to hypoxia via HIF in model invertebrates. *J Insect Physiol,* 52**,** 349-64.

GOSAI, S. J., KWAK, J. H., LUKE, C. J., LONG, O. S., KING, D. E., KOVATCH, K. J., JOHNSTON, P. A., SHUN, T. Y., LAZO, J. S., PERLMUTTER, D. H., SILVERMAN, G. A. & PAK, S. C. 2010. Automated high-content live animal drug screening using C. elegans expressing the aggregation prone serpin alpha1-antitrypsin Z. *PLoS One,* 5**,** e15460.

GRANT, B. & HIRSH, D. 1999. Receptor-mediated endocytosis in the Caenorhabditis elegans oocyte. *Mol Biol Cell,* 10**,** 4311-26.

GREENSPAN, P., MAYER, E. P. & FOWLER, S. D. 1985. Nile red: a selective fluorescent stain for intracellular lipid droplets. *J Cell Biol,* 100**,** 965-73.

GREER, E. L. & BRUNET, A. 2009. Different dietary restriction regimens extend lifespan by both independent and overlapping genetic pathways in C. elegans. *Aging Cell,* 8**,** 113-27.

GROEN, A. K. 2001. The pros and cons of gene expression analysis by microarrays. *Journal of Hepatology,* 35**,** 295-296.

GUARENTE, L. & KENYON, C. 2000. Genetic pathways that regulate ageing in model organisms. *Nature,* 408**,** 255-62.

HALASCHEK-WIENER, J., KHATTRA, J. S., MCKAY, S., POUZYREV, A., STOTT, J. M., YANG, G. S., HOLT, R. A., JONES, S. J., MARRA, M. A., BROOKS-WILSON, A. R. & RIDDLE, D. L. 2005. Analysis of long-lived C. elegans daf-2 mutants using serial analysis of gene expression. *Genome Res,* 15**,** 603-15.

HARA, K., MARUKI, Y., LONG, X., YOSHINO, K., OSHIRO, N., HIDAYAT, S., TOKUNAGA, C., AVRUCH, J. & YONEZAWA, K. 2002. Raptor, a binding partner of target of rapamycin (TOR), mediates TOR action. *Cell,* 110**,** 177-89.

HARR, B. & SCHLOTTERER, C. 2006. Comparison of algorithms for the analysis of Affymetrix microarray data as evaluated by co-expression of genes in known operons. *Nucleic Acids Res,* 34**,** e8.

HAZELRIGG, T. & PETERSEN, S. 1992. An unusual genomic position effect on Drosophila white gene expression: pairing dependence, interactions with zeste, and molecular analysis of revertants. *Genetics,* 130**,** 125-38.

HEINE, U. & BLUMENTHAL, T. 1986. Characterization of regions of the Caenorhabditis elegans X chromosome containing vitellogenin genes. *J Mol Biol,* 188**,** 301-12.

HELLERER, T., AXANG, C., BRACKMANN, C., HILLERTZ, P., PILON, M. & ENEJDER, A. 2007. Monitoring of lipid storage in Caenorhabditis elegans using coherent anti-Stokes Raman scattering (CARS) microscopy. *Proc Natl Acad Sci U S A,* 104**,** 14658-63.

HILLIER, L. W., COULSON, A., MURRAY, J. I., BAO, Z., SULSTON, J. E. & WATERSTON, R. H. 2005. Genomics in C. elegans: so many genes, such a little worm. *Genome Res,* 15**,** 1651-60.

HILLS, T., BROCKIE, P. J. & MARICQ, A. V. 2004. Dopamine and glutamate control area-restricted search behavior in Caenorhabditis elegans. *J Neurosci,* 24**,** 1217-25.

HOBSON, R. J., HAPIAK, V. M., XIAO, H., BUEHRER, K. L., KOMUNIECKI, P. R. & KOMUNIECKI, R. W. 2006. SER-7, a Caenorhabditis elegans 5-HT7-like receptor, is essential for the 5-HT stimulation of pharyngeal pumping and egg laying. *Genetics,* 172**,** 159-69.

HOLLAND, L. Z. & GIBSON-BROWN, J. J. 2003. The Ciona intestinalis genome: when the constraints are off. *Bioessays,* 25**,** 529-32.

HOPE, I. A. 1999. *C. elegans: a practical approach*, Oxford University Press (OUP).

HOU, N. S. & TAUBERT, S. 2012. Function and Regulation of Lipid Biology in Caenorhabditis elegans Aging. *Front Physiol,* 3**,** 143.

HU, P. J. 2007. Dauer. *WormBook***,** 1-19.

HUANG DA, W., SHERMAN, B. T. & LEMPICKI, R. A. 2009. Systematic and integrative analysis of large gene lists using DAVID bioinformatics resources. *Nat Protoc,* 4**,** 44-57.

HUANG, J., WEI, W., ZHANG, J., LIU, G., BIGNELL, G. R., STRATTON, M. R., FUTREAL, P. A., WOOSTER, R., JONES, K. W. & SHAPERO, M. H. 2004. Whole genome DNA copy number changes identified by high density oligonucleotide arrays. *Hum Genomics,* 1**,** 287-99.

HUGHES, A. L., TODD, B. L. & ESPENSHADE, P. J. 2005. SREBP pathway responds to sterols and functions as an oxygen sensor in fission yeast. *Cell,* 120**,** 831-42.

IMANIKIA, S. & STÜRZENBAUM, S. R. 2013. Chapter 12 - Invertebrates in Obesity Research: A Worm's Perspective. *In:* CONN, P. M. (ed.) *Animal Models for the Study of Human Disease.* Boston: Academic Press.

JIA, K., CHEN, D. & RIDDLE, D. L. 2004. The TOR pathway interacts with the insulin signaling pathway to regulate C. elegans larval development, metabolism and life span. *Development,* 131**,** 3897-906.

JOKIEL, P. L. & BIGGER, C. H. 1994. Aspects of histocompatibility and regeneration in the solitary reef coral Fungia scutaria. *Biol Bull,* 186**,** 72-80.

JONES, K. T. & ASHRAFI, K. 2009. Caenorhabditis elegans as an emerging model for studying the basic biology of obesity. *Dis Model Mech,* 2**,** 224-9.

JORGENSEN, E. M., HARTWIEG, E., SCHUSKE, K., NONET, M. L., JIN, Y. & HORVITZ, H. R. 1995. Defective recycling of synaptic vesicles in synaptotagmin mutants of Caenorhabditis elegans. *Nature,* 378**,** 196-9.

JORGENSEN, E. M. & MANGO, S. E. 2002. The art and design of genetic screens: caenorhabditis elegans. *Nat Rev Genet,* 3**,** 356-69.

KALETTA, T. & HENGARTNER, M. O. 2006. Finding function in novel targets: C. elegans as a model organism. *Nat Rev Drug Discov,* 5**,** 387-98.

KAMATH, R. S., FRASER, A. G., DONG, Y., POULIN, G., DURBIN, R., GOTTA, M., KANAPIN, A., LE BOT, N., MORENO, S., SOHRMANN, M., WELCHMAN, D. P., ZIPPERLEN, P. & AHRINGER, J. 2003. Systematic functional analysis of the Caenorhabditis elegans genome using RNAi. *Nature,* 421**,** 231-7.

KAMATH, R. S., MARTINEZ-CAMPOS, M., ZIPPERLEN, P., FRASER, A. G. & AHRINGER, J. 2001. Effectiveness of specific RNA-mediated interference through ingested double-stranded RNA in Caenorhabditis elegans. *Genome Biol,* 2**,** Research0002.

KAUFMANN, S. H. & HENGARTNER, M. O. 2001. Programmed cell death: alive and well in the new millennium. *Trends Cell Biol,* 11**,** 526-34.

KAUR, H., ARORA, A., WENGEL, J. & MAITI, S. 2006. Thermodynamic, counterion, and hydration effects for the incorporation of locked nucleic acid nucleotides into DNA duplexes. *Biochemistry,* 45**,** 7347-55.

KENNEDY, B. K., AUSTRIACO, N. R., JR., ZHANG, J. & GUARENTE, L. 1995. Mutation in the silencing gene SIR4 can delay aging in S. cerevisiae. *Cell,* 80**,** 485-96.

KENYON, C. J. 2010. The genetics of ageing. *Nature,* 464**,** 504-12.

KIMURA, K. D., TISSENBAUM, H. A., LIU, Y. & RUVKUN, G. 1997. daf-2, an insulin receptor-like gene that regulates longevity and diapause in Caenorhabditis elegans. *Science,* 277**,** 942-6.

KLAPPER, M., EHMKE, M., PALGUNOW, D., BOHME, M., MATTHAUS, C., BERGNER, G., DIETZEK, B., POPP, J. & DORING, F. 2011. Fluorescence-based fixative and vital staining of lipid droplets in Caenorhabditis elegans reveal fat stores using microscopy and flow cytometry approaches. *J Lipid Res,* 52**,** 1281-93.

KNIAZEVA, M., CRAWFORD, Q. T., SEIBER, M., WANG, C. Y. & HAN, M. 2004. Monomethyl branched-chain fatty acids play an essential role in Caenorhabditis elegans development. *PLoS Biol,* 2**,** E257.

KNOX, C., LAW, V., JEWISON, T., LIU, P., LY, S., FROLKIS, A., PON, A., BANCO, K., MAK, C., NEVEU, V., DJOUMBOU, Y., EISNER, R.,

GUO, A. C. & WISHART, D. S. 2011. DrugBank 3.0: a comprehensive resource for 'omics' research on drugs. *Nucleic Acids Res,* 39**,** D1035-41.

KOPELMAN, P. G. 2000. Obesity as a medical problem. *Nature,* 404**,** 635-43.

KULAS, J., SCHMIDT, C., ROTHE, M., SCHUNCK, W. H. & MENZEL, R. 2008. Cytochrome P450-dependent metabolism of eicosapentaenoic acid in the nematode Caenorhabditis elegans. *Arch Biochem Biophys,* 472**,** 65-75.

KUO, Y., HSU, T. Y., WU, Y. C. & CHANG, H. C. 2013. Fluorescent nanodiamond as a probe for the intercellular transport of proteins in vivo. *Biomaterials,* 34**,** 8352-60.

LAKOWSKI, B. & HEKIMI, S. 1998. The genetics of caloric restriction in Caenorhabditis elegans. *Proc Natl Acad Sci U S A,* 95**,** 13091-6.

LAMB, D. C. & WATERMAN, M. R. 2013. Unusual properties of the cytochrome P450 superfamily. *Philos Trans R Soc Lond B Biol Sci,* 368**,** 20120434.

LAPIERRE, L. R., MELENDEZ, A. & HANSEN, M. 2012. Autophagy links lipid metabolism to longevity in C. elegans. *Autophagy,* 8**,** 144-6.

LARSEN, M. K., TUCK, S., FAERGEMAN, N. J. & KNUDSEN, J. 2006. MAA-1, a novel acyl-CoA-binding protein involved in endosomal vesicle transport in Caenorhabditis elegans. *Mol Biol Cell,* 17**,** 4318-29.

LAWRENCE, V. J. & KOPELMAN, P. G. 2004. Medical consequences of obesity. *Clin Dermatol,* 22**,** 296-302.

LEE, S. S., KENNEDY, S., TOLONEN, A. C. & RUVKUN, G. 2003. DAF-16 target genes that control C. elegans life-span and metabolism. *Science,* 300**,** 644-7.

LEMIEUX, G. A. & ASHRAFI, K. 2014. Insights and challenges in using C. elegans for investigation of fat metabolism. *Crit Rev Biochem Mol Biol***,** 1-16.

LEMIEUX, G. A., LIU, J., MAYER, N., BAINTON, R. J., ASHRAFI, K. & WERB, Z. 2011. A whole-organism screen identifies new regulators of fat storage. *Nat Chem Biol,* 7**,** 206-13.

LENAERTS, I., WALKER, G. A., VAN HOOREBEKE, L., GEMS, D. & VANFLETEREN, J. R. 2008. Dietary restriction of Caenorhabditis elegans by axenic culture reflects nutritional requirement for constituents provided by metabolically active microbes. *J Gerontol A Biol Sci Med Sci,* 63**,** 242-52.

LEVITT, J. A., MATTHEWS, D. R., AMEER-BEG, S. M. & SUHLING, K. 2009. Fluorescence lifetime and polarization-resolved imaging in cell biology. *Curr Opin Biotechnol,* 20**,** 28-36.

LEWIS, G. F., CARPENTIER, A., ADELI, K. & GIACCA, A. 2002. Disordered fat storage and mobilization in the pathogenesis of insulin resistance and type 2 diabetes. *Endocr Rev,* 23**,** 201-29.

LI, D. U., ARLT, J., RICHARDSON, J., WALKER, R., BUTS, A., STOPPA, D., CHARBON, E. & HENDERSON, R. 2010. Real-time fluorescence lifetime imaging system with a 32 x 32 0.13microm CMOS low dark-count single-photon avalanche diode array. *Opt Express,* 18**,** 10257-69.

LI, X. & GREENWALD, I. 1996. Membrane topology of the C. elegans SEL-12 presenilin. *Neuron,* 17**,** 1015-21.

LIGHTNER, A., SCHUST, D. J., CHEN, Y. B. & BARRIER, B. F. 2008. The fetal allograft revisited: does the study of an ancient invertebrate species shed light on the role of natural killer cells at the maternal-fetal interface? *Clin Dev Immunol,* 2008**,** 631920.

LIM, W. K., WANG, K., LEFEBVRE, C. & CALIFANO, A. 2007. Comparative analysis of microarray normalization procedures: effects on reverse engineering gene networks. *Bioinformatics,* 23**,** i282-8.

LIN, K., HSIN, H., LIBINA, N. & KENYON, C. 2001. Regulation of the Caenorhabditis elegans longevity protein DAF-16 by insulin/IGF-1 and germline signaling. *Nat Genet,* 28**,** 139-45.

LINK, C. D., TAFT, A., KAPULKIN, V., DUKE, K., KIM, S., FEI, Q., WOOD, D. E. & SAHAGAN, B. G. 2003. Gene expression analysis in a transgenic Caenorhabditis elegans Alzheimer's disease model. *Neurobiol Aging,* 24**,** 397-413.

LONG, X., SPYCHER, C., HAN, Z. S., ROSE, A. M., MULLER, F. & AVRUCH, J. 2002. TOR deficiency in C. elegans causes developmental arrest and intestinal atrophy by inhibition of mRNA translation. *Curr Biol,* 12**,** 1448-61.

MACLEAN, D. B. & LUO, L. G. 2004. Increased ATP content/production in the hypothalamus may be a signal for energy-sensing of satiety: studies of the anorectic mechanism of a plant steroidal glycoside. *Brain Res,* 1020**,** 1-11.

MAESTRO, M. A., CARDALDA, C., BOJ, S. F., LUCO, R. F., SERVITJA, J. M. & FERRER, J. 2007. Distinct roles of HNF1beta, HNF1alpha, and HNF4alpha in regulating pancreas development, beta-cell function and growth. *Endocr Dev,* 12**,** 33-45.

MAIR, W. & DILLIN, A. 2008. Aging and survival: the genetics of life span extension by dietary restriction. *Annu Rev Biochem,* 77**,** 727-54.

MAK, H. Y. 2012. Lipid droplets as fat storage organelles in Caenorhabditis elegans: Thematic Review Series: Lipid Droplet Synthesis and Metabolism: from Yeast to Man. *J Lipid Res,* 53**,** 28-33.

MARCOTTE, E. M., XENARIOS, I., VAN DER BLIEK, A. M. & EISENBERG, D. 2000. Localizing proteins in the cell from their phylogenetic profiles. *Proc Natl Acad Sci U S A,* 97**,** 12115-20.

MASORO, E. J., SHIMOKAWA, I. & YU, B. P. 1991. Retardation of the aging processes in rats by food restriction. *Ann N Y Acad Sci,* 621**,** 337-52.

MCKAY, R. M., MCKAY, J. P., AVERY, L. & GRAFF, J. M. 2003. C elegans: a model for exploring the genetics of fat storage. *Dev Cell,* 4**,** 131-42.

MENZEL, R., BOGAERT, T. & ACHAZI, R. 2001. A systematic gene expression screen of Caenorhabditis elegans cytochrome P450 genes reveals CYP35 as strongly xenobiotic inducible. *Arch Biochem Biophys,* 395**,** 158-68.

MENZEL, R., RODEL, M., KULAS, J. & STEINBERG, C. E. 2005. CYP35: xenobiotically induced gene expression in the nematode Caenorhabditis elegans. *Arch Biochem Biophys,* 438**,** 93-102.

MENZEL, R., YEO, H. L., RIENAU, S., LI, S., STEINBERG, C. E. & STURZENBAUM, S. R. 2007. Cytochrome P450s and short-chain dehydrogenases mediate the toxicogenomic response of PCB52 in the nematode Caenorhabditis elegans. *J Mol Biol,* 370**,** 1-13.

MULLANEY, B. C. & ASHRAFI, K. 2009. C. elegans fat storage and metabolic regulation. *Biochim Biophys Acta,* 1791**,** 474-8.

MURPHY, C. T., MCCARROLL, S. A., BARGMANN, C. I., FRASER, A., KAMATH, R. S., AHRINGER, J., LI, H. & KENYON, C. 2003. Genes that act downstream of DAF-16 to influence the lifespan of Caenorhabditis elegans. *Nature,* 424**,** 277-83.

NAKAMURA, M. T. & NARA, T. Y. 2004. Structure, function, and dietary regulation of delta6, delta5, and delta9 desaturases. *Annu Rev Nutr,* 24**,** 345-76.

NARBONNE, P. & ROY, R. 2009. Caenorhabditis elegans dauers need LKB1/AMPK to ration lipid reserves and ensure long-term survival. *Nature,* 457**,** 210-4.

NCBI. 2014. *stearoyl-CoA desaturase (delta-9-desaturase) [ Homo sapiens (human) ]* [Online]. Available: http://www.ncbi.nlm.nih.gov/gene/6319 2013].

NOMURA, T., HORIKAWA, M., SHIMAMURA, S., HASHIMOTO, T. & SAKAMOTO, K. 2010. Fat accumulation in Caenorhabditis elegans is mediated by SREBP homolog SBP-1. *Genes Nutr,* 5**,** 17-27.

O'ROURKE, E. J., SOUKAS, A. A., CARR, C. E. & RUVKUN, G. 2009. C. elegans major fats are stored in vesicles distinct from lysosome-related organelles. *Cell Metab,* 10**,** 430-5.

OH, S. W., MUKHOPADHYAY, A., DIXIT, B. L., RAHA, T., GREEN, M. R. & TISSENBAUM, H. A. 2006. Identification of direct DAF-16 targets controlling longevity, metabolism and diapause by chromatin immunoprecipitation. *Nat Genet,* 38**,** 251-7.

OIDA, T., SAKO, Y. & KUSUMI, A. 1993. Fluorescence lifetime imaging microscopy (flimscopy). Methodology development and application to studies of endosome fusion in single cells. *Biophys J,* 64**,** 676-85.

PALANKER, L., TENNESSEN, J. M., LAM, G. & THUMMEL, C. S. 2009. Drosophila HNF4 regulates lipid mobilization and beta-oxidation. *Cell Metab,* 9**,** 228-39.

PASSAMANECK, Y. J. & DI GREGORIO, A. 2005. Ciona intestinalis: chordate development made simple. *Dev Dyn,* 233**,** 1-19.

PEREZ, V. I., BOKOV, A., VAN REMMEN, H., MELE, J., RAN, Q., IKENO, Y. & RICHARDSON, A. 2009. Is the oxidative stress theory of aging dead? *Biochim Biophys Acta,* 1790**,** 1005-14.

PFAFFL, M. W. 2001. A new mathematical model for relative quantification in real-time RT-PCR. *Nucleic Acids Res,* 29**,** e45.

PIANO, F., SCHETTER, A. J., MORTON, D. G., GUNSALUS, K. C., REINKE, V., KIM, S. K. & KEMPHUES, K. J. 2002. Gene clustering based on RNAi phenotypes of ovary-enriched genes in C. elegans. *Curr Biol,* 12**,** 1959-64.

PIETSCH, K., SAUL, N., SWAIN, S. C., MENZEL, R., STEINBERG, C. E. & STURZENBAUM, S. R. 2012. Meta-Analysis of Global Transcriptomics Suggests that Conserved Genetic Pathways are Responsible for Quercetin and Tannic Acid Mediated Longevity in C. elegans. *Front Genet,* 3**,** 48.

PIPER, M. D. & PARTRIDGE, L. 2007. Dietary restriction in Drosophila: delayed aging or experimental artefact? *PLoS Genet,* 3**,** e57.

PLENEFISCH, J., XIAO, H., MEI, B., GENG, J., KOMUNIECKI, P. R. & KOMUNIECKI, R. 2000. Secretion of a novel class of iFABPs in nematodes: coordinate use of the Ascaris/Caenorhabditis model systems. *Mol Biochem Parasitol,* 105**,** 223-36.

PROMEGA. 2013. *MSDS* [Online]. Promega Corporation. Available: https://www.promega.co.uk/~/media/files/resources/msds/m8000/m8302.pdf?la=en-gb 2014].

QABAZARD, B., AHMED, S., LI, L., ARLT, V. M., MOORE, P. K. & STURZENBAUM, S. R. 2013. C. elegans aging is modulated by hydrogen sulfide and the sulfhydrylase/cysteine synthase cysl-2. *PLoS One,* 8**,** e80135.

RANKIN, C. H. 2002. From gene to identified neuron to behaviour in Caenorhabditis elegans. *Nat Rev Genet,* 3**,** 622-30.

RIDDLE, D. L., BLUMENTHAL, T., MEYER, B. J. & PRIESS, J. R. 1997. Introduction to C. elegans. *In:* RIDDLE, D. L., BLUMENTHAL, T.,

MEYER, B. J. & PRIESS, J. R. (eds.) *C. elegans II.* Cold Spring Harbor (NY): Cold Spring Harbor Laboratory Press.

ROBINSON-RECHAVI, M., MAINA, C. V., GISSENDANNER, C. R., LAUDET, V. & SLUDER, A. 2005. Explosive lineage-specific expansion of the orphan nuclear receptor HNF4 in nematodes. *J Mol Evol,* 60**,** 577-86.

ROMERO, N. M., DEKANTY, A. & WAPPNER, P. 2007. Cellular and developmental adaptations to hypoxia: a Drosophila perspective. *Methods Enzymol,* 435**,** 123-44.

ROSEN, E. D., WALKEY, C. J., PUIGSERVER, P. & SPIEGELMAN, B. M. 2000. Transcriptional regulation of adipogenesis. *Genes Dev,* 14**,** 1293-307.

SAWIN, E. R., RANGANATHAN, R. & HORVITZ, H. R. 2000. C. elegans locomotory rate is modulated by the environment through a dopaminergic pathway and by experience through a serotonergic pathway. *Neuron,* 26**,** 619-31.

SCHLEGEL, A. & STAINIER, D. Y. 2007. Lessons from "lower" organisms: what worms, flies, and zebrafish can teach us about human energy metabolism. *PLoS Genet,* 3**,** e199.

SCHULZ, T. J., ZARSE, K., VOIGT, A., URBAN, N., BIRRINGER, M. & RISTOW, M. 2007. Glucose restriction extends Caenorhabditis elegans life span by inducing mitochondrial respiration and increasing oxidative stress. *Cell Metab,* 6**,** 280-93.

SCHWARZ, D., KISSELEV, P., ERICKSEN, S. S., SZKLARZ, G. D., CHERNOGOLOV, A., HONECK, H., SCHUNCK, W. H. & ROOTS, I. 2004. Arachidonic and eicosapentaenoic acid metabolism by human

CYP1A1: highly stereoselective formation of 17(R),18(S)-epoxyeicosatetraenoic acid. *Biochem Pharmacol,* 67**,** 1445-57.

SHANKLIN, J., WHITTLE, E. & FOX, B. G. 1994. Eight histidine residues are catalytically essential in a membrane-associated iron enzyme, stearoyl-CoA desaturase, and are conserved in alkane hydroxylase and xylene monooxygenase. *Biochemistry,* 33**,** 12787-94.

SHANLEY, D. P. & KIRKWOOD, T. B. 2000. Calorie restriction and aging: a life-history analysis. *Evolution,* 54**,** 740-50.

SHMOOKLER REIS, R. J., XU, L., LEE, H., CHAE, M., THADEN, J. J., BHARILL, P., TAZEARSLAN, C., SIEGEL, E., ALLA, R., ZIMNIAK, P. & AYYADEVARA, S. 2011. Modulation of lipid biosynthesis contributes to stress resistance and longevity of C. elegans mutants. *Aging (Albany NY),* 3**,** 125-47.

SHTONDA, B. B. & AVERY, L. 2006. Dietary choice behavior in Caenorhabditis elegans. *J Exp Biol,* 209**,** 89-102.

SMITH, E. D., KAEBERLEIN, T. L., LYDUM, B. T., SAGER, J., WELTON, K. L., KENNEDY, B. K. & KAEBERLEIN, M. 2008. Age- and calorie-independent life span extension from dietary restriction by bacterial deprivation in Caenorhabditis elegans. *BMC Dev Biol,* 8**,** 49.

SOUKAS, A. A., CARR, C. E. & RUVKUN, G. 2013. Genetic regulation of Caenorhabditis elegans lysosome related organelle function. *PLoS Genet,* 9**,** e1003908.

SRINIVASAN, S., SADEGH, L., ELLE, I. C., CHRISTENSEN, A. G., FAERGEMAN, N. J. & ASHRAFI, K. 2008. Serotonin regulates C. elegans fat and feeding through independent molecular mechanisms. *Cell Metab,* 7**,** 533-44.

STEINKRAUS, K. A., SMITH, E. D., DAVIS, C., CARR, D., PENDERGRASS, W. R., SUTPHIN, G. L., KENNEDY, B. K. & KAEBERLEIN, M. 2008. Dietary restriction suppresses proteotoxicity and enhances longevity by an hsf-1-dependent mechanism in Caenorhabditis elegans. *Aging Cell,* 7**,** 394-404.

STEYN, P. S., VAN HEERDEN, F. R. & VLEGGAAR, R. 1989. Toxic constituents of the Asclepiadaceae. Structure elucidation of the cynafosides, toxic pregnane glycosides of Cynanchum africanum R. *British South African Journal of Chemistry,* 42**,** 29-37.

STIERNAGLE, T. 2006. Maintenance of C. elegans. *WormBook***,** 1-11.

STRITTMATTER, P., SPATZ, L., CORCORAN, D., ROGERS, M. J., SETLOW, B. & REDLINE, R. 1974. Purification and properties of rat liver microsomal stearyl coenzyme A desaturase. *Proc Natl Acad Sci U S A,* 71**,** 4565-9.

SUBRAMANIAM, S., FAHY, E., GUPTA, S., SUD, M., BYRNES, R. W., COTTER, D., DINASARAPU, A. R. & MAURYA, M. R. 2011. Bioinformatics and systems biology of the lipidome. *Chem Rev,* 111**,** 6452-90.

TAUBERT, S., VAN GILST, M. R., HANSEN, M. & YAMAMOTO, K. R. 2006. A Mediator subunit, MDT-15, integrates regulation of fatty acid metabolism by NHR-49-dependent and -independent pathways in C. elegans. *Genes Dev,* 20**,** 1137-49.

TECOTT, L. H., SUN, L. M., AKANA, S. F., STRACK, A. M., LOWENSTEIN, D. H., DALLMAN, M. F. & JULIUS, D. 1995. Eating disorder and epilepsy in mice lacking 5-HT2c serotonin receptors. *Nature,* 374**,** 542-6.

THOMAS, J. H. 1990. Genetic analysis of defecation in Caenorhabditis elegans. *Genetics,* 124**,** 855-72.

THOMAS, J. H. 2007. Rapid birth-death evolution specific to xenobiotic cytochrome P450 genes in vertebrates. *PLoS Genet,* 3**,** e67.

TIMMONS, L. & FIRE, A. 1998. Specific interference by ingested dsRNA. *Nature,* 395**,** 854.

TISSENBAUM, H. A. & RUVKUN, G. 1998. An insulin-like signaling pathway affects both longevity and reproduction in Caenorhabditis elegans. *Genetics,* 148**,** 703-17.

TREGIDGO, C., LEVITT, J. A. & SUHLING, K. 2008. Effect of refractive index on the fluorescence lifetime of green fluorescent protein. *J Biomed Opt,* 13**,** 031218.

TUCCI, S. A. 2010. Phytochemicals in the Control of Human Appetite and Body Weight. *Pharmaceuticals,* 3**,** 748-763.

TULLET, J. M., HERTWECK, M., AN, J. H., BAKER, J., HWANG, J. Y., LIU, S., OLIVEIRA, R. P., BAUMEISTER, R. & BLACKWELL, T. K. 2008. Direct inhibition of the longevity-promoting factor SKN-1 by insulin-like signaling in C. elegans. *Cell,* 132**,** 1025-38.

URLACHER, V. B. & EIBEN, S. 2006. Cytochrome P450 monooxygenases: perspectives for synthetic application. *Trends Biotechnol,* 24**,** 324-30.

VAN GILST, M. R., HADJIVASSILIOU, H., JOLLY, A. & YAMAMOTO, K. R. 2005a. Nuclear hormone receptor NHR-49 controls fat consumption and fatty acid composition in C. elegans. *PLoS Biol,* 3**,** e53.

VAN GILST, M. R., HADJIVASSILIOU, H. & YAMAMOTO, K. R. 2005b. A Caenorhabditis elegans nutrient response system partially dependent on nuclear receptor NHR-49. *Proc Natl Acad Sci U S A,* 102**,** 13496-501.

VAN HEERDEN, F. R. 2008. Hoodia gordonii: a natural appetite suppressant. *J Ethnopharmacol,* 119**,** 434-7.

VAN HEERDEN, F. R., MARTHINUS HORAK, R., MAHARAJ, V. J., VLEGGAAR, R., SENABE, J. V. & GUNNING, P. J. 2007. An appetite suppressant from Hoodia species. *Phytochemistry,* 68**,** 2545-53.

VAN HEERDEN, F. R., VLEGGAAR, R., HORAK, R. M., LEARMONTH, R. A., MAHARAJ, V. & WHITTAL, R. D. 2002. Pharmaceutical compositions having appetite suppressant activity. Google Patents.

VAN RAAMSDONK, J. M. & HEKIMI, S. 2010. Reactive Oxygen Species and Aging in Caenorhabditis elegans: Causal or Casual Relationship? *Antioxid Redox Signal,* 13**,** 1911-53.

VANFLETEREN, J. R. & DE VREESE, A. 1994. Analysis of the proteins of aging Caenorhabditis elegans by high resolution two-dimensional gel electrophoresis. *Electrophoresis,* 15**,** 289-96.

VERMAAK, I., HAMMAN, J. H. & VILJOEN, A. M. 2011a. Hoodia gordonii: an up-to-date review of a commercially important anti-obesity plant. *Planta Med,* 77**,** 1149-60.

VERMAAK, I., VILJOEN, A. M., CHEN, W. & HAMMAN, J. H. 2011b. In vitro transport of the steroidal glycoside P57 from Hoodia gordonii across excised porcine intestinal and buccal tissue. *Phytomedicine,* 18**,** 783-7.

VILCHEZ, D., MORANTTE, I., LIU, Z., DOUGLAS, P. M., MERKWIRTH, C., RODRIGUES, A. P., MANNING, G. & DILLIN, A. 2012. RPN-6 determines C. elegans longevity under proteotoxic stress conditions. *Nature,* 489**,** 263-8.

WATTS, J. 2013. Physiological Functions and Regulation of C. elegans Stearoyl-CoA Desaturases. *In:* NTAMBI, P. D. J. M. (ed.) *Stearoyl-CoA Desaturase Genes in Lipid Metabolism.* Springer New York.

WATTS, J. L. 2009. Fat synthesis and adiposity regulation in Caenorhabditis elegans. *Trends Endocrinol Metab,* 20**,** 58-65.

WATTS, J. L. & BROWSE, J. 2000. A palmitoyl-CoA-specific delta9 fatty acid desaturase from Caenorhabditis elegans. *Biochem Biophys Res Commun,* 272**,** 263-9.

WATTS, J. L. & BROWSE, J. 2002. Genetic dissection of polyunsaturated fatty acid synthesis in Caenorhabditis elegans. *Proc Natl Acad Sci U S A,* 99**,** 5854-9.

WESSEL, G. M., REICH, A. M. & KLATSKY, P. C. 2010. Use of sea stars to study basic reproductive processes. *Syst Biol Reprod Med,* 56**,** 236-45.

WHO. 2013. *Obesity and Overweight* [Online]. Available: http://www.who.int/mediacentre/factsheets/fs311/en/ [Accessed 10th December 2013].

WILSON-SANDERS, S. E. 2011. Invertebrate models for biomedical research, testing, and education. *Ilar j,* 52**,** 126-52.

WOOD, W. B. 1988a. *1 Introduction to C. elegans Biology*.

WOOD, W. B. 1988b. *8 Embryology*.

YANG, F., VOUGHT, B. W., SATTERLEE, J. S., WALKER, A. K., JIM SUN, Z. Y., WATTS, J. L., DEBEAUMONT, R., SAITO, R. M., HYBERTS, S. G., YANG, S., MACOL, C., IYER, L., TJIAN, R., VAN DEN HEUVEL, S., HART, A. C., WAGNER, G. & NAAR, A. M. 2006. An ARC/Mediator subunit required for SREBP control of cholesterol and lipid homeostasis. *Nature,* 442**,** 700-4.

YANG, W. & HEKIMI, S. 2010. A mitochondrial superoxide signal triggers increased longevity in Caenorhabditis elegans. *PLoS Biol,* 8**,** e1000556.

YANG, Y., CAO, J. & SHI, Y. 2004. Identification and characterization of a gene encoding human LPGAT1, an endoplasmic reticulum-associated lysophosphatidylglycerol acyltransferase. *J Biol Chem,* 279**,** 55866-74.

YEN, K., LE, T. T., BANSAL, A., NARASIMHAN, S. D., CHENG, J. X. & TISSENBAUM, H. A. 2010. A comparative study of fat storage quantitation in nematode Caenorhabditis elegans using label and label-free methods. *PLoS One*, 5.

YEN, K., NARASIMHAN, S. D. & TISSENBAUM, H. A. 2011. DAF-16/Forkhead box O transcription factor: many paths to a single Fork(head) in the road. *Antioxid Redox Signal,* 14**,** 623-34.

YEOH, E. J., ROSS, M. E., SHURTLEFF, S. A., WILLIAMS, W. K., PATEL, D., MAHFOUZ, R., BEHM, F. G., RAIMONDI, S. C., RELLING, M. V., PATEL, A., CHENG, C., CAMPANA, D., WILKINS, D., ZHOU, X., LI, J., LIU, H., PUI, C. H., EVANS, W. E., NAEVE, C., WONG, L. & DOWNING, J. R. 2002. Classification, subtype discovery, and prediction of outcome in pediatric acute lymphoblastic leukemia by gene expression profiling. *Cancer Cell,* 1**,** 133-43.

YOU, Y. J., KIM, J., RAIZEN, D. M. & AVERY, L. 2008. Insulin, cGMP, and TGF-beta signals regulate food intake and quiescence in C. elegans: a model for satiety. *Cell Metab,* 7**,** 249-57.

ZHANG, S. O., BOX, A. C., XU, N., LE MEN, J., YU, J., GUO, F., TRIMBLE, R. & MAK, H. Y. 2010. Genetic and dietary regulation of lipid droplet expansion in Caenorhabditis elegans. *Proc Natl Acad Sci U S A,* 107**,** 4640-5.

ZHENG, J. & GREENWAY, F. L. 2012. Caenorhabditis elegans as a model for obesity research. *Int J Obes (Lond),* 36**,** 186-94.

ZHOU, X. R., GREEN, A. G. & SINGH, S. P. 2011. Caenorhabditis elegans Delta12-desaturase FAT-2 is a bifunctional desaturase able to desaturate a diverse range of fatty acid substrates at the Delta12 and Delta15 positions. *J Biol Chem,* 286**,** 43644-50.

# *Appendices*

# 10 Appendices

## Appendix One.

Individual Nile Red stained compartments were analyzed and the peak fluorescent intensity was determined to be approximately 616 nm (approx. 620 nm) when Nile Red was dissolved in acetone. Note that the red fluorescence was converted to green by the TRI2 software (Physics department, King's College London), (Figures S.1 and S.2).

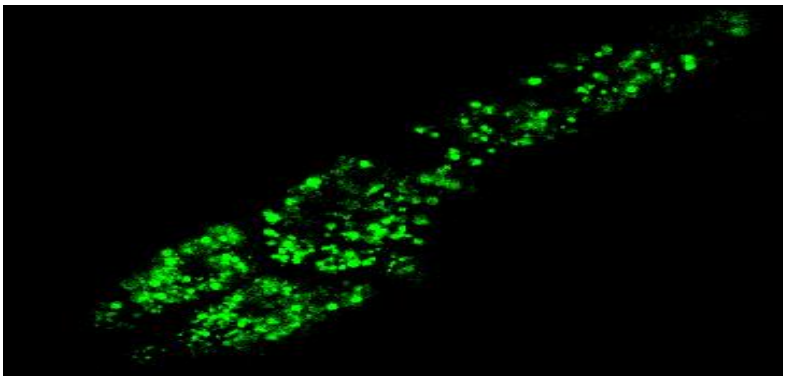

**Figure S.1 A nominated nematode, for analysis of the Nile Red fluorescent wavelength assessment.** The green compartments are likely to be the lipid droplets. Green fluorescence corresponds to the Nile Red stained areas by the TRI2 software (X20).

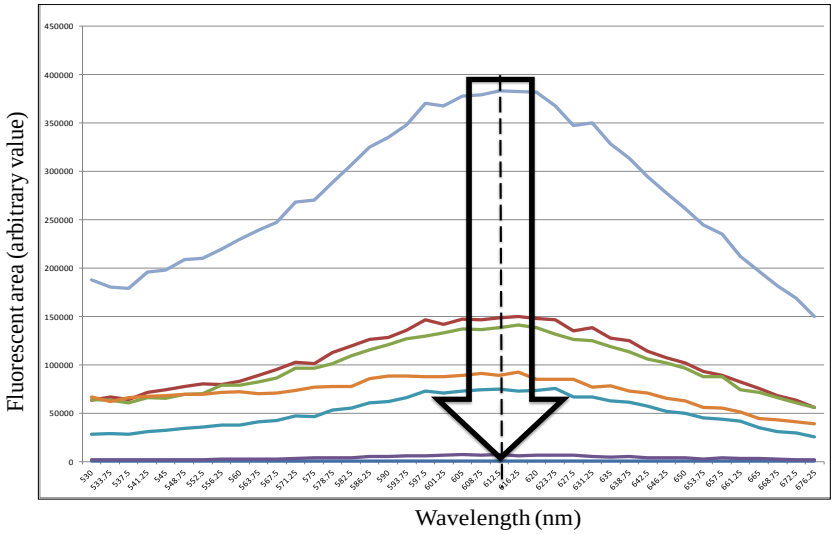


**Figure S. 2 Each color corresponds to the fluorescent peak wavelength of individual organelles taken from Figure S.1.** As demonstrated, all peaks are within the expected peak range, confirming that the stained areas are true fluorescence.

**Appendix Two.**

Developmental changes in wild-type nematodes treated with two initial doses of *H. gordonii* plant extract (Chapter Four, Figure 4.1).

| | Vehicle control | | 1 mg/mL *H. gordonii* | | 10 mg/mL *H. gordonii* | |
|---|---|---|---|---|---|---|
| **48 hrs** | **Body surface area (micron$^2$)** | **Body length (micron)** | **Body surface area (micron$^2$)** | **Body length (micron)** | **Body surface area (micron$^2$)** | **Body length (micron)** |
| **Average** | 34622.632 | 753.89639 | 22135.6795 | 683.40111 | 17526.98355 | 626.73906 |
| **STDEV.** | 3381.311593 | 43.59804375 | 3820.666946 | 64.73645216 | 4964.306055 | 93.99756972 |
| **COUNT** | 20 | 20 | 20 | 20 | 20 | 20 |
| **72 hrs** | | | | | | |
| **Average** | 85688.132 | 1179.96565 | 48218.81 | 977.004885 | 30457.4 | 792.46672 |
| **STDEV.** | 5214.941957 | 57.04649879 | 6192.655679 | 69.81246329 | 5647.119781 | 75.87044692 |
| **COUNT** | 20 | 20 | 20 | 20 | 20 | 20 |
| **96 hrs** | | | | | | |
| **Average** | 91220.209 | 1225.48625 | 60428.461 | 1049.33549 | 51697.99357 | 998.7007929 |
| **STDEV.** | 9130.330937 | 53.77233298 | 9238.270218 | 109.3638326 | 7203.338744 | 85.333986 |
| **COUNT** | 20 | 20 | 20 | 20 | 14 | 14 |
| **120 hrs** | | | | | | |
| **Average** | 96856.739 | 1240.1497 | 60555.15 | 1015.945525 | 51173.79143 | 977.9660143 |
| **STDEV.** | 9870.344488 | 41.90854599 | 11256.59652 | 95.95333611 | 10911.61462 | 121.3596506 |
| **COUNT** | 20 | 20 | 20 | 20 | 14 | 14 |

**Table S. 1 Growth measurements were performed on three biologically independent trials of wild-type worms. The average body surface area/ length are presented as well as the standard deviation and the number of nematodes used in each trial is also displayed.**

**Appendix Three.**

Growth measurements of wild-type worms incubated with *H. gordonii* extract infused OP50, for a period of six days. Table S. 2 corresponds to the average body surface area changes traced in three biologically independent groups and Table S. 3 presents the data from body length changes in the same nematodes. Standard deviation and the number of nematodes for each trial are also presented (Note. The total number of nematodes traced for volumetric changes added up to 60, 3x20).

| **Body surface area (micron$^2$)** | | | | | |
|---|---|---|---|---|---|
| **24 hrs** | **Vehicle control** | **0.01 mg/mL *H. gordonii*** | **0.05 mg/mL *H. gordonii*** | **0.1 mg/mL *H. gordonii*** | **0.5 mg/mL *H. gordonii*** |
| **Average** | 4574.6102 | 3923.1482 | 3671.6933 | 3635.7785 | 3595.4109 |
| **STDEV.** | 803.357134 | 747.4078846 | 723.8765289 | 1004.00278 | 507.5552409 |
| **COUNT** | 20 | 20 | 20 | 20 | 20 |
| **48 hrs** | | | | | |
| **Average** | 29100.846 | 25511.606 | 24579.484 | 23479.012 | 18578.979 |
| **STDEV.** | 4388.185669 | 5577.784723 | 3869.187534 | 8151.070215 | 6199.822938 |
| **COUNT** | 20 | 20 | 20 | 20 | 20 |
| **72 hrs** | | | | | |
| **Average** | 59294.49 | 54532.365 | 53371.286 | 55370.756 | 52626.366 |

| | | | | | |
|---|---|---|---|---|---|
| **STDEV.** | 7217.156914 | 6942.60087 | 8842.906765 | 4382.711319 | 12130.29198 |
| **COUNT** | 20 | 20 | 20 | 20 | 20 |
| **96 hrs** | **Vehicle control** | **0.01 mg/mL *H. gordonii*** | **0.05 mg/mL *H. gordonii*** | **0.1 mg/mL *H. gordonii*** | **0.5 mg/mL *H. gordonii*** |
| **Average** | 71193.45 | 61990.905 | 59075.628 | 56368.322 | 66273.715 |
| **STDEV.** | 11381.58279 | 9415.840609 | 5965.360965 | 10930.91835 | 8045.580767 |
| **COUNT** | 20 | 20 | 20 | 20 | 20 |
| **120 hrs** | | | | | |
| **Average** | 83819.379 | 73260.361 | 65278.752 | 72096.029 | 72243.278 |
| **STDEV.** | 5548.322683 | 5315.816662 | 9039.208492 | 5668.49111 | 5490.254818 |
| **COUNT** | 20 | 20 | 20 | 20 | 20 |
| **144 hrs** | | | | | |
| **Average** | 85383.604 | 76230.288 | 66761.221 | 73782.132 | 74959.042 |
| **STDEV.** | 9432.787026 | 11172.56777 | 10800.57064 | 10938.74649 | 6951.218354 |
| **COUNT** | 20 | 20 | 20 | 20 | 20 |

**Table S. 2 Body surface area changes in wild-type nematodes upon treatment with different concentrations of *H. gordonii* extract (refer to Chapter Four, Figure 4.4).**

| Body length (micron) | | | | | |
|---|---|---|---|---|---|
| **24 hrs** | **Vehicle control** | **0.01 mg/mL *H. gordonii*** | **0.05 mg/mL *H. gordonii*** | **0.1 mg/mL *H. gordonii*** | **0.5 mg/mL *H. gordonii*** |
| **Average** | 347.56445 | 333.10307 | 325.81279 | 335.29399 | 327.87752 |
| **STDEV.** | 22.22043364 | 26.48633087 | 36.59750428 | 44.90774345 | 29.49413164 |
| **COUNT** | 20 | 20 | 20 | 20 | 20 |
| **48 hrs** | | | | | |
| **Average** | 743.21007 | 719.31886 | 748.46003 | 717.18213 | 650.60226 |
| **STDEV.** | 38.18475931 | 75.4748718 | 68.13165758 | 103.3576101 | 95.98146966 |
| **COUNT** | 20 | 20 | 20 | 20 | 20 |
| **72 hrs** | | | | | |
| **Average** | 1040.05477 | 1018.88467 | 1009.38373 | 1004.79132 | 994.59623 |
| **STDEV.** | 41.76434594 | 56.44301634 | 68.70272077 | 65.17539235 | 159.6540598 |
| **COUNT** | 20 | 20 | 20 | 20 | 20 |
| **96 hrs** | | | | | |
| **Average** | 1143.4588 | 1068.57771 | 1088.27654 | 1031.12087 | 1095.1237 |
| **STDEV.** | 59.50914957 | 61.58267936 | 94.14474224 | 152.2745438 | 52.7960288 |
| **COUNT** | 20 | 20 | 20 | 20 | 20 |
| **120 hrs** | | | | | |
| **Average** | 1212.0567 | 1150.1711 | 1114.1795 | 1184.6157 | 1184.6082 |
| **STDEV.** | 58.62321956 | 64.67917866 | 76.06885989 | 60.68455242 | 71.51314445 |
| **COUNT** | 20 | 20 | 20 | 20 | 20 |

| 144 hrs | Vehicle control | 0.01 mg/mL *H. gordonii* | 0.05 mg/mL *H. gordonii* | 0.1 mg/mL *H. gordonii* | 0.5 mg/mL *H. gordonii* |
|---|---|---|---|---|---|
| **Average** | 1199.8023 | 1169.8554 | 1080.99858 | 1162.5878 | 1198.004 |
| **STDEV.** | 51.16407241 | 65.4606954 | 111.827078 | 75.45851776 | 88.00850353 |
| **COUNT** | 20 | 20 | 20 | 20 | 20 |

**Table S. 3 Body length changes in wild-type nematodes upon treatment with different concentrations of *H. gordonii* extract (refer to Chapter Four, Figure 4.5).**

**Appendix Four.**

Lifespan of wild-nematodes in response to *H. gordonii* extract concentrations was determined and Kaplan-Meier curves were plotted. Thereafter, Log-rank statistical analysis was conducted to find out whether the changes were significant (Chapter Four, Figure 4.10).

| **wild-type** | | | | | |
|---|---|---|---|---|---|
| Condition | Mean lifespan ± SEM (days) | Median lifespan (days) | Log-rank test | Control/treatment (n) | Censored (n) |
| Vehicle control | 13.1 ± 0.2 | 15 | - | - | 42 |
| 0.01 mg/mL | 12.8 ± 0.3 | 14.5 | 0.218 | 358/317 | 83 |
| 0.05 mg/mL | 13.2 ± 0.2 | 14.5 | 0.134 | 358/339 | 61 |
| 0.1 mg/mL | 13.1 ± 0.2 | 15 | 0.160 | 358/375 | 25 |
| 0.5 mg/mL | 13.1 ± 0.2 | 14.5 | 0.08 | 358/329 | 71 |

**Table S. 4 Survival data collected from wild-type nematodes in response to *H. gordonii* extract treatment.**

## Appendix Five.

Venn diagrams in Figure 4. 12, Chapter Four revealed the overlapping genes among responsive genes within different *H. gordonii* extract doses. The statistical significance within overlaps was quantified and data are presented below.

| Up-regulated | | | |
|---|---|---|---|
| **Comparison groups (mg/mL)** | **Expected overlap data** | **Actual observed overlap** | **P values (Fisher exact test)** |
| **0.1 & 0.05** | 5 | 100 | 8.470E-120 |
| **0.1 & 0.01** | 7 | 105 | 1.864E-105 |
| **0.05 & 0.01** | 2 | 37 | 9.047E-046 |

| Down-regulated | | | |
|---|---|---|---|
| **Comparison groups (mg/mL)** | **Expected overlap data** | **Actual observed overlap** | **P values (Fisher test)** |
| **0.1 & 0.05** | 1 | 25 | 2.590E-030 |
| **0.1 & 0.01** | 3 | 41 | 1.274E-30 |
| **0.05 & 0.01** | 13 | 10 | 1.365E-012 |

**Table S. 5 The Fisher's Exact Test analysis pinpointed the statistical significance among different doses of *H. gordonii* extract-exposed nematodes to be highly pronounced in either up and/or down-regulated gene groups.**

**Appendix Six.**

A list of UPL probe and oligonucleotide sets that were custom designed for pinpointed genes of the microarray experiment are presented. For further information refer to: http://lifescience.roche.com.

| Oligo name | Sequence (5'-3") |
|---|---|
| EEED8.3 Fwd | GGTTTTAATTCTACTCTTCGCTTCAAT |
| EEED8.3 Rev | CAACAAGGTGAACGGTAGAGAAT |
| F49E10.2 Fwd | ATGGCAATCCATGAGCGTA |
| F49E10.2 Rev | TTGTGTCGACAGTGAAGATGC |
| Y62H9A.5 Fwd | TTCTCGGGAACACAGAAGAGA |
| Y62H9A.5 Rev | TGGGCAGCTAATTTCTGCAT |
| Y62H9A.6 Fwd | AACCATCGTCTCATCTTTCCA |
| Y62H9A.6 Rev | AGCGGTGCATACAAGAGCA |
| ZK813.1 Fwd | GCTCTCATCGCTGTTGTTGT |
| ZK813.1 Rev | AGAAGGGATTTCCGTTGTCAT |

| | |
|---|---|
| *acl-12* Fwd | TCTCGGTCCCACTGATGATT |
| *acl-12* Rev | CCCATCATCACATCACAAATG |
| *cdh-12* Fwd | CGAGTTTCGGCAGTGTCA |
| *cdh-12* Rev | CTACCAGGTGATTGGCGACT |
| *col-19* Fwd | TTCCAGGATGGTATGGTTGAA |
| *col-19* Rev | GGCTCCGAAGAGAGTCTCAA |
| *col-41* Fwd | AGGAAACGCTGGTCACGA |
| *col-41* Rev | TGGGCAGTAGTTGGCATCTT |
| *fat-5* Fwd | GAGGATCCGGTGCTGATG |
| *fat-5* Rev | AGCAGAAGATTCCGACCAAG |
| *nspd-2* Fwd | CAATCTTGTTACCTCGGACCA |
| *nspd-2* Rev | AGACGGATGAGTTGCGTGTT |
| *cyp-35A2* Fwd | TCAGAAAGTGATTCCTTTTGGAG |
| *cyp-35A2* Rev | AGGAGAAGGTTACCGAAGATCA |

**Table S. 6 UPL oligos utilized in the RT-PCR for nominated genes of the microarray experiment.**

| Gene name | UPL probe ID number |
|---|---|
| EEED8.3 | 120 |
| F49E10.2 | 156 |
| Y62H9A.5 | 148 |
| Y62H9A.6 | 143 |
| ZK813.1 | 78 |
| *acl-12* | 24 |
| *cdh-12* | 1 |
| *col-19* | 22 |
| *col-41* | 1 |
| *fat-5* | 6 |
| *nspd-2* | 137 |
| *cyp-35A2* | 103 |

**Table S. 7 Probe list of the chosen microarray transcripts.**

**Appendix Seven.**

The expression patterns of 11 nominated transcripts pinpointed by the microarray experiment are compared.

| | ***H. gordonii*** **treatment (mg/mL)** | | | | | |
|---|---|---|---|---|---|---|
| | **Microarray** | | | **RT-PCR the same RNA as for the microarray** | | |
| **Gene** | **0.01** | **0.05** | **0.1** | **0.01** | **0.05** | **0.1** |
| Y62H9A.5 | 4.4 | 5.5 | 7.0 | 1.8 ± 0.3 | 3.2 ± 0.4 | 7.8 ± 0.6 |
| *fat-5* | 1.1 | 1.5 | 1.7 | 1.1 ± 0.1 | 1.3 ± 0.1 | 1.7 ± 0.2 |
| *col-19* | 1.1 | 1.3 | 4.1 | 1.2 ± 0.2 | 1.7 ± 0.4 | 4.8 ± 1.1 |
| *acl-12* | 1.4 | | 1.4 | 0.8 ± 0.0 | 1.4 ± 0.0 | 1.5 ± 0.1 |
| EEED8.3 | 2.2 | 2.1 | 4.0 | 2.2 ± 0.6 | 2.1 ± 0.2 | 4.0 ± 0.6 |
| Y62H9A.6 | 1.4 | 2.4 | 4.4 | 0.6 ± 0.1 | 1.0 ± 0.1 | 1.2 ± 0.2 |
| ZK813.1 | 1.6 | 2.0 | 5.8 | 0.4 ± 0.0 | 0.6 ± 0.0 | 1.6 ± 0.1 |
| *nspd-2* | -1.3 | -1.3 | -2.5 | 0.3 ± 0.0 | 0.3 ± 0.0 | 0.9 ± 0.0 |
| *col-41* | -1.8 | -1.8 | -2.6 | -1.8 ± 0.1 | -1.8 ± 0.2 | -2.6 ± 0.4 |
| F49E10.2 | -1.3 | -3.1 | -6.0 | -1.5 ± 0.2 | -3.1 ± 0.3 | -6.0 ± 0.8 |
| *cdh-12* | -1.3 | -1.9 | -2.5 | -1.3 ± 0.1 | -1.3 ± 0.1 | -2.5 ± 0.3 |

**Table S. 8 Transcriptional responses of 11 selected genes were compared using two different platforms are microarray and RT-PCR to validate the efficiency of the genome-wide microarray experiment.**

**Appendix Eight.**

Growth measurement of wild-type nematodes in response to P57 treatment is plotted in Figures 5.5 and 5.6, data corresponding to body length is presented in Table S. 9 and body surface area in Table S. 10 (Note. The average data points are calculated from three biologically independent experiments and 20 nematodes per biological trial were measured).

| Average body length (µ) ± SEM | | | |
|---|---|---|---|
| **hrs post hatch** | **Control+MeOH** | **0.03 µg/mL** | **0.3 µg/mL** |
| **0** | 0 | 0 | 0 |
| **24** | 434.619755 ± 8.695 | 399.96974 ± 9.224 | 345.01256 ± 13.483 |
| **48** | 862.350335 ± 16.684 | 731.24872 ± 17.361 | 720.958905 ± 21.391 |
| **72** | 1058.57288 ± 11.187 | 974.99301 ± 13.370 | 974.82813 ± 11.285 |
| **96** | 1103.80295 ± 12.436 | 1065.11997 ± 11.788 | 1040.31526 ± 15.298 |
| **120** | 1115.746415 ± 11.828 | 1046.772625 ± 16.496 | 1070.189345 ± 14.808 |
| **144** | 1140.22305 ± 14.406 | 1071.55601 ± 16.022 | 1065.0213 ± 10.332 |

**Table S. 9 Body length changes following a six day incubation with P57 doses.**

| Average body surface area (μ²) ± SEM | | | |
|---|---|---|---|
| **hrs post hatch** | **Control+MeOH** | **0.03 μg/mL** | **0.3 μg/mL** |
| **0** | 0 | 0 | 0 |
| **24** | 7329.2966 ± 224.915 | 5841.1087 ± 220.925 | 4375.06475 ± 340.094 |
| **48** | 33065.0885 ± 1374.09 | 23608.9245 ± 1039.53 | 21249.00405 ± 1333.86 |
| **72** | 58445.2845 ± 1178.26 | 47285.2505 ± 946.508 | 45302.769 ± 1268.45 |
| **96** | 66657.6555 ± 1589.5 | 55691.5005 ± 1183.39 | 52682.635 ± 1260.87 |
| **120** | 65697.1235 ± 998.014 | 56230.4285 ± 1231.01 | 55030.061 ± 989.448 |
| **144** | 65502.703 ± 1481.14 | 56529.735 ± 1392.42 | 56442.4735 ± 881.094 |

**Table S. 10 Body surface area changes following a six day incubation with P57 doses.**

**Appendix Nine.**

Wild-type nematodes were incubated with a combination of Nile Red, *E. coli* OP50 and different doses of P57 and assessed after 72 hours. The red fluorescent intensity of stained organelles was not consistent amongst the individual nematodes of the same P57 treatment groups therefore the data were not analyzed quantitatively. To highlight this issue, few nematodes are presented below.

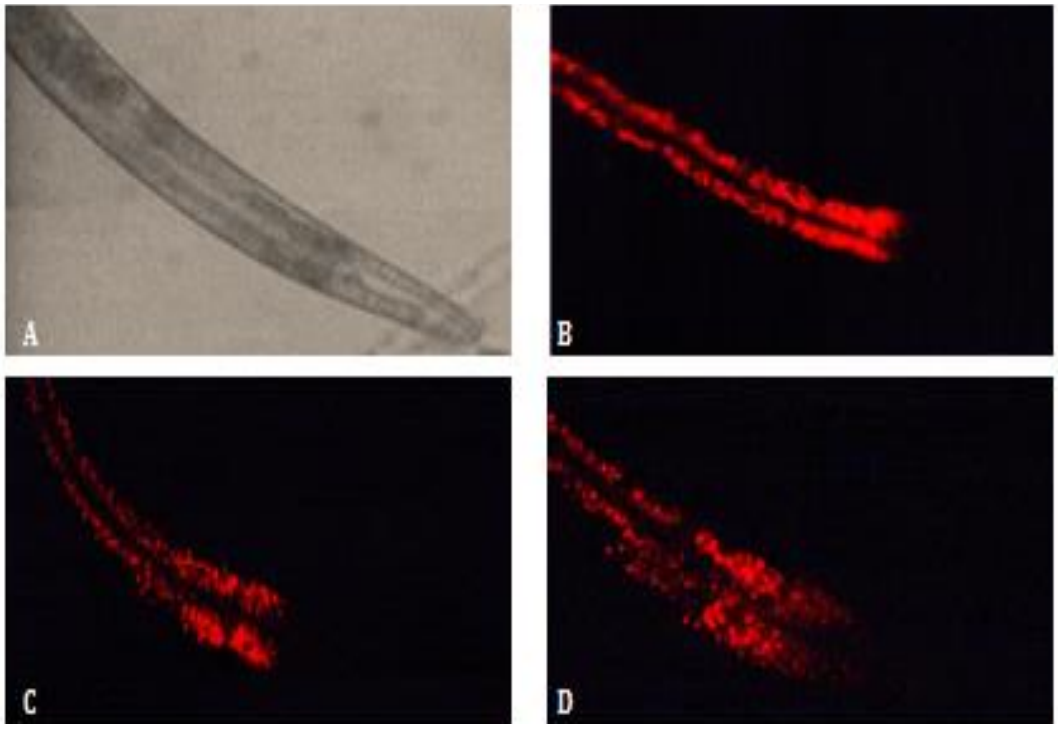


**Figure S.3 Nile Red stained nematodes incubated with different doses of P57.** A representative nematode (A) indicated the visualized area of the nematode. A non-exposed worm (B) followed by 0.03 and 0.3 µg/mL P57-treated nematodes (C and D, respectively). Note that no significance difference is observed among the samples (Magnification X20).

**Appendix Ten.**

Kaplan-Meier curves presenting survival percentages of wild-type nematodes upon treatment with P57 were plotted (Figure 5.9) and data were further analyzed via Log-rank (Mantel-Cox) method using GraphPad Prism v5 software (GraphPad Software Inc., La Jolla USA).

| wild-type | | | | | |
|---|---|---|---|---|---|
| condition | Mean lifespan ± SEM (days) | Median lifespan (days) | Log-rank test | Control/treatment (n) | censored |
| Vehicle control | 12.6 ± 0.2 | 12 | - | - | 5 |
| 0.03 μg/mL | 13.7 ± 0.2 | 13 | < 0.0001 | 395/385 | 15 |
| 0.3 μg/mL | 14.0 ± 0.1 | 14 | < 0.0001 | 395/398 | 2 |

**Table S. 11 Lifespan data, performed on wild-type nematodes treated with P57 doses.**

**Appendix Eleven.**

Quantitative analysis on growth changes traced in *fat-5(tm420)* nematodes upon treatment with P57 over a period of six days. Table S. 12 presents the changes in body surface area of the worms whereas Table S. 13 is the length measurements within the period of six days.

| ***fat-5(tm420)* Body surface area (micron$^2$)** | | | | | | |
|---|---|---|---|---|---|---|
| **Vehicle control** | **24 hrs** | **48 hrs** | **72 hrs** | **96 hrs** | **120 hrs** | **144 hrs** |
| **AVE.** | 6623.0458 | 36167.8525 | 76632.809 | 100559.102 | 101312.9395 | 103021.2595 |
| **STDEV.** | 563.7372112 | 4403.159683 | 7026.482208 | 10483.89163 | 10662.34973 | 10049.15503 |
| **COUNT** | 20 | 20 | 20 | 20 | 20 | 20 |
| **0.03 µg/mL P57** | | | | | | |
| **AVE.** | 6680.90135 | 35346.944 | 78629.341 | 98503.4495 | 100151.4625 | 102628.253 |
| **STDEV.** | 636.0107621 | 6010.108466 | 8413.224577 | 12053.824 | 14013.02019 | 15335.71272 |
| **COUNT** | 20 | 20 | 20 | 20 | 20 | 20 |
| **0.3 µg/mL P57** | | | | | | |
| **AVE.** | 6775.5979 | 36059.749 | 76683.4845 | 97827.811 | 99899.2145 | 103376.544 |
| **STDEV.** | 679.3828427 | 5062.802066 | 9920.530639 | 9089.518303 | 10633.47311 | 21127.44822 |
| **COUNT** | 20 | 20 | 20 | 20 | 20 | 20 |

**Table S. 12 Volumetric changes upon treatment with P57 in *fat-5(tm420)* mutant. Presented data are combined results of three biologically independent trials.**

| *fat-5(tm420)* **Body length (micron)** | | | | | | |
|---|---|---|---|---|---|---|
| **Vehicle control** | **24 hrs** | **48 hrs** | **72 hrs** | **96 hrs** | **120 hrs** | **144 hrs** |
| **AVE.** | 396.95079 | 816.86736 | 1144.89665 | 1304.6352 | 1364.76945 | 1392.06425 |
| **STDEV.** | 16.47320545 | 49.90627276 | 64.05793208 | 77.56487498 | 97.17568661 | 91.54239338 |
| **COUNT** | 20 | 20 | 20 | 20 | 20 | 20 |
| **0.03 µg/mL P57** | | | | | | |
| **AVE.** | 401.067015 | 822.73582 | 1144.836745 | 1274.24775 | 1330.60955 | 1358.43785 |
| **STDEV.** | 24.52708659 | 65.65090016 | 69.72816927 | 83.35219769 | 100.4624542 | 118.0311086 |
| **COUNT** | 20 | 20 | 20 | 20 | 20 | 20 |
| **0.3 µg/mL P57** | | | | | | |
| **AVE.** | 406.470375 | 839.05864 | 1137.7671 | 1285.61175 | 1300.87735 | 1307.29445 |
| **STDEV.** | 21.52620669 | 61.37329216 | 77.14643381 | 62.8543782 | 92.99857236 | 170.9441891 |
| **COUNT** | 20 | 20 | 20 | 20 | 20 | 20 |

**Table S. 13 Body length changes upon treatment with P57 in *fat-5(tm420)* mutant. Presented data are combined results of three biologically independent trials.**

**Appendix Twelve.**

Once the Kaplan-Meier graphs were created for the survival rate *fat-5(tm420)* mutants upon exposure to P57 doses, results were assessed using GraphPad Prism v5 software (GraphPad Software Inc., La Jolla USA).

| ***fat-5(tm420)*** | | | | | |
|---|---|---|---|---|---|
| Condition | Mean lifespan ± SEM (days) | Median lifespan (days) | Log-rank test | Control/treatment (n) | Censored |
| Vehicle control | 11.1 ± 0.2 | 11 | - | - | 95 |
| 0.03 μg/mL | 9.4 ± 0.1 | 10 | 0.0007 | 305/330 | 70 |
| 0.3 μg/mL | 10.3 ± 0.1 | 10 | 0.3414 | 325/330 | 75 |

**Table S. 14 survival data for *fat-5(tm420)* nematodes upon exposure to P57. The average mean and median survival are presented by calculating from three independet trials.**

**Appendix Thirteen.**

Body size measurements were performed and graphs were plotted for *cyp-35A2(gk317)* mutant in response to P57. The average size changes (Body area Table. S15 and length Table. S16), results of three biologically independent trials are presented.

| ***cyp-35A2(gk317)* Body surface area (micron$^2$)** | | | | | | |
|---|---|---|---|---|---|---|
| **Vehicle control** | **24 hrs** | **48 hrs** | **72 hrs** | **96 hrs** | **120 hrs** | **144 hrs** |
| **AVE.** | 5060.1023 | 28887.3485 | 75533.7865 | 101856.743 | 102000.026 | 106153.2555 |
| **STDEV.** | 865.4631995 | 2286.756089 | 3978.693386 | 6659.509207 | 9195.684021 | 8941.181275 |
| **COUNT** | 20 | 20 | 20 | 20 | 20 | 20 |
| **0.03 µg/mL P57** | | | | | | |
| **AVE.** | 6008.49185 | 30479.6785 | 73204.697 | 99649.963 | 104342.525 | 105274.3775 |
| **STDEV.** | 649.4377096 | 3256.576867 | 6826.347208 | 7347.819668 | 9776.189017 | 10067.00278 |
| **COUNT** | 20 | 20 | 20 | 20 | 20 | 20 |
| **0.3 µg/mL P57** | | | | | | |
| **AVE.** | 5321.4228 | 29312.5135 | 74253.0485 | 104548.093 | 108448.5645 | 110078.155 |
| **STDEV.** | 843.6815338 | 2076.816232 | 8533.475681 | 7999.023822 | 10474.86171 | 9759.123923 |
| **COUNT** | 20 | 20 | 20 | 20 | 20 | 20 |

**Table S. 15 Body surface area growth in *cyp-35A2(gk317)* worms treated with two doses of P57. The average volumetric measurements are taken from three biological groups.**

| *cyp-35A2(gk317)* **Body length (micron)** | | | | | | |
|---|---|---|---|---|---|---|
| **Vehicle control** | **24 hrs** | **48 hrs** | **72 hrs** | **96 hrs** | **120 hrs** | **144 hrs** |
| **AVE.** | 378.650765 | 743.59342 | 1131.94915 | 1300.93285 | 1317.9227 | 1358.7894 |
| **STDEV.** | 35.42569618 | 42.97857978 | 51.74446075 | 73.58744734 | 65.29069884 | 72.20619478 |
| **COUNT** | 20 | 20 | 20 | 20 | 20 | 20 |
| **0.03 µg/mL P57** | | | | | | |
| **AVE.** | 379.152025 | 750.47528 | 1112.0301 | 1292.81525 | 1342.4506 | 1349.25065 |
| **STDEV.** | 18.9915866 | 47.21799337 | 59.00700514 | 43.0026167 | 65.13967825 | 79.92460197 |
| **COUNT** | 20 | 20 | 20 | 20 | 20 | 20 |
| **0.3 µg/mL P57** | | | | | | |
| **AVE.** | 375.842835 | 765.416505 | 1113.8644 | 1279.7099 | 1335.4435 | 1376.77565 |
| **STDEV.** | 28.81943044 | 31.35835528 | 67.96336387 | 77.29705148 | 56.48557358 | 60.38489364 |
| **COUNT** | 20 | 20 | 20 | 20 | 20 | 20 |

**Table S. 16 Body length growth in *cyp-35A2(gk317)* worms treated with two doses of P57. The average volumetric measurements are taken from three biological groups.**

**Appendix Fourteen.**

The lifespan of *cyp-35A2(gk317)* was determined with or without the presence of P57 and plotted using Kaplan-Meier curves. Thereafter utilizing Log-rank (Mantel-Cox) procedure the significance in changes within the median lifespan and mean survival of each experimental nematode group was pinpointed which is displayed. Analysis was applied via GraphPad Prism v5. Software (GraphPad Software Inc., La Jolla USA).

| ***cyp-35A2(gk317)*** | | | | | |
|---|---|---|---|---|---|
| Condition | Mean lifespan ± SEM (days) | Median lifespan (days) | Log-rank test | Control/treatment (n) | censored |
| Vehicle control | 10.8 ± 0.2 | 12 | - | - | 62 |
| 0.03 µg/mL | 10.6 ± 0.1 | 11 | 0.033 | 338/357 | 43 |
| 0.3 µg/mL | 11.3 ± 0.3 | 12 | 0.084 | 338/376 | 24 |

**Table S. 17 Survival data gathered from *cyp-35A2(gk317)* in response to P57 treatment. Results present the outcomes of three biologically indpeendent trials.**

**Appendix Fifteen.**

Growth measurements in response to silencing of *cyp-35A2* in wild-type and/or *fat-5(tm420)* background worms. Both body length and surface area changes are displayed as the average of three biological repeats.

| | **wild-type** | | **wild-type (*cyp-35A2* RNAi)** | | ***fat-5(tm420)*** | | ***fat-5* (*cyp-35A2* RNAi)** | |
|---|---|---|---|---|---|---|---|---|
| **24 hrs** | **Body surface area (micron$^2$)** | **Body length (micron)** | **Body surface area (micron$^2$)** | **Body length (micron)** | **Body surface area (micron$^2$)** | **Body length (micron)** | **Body surface area (micron$^2$)** | **Body length (micron)** |
| **Average** | 7475.1888 | 413.88485 | 7880.7567 | 395.51566 | 7092.96925 | 401.83969 | 7070.05335 | 418.18783 |
| **STDEV.** | 853.0003155 | 29.02051391 | 680.4731782 | 23.08132112 | 1022.809597 | 32.55399209 | 756.8809466 | 26.52696269 |
| **COUNT** | 20 | 20 | 20 | 20 | 20 | 20 | 20 | 20 |
| **48 hrs** | | | | | | | | |
| **Average** | 31885.33 | 809.02656 | 40111.571 | 922.451945 | 32108.2135 | 829.094805 | 28146.436 | 799.06426 |
| **STDEV.** | 1856.448952 | 44.74568849 | 3787.198443 | 44.63835264 | 4624.907981 | 83.32082972 | 5070.362001 | 91.17065255 |
| **COUNT** | 20 | 20 | 20 | 20 | 20 | 20 | 20 | 20 |
| **72 hrs** | | | | | | | | |
| **Average** | 84424.08 | 1145.3829 | 96578.2515 | 1275.5786 | 79006.1165 | 1223.842 | 78906.2505 | 1265.4081 |
| **STDEV.** | 9713.878386 | 70.0601928 | 8326.518752 | 102.6757936 | 11929.86389 | 66.81655495 | 6152.497744 | 76.64671005 |
| **COUNT** | 20 | 20 | 20 | 20 | 20 | 20 | 20 | 20 |
| **96 hrs** | | | | | | | | |
| **Average** | 108325.539 | 1278.19555 | 113588.265 | 1388.2263 | 101976.817 | 1367.1245 | 92008.878 | 1325.99405 |
| **STDEV.** | 7998.790461 | 45.66580773 | 5607.048002 | 61.17512065 | 6603.087312 | 72.16650659 | 6800.708226 | 58.88965883 |
| **COUNT** | 20 | 20 | 20 | 20 | 20 | 20 | 20 | 20 |
| **120 hrs** | | | | | | | | |
| **Average** | 114826.053 | 1367.5587 | 123333.085 | 1441.0998 | 109006.9075 | 1405.90435 | 103061.6455 | 1429.2422 |
| **STDEV.** | 9076.158256 | 60.44946341 | 6256.843028 | 41.99386743 | 10828.93611 | 76.1217877 | 8795.042769 | 61.8962890 |

| | | | | | | | | |
|---|---|---|---|---|---|---|---|---|
| **COUNT** | 20 | 20 | 20 | 20 | 20 | 20 | 20 | 20 |
| **144 hrs** | **Body surface area (micron$^2$)** | **Body length (micron)** | **Body surface area (micron$^2$)** | **Body length (micron)** | **Body surface area (micron$^2$)** | **Body length (micron)** | **Body surface area (micron$^2$)** | **Body length (micron)** |
| **Average** | 117403.785 | 1388.5337 | 125124.41 | 1467.6449 | 112549.0835 | 1453.6146 | 105205.0995 | 1460.77375 |
| **STDEV.** | 7053.16225 | 82.28079073 | 10686.5198 | 96.13300678 | 9227.463377 | 61.29429275 | 13563.56622 | 68.62872282 |
| **COUNT** | 20 | 20 | 20 | 20 | 20 | 20 | 20 | 20 |

**Table S. 18 Growth measurements performed in wild-type and *fat-5(tm420)* strains upon *cyp-35A2* RNAi.**

**Appendix Sixteen.**

Upon Knockdown of *cyp-35A2* in wild-type and a *fat-5(tm420)* background, survival curves were plotted with Kaplan-Meier method and further analyzed using Log-rank (Mantel-Cox) statistical approaches and data are displayed.

| Condition | Mean lifespan ± SEM (days) | | Median lifespan (days) | | Log-rank test | Control/treated (n) | Censored |
|---|---|---|---|---|---|---|---|
| wild-type | control | *cyp-35A2* RNAi | control | *cyp-35A2* RNAi | | | |
| | 11.5 ± 0.1 | 10.1 ± 0.1 | 12 | 10 | <0.0001 | 363/351 | 37/49 |
| | | | | | | | |
| *fat-5(tm420)* | control | *cyp-35A2* RNAi | control | *cyp-35A2* RNAi | | | |
| | 13.9 ± 0.2 | 15.9 ± 0.3 | 15 | 17 | <0.0001 | 361/382 | 39/18 |

**Table S. 19 Lifespan data performed on three trials and average is presented for each data set.**

**Appendix Seventeen.**

Survival rate of wild-type, *fat-5(tm420), cyp-35A2(gk317)* and the double knockout *fat-5(tm420);cyp-35A2(gk317)* were determined and plotted.

Addition statistical analysis was applied via Log-rank (Mantel-Cox) method and results are displayed.

| Nematode strain | Mean lifespan ± SEM (days) | Median lifespan (days) | Log-rank test | Control/mutant (n) | Censored (n) |
|---|---|---|---|---|---|
| wild-type | 12.4 ± 0.2 | 13 | - | - | 57 |
| *fat-5(tm420)* | 11.1 ± 0.1 | 11 | < 0.0001 | 343/374 | 26 |
| *cyp-35A2(gk317)* | 10.8 ± 0.2 | 12 | < 0.0001 | 343/338 | 62 |
| *fat-5(tm420);cyp-35A2(gk317)* | 14.7 ± 0.3 | 17 | < 0.0001 | 343/341 | 59 |

**Table S. 20 survival data quantified within four strains and performed on three biologically independent trials.**

**Appendix Eighteen.**

Data consist of body growth changes in double knockout *fat-5(tm420);cyp-35A2(gk317)* nematodes treated with and without P57. Each data point is the average body surface area/length of three biological trials where in each trial 20 worms were analyzed.

| | Vehicle control | | 0.03 µg/mL P57 | | 0.3 µg/mL P57 | |
|---|---|---|---|---|---|---|
| **24 hrs** | **Body surface area (micron$^2$)** | **Body length (micron)** | **Body surface area (micron$^2$)** | **Body length (micron)** | **Body surface area (micron$^2$)** | **Body length (micron)** |
| **Average** | 5978.22555 | 373.830455 | 6493.08685 | 389.991875 | 7115.2322 | 385.49436 |
| **STDEV.** | 996.0106859 | 31.6515612 | 1035.701157 | 26.07041225 | 678.1988097 | 20.76461514 |
| **COUNT** | 20 | 20 | 20 | 20 | 20 | 20 |
| **48 hrs** | | | | | | |
| **Average** | 31096.36 | 782.77275 | 33117.761 | 786.920605 | 30668.493 | 765.999215 |
| **STDEV.** | 2493.301146 | 36.99785821 | 2355.763559 | 38.66469241 | 4182.928757 | 53.21092592 |
| **COUNT** | 20 | 20 | 20 | 20 | 20 | 20 |
| **72 hrs** | | | | | | |
| **Average** | 69805.2135 | 1134.30645 | 76168.7365 | 1169.459315 | 81268.372 | 1170.3099 |
| **STDEV.** | 7226.84971 | 66.16904762 | 9780.359204 | 92.45414213 | 7058.274059 | 60.85558532 |
| **COUNT** | 20 | 20 | 20 | 20 | 20 | 20 |
| **96 hrs** | | | | | | |
| **Average** | 88399.4185 | 1290.3296 | 105770.1625 | 1337.6904 | 105854.58 | 1318.18155 |
| **STDEV.** | 7347.826791 | 51.31805074 | 8884.83949 | 80.11862888 | 10896.69289 | 101.4946495 |
| **COUNT** | 20 | 20 | 20 | 20 | 20 | 20 |

| | | | | | | |
|---|---|---|---|---|---|---|
| **120 hrs** | | | | | | |
| **Average** | 89490.9215 | 1242.1505 | 105759.4595 | 1351.25705 | 105736.8735 | 1288.64005 |
| **STDEV.** | 9205.842562 | 65.38175843 | 9866.606477 | 84.73707286 | 9969.52057 | 88.95959092 |
| **COUNT** | 20 | 20 | 20 | 20 | 20 | 20 |
| **144 hrs** | | | | | | |
| **Average** | 91572.252 | 1276.33195 | 109168.937 | 1335.179775 | 109155.8505 | 1329.3647 |
| **STDEV.** | 9579.134731 | 131.6827984 | 16800.60116 | 127.9586085 | 11897.1407 | 82.03662548 |
| **COUNT** | 20 | 20 | 20 | 20 | 20 | 20 |

**Table S. 21 Growth measurements in *fat-5(tn420);cyp-35A2(gk317)* double knockout upon treatment with P57 concentrations.**

**Appendix Nineteen**

Survival data of double knockout nematodes upon exposure to P57 doses are displayed. The mean lifespan and median survival are the average taken from three biologically independent assays.

| ***fat-5(tm420);cyp-35A2(gk317)* double knockout** | | | | | |
|---|---|---|---|---|---|
| condition | Mean lifespan ± SEM (days) | Median lifespan (days) | Log-rank test | Control/treatment (n) | Censored (n) |
| Vehicle control | 14.1 ± 0.3 | 17 | - | - | 60 |
| 0.03 μg/mL | 9.9 ± 0.2 | 10 | < 0.0001 | 340/312 | 88 |
| 0.3 μg/mL | 9.8 ± 0.2 | 10 | < 0.0001 | 340/326 | 74 |

**Table S. 22Data corresponding to the Kaplan-Meier survival curves of the double knockout strain upon treatment with P57.**

**Appendix Twenty.**

Probe and primer sets designed by the UPL software for transcription factors. For further details refer to: http://lifescience.roche.com.

| Gene | Forward primer | Reverse primer | UPL probe ID number |
|---|---|---|---|
| *nhr-49* | ACAAGTTGGAATGAAACGAGAAG | TTGAATGGAGTCCCGTTGA | 36 |
| *sbp-1* | CAGCGTCGCTTTTTGTTAATAC | TTGAGGAGTCATTGAGGTATGG | 22 |
| *cyp-35A5* | TGTGAAAGGAGAAGACGAGAAA | CTGTCGTGGTTTCTTGACCA | 5 |
| *daf-16* | TGTGCCAAGCACTAACTTCAA | GCAGTGGAGATGAGTTGGATG | 31 |
| *cyp-35C1* | CGTTTGGAATTGGAAAAAGG | GCGGAGTAGTAGGTTTCCAATG | 14 |

**Table S.23 Probe and Primer sets designed by UPL software.**